

OCTOBER 1971

LMSC-D243938

7 ml

REVIEW OF DELTA WING SPACE SHUTTLE VEHICLE DYNAMICS

Final Technical Report

Prepared by:

J. Peter Reding

Research Specialist, Aero-Thermodynamics

Lars E. Ericsson

Senior Staff Engineer, Engineering Technology

Prepared under Contract NAS 9-11495

For

National Aeronautics and Space Administration

FACILITY FORM 602

N 72-15941
(ACCESSION NUMBER)

164
(PAGES)

CR-115-357
(NASA CR OR TMX OR AD NUMBER)

(THRU)

63
(CODE)

01
(CATEGORY)

Lockheed

MISSILES & SPACE COMPANY, INC.

A SUBSIDIARY OF LOCKHEED AIRCRAFT CORPORATION

SUNNYVALE, CALIFORNIA

A Reproduced Copy OF

(NASA-CR-115357)	REVIEW OF DELTA WING	N72-15941
SPACE SHUTTLE VEHICLE DYNAMICS	Final	
Technical Report	J.P. Reding, et al	
(Lockheed Missiles and Space Co.)	Oct.	Unclas
1971 164 p	CSSL 01A G3/01	14400

Reproduced for NASA
by the
NASA Scientific and Technical Information Facility

Reproduced by
**NATIONAL TECHNICAL
 INFORMATION SERVICE**
 Springfield, Va. 22151

PRECEDING PAGE BLANK NOT FILMED

ABSTRACT

The unsteady aerodynamics of the proposed delta planform, high cross range, shuttle orbiters, are investigated. It is found that these vehicles are subject to five unsteady-flow phenomena that could compromise the flight dynamics.

They are as follows:

- Leaside shock-induced separation
- Sudden leading-edge stall
- Vortex burst
- Bow shock-flap shock interaction
- Forebody vorticity

Trajectory shaping is seen as the most powerful means of avoiding detrimental effects of the stall phenomena; however, stall must be fixed or controlled when traversing the stall region. Other phenomena may be controlled by carefully programmed control deflections and some configuration modifications. Ways to alter the occurrence of the various flow conditions are explored.

A companion study of the aeroelastic stability of typical boost configurations indicates that both parallel- and series-boost configurations will be subject to unsteady aerodynamic effects that could cause aerodynamic undamping of one or more of the low-frequency bending modes.

PRECEDING PAGE BLANK NOT FILMED

CONTENTS

Section		Page
	ABSTRACT	iii
	ILLUSTRATIONS	vii
1	INTRODUCTION	1-1
2	DISCUSSION	2-1
	2.1 Leaside Shock Induced Separation	2-1
	2.2 Sudden Leading Edge Stall	2-20
	2.3 Vortex Burst	2-30
	2.4 Control Interference	2-57
	2.5 Forebody Vortices	2-71
	2.6 Avoiding the Problems	2-84
	2.7 Experimental Program	2-110
3	CONCLUSIONS	3-1
4	RECOMMENDATIONS FOR FUTURE STUDY	4-1
5	REFERENCES	5-1
Appendix		
A	NOMENCLATURE	A-1
B	LAUNCH CONFIGURATION AEROELASTIC STABILITY	B-1

REVIEW OF DELTA WING SPACE
SHUTTLE VEHICLE DYNAMICS

by

J. Peter Reding and Lars E. Ericsson

LMSC-D243938

October 1971

Prepared Under Contract NAS 9-11445
for
National Aeronautics and Space Administration

LOCKHEED MISSILES & SPACE COMPANY
A Group Division of Lockheed Aircraft Corporation
Sunnyvale, California

ILLUSTRATIONS

Figure		Page
1	Comparison of Entry Attitudes for Proposed Delta Planform Shuttle Orbiters (Ref. 21)	2-2
2	Hypersonic Leaside Oil Flow Photographs on NAR Orbiter, $M = 7.4$ (Ref. 22)	2-3
3	Hypersonic Leaside Flow Field	2-4
4	Hypersonic Leaside Flows on Delta Wing at $M = 10.16$ (Ref. 23)	2-5
5	Experimental Separation Line Position (Ref. 23)	2-7
6	Hypersonic Leaside Flow Boundaries, NAR Delta Orbiter at $M = 7.4$ (Ref. 22)	2-8
7	Wing Pitching Moment and Lift Increments of NAR Delta Orbiter (Refs. 24 and 26)	2-9
8	Wing-Induced Rolling Moment Derivative NAR Orbiter, $M = 7.4$ (Ref. 26)	2-12
9	Shock-Induced Leading-Edge Separation Boundary as Defined by Rolling Moment Derivative Nonlinearity (Ref. 27)	2-13
10	Comparison of Leaside Wing Flow Boundaries with α_{trim} Schedule for NAR Delta Orbiter	2-14
11	Comparison of Theoretical and Experimental Spanwise Pressure Distributions on Leaside of Delta Wing at Hypersonic Speeds, $M = 10.16$ (Ref. 23)	2-15
12	Steady and Unsteady Flow Patterns of Nose-Induced Separation	2-17
13	Comparison of Steady and Unsteady Vortex Positions (Ref. 29)	2-18
14	Vortex Position as Function of Time for Plunging Delta Wing (Ref. 30)	2-19
15	Estimated Roll Damping Characteristics at $M = 6.0$, NAR Orbiter	2-21
16	Estimated Roll Damping Characteristics for Design α_{trim} Schedule for NAR Orbiter	2-22
17	Windward Side Wing Body Hypersonic Flow Field (Ref. 33)	2-23
18	Transonic Flow Boundaries for Two-Dimensional NACA 64A012 Airfoil Section (Ref. 39)	2-24

Figure		Page
19	Flow Boundaries for NACA 16-006 Airfoil (Ref. 39)	2-26
20	Comparison of Pressure Distributions for Sudden Separation	2-27
21	Dynamic Effects of Sudden Separation	2-28
22	Flow Breakdown at $M = 1.05$ Showing Region of Outboard Attached Flow (Ref. 43)	2-29
23	Measured Isolated Data Point for Bending Instability (Ref. 44)	2-31
24	Effect of Mach Number on Damping (Ref. 45)	2-32
25	Effect of Vortex Burst on Longitudinal and Lateral Characteristics (Ref. 48)	2-33
26	Effect of Vortex Breakdown on Static Pressure (Ref. 48)	2-35
27	Effect of Leading Edge Sweep on Vortex Burst (Ref. 58)	2-36
28	Low-Speed Vortex Burst on 76-deg Delta Wing at Angle-of-Attack and Sideslip (Refs. 48 and 59)	2-37
29	Vortex Breakdown Position – Delta Wings (Ref. 60)	2-39
30	Hysteresis and Unstable Vortex Burst Locations (Ref. 61)	2-40
31	Comparison of Breakdown Measurements on Delta Wings Measured in Different Tunnels (Ref. 62)	2-41
32	Vortices for Cambered Delta Plate, $\Lambda = 80$ deg; Water Tunnel, $U = 2$ in./sec (Ref. 58)	2-42
33	Interaction of Shock Wave With Leading-Edge Vortices; Schlieren Observation, Sharp-Edged Plate Delta; $\Lambda = 50$ deg, $\alpha = 10$ deg (Ref. 58)	2-43
34	Low-Frequency ($f\bar{c}/U = 0.05$) Vibration Load on Delta Wings Due to Vortex Burst (Ref. 63)	2-44
35	Vortex Burst Effects on the Concorde Aircraft (Ref. 64)	2-45
36	Lateral Characteristics of Cone-Flow Wave Rider (Ref. 65)	2-46
37	Sensitivity of Vortex Burst to Planform and Section Geometry	2-47
38	Variation of Breakdown Position With Incidence (Ref. 62)	2-49
39	Effect of Vortex Burst on the Aerodynamic Characteristics of the NAR Delta Orbiter, $M = 0.6$ (Ref. 66)	2-50
40	Vortex Burst Interference Effects	2-53
41	Yaw Interference Loads on Straight Wing Orbiter, $\alpha = 57$ deg (Ref. 67)	2-55
42	Yaw Stability on Straight Wing Orbiter, $\alpha = 57$ deg (Ref. 67)	2-56
43	Correlation of Delta Body Pitch and Yaw Characteristics (Ref. 69)	2-58

Figure		Page
44	Delta Body Leaside Flow Patterns, $M = 1.0$ (Ref. 69)	2-59
45	$M_\infty \theta_{incip}$ Versus \bar{x}_L for Incipient Separation Condition (Ref. 71)	2-60
46	Supersonic Control Interference for NAR Orbiter, $M = 5$	2-61
47	Effect of Combined Elevator - Aileron Deflection on Aerodynamic Characteristics, NAR Orbiter With Split Elevon, $M = 60$ (Ref. 24)	2-63
48	Possible Control Induced Hysteresis	2-64
49	Vortex Burst Caused by Downstream Obstacle on 76-deg Delta Wing at $\alpha = 20$ deg (Ref. 48)	2-65
50	Control-Induced Vortex Burst (Ref. 24)	2-67
51	Effect of Vortex Burst on Control Demand, Flight Results on a Modified F5D Aircraft (Ref. 75)	2-68
52	Unsteady Aerodynamic Flow Boundaries Superimposed on NAR Orbiter Entry Corridor (Ref. 21)	2-69
53	Probable Occurrence and Possible Results of Bow Shock-Flap Shock Interference	2-70
54	Side Force at Zero Yaw as Function of Angle-of-Attack for Cone-Cylinder Body at $M = 2$ and $R_d = 2.6 \times 10^6$ (Ref. 87)	2-72
55	Side Moment Coefficients Measured on Tomahawk With ± 15 -deg Fin Cant (Ref. 88)	2-73
56	Side Force Coefficient at Zero Yaw and Various Roll Angles for an Ogive-Cylinder at $M = 0.7$ (Ref. 89)	2-74
57	Side Moment at Zero Yaw for Cone-Cylinder at $M = 0.5$ (Ref. 87)	2-75
58	Side Force Coefficients on Tomahawk at Zero Spin With and Without 1/4-in. -Wide Longitudinal Strips of No. 40 Grit (Ref. 88)	2-76
59	Effect of Roll Orientation and Roll Rate on Side Force at $\alpha = 18$ deg and $\beta = 0$ for Cone-Cylinder at $M = 0.5$ (Ref. 87)	2-78
60	Yaw Rate Damping Characteristics as Function of Angle-of-Attack for Several High Performance Fighter Aircraft (Ref. 91)	2-79
61	Example of Yawing Moments at $\beta = 0^\circ$ (Ref. 92)	2-80
62	Lack of Repeatability of Side Moments Induced by Free Forebody Vortices at Zero Yaw (Ref. 93)	2-81
63	Correlation of Dynamic Vortex Induced Yaw Moment (Ref. 101)	2-82
64	Effect of Forebody Vorticity on Velocity Profile at Tail	2-83

Figure		Page
65	Effect of Shear Flow on Fin-Induced Pitching Moment (Ref. 105)	2-85
66	Effect of Drag Brake on Directional Stability, NAR Orbiter (Ref. 24)	2-86
67	Component Buildup Yaw Characteristics, NAR Orbiter, $M = 6.0$ (Ref. 25)	2-87
68	Sample Trajectories to Minimize Unsteady Aerodynamic Effects	2-89
69	Effect of Leading Edge Sweep on Mixed Leading Edge Flow Conditions	2-91
70	Leading Edge Vortex Flow Characteristics of Double-Delta Wings	2-92
71	Swedish Fighter Aircraft Draken (Ref. 113)	2-96
72	Effect of Double-Strake Configuration on Aerodynamic Damping in Yaw With Angle-of-Attack for a High Performance Aircraft Configuration (Ref. 84)	2-98
73	Mischievous Centerline Spline Effects on Vortex Shedding	2-99
74	Variation of Yawing-Moment Coefficient With Angle-of-Attack for Several Aircraft Configurations at $\beta = 0$ deg, $R = 0.3 \times 10^6$ (Ref. 94)	2-100
75	Side Force Coefficients at Zero Yaw for Ogive-Cylinder With Various Nose Tip Bluntness Ratios, $M = 0.6$ (Ref. 89)	2-101
76	Effect of Nose-Tip Shape on Side Moment of a High Performance Aircraft at Zero Yaw (Ref. 94)	2-102
77	Effect of Asymmetric Nose-Tip on Side Moment of a High Perform- ance Aircraft at Zero Yaw (Ref. 94)	2-104
78	Variation of Side Moment at Zero Yaw Between "Identical" Models (Ref. 94)	2-105
79	Effect of Wing Sweep Angle on $C_{y\beta}$ and $C_{n\beta}$ of a High Performance Aircraft at Zero Yaw (Ref. 94)	2-106
80	Effect of Configuration Modifications on Directional Stability of the Grumman Orbiter (Ref. 106)	2-107
81	Suggested Orbiter Modifications	2-108
82	Shock Induced Separation, Comparison Between Wind Tunnel and Flight-Test Results (Ref. 127)	4-3
83	Effect of Boundary Layer Transition on Leading Edge Vortex Formation (Ref. 59)	4-4
84	Effect of Reynolds Number on Forebody Asymmetric Vortex Shedding at Zero Yaw (Ref. 94)	4-6
B-1	Shadowgraph of Flow Over Saturn-V Launch Vehicle at $M = 1.46$	B-2
B-2	Static Load Distribution on Saturn-V Launch Vehicle at $M = 1.3$ (Ref. 133)	B-3

Figure		Page
B-3	Comparison Between Computed and Measured Time Lags In Escape-System Wake (Ref. 134)	B-4
B-4	Comparison Between Quasi-Steady Predictions and Rigid-Body Experimental Results (Ref. 135)	B-5
B-5	Aerodynamic Damping at $\alpha = 0^\circ$ of Apollo-Saturn I Launch Vehicle With Disk-On Escape Rocket (Ref. 3)	B-7
B-6	Correlation of Wake Source Base Pressure Sensitivity With Submerged Conic Forebody Local Loads (Ref. 135)	B-8
B-7	Correlation of Instability Region With Wake Neck Induced Drag Rise	B-9
B-8	Launch Configuration, Upstream Communication Load (Ref. 137)	B-10
B-9	Yaw Plane Bending Modes (Ref. 138)	B-11
B-10	Effect of Relative Magnitude of Induced Booster Tail Load on Yaw Damping	B-12
B-11	Pitch Plane Mode Shapes (Ref. 138)	B-14
B-12	Straight Wing Boost Configuration Free-Free Mode Aerodynamic Damping	B-15
B-13	Second Mode Aerodynamic Damping Bounds for S-1C NAR Orbiter Launch Configuration	B-16
B-14	Mode Shape Comparison for S-1C-NAR Orbiter Launch Configuration and Saturn 203 Launch Vehicle	B-17

Section 1
INTRODUCTION

The high cross range, delta wing, space shuttle configurations present the flight dynamicist with a challenging set of flight conditions. These vehicles must fly at speeds from hypersonic down to low subsonic, they must traverse altitudes from orbit to sea level, and are required to fly at angles of attack from zero to as high as 50 deg in some cases. The angle of attack requirements probably cause the most severe aerodynamic stability problems since the vehicle is stalled, or, what is worse, nearly stalled, for much of the trajectory. There is the danger of experiencing a sudden, discontinuous change in stability when flying near incipient stall (either stalled or unstalled) which will raise havoc with the flight dynamics.

The effects of flow separation and other similar unsteady flow phenomena have been under study for quite some time at Lockheed (e. g. , Refs. 1-17). Quasi-steady techniques have been used extensively and with a great degree of success for the prediction of the dynamic effects of a variety of unsteady flow phenomena. Perhaps the most notable success has been the application of these techniques in the prediction of the aerodynamic damping of the first few elastic modes of the Apollo-Saturn family of boost vehicles. The predictions agreed so well with experiment (Refs. 2, 18, 19) for the Saturn I booster that this technique was used to predict the damping of all further Saturns (Ref. 20), thus eliminating the need for further complicated elastic model tests (e. g. , Ref. 18).

For these reasons, Lockheed was chosen by the NASA Manned Spacecraft Center to investigate the unsteady aerodynamics of the high cross range, delta planform, shuttle vehicles. This work, reported herein, is exploratory in nature. Possible problem areas are identified, their impact on the flight dynamics is explored, and fixes are suggested.

The major portion of this report deals with the North American Rockwell (NAR) delta orbiter. This is wholly the result of the availability of wind tunnel data at the time of the study. The problems discussed are by no means peculiar to the NAR orbiter. They are, in fact, common to the various delta wing designs, the only difference being minor shifts of the ranges of the instabilities.

Section 2 DISCUSSION

Generally the various delta orbiters follow a similar angle of attack-Mach number profile (Fig. 1 and Ref. 21). Entry occurs at a high initial angle of attack (up to 53 deg). At $M \approx 20.0$ pitchover to between 20 deg and 35 deg is accomplished where a bank angle program is initiated to achieve the required cross range. This continues to $M \approx 7.0$ where pitchover to the subsonic cruise attitude, which varies between 5 deg and 10 deg, is initiated. The pitchover maneuver may last down to $M \approx 1.0$. A very important part of the trajectory is flown at high angle of attack and high Mach number.

It is quite possible to arrive at some very erroneous conclusions if one approaches the high α - M regime with Newtonian theory in mind. Leaside effects are not negligible as Seegmiller's excellent flow photographs demonstrate (Fig. 2 and Ref. 22). At moderate angle of attack a significant region of attached flow exists on the leeward side of the delta wing (Fig. 2a). Also relatively strong reattachment zones may be seen on the sides of the fuselage at all angles of attack. Furthermore, a reattachment zone exists on the leeward fuselage, which, like the region of attached flow on the wing, is sensitive to yaw angle.* As angle of attack is increased the wing separation grows until nearly the entire wing - in fact, nearly the entire leaside of the vehicle - is separated (Figs. 2b and 2c). However, this does not occur until very high angles of attack. These salient features of the leaside flow are illustrated in Fig. 3. The strong leaside flows have a significant, sometimes a dominant, effect on orbiter stability as the following discussion will demonstrate.

2.1 LEESIDE SHOCK INDUCED SEPARATION

The surface flow patterns presented by Cross (Ref. 23) suggest a number of distinct flows on the leaside of a delta wing at hypersonic speeds (Fig. 4). At low angles of

*Note the asymmetry of both due to the negative yaw angle in Fig. 2a.

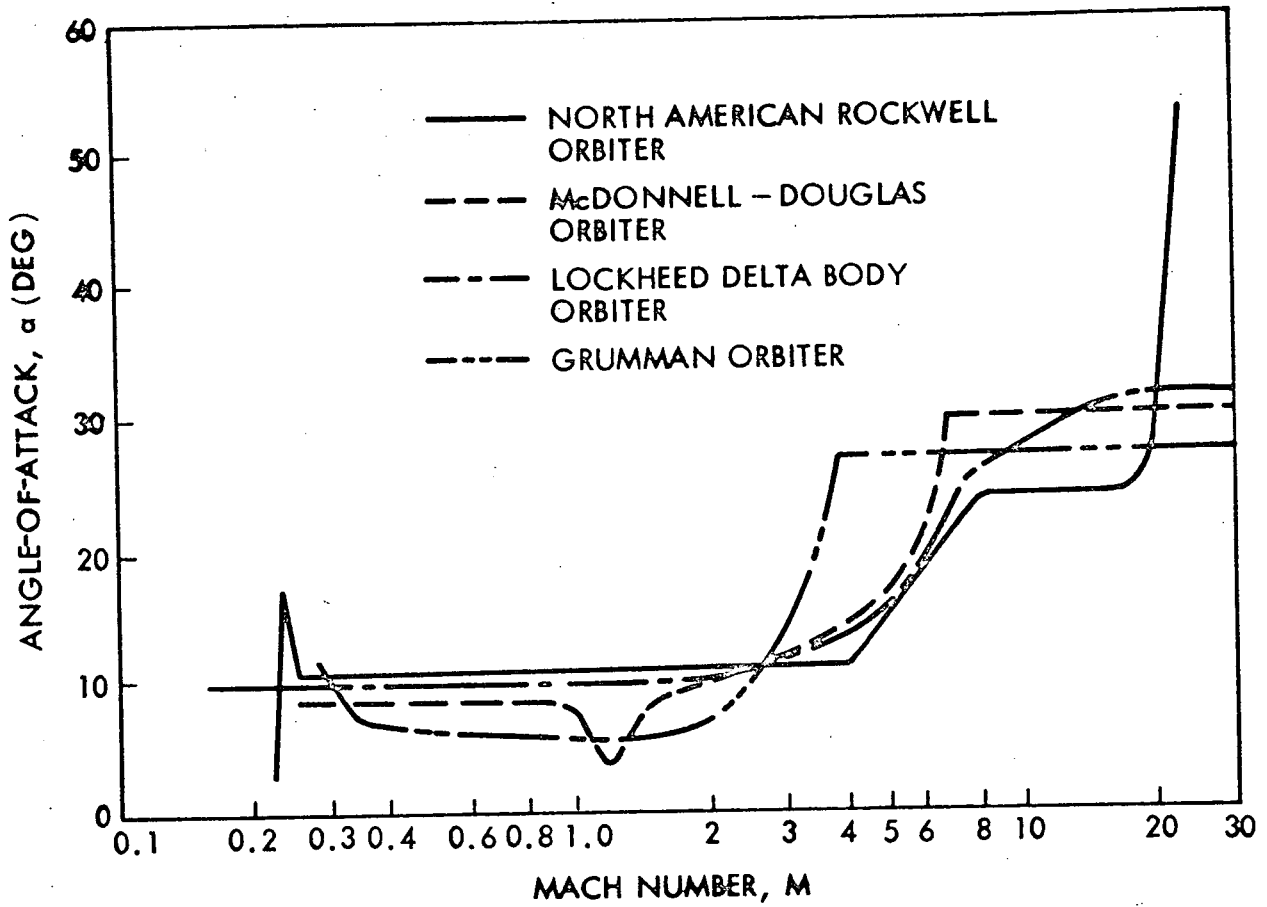
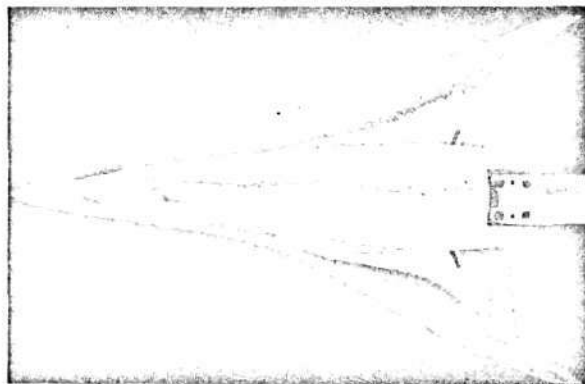


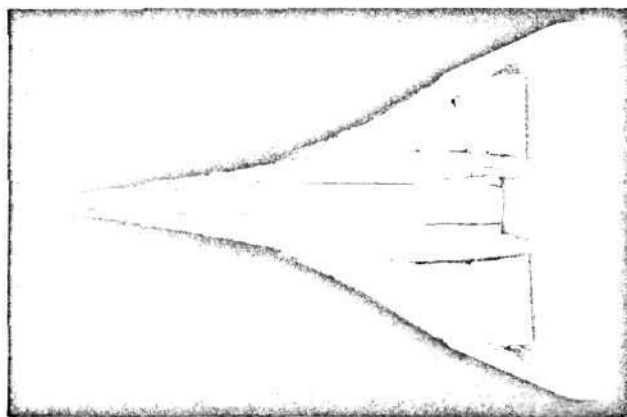
Fig. 1 Comparison of Entry Attitudes for Proposed Delta Platform Shuttle Orbiters (Ref. 21)



(a) $\alpha = 15 \text{ DEG}$, $\beta = -5 \text{ DEG}$



(b) $\alpha = 30 \text{ DEG}$, $\beta = 0 \text{ DEG}$



(c) $\alpha = 45 \text{ DEG}$, $\beta = 0 \text{ DEG}$

Reproduced from
best available copy.

Fig. 2 Hypersonic Leeside Oil Flow Photographs on NAR Orbiter, $M = 7.4$ (Ref. 22)

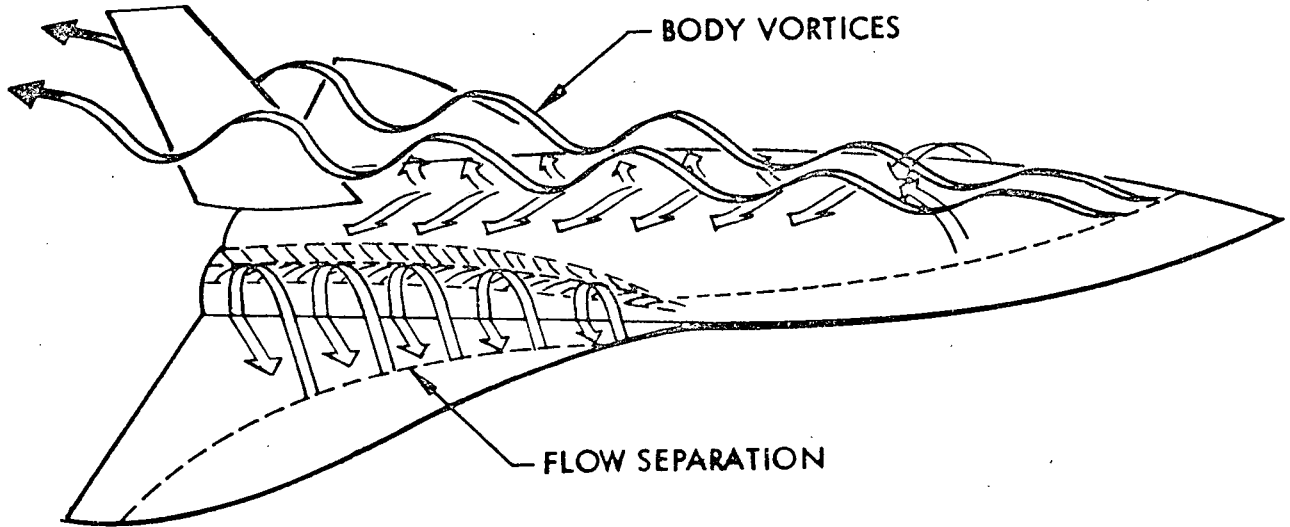


Fig. 3 Hypersonic Leeside Flow Field

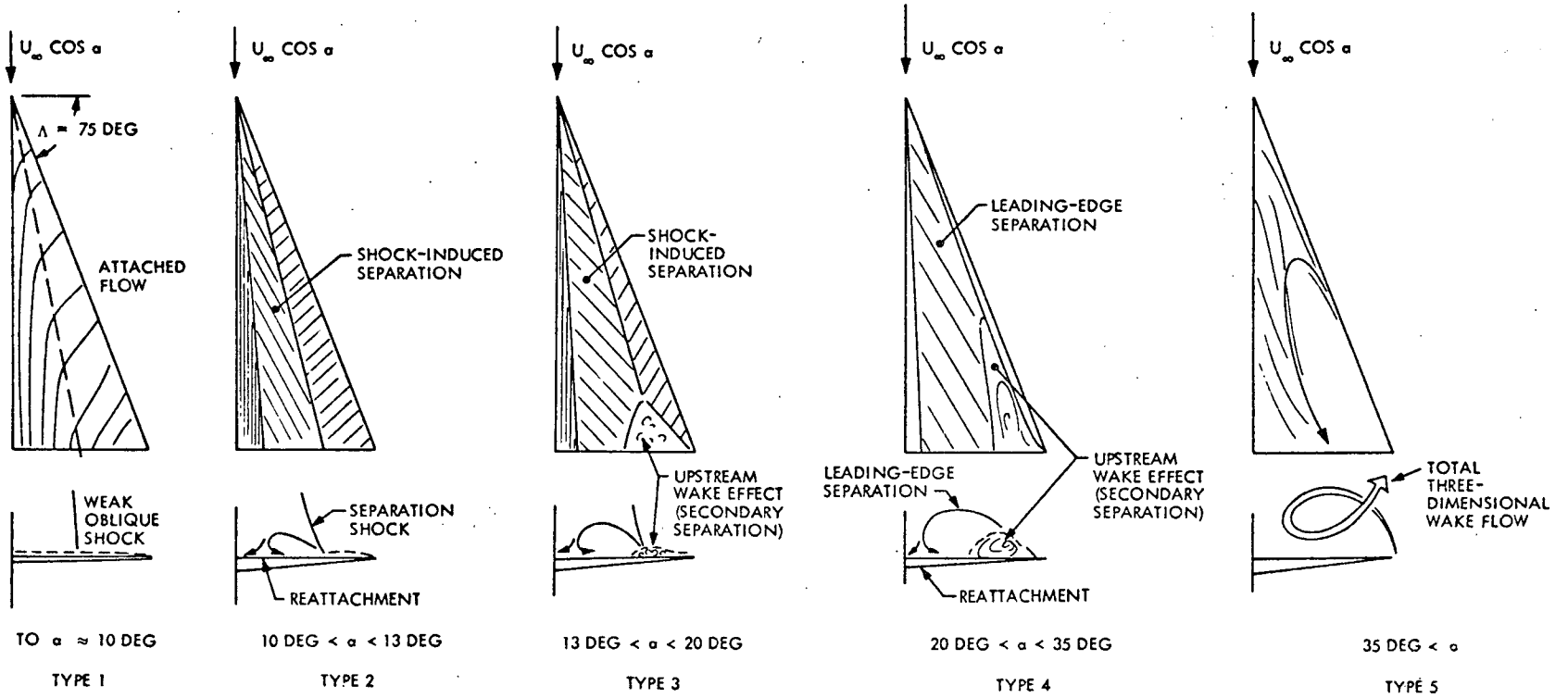


Fig. 4 Hypersonic Leeside Flows on Delta Wing at $M = 10.16$ (Ref. 23)

attack the flow converging from opposite wing panels (in the case of the pure delta wing) or from wing and fuselage (in the case of the shuttle) is turned parallel to the free stream by a weak shock (Type 1). When the angle of attack is great enough to cause the wing leading edge shock to detach the embedded terminal leeside shock becomes strong enough to separate the boundary layer (Type 2). That is, the subsonic flow aft of the detached shock expands around the leeward leading edge reattaining supersonic speeds. The flow is still constrained to turn downstream near the root as before. This turning is accomplished by a strong shock that causes the boundary layer to separate. The wake begins to affect the flow patterns at higher angle of attack, causing a secondary separation (Type 3). This is undoubtedly promoted by the thick, laminar, leeside boundary layer. As angle of attack is increased further the leeward boundary layer is weakened. This couples with the increased leeside expansion to promote separation. The separation region, therefore, grows until it reaches the leading edge (Type 4). This type of flow is somewhat similar to the subsonic delta wing flow with a vortex bound to the leading edge. Increasing the angle of attack still further results in a breakdown or burst of the bound vortex near the trailing edge. Finally, at still larger angles of attack, the leeward flow separation takes on a complicated three-dimensional, wake-like character (Type 5).

The changes of flow type correlates with discontinuities in the α -dependence of the terminal shock position (Fig. 5). Of course, the delta wing space shuttle orbiter will experience similar flow phenomena (compare Figs. 5 and 6).^{*} The data seem to indicate the possibility of a hysteresis region associated with the occurrence of shock induced separation. The angle of attack for shock detachment correlates with α for first occurrence of shock induced separation (Fig. 6) and also with the angle of attack where the wing pitching moment slope discontinuity occurs (Fig. 7). The change to a more stable pitching moment slope is the result of increased subsonic type leading edge

^{*}The data were measured on a double tail configuration (Ref. 22). However, the relative spanwise shock position (b_s/b) was measured at a chord station that appeared to be unaffected by the leading edge-fuselage interaction or by the wing-tail interaction; that is, where the separation line was relatively straight.

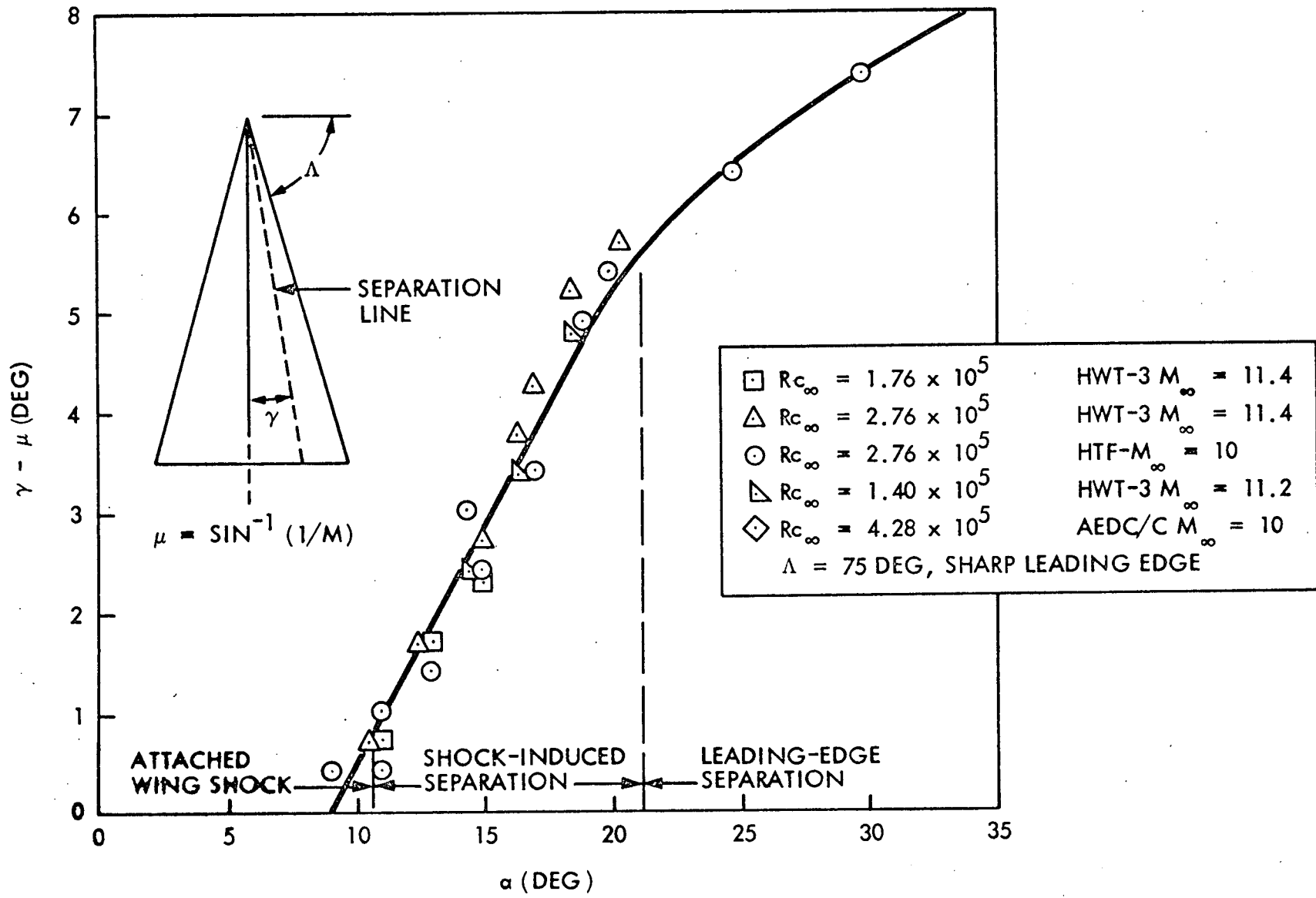


Fig. 5 Experimental Separation Line Position (Ref. 23)

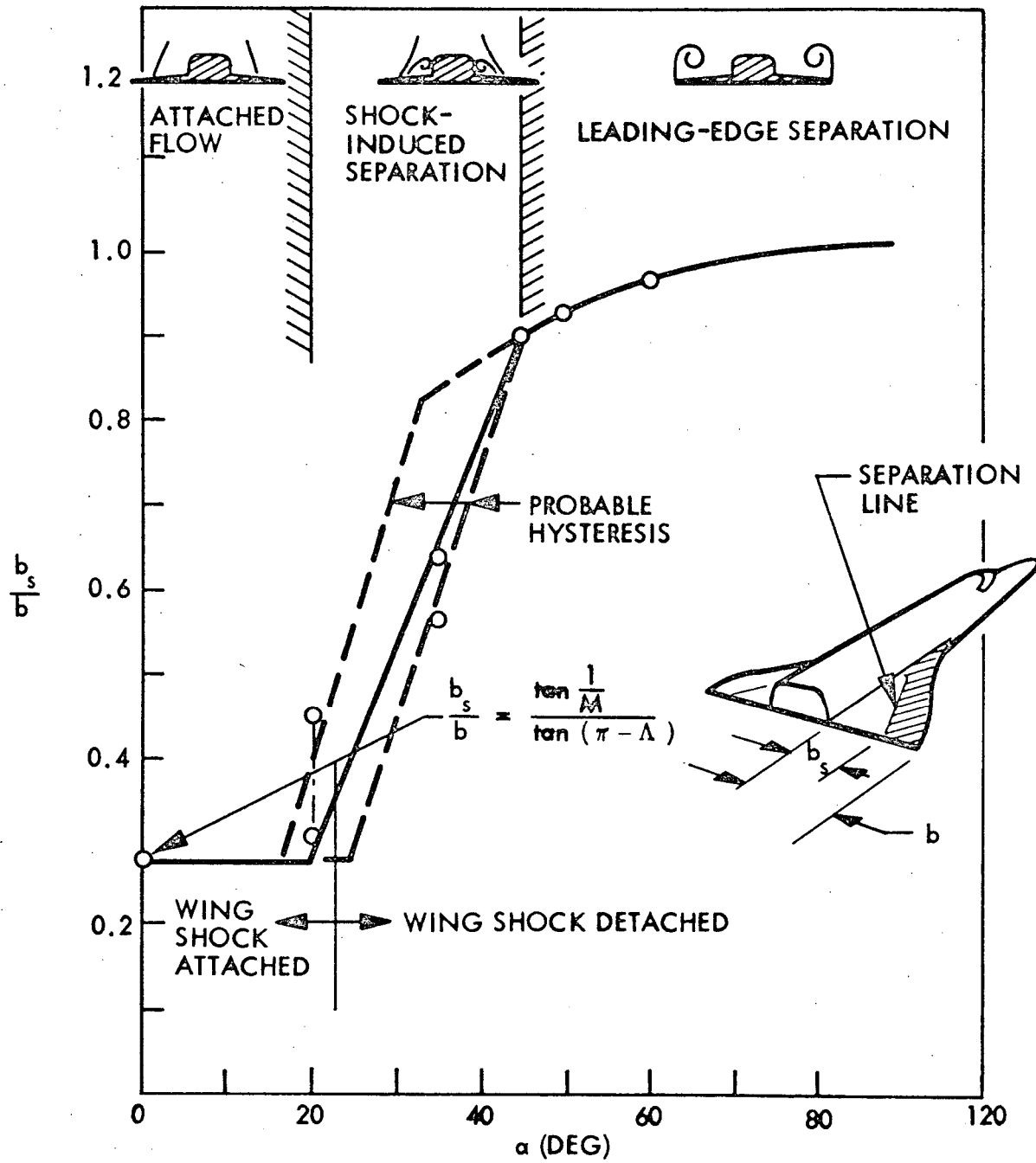


Fig. 6 Hypersonic Leeside Flow Boundaries, NAR Delta Orbiter at M=7.4 (Ref. 22)

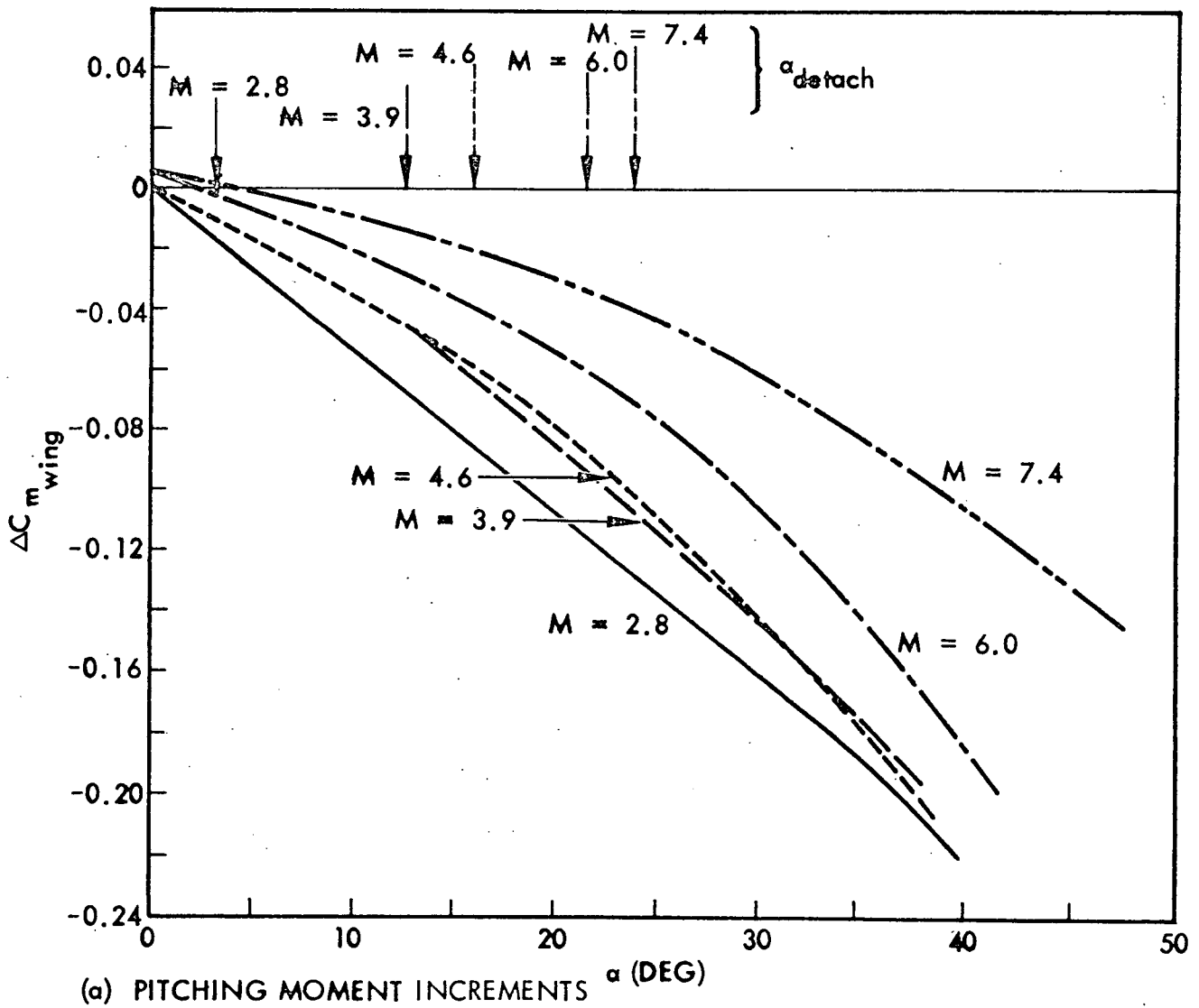
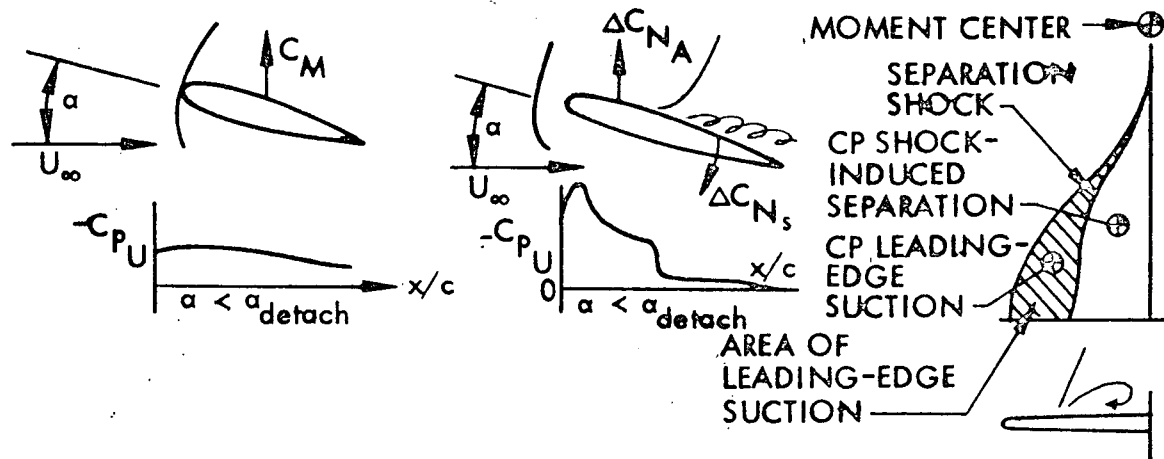
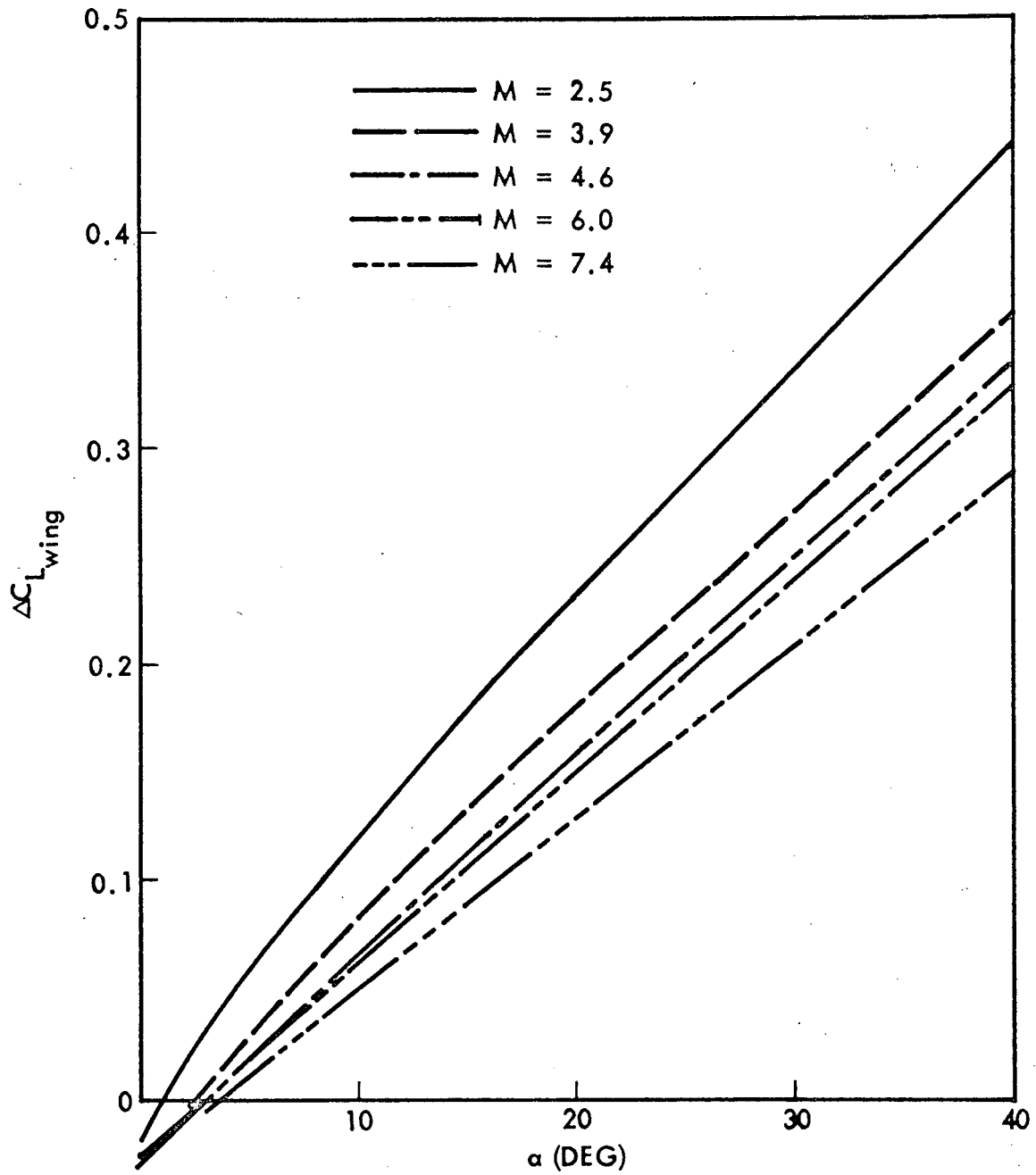


Fig. 7 Wing Pitching Moment and Lift Increments of NAR Delta Orbiter (Refs. 24 and 26)



(b) LIFT INCREMENTS

Fig. 7 (Cont.)

suction when the wing bow shock detaches. In addition there is a reduction of the lift over the wing area aft of separation (see sketches in Fig. 7a). Due to the increasing leading edge sweep towards the trailing edge, the center of pressure is more aft for the lift gain (due to L.E. suction) than for the lift loss (due to shock induced pressure increase aft of separation line). Thus, the wing pitching moment becomes more stable (Fig. 7a) although the incremental lift remains nearly linear (Fig. 7b).

This lift redistribution also explains the nonlinear roll characteristics. As the body is yawed the shock induced separation becomes asymmetric (Fig. 2). The separation grows on the leeward side giving a negative incremental lift, and shrinks on the windward side causing a positive incremental lift. The result is a stable (negative) incremental roll moment of larger magnitude than for attached flow. When leading edge separation occurs the growth of the negative lift increment is arrested and a less negative $C_{l\beta}$ results (Fig. 8). Thus, the nonlinearity in the roll curve indicates the occurrence of leading edge separation (Fig. 9). Likewise, a nonlinearity in the incremental wing pitching moment occurs due to leading edge separation, although the discontinuity is less distinct than that for the roll moment characteristics. Thus, the α -M range of shock induced separation may be obtained directly from the static data. It appears that this flow condition is of great practical importance as the orbiter will transverse this α -M region (Fig. 10).

Shock induced separation is characterized by an extreme (maximum) sensitivity of shock position and wing loading to angle to attack. This is undoubtedly due to the sensitivity of the boundary layer, hence the separation, to angle of attack. The dominance of viscous effects is demonstrated by the poor agreement between the actual surface pressure measurements and inviscid predictions from an equivalent solid body (Ref. 23 and Fig. 11). The implied assumption of zero pressure gradient normal to the wing surface is invalid for both separated and reattaching flow regions. This dominance of viscous effects indicates that the separation extent, and thus the wing loads, will be extremely sensitive to all factors affecting boundary layer strength (e.g., angle of attack, yaw angle, Reynolds number, pitch rate, yaw rate, etc.). The dominance of viscous effects will have a particularly strong impact on the dynamic characteristics.

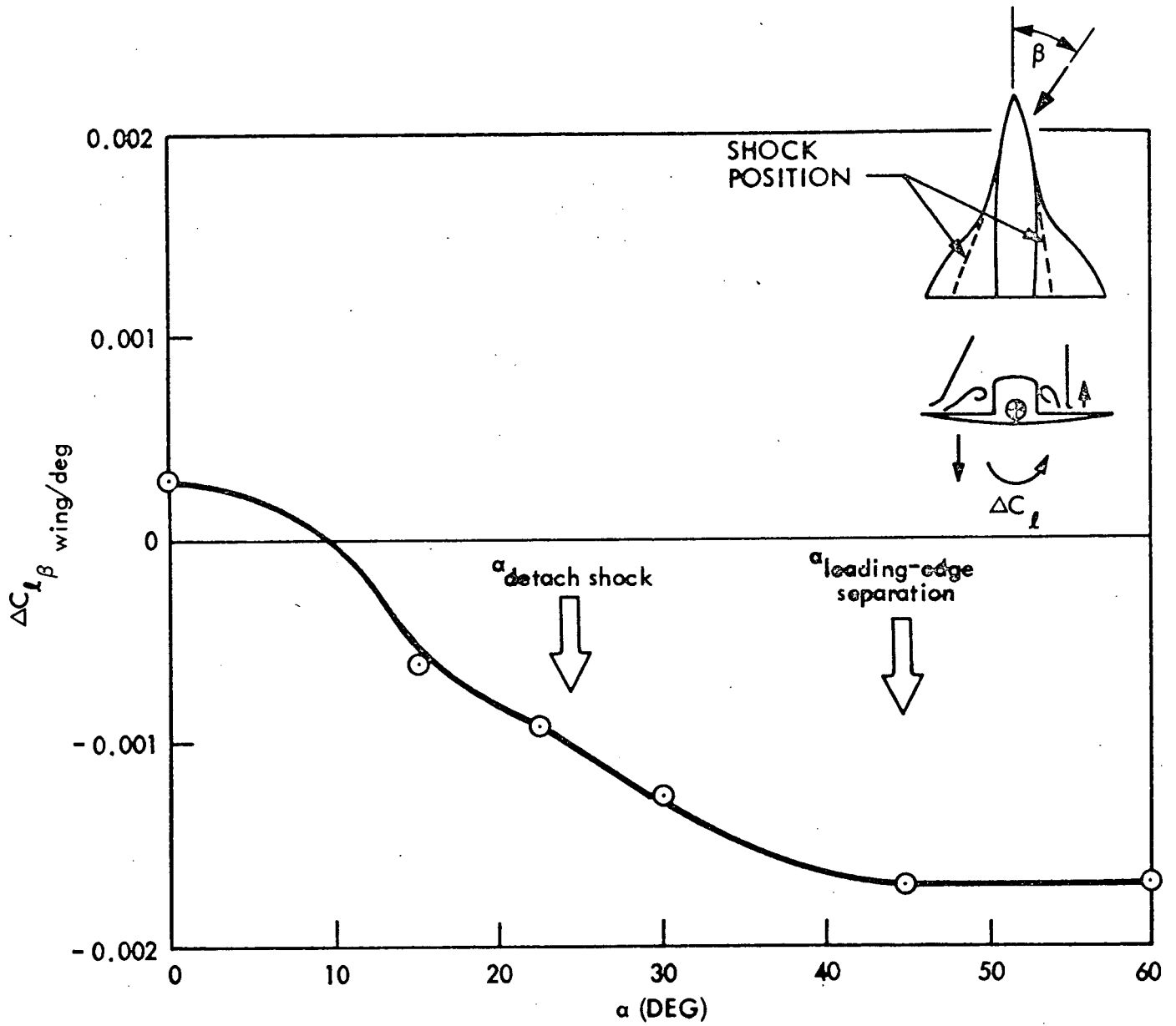


Fig. 8 Wing-Induced Rolling Moment Derivative NAR Orbiter, M = 7.4 (Ref. 26)

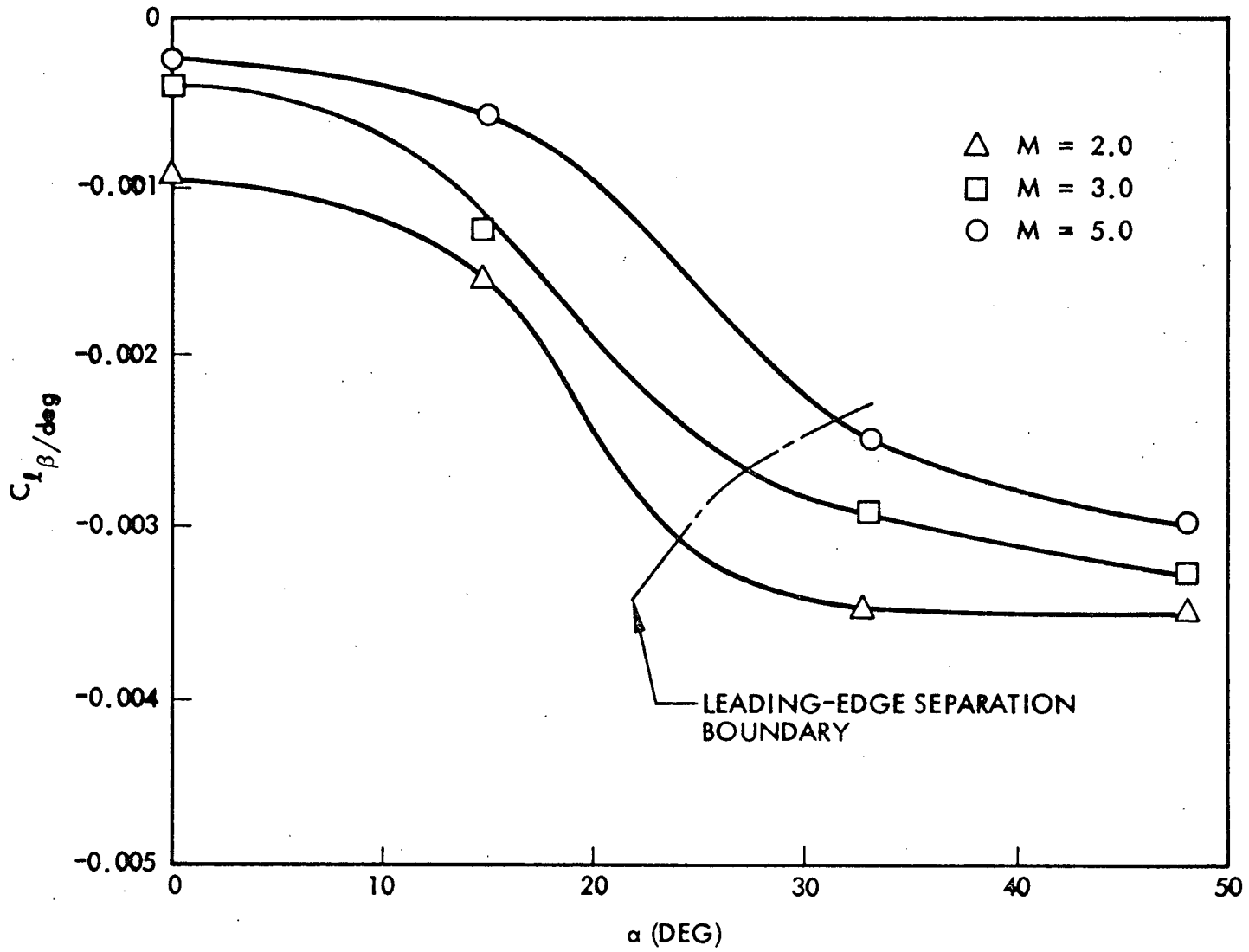


Fig. 9 Shock-Induced Leading-Edge Separation Boundary as Defined by Rolling Moment Derivative Nonlinearity (Ref. 27)

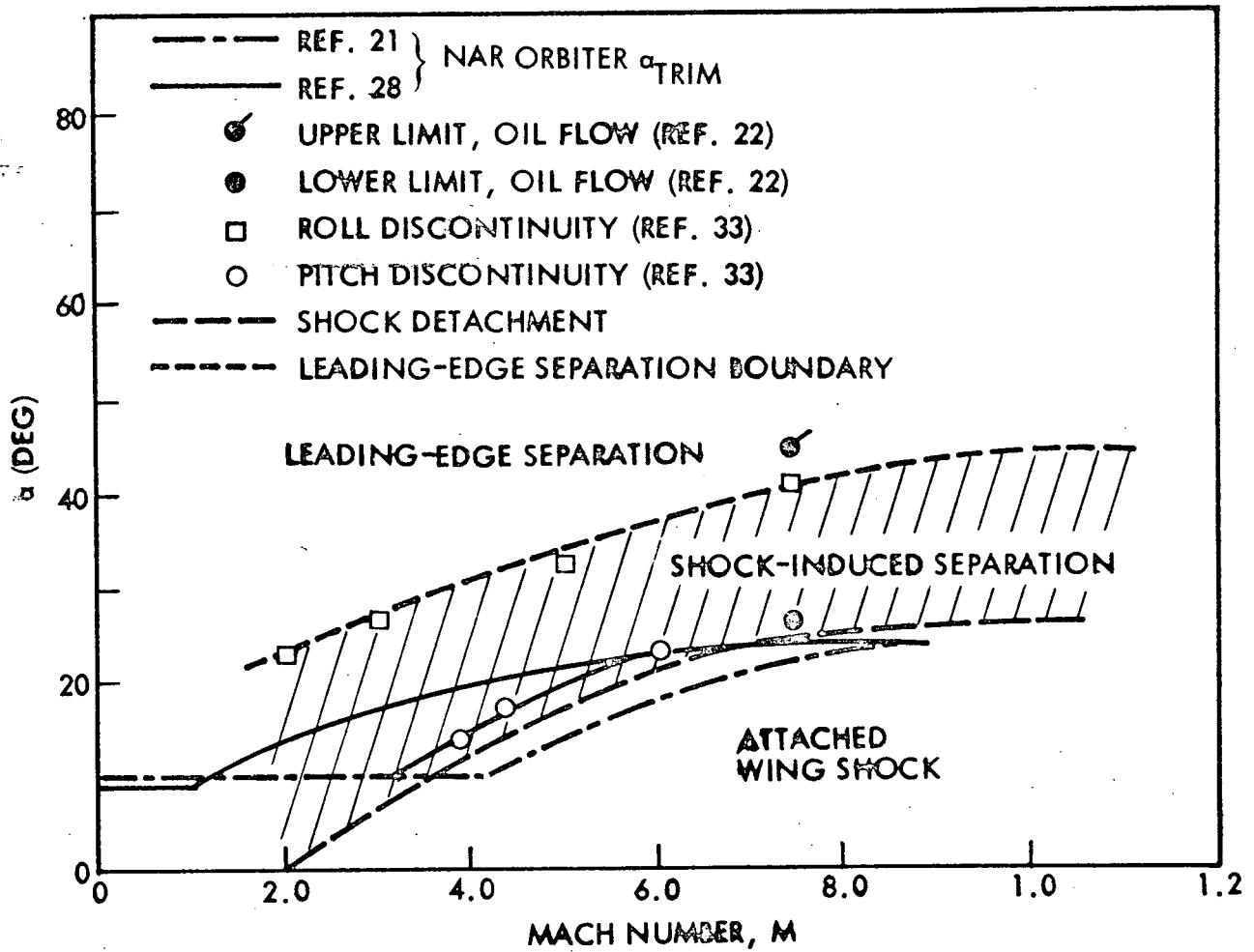


Fig. 10 Comparison of Leaside Wing Flow Boundaries With α_{trim} Schedule for NAR Delta Orbiter

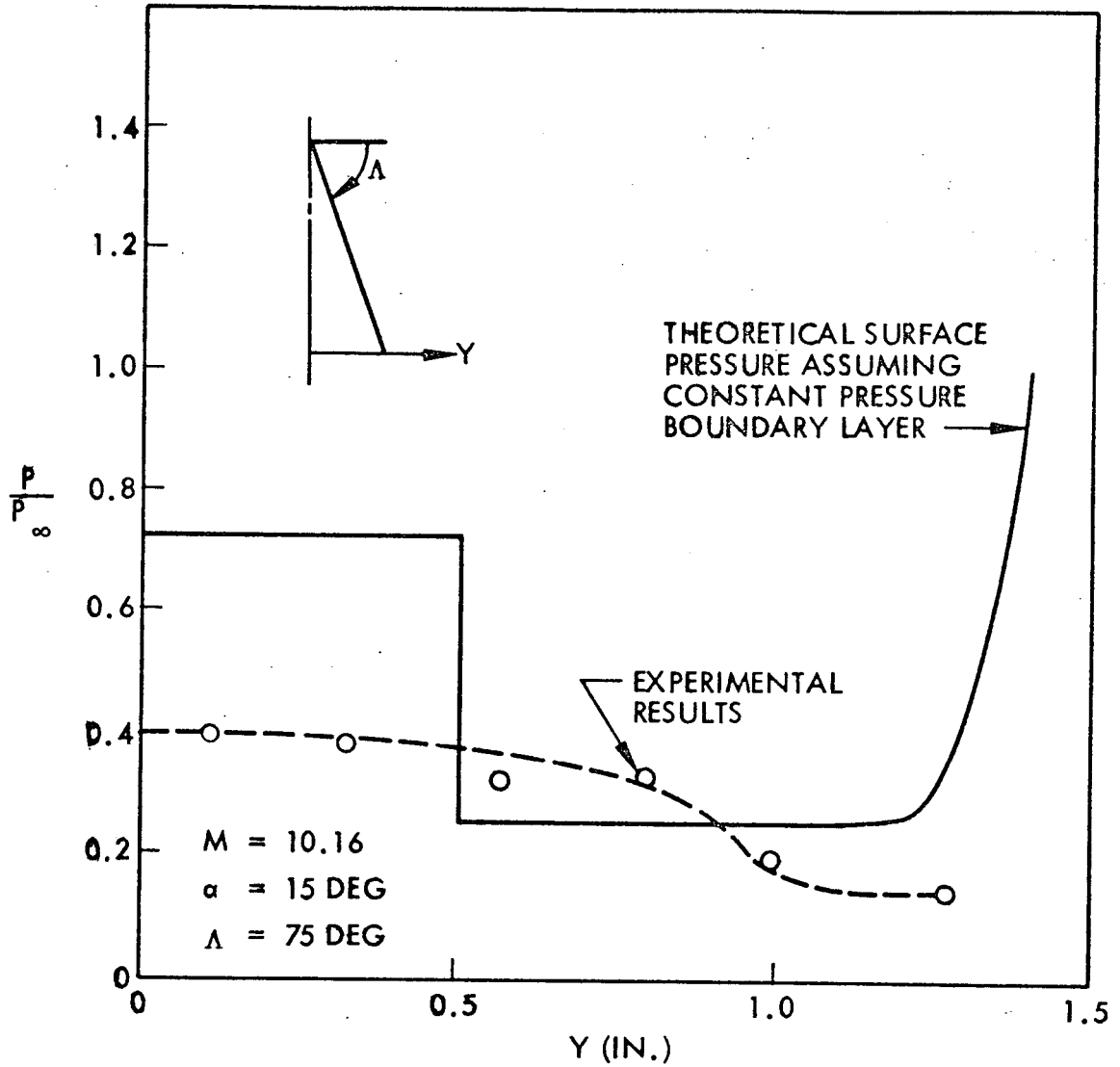
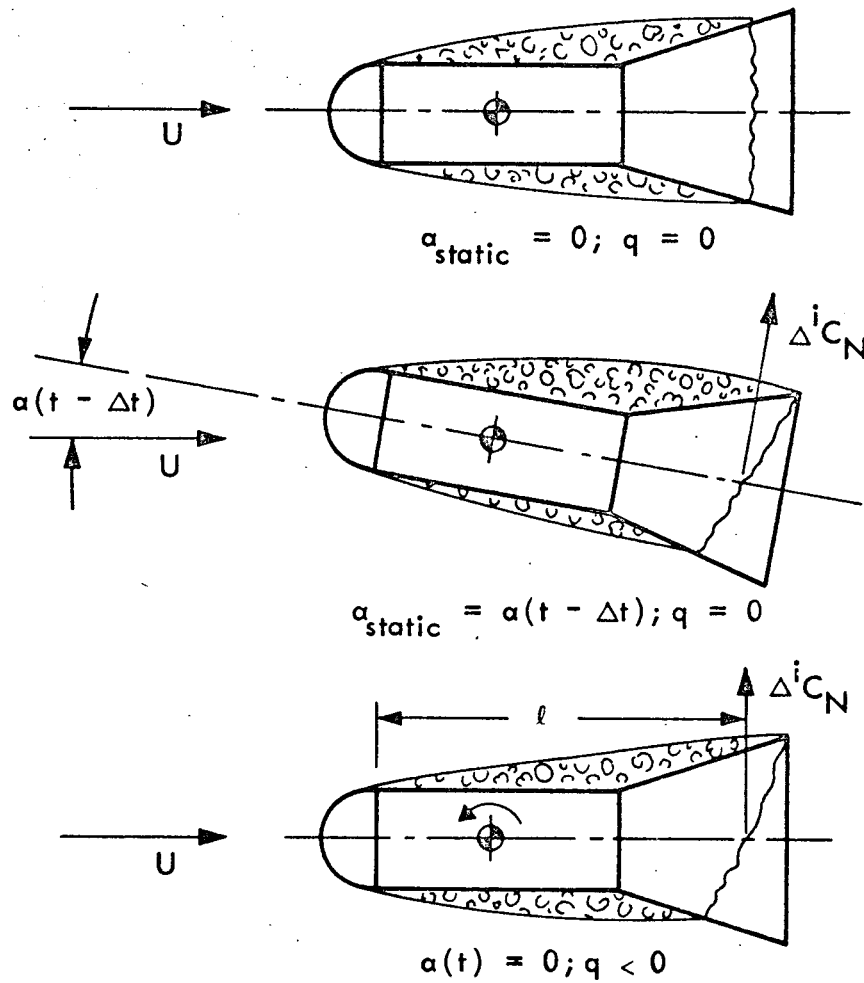


Fig. 11 Comparison of Theoretical and Experimental Spanwise Pressure Distributions on Leeside of Delta Wing at Hypersonic Speeds, $M = 10.16$ (Ref. 23)

The fundamental principle in the application of quasi-steady theory to the dynamics of bodies dominated by separated flow is that of the time lag (Refs. 1 to 17). In the case of shock induced separation the time lag due to the finite convection speed within the boundary layer is amplified by accelerated flow effects, which change the boundary layer strength. Because of this lag, one can apply the so called reversed reactions rule. That is, if the induced load is statically stabilizing it will be undamping dynamically. This is illustrated simply in Fig. 12, using the classic example of nose induced separation. It is shown that as the body pitches downward through $\alpha = 0$ a residual flare load occurs that tends to drive the motion (is undamping). Statically the separation induced flare load is, of course, stabilizing. Since the induced flare load results from a separation asymmetry generated at the nose, and since the convection speed within the separated region (\bar{U}) is finite, the load at $\alpha(t) = 0$ (residual load) is the result of flow conditions generated earlier when $\alpha = \alpha(t - \Delta t)$ where $\Delta t = \ell/\bar{U}$.

It was shown earlier that the shock induced separation produced a statically stabilizing contribution to the pitching and roll moments. Consequently, the shuttle vehicle will experience degraded pitch and roll damping as the results of shock induced separation. Likewise, a damping degradation will be caused by the leading edge separation. Leading edge separation at high Mach numbers is similar to subsonic delta wing flow; in both cases a vortex is bound to the wing leading edge. Lambourne (Ref. 29) has shown that the leading edge vortex position lags dynamically (Fig. 13). If one assumes it is the crossflow velocity at the leading edge that sets the vortex position,* then the lag will produce static roll stability and roll undamping. Lamborne et al. have also measured the time lag required for the vortex to reach its steady state position (Ref. 30). These results indicate that the vortex travels downstream with free stream velocity (Fig. 14). By applying the shock induced time lag and accelerated flow effect derived in Ref. 15 (from the data of Ref. 31) to the crossflow normal to the leading edge, and using free stream speed for the vortex convection velocity also at supersonic Mach numbers (measured for subsonic Mach numbers in Ref. 30), it is possible to get an estimate of the leeward side contribution to the roll damping. The estimated lee side damping ($C_{\ell\beta} \tan \phi$), obtained by assuming that the large statically stabilizing roll derivative

*This is consistent with subsonic L. E. separation on two-dimensional airfoils (Ref. 15) as will be discussed in detail later.



α DECREASED FROM $\alpha(t - \Delta t)$ to $\alpha = 0$
 (Δt IS THE TIME REQUIRED FOR THE NOSE-INDUCED
 SEPARATION TO TRAVEL FROM NOSE TO FLARE)

Fig. 12 Steady and Unsteady Flow Patterns of Nose-Induced Separation

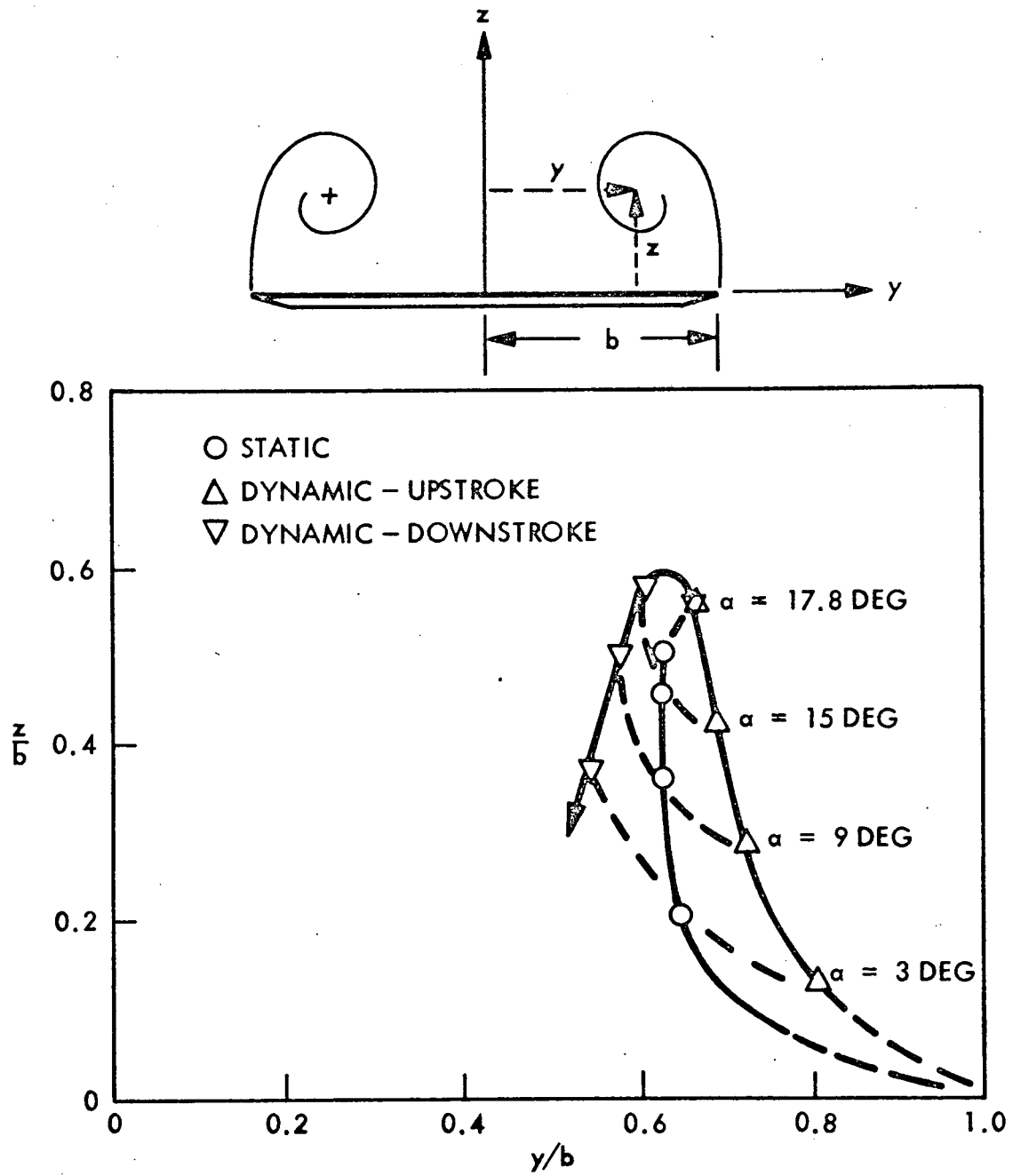


Fig. 13 Comparison of Steady and Unsteady Vortex Positions (Ref. 29)

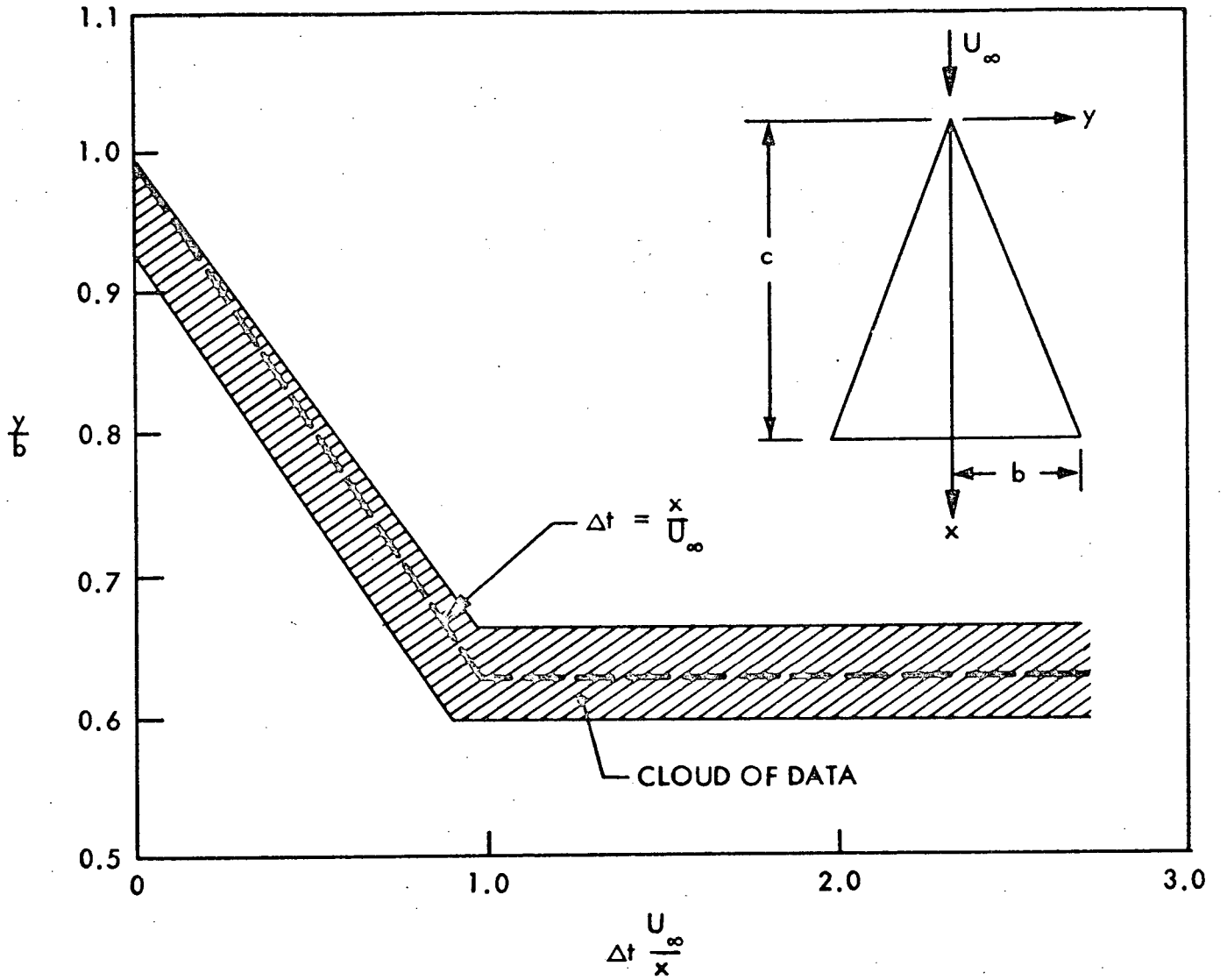


Fig. 14 Vortex Position as Function of Time for Plunging Delta Wing (Ref. 30)

measured in wind tunnel tests (Fig. 9) is in totality the result of the separation induced loads, is in Fig. 15 compared to the windward side damping derivative ($-C_{\ell p}$) as given by hypersonic small disturbance theory (Ref. 32). It is evident the roll undamping can result due to shock induced separation, and for the trajectory given in Ref. 28 it could exist over a considerable Mach number range (Fig. 16). While the results are only approximate, they do demonstrate that shock induced separation could cause roll undamping of the delta orbiter.

For a mid- or high-wing vehicle, shock induced separation can occur on the windward side even for supersonic leading edge conditions (Refs. 33 and 34, Fig. 17). The associated force changes in the wing body juncture could have a decisive influence on lateral vehicle dynamics. For the low wing vehicles, however, its effects are small compared to the other leeside flow separations. Even if the body-wing juncture is shaped so it becomes a flow streamline, there will still be flow separations, as Charwat has shown (Ref. 35), usually involving formation of corner vortices (Ref. 36). Fins often form such parallel corners with body or wing, with separation and vortex formations as the usual results (Refs. 37 and 38). These viscous corner interactions have, in general, more impact on heating than on vehicle stability and control.

2.2 SUDDEN LEADING EDGE STALL

When the Mach number normal to the leading edge is slightly less than unity ($M = 2.0$ for NAR shuttle) the separation can suddenly switch from the shock induced variety to leading edge separation with a corresponding discontinuous change in wing loading. This phenomenon is analogous to the switch between transonic flow attachment and leading edge stall and is, therefore, dependent upon the airfoil section configuration (Ref. 39). Typical boundaries for sudden leading edge stall are shown in Fig. 18 for a practical airfoil section. The disconcerting feature of this plot is that the jump is from an aft shock induced separation (transonic L.E. attachment) to L.E. separation, which implies a very large change in loading.

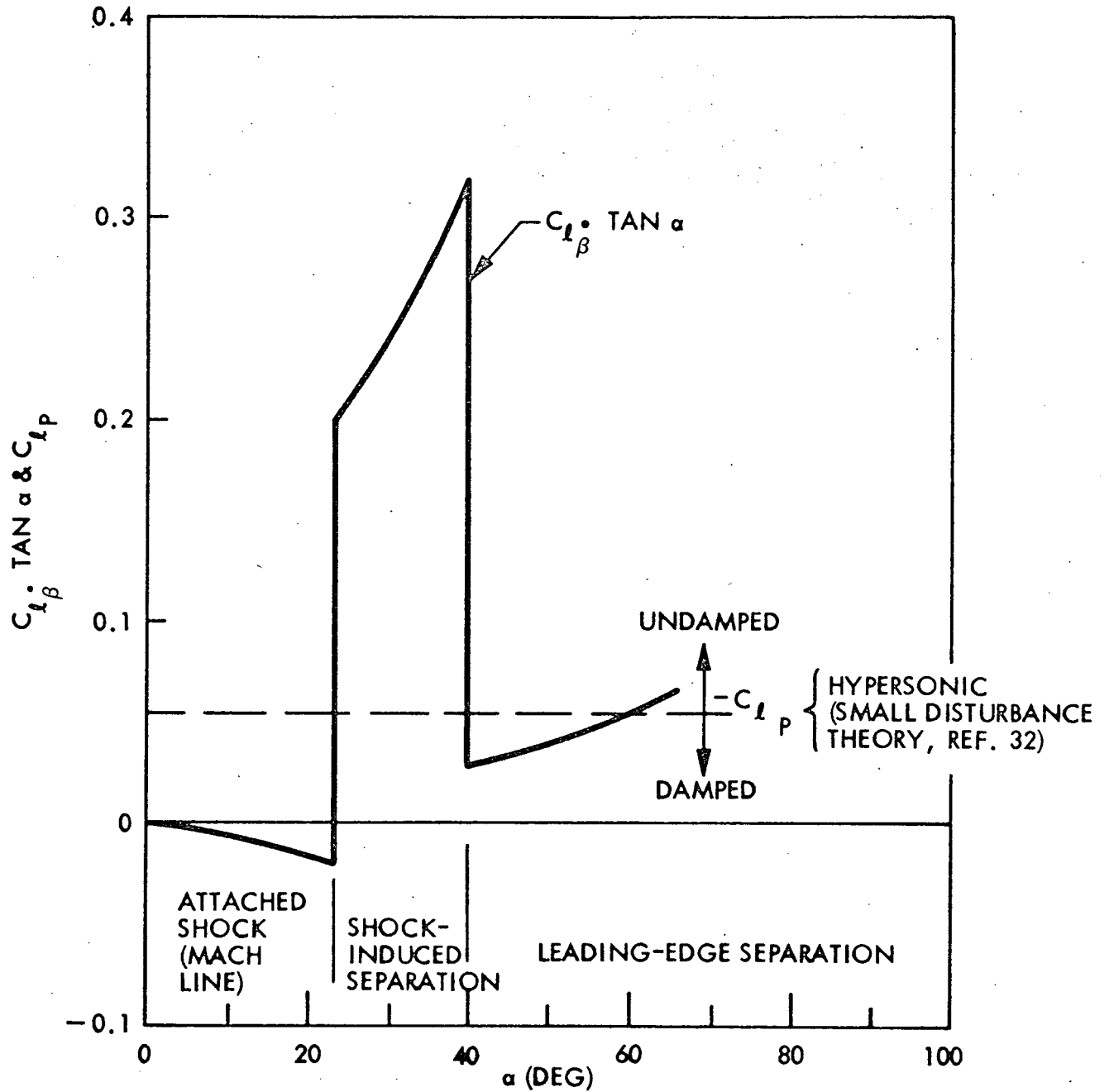


Fig. 15 Estimated Roll Damping Characteristics at M = 6.0, NAR Orbiter

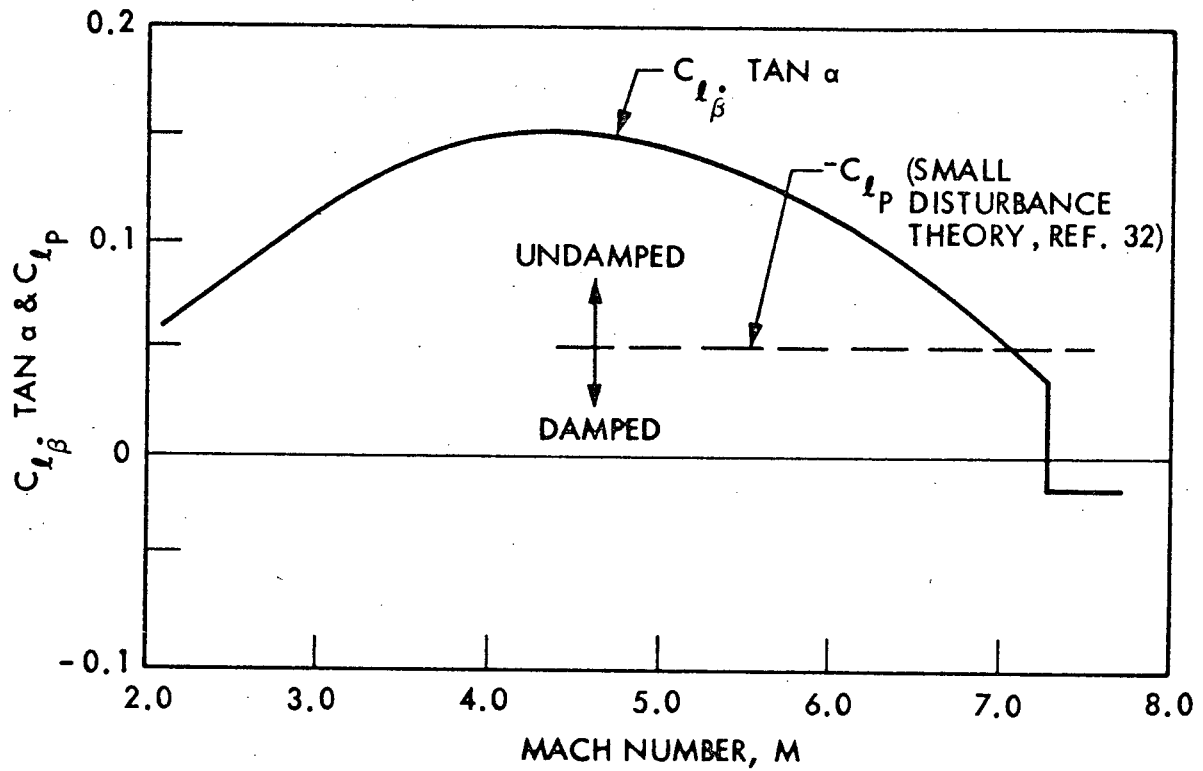


Fig. 16 Estimated Roll Damping Characteristics for Design α_{trim} Schedule for NAR Orbiter

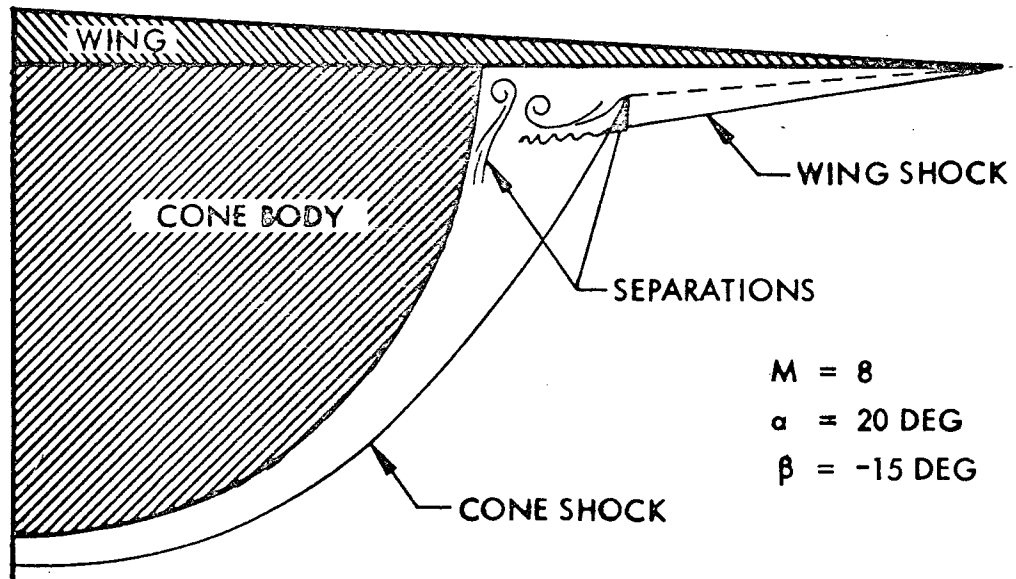
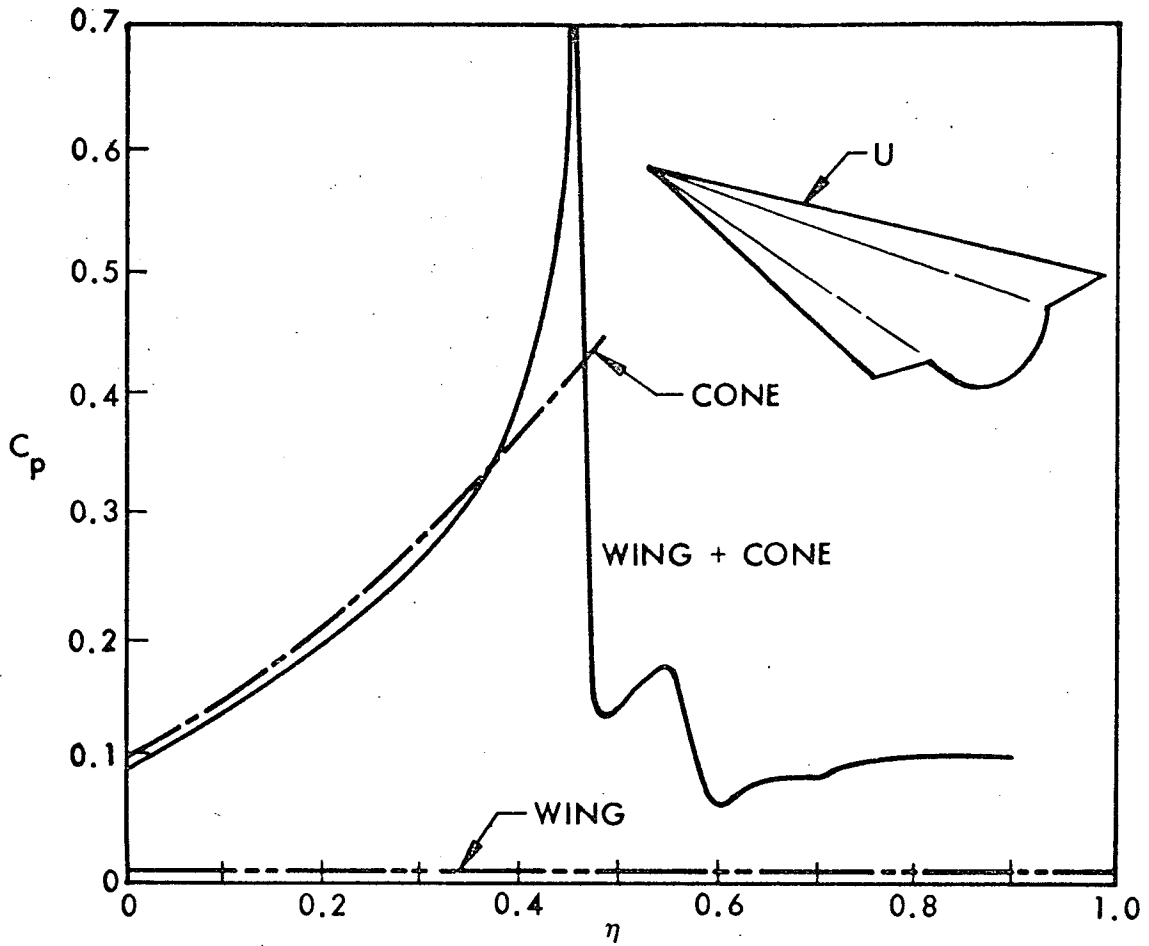


Fig. 17 Windward Side Wing Body Hypersonic Flow Field (Ref. 33)

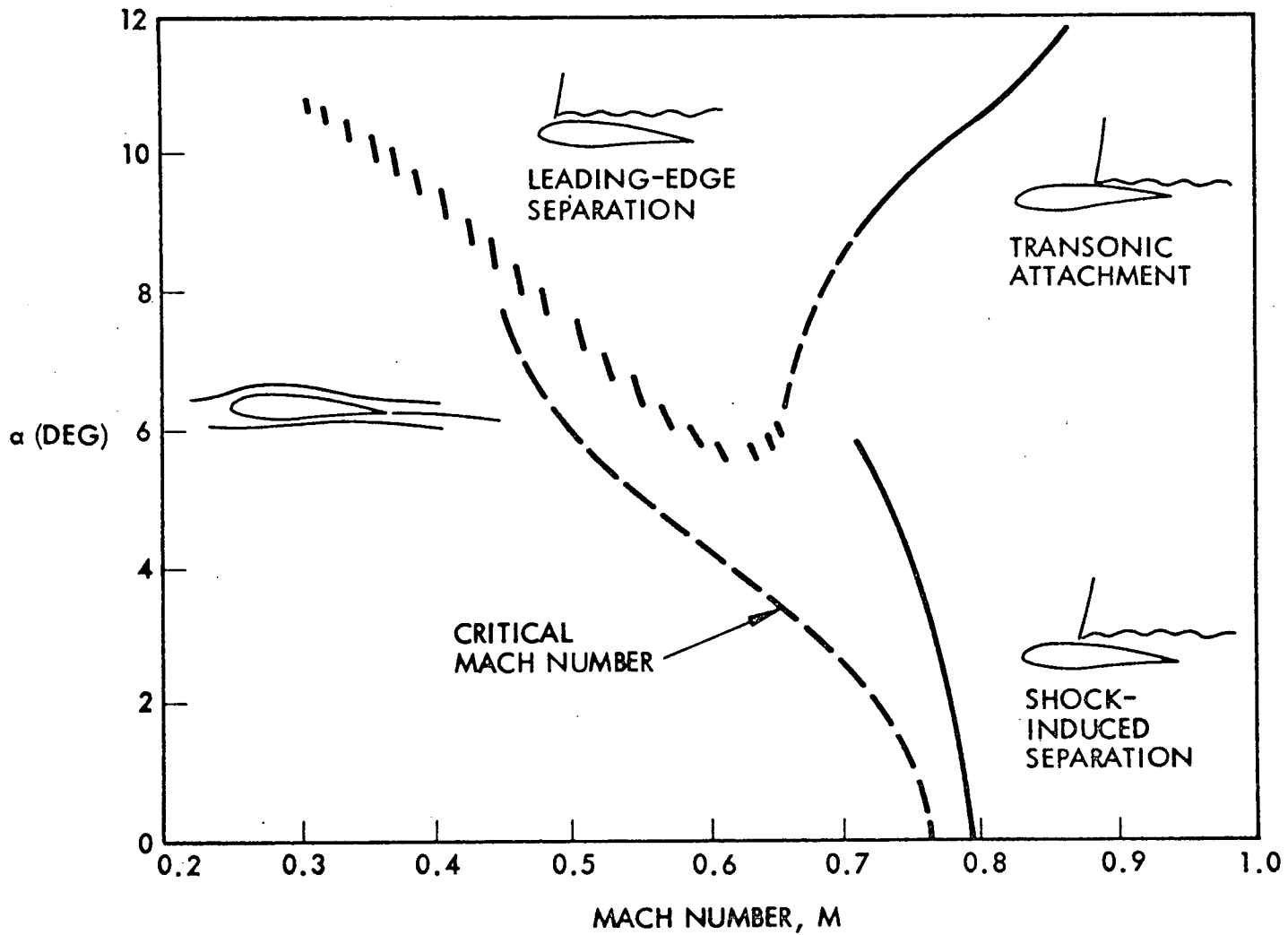


Fig. 18. Transonic Flow Boundaries for Two-Dimensional NACA 64A012 Airfoil Section (Ref. 39)

For some rather thin airfoils the flow was observed to oscillate between L. E. separation and transonic attachment followed by a region where the terminal normal shock position was unsteady (Fig. 19). This behavior is reminiscent of the results of Robertson and Chevalier (Ref. 40). They observed that the flow aft of the shoulder of a cone-cylinder body alternated between totally separated and attached. The body of revolution results are simply the three-dimensional analog to the airfoil results.

The discontinuous jump from attached to separated flow occurs when the terminal normal shock enters the near nose region with its adverse pressure gradient. At some point the shock induced pressure rise, coupled with the near nose adverse pressure gradient, is just too much for the boundary layer, and separation jumps to the shoulder (in the case of the cone-cylinder) or to the point where the boundary layer encounters a pressure gradient that it can tolerate. The similarity between the two- and three-dimensional flows is illustrated in Fig. 20. Both result in large discontinuous, statically stabilizing, pitching moments when the sudden nose stall is established. For the cone-cylinder body it has been shown that dynamically the jump will lag the body motion due mainly to the accelerated flow relief of the adverse pressure gradient, and to a lesser extent due to the delay of boundary layer buildup on the leeward side (as the result of a finite convection speed in the boundary layer, Refs. 4 and 5). Likewise, pitch rate induced camber and accelerated flow effects have a large influence on the jump to leading edge stall, perhaps even larger than their influence on regular (low speed) dynamic airfoil stall (Refs. 14 to 16 and 41). The jump represents an infinitely stable moment derivative which results in infinite undamping for infinitesimal amplitude oscillation at the jump angle of attack. However, as oscillation amplitude is increased the undamping becomes finite due to the finite moment derivatives on either side of the jump (Refs. 4 and 5). Thus, the damping is a function of oscillation amplitude (Fig. 21a). It has been shown that the experimentally observed undamping of the Saturn I vehicle with a Jupiter nose cone (Refs. 5 and 42) was the result of sudden separation (Fig. 21b).

On the swept wing a mixed flow condition can result (Fig. 22, Ref. 43). That is, the inner portion of the wing may have laminar L. E. separation while the turbulent flow over

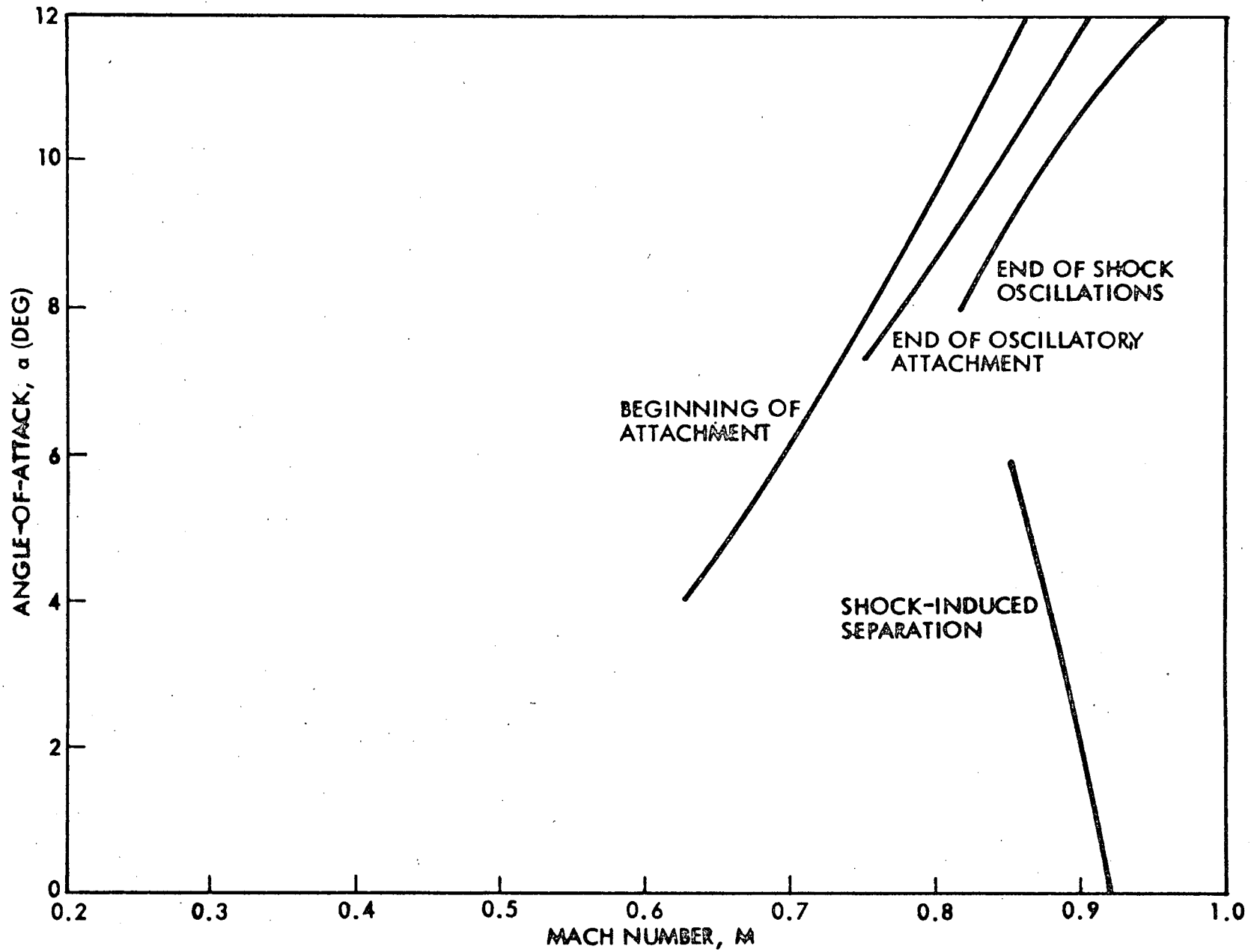
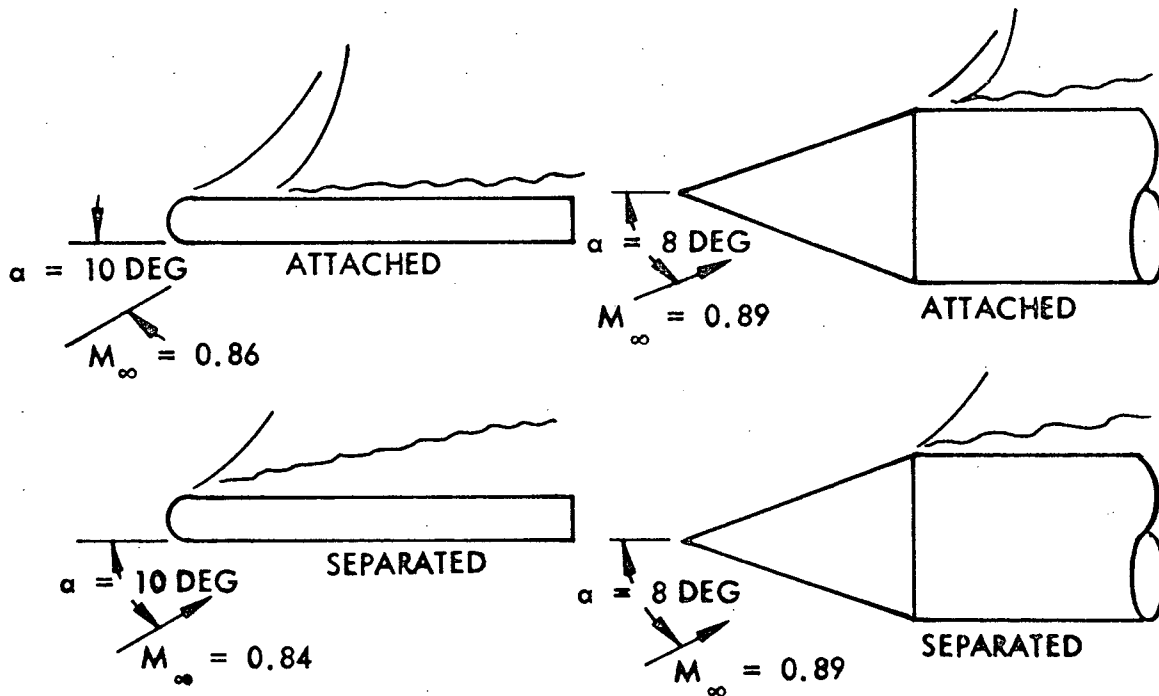
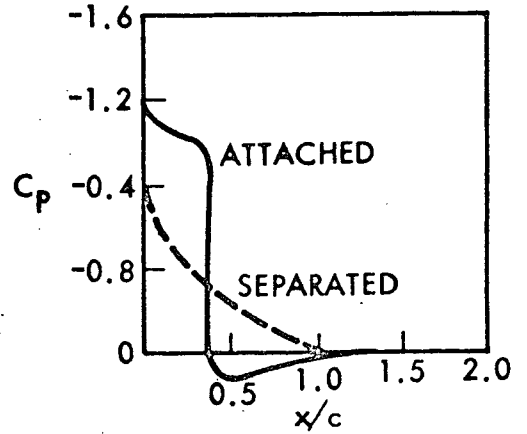
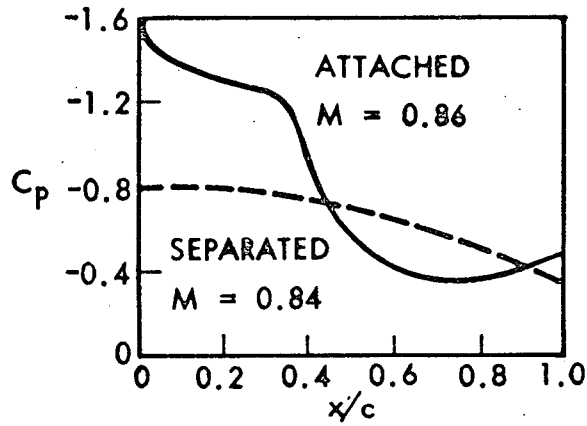


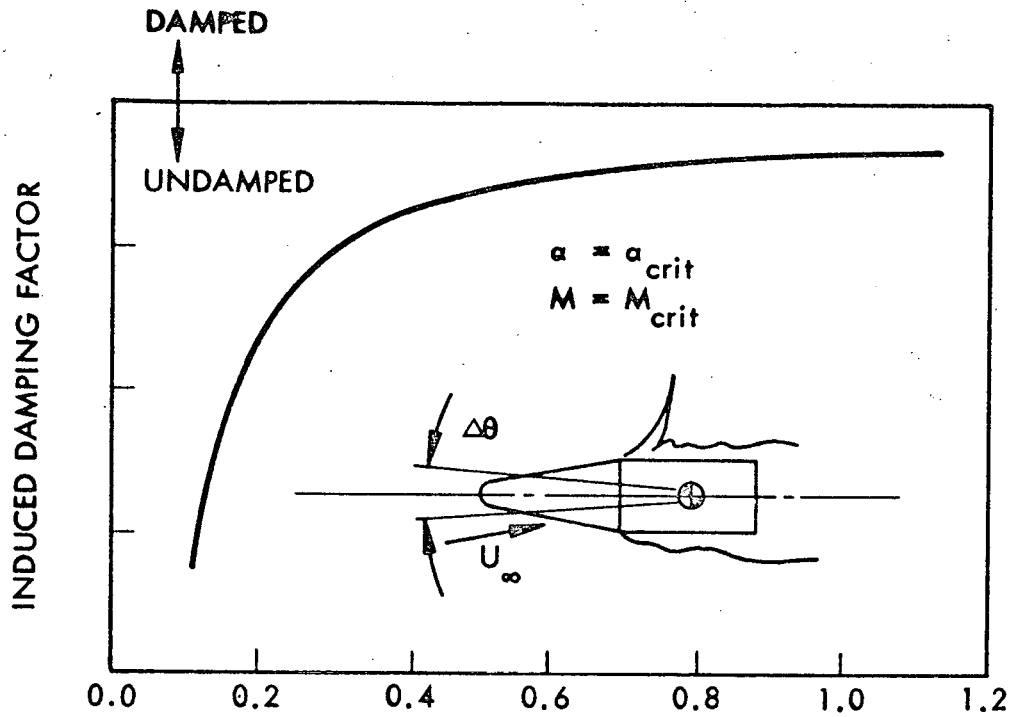
Fig. 19 Flow Boundaries for NACA 16-006 Airfoil (Ref. 39)



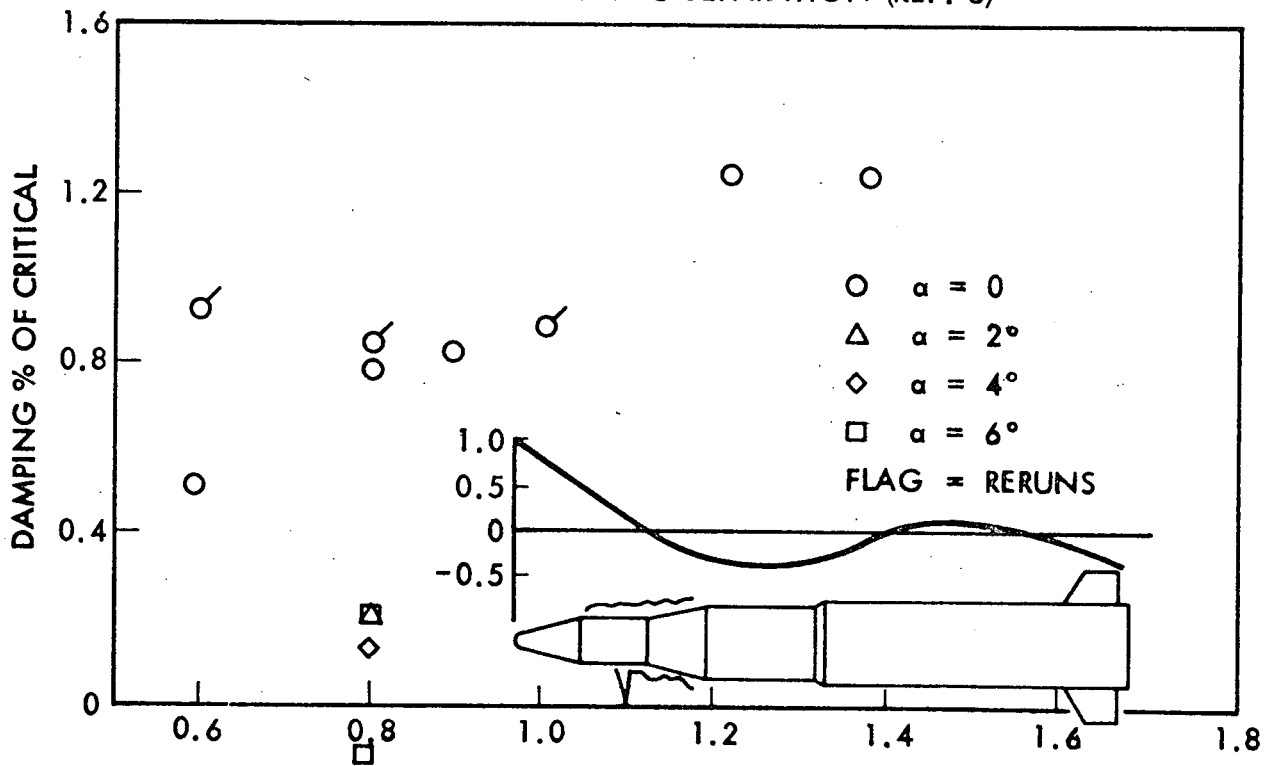
(a) SLAB WING (REF. 39)

(b) 15-DEG CONE-CYLINDER (REF. 40)

Fig. 20 Comparison of Pressure Distributions for Sudden Separation



(a) EFFECT OF AMPLITUDE ON DAMPING FOR COLLAPSING SEPARATION (REF. 5)



(b) EFFECT OF SUDDEN SEPARATION ON SECOND MODE DAMPING OF SATURN I W/JUPITER NOSE (REF. 42)

Fig. 21 Dynamic Effects of Sudden Separation

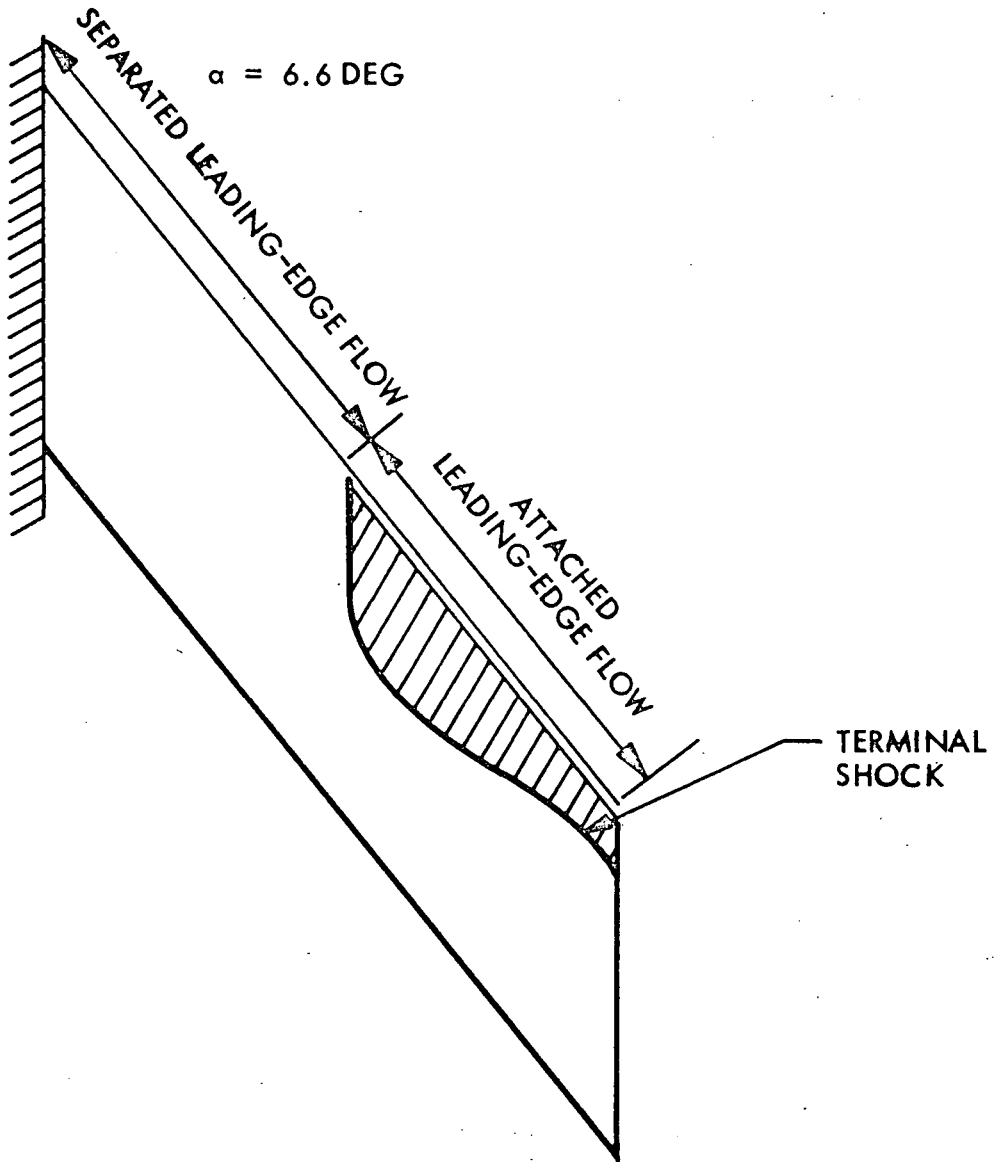


Fig. 22 Flow Breakdown at $M = 1.05$ Showing Region of Outboard Attached Flow (Ref. 43)

the outer wing leading edge is attached with shock induced separation occurring a short distance downstream. In the unsteady case the demarkation line between the flow conditions will oscillate spanwise as the wing pitches or plunges. There will undoubtedly be a random (motion independent) oscillation superimposed on the motion dependent oscillation. It is likely that the motion dependent oscillation of this separation boundary was the cause of the large amplitude bending response measured on the wing of the earlier straight wing shuttle (Figs. 23 and 24, Refs. 44 and 45). Likewise, the spanwise, motion dependent, oscillation of the demarkation line can degrade roll damping of the delta wing shuttle. This separation phenomenon also serves to couple the effects of pitch, yaw, and roll motions.

The mixed separated-attached flow condition has not, to the knowledge of the authors, been observed on any of the delta orbiters (possibly because no one has really looked for it), but it is certainly possible that it could occur. It is important to determine whether it is there or not, as its effects can be disastrous, and there are ways to alleviate these effects and possibly avoid the flow phenomena altogether, as will be discussed later.*

2.3 VORTEX BURST

It is well known that vortex lift is a major portion of the lift on delta wings at subsonic speeds. Polhamus' "turned-up" leading edge suction predicts vortex lift and drag quite well (Refs. 46 and 47). However, as yet there is no similarly simple means of predicting vortex burst which has drastic effects on delta wing characteristics (Fig. 25 and Ref. 48). It remains a well documented but still not fully understood phenomenon. Ludwig (Ref. 49) showed that a cylindrical vortex experienced spiral instability if the peripheral to axial velocity ratio exceeded the value 1.12, i. e., the helix angle of the fluid particles on the vortex boundary exceeded 48 deg. Benjamin (Ref. 50) demonstrates that vortex breakdown is simply the transition between two stable rotating flow states, similar to the Rankin-Hugiot shock or the hydraulic jump; i. e., it is a transition between supercritical and subcritical flow states. Harvey (Ref. 51) thought that

*See section "Avoiding the Problems."

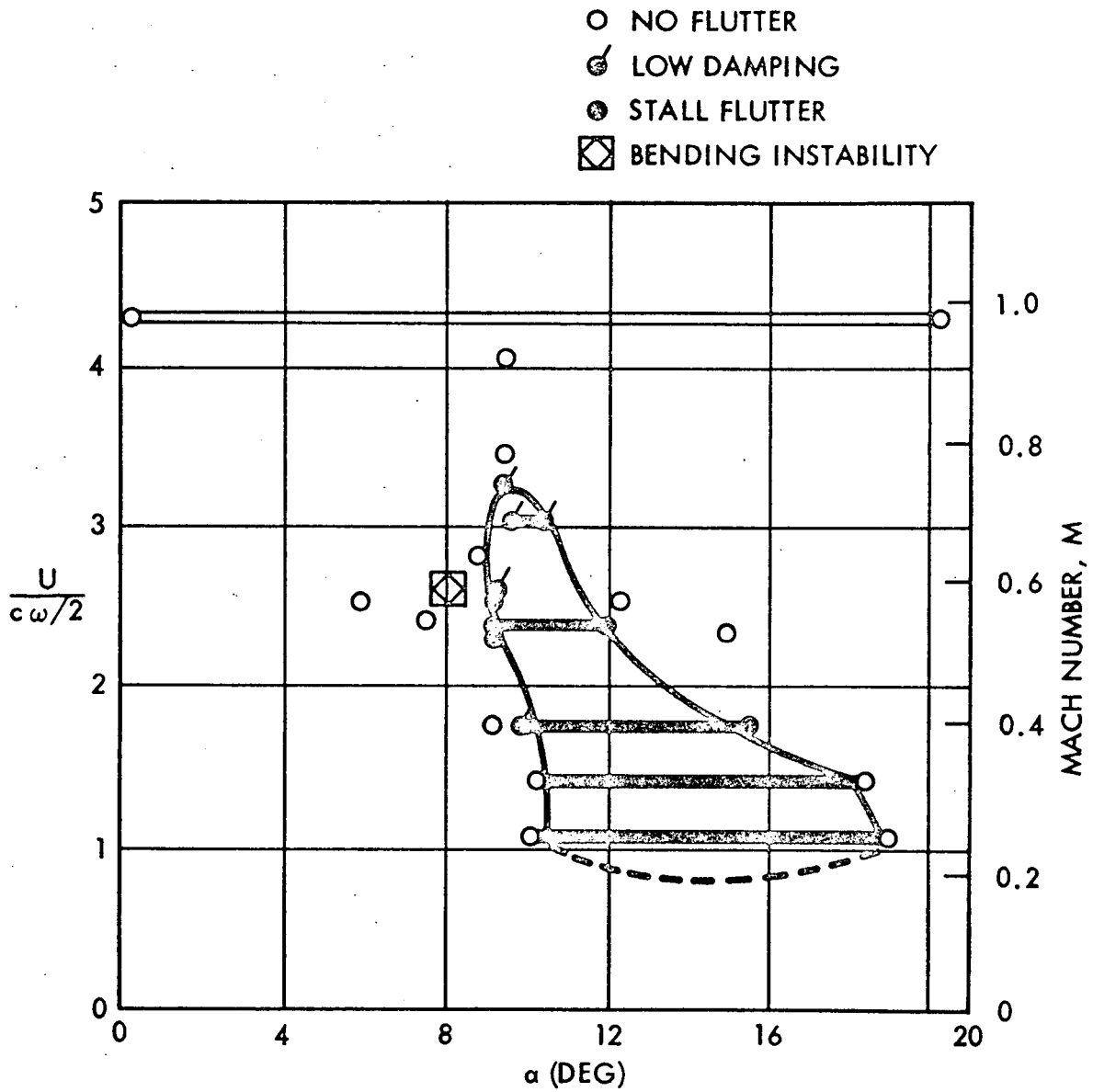


Fig. 23 Measured Isolated Data Point for Bending Instability (Ref. 44)

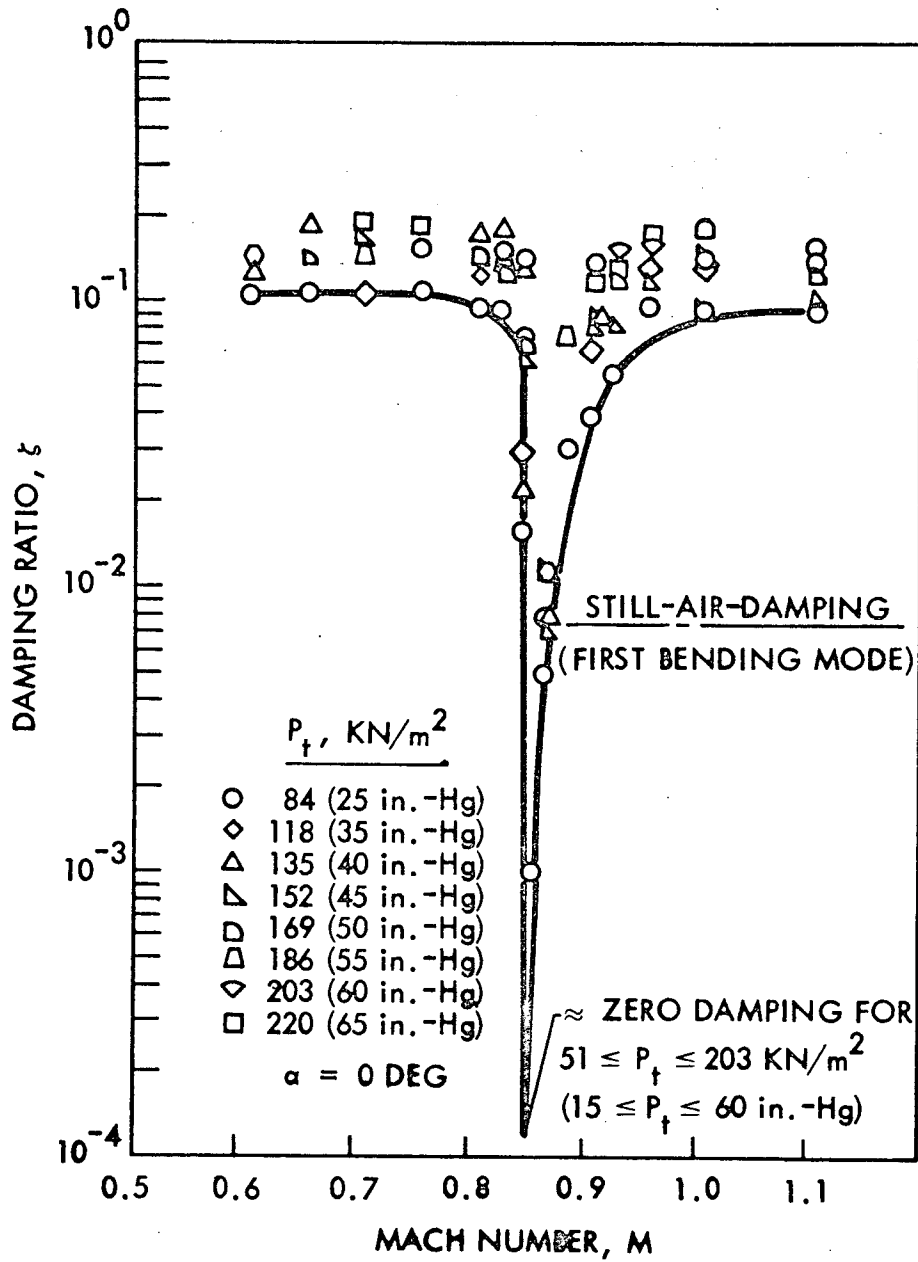


Fig. 24 Effect of Mach Number on Damping (Ref. 45)

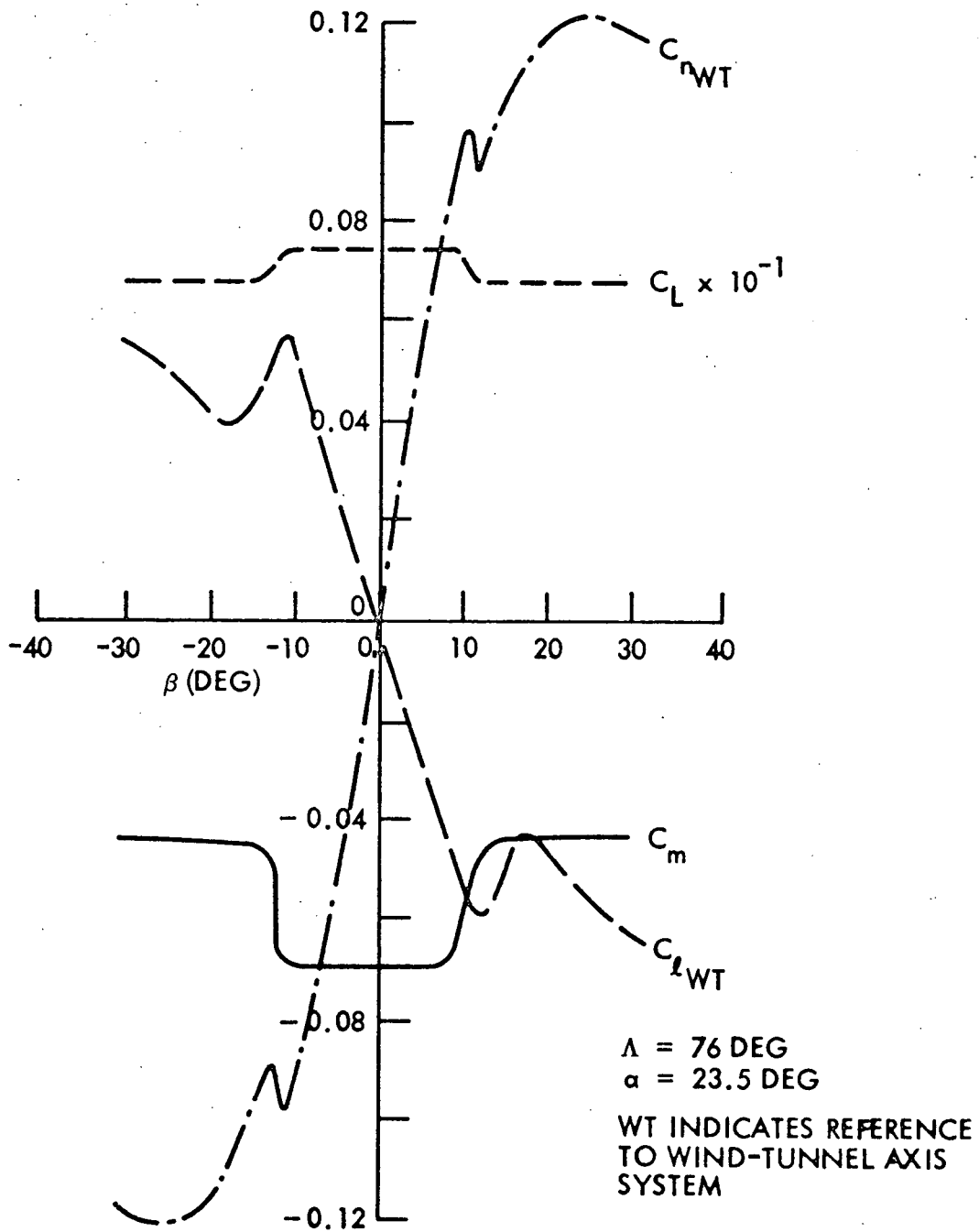
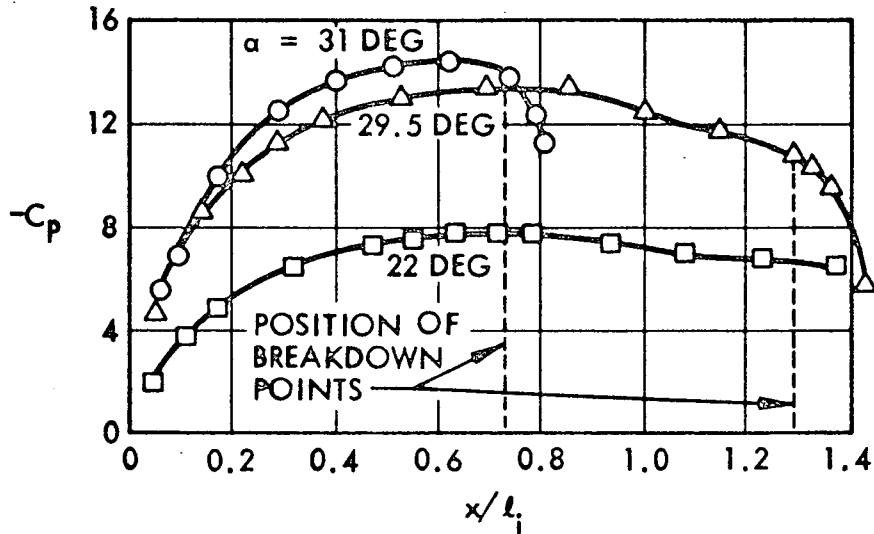


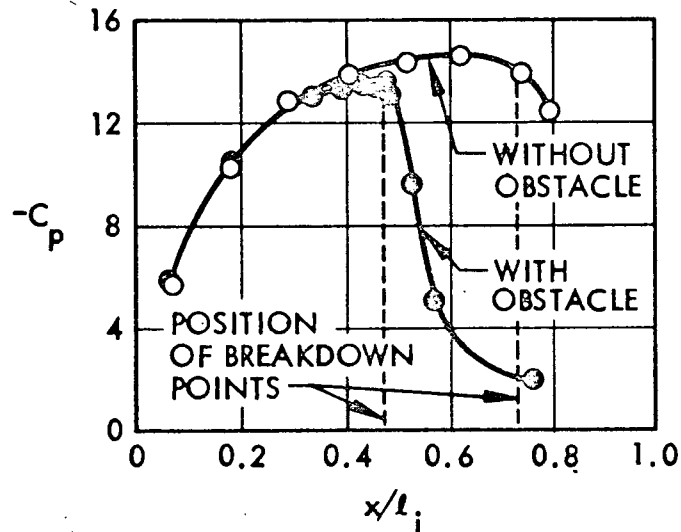
Fig. 25 Effect of Vortex Burst on Longitudinal and Lateral Characteristics (Ref. 48)

his experiments verified Benjamin's hypothesis, whereas Sarpkaya finds his experimental results to indicate that the breakdown is an instability phenomenon (Ref. 52). Petersohn (Ref. 53) also finds that Ludwig's stability criterion applies, and that the effect of viscosity, which was neglected by Ludwig, is simply to cause the instability to start in the center of the vortex rather than at the edge. Hall's results (Ref. 54) also support Ludwig's instability hypothesis. His description of "axial flow in vortex stops and reverses as if hitting an obstacle" at vortex breakdown agrees with Elle's concept that failing downstream transport in the vortex core is the cause of breakdown (Ref. 55). Bossel uses this concept, together with Hall's results, to define a critical velocity ratio of 2, i. e., instability results when the helix angle is larger than 54.8 deg (Ref. 56). This is in better agreement with experimental results than Ludwig's value of 48 deg. In the case of a leading edge vortex one would think that the vortex together with its image, needed to assure zero flow through the wing surface, forms a vortex pair similar to that treated by Crow (Ref. 57), in which case spiral instability via or without an interim stage leads to a breakdown to large scale turbulence. Thus, it appears that vortex breakdown is an instability phenomenon somewhat similar to boundary layer transition. That is, adverse pressure gradients will have a dominant influence, and large dynamic effects of convective time lag and accelerated flow are to be expected.

When leading edge vortex breakdown occurs over the delta wing, a loss of lift due to the decreased suction results (Ref. 48 and Fig. 26), usually also resulting in reduced longitudinal and lateral stability (Fig. 25). There has, therefore, been extensive experimental research aimed at defining the vortex breakdown phenomenon for delta wings. Lambourne showed that the delay of vortex breakdown with increasing leading edge sweep could be scaled by using the angle the leading edge forms with the free stream velocity vector (Ref. 58 and Fig. 27). He found also that vortex breakdown is relatively insensitive to Reynolds number. (As Ludwig's inviscid analysis predicts experimentally observed vortex bursts, this result is not unexpected.) Side-slip effects on vortex breakdown could probably be accounted for by adding the yaw angle to Lambourne's scaling (Fig. 27). The effect of yaw is, of course, to cause earlier breakdown on the windward wing with its less effective sweep angle (Fig. 28 and Refs. 48 and 59).

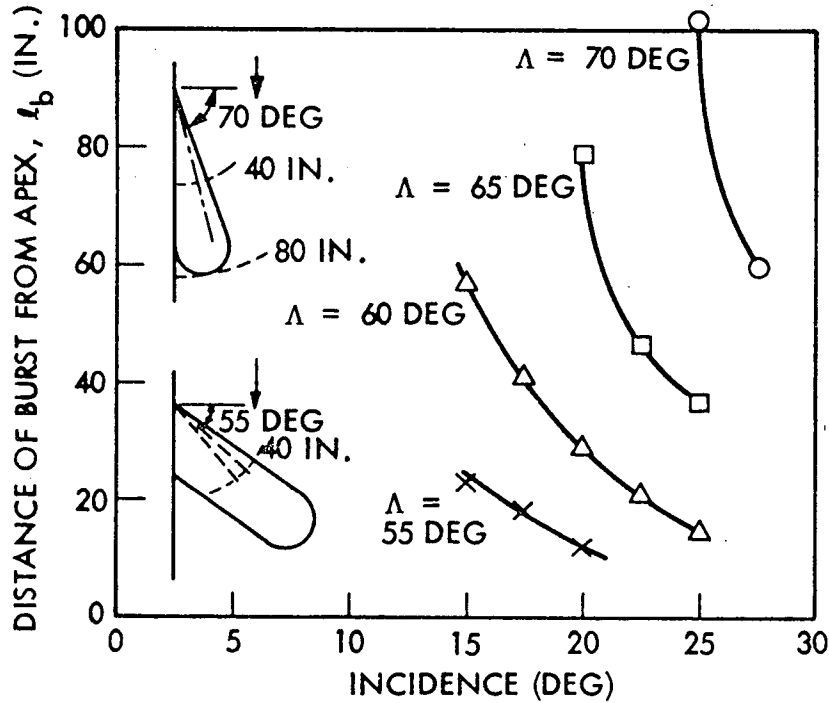


(a) RANGE OF STATIC PRESSURES
 $C_p = (p - p_\infty)/q_\infty$ ALONG VORTEX
 AXIS AT VARIOUS ANGLES OF INCIDENCE

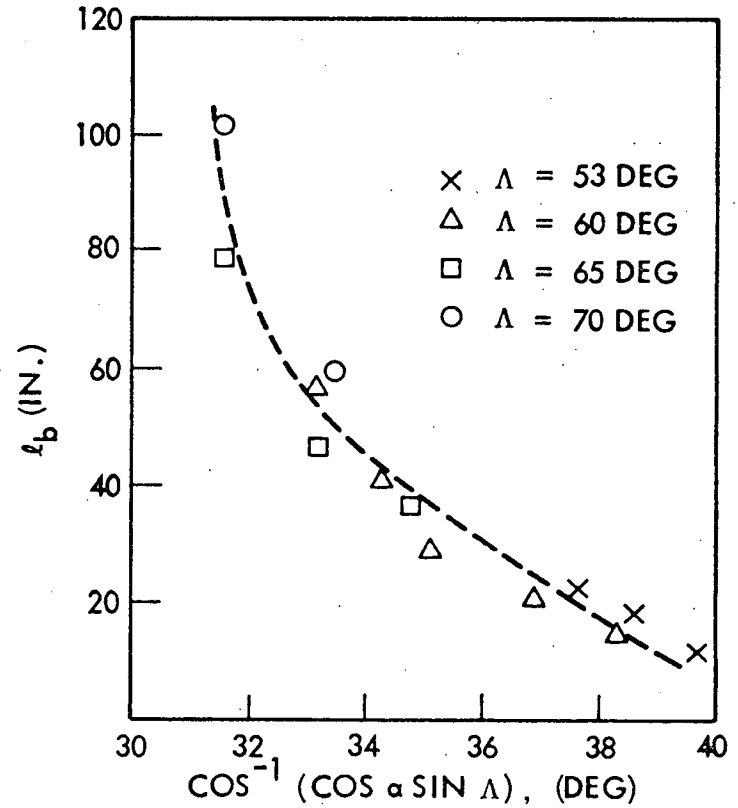


(b) RANGE OF STATIC PRESSURES
 $C_p = (p - p_\infty)/q_\infty$ ALONG VORTEX
 AXIS AT ANGLE OF INCIDENCE $\alpha = 31$ DEG
 WITH AND WITHOUT OBSTACLES BEHIND
 WING

Fig. 26 Effect of Vortex Breakdown on Static Pressure (Ref. 48)



(a) VARIATION OF BURST POSITION WITH INCIDENCE AND SWEEPBACK - SWEEP PLATE, 180 FT/SEC



(b) BURST POSITION PLOTTED AGAINST THE ANGLE BETWEEN THE LEADING EDGE AND FREE STREAM - SWEEP PLATE, 180 FT/SEC

Fig. 27 Effect of Leading Edge Sweep on Vortex Burst (Ref. 58)

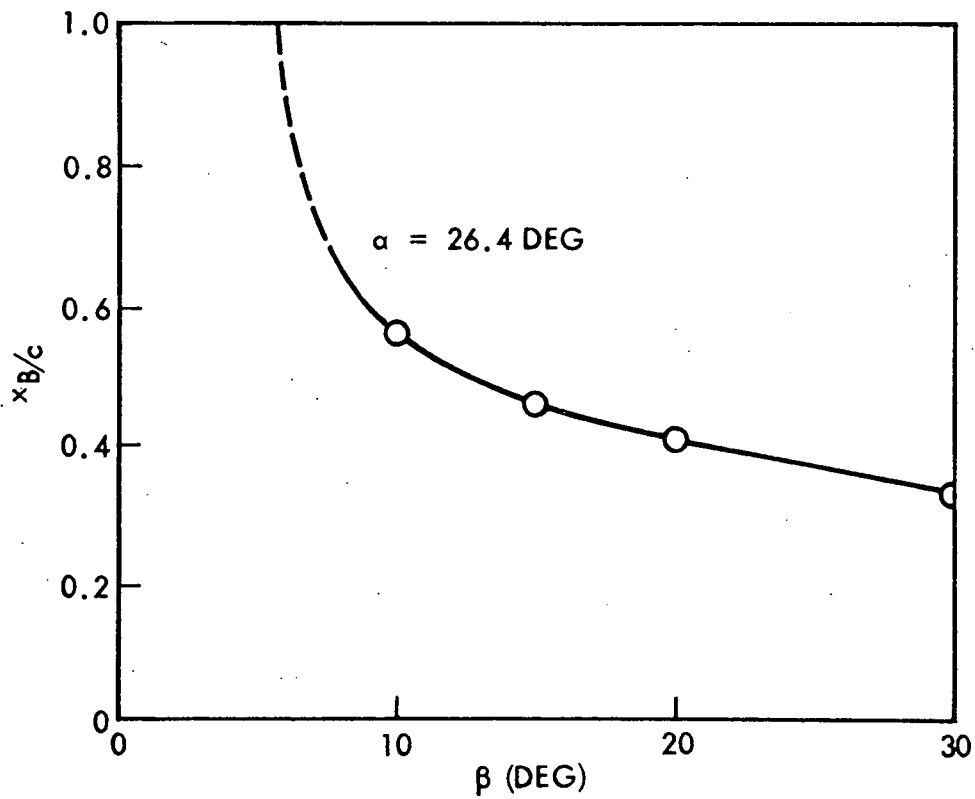
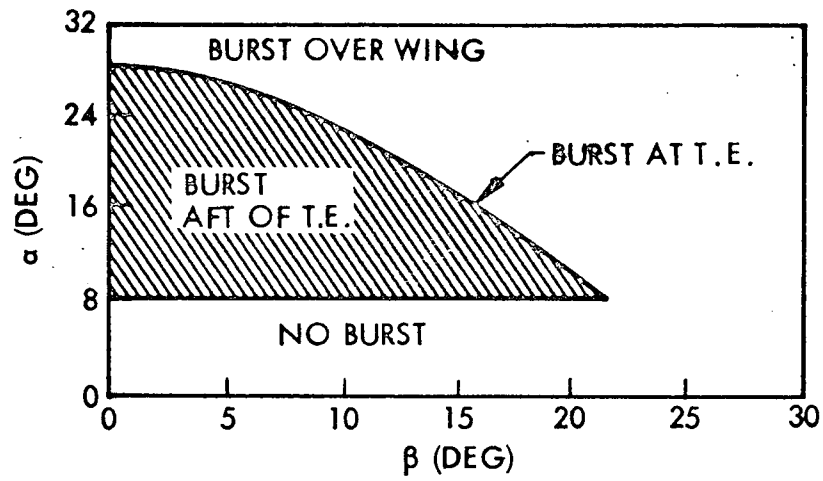


Fig. 28 Low-Speed Vortex Burst on 76-Deg Delta Wing at Angle-of-Attack and Sideslip (Refs. 48 and 59)

The vortex breakdown is very sensitive to angle of attack, moving almost jump-wise from trailing edge to 2/3 chord (Fig. 28 and Ref. 60), at least for high sweep angles. Lowson finds that he has to "undershoot" angle of attack to bring vortex breakdown back to the "upstroke" position, i. e., there is an α -hysteresis (Fig. 30 and Ref. 61). He also finds that the vortex breakdown is asymmetric, i. e., at different axial positions for right and left half span. Which side gets the earlier breakdown is a random event, but once established the asymmetry prevails throughout the angle of attack range. The distance axially between the two breakdowns was in his case approximately the same as their spanwise separation distance. Lowson speculates that his asymmetry may be limited to highly swept delta wings where the two breakdowns get close to each other. This is verified by others' results (Refs. 48 and 60).

The sensitivity to angle of attack remains high also for vortex breakdown further forward on the wing (see Figs. 29 and 30, and also Fig. 31, Ref. 62). This α -sensitivity implies that the down-going wing during roll will get earlier breakdown due to the roll rate induced angle of attack, causing a roll moment that will sustain the roll rate, i. e., an undamping effect. Vortex breakdown plays the same role for delta wings as nose stall does for airfoils. One can, therefore, expect that pitch rate induced camber and accelerated flow effects, which have proven to have a powerful influence on dynamic stall (Refs. 14 to 16 and 41) also will dominate dynamic vortex breakdown. This is verified by experiments with cambered delta wings (Fig. 32 and Ref. 58). At transonic speeds the terminal shock will cause vortex breakdown, again creating a situation similar to dynamic airfoil stall (Fig. 33 and Ref. 58, compared to Ref. 15). Not only does vortex breakdown cause drastically increased static pressures (Fig. 26), the increase of fluctuating pressure level is even more dramatic due to the large scale turbulence associated with vortex breakdown (Fig. 34 and Ref. 63). It should be pointed out that vortex breakdown is not limited to extremely large angles of attack. The Anglo-French Concorde has experienced it at somewhat abnormal landing conditions (Ref. 64 and Fig. 35). A "wave-rider" configuration shows nonlinear lateral characteristics due to vortex breakdown already at $\alpha = 17$ deg and $\beta = 2$ deg (Fig. 36 and Ref. 65).

While vortex burst is sensitive to both planform and section shape, planform shape is the dominant parameter (compare Figs. 37a and 37b). Furthermore, leading edge

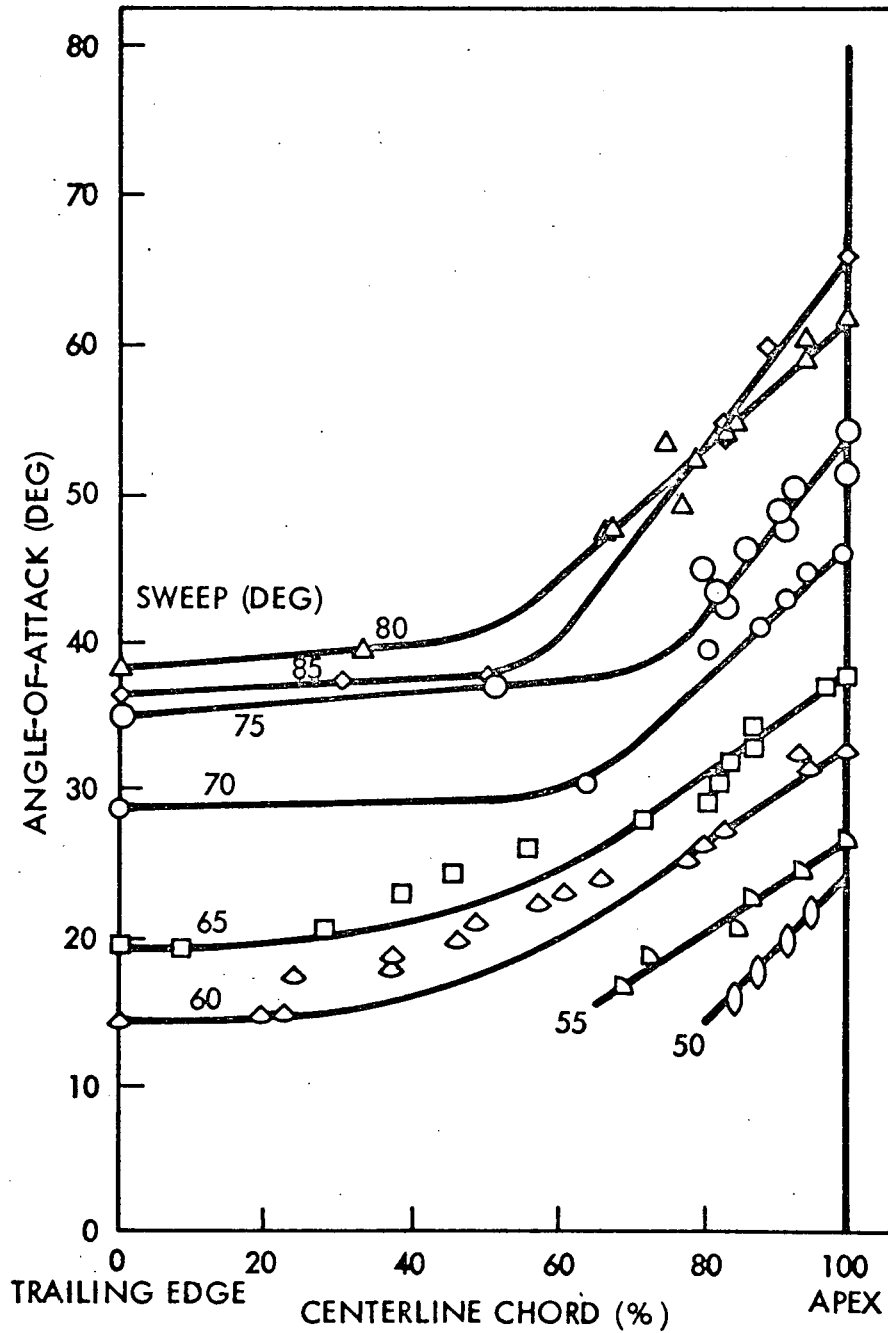


Fig. 29 Vortex Breakdown Position – Delta Wings (Ref. 60)

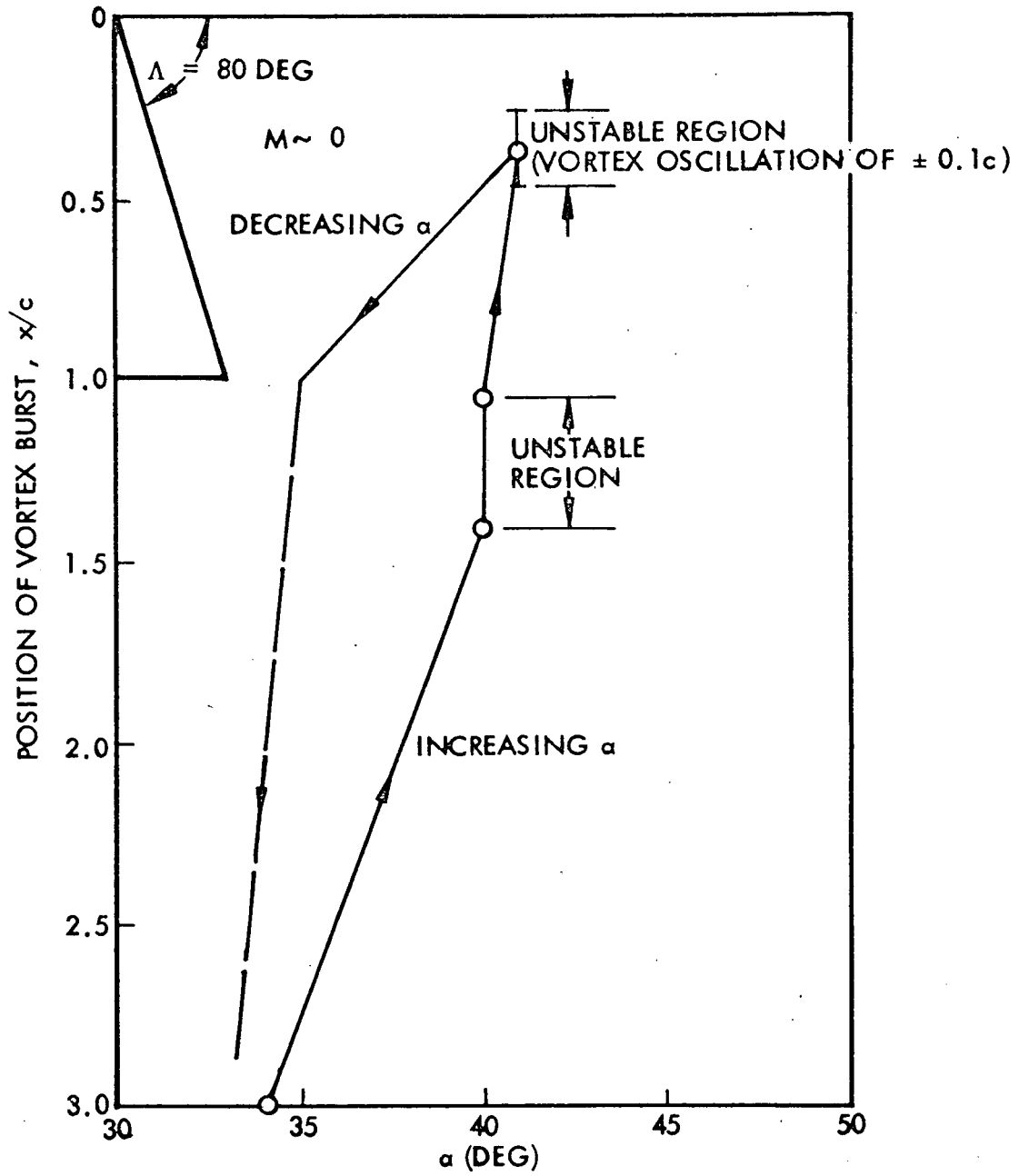


Fig. 30 Hysteresis and Unstable Vortex Burst Locations (Ref. 61)

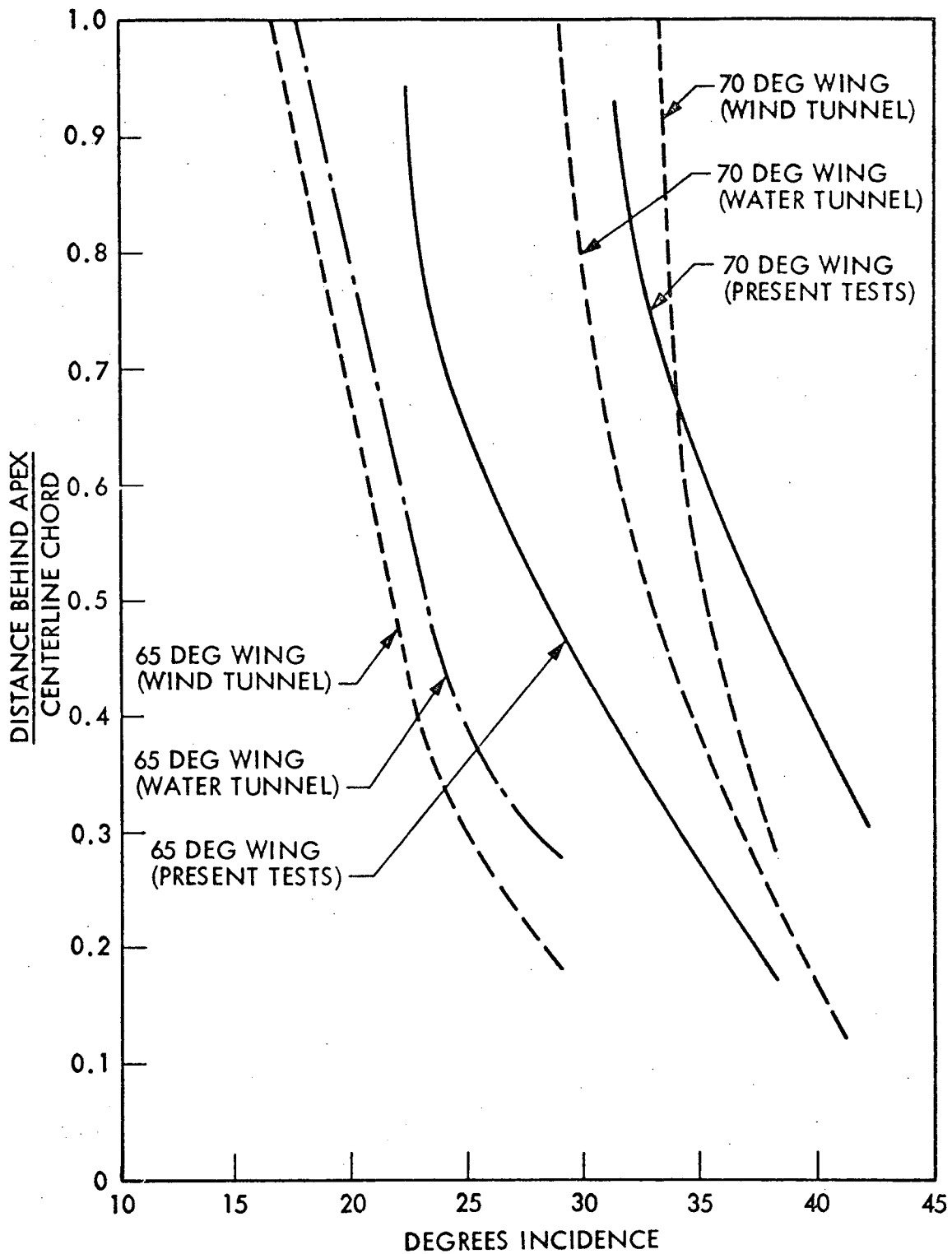
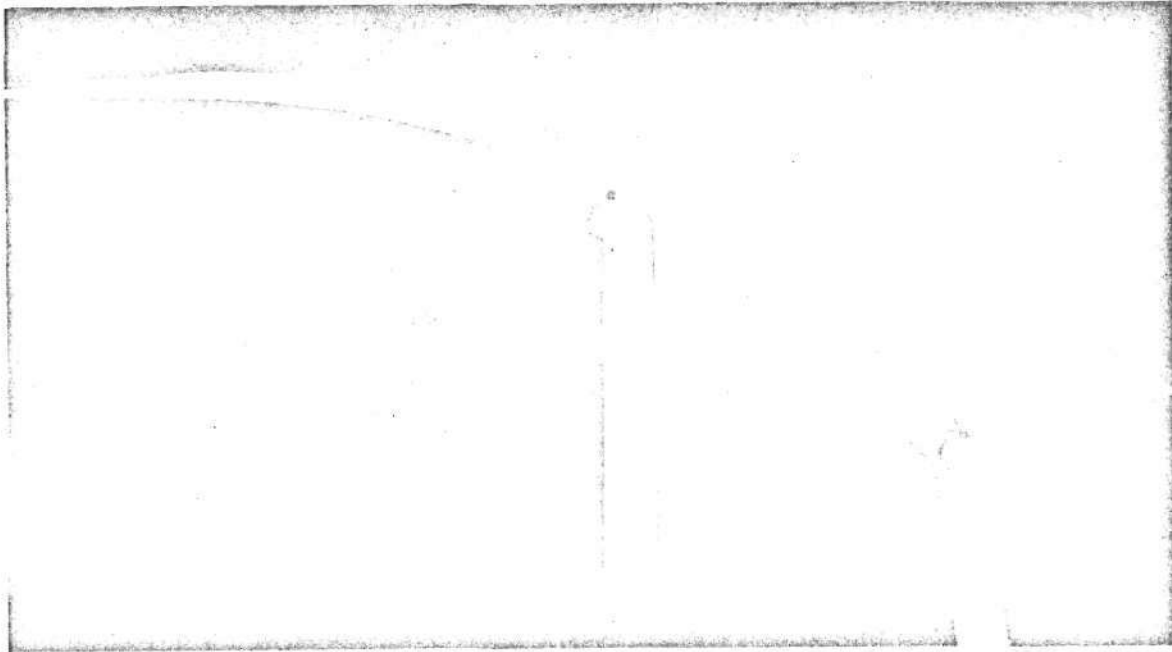
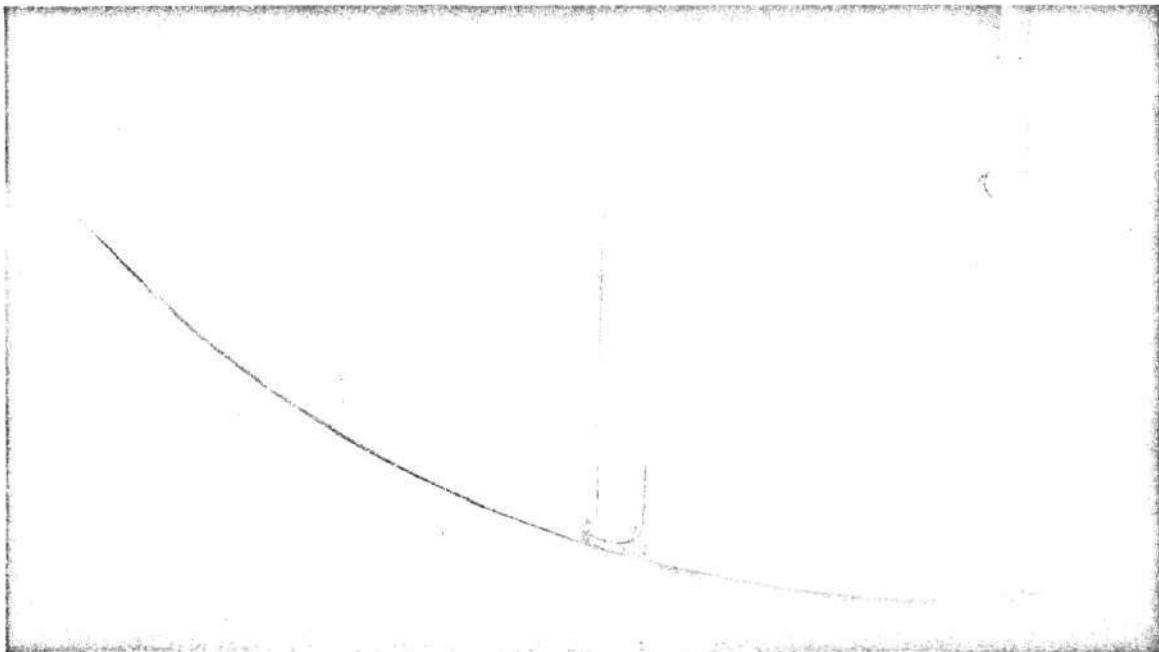


Fig. 31 Comparison of Breakdown Measurements on Delta Wings Measured in Different Tunnels (Ref. 62)

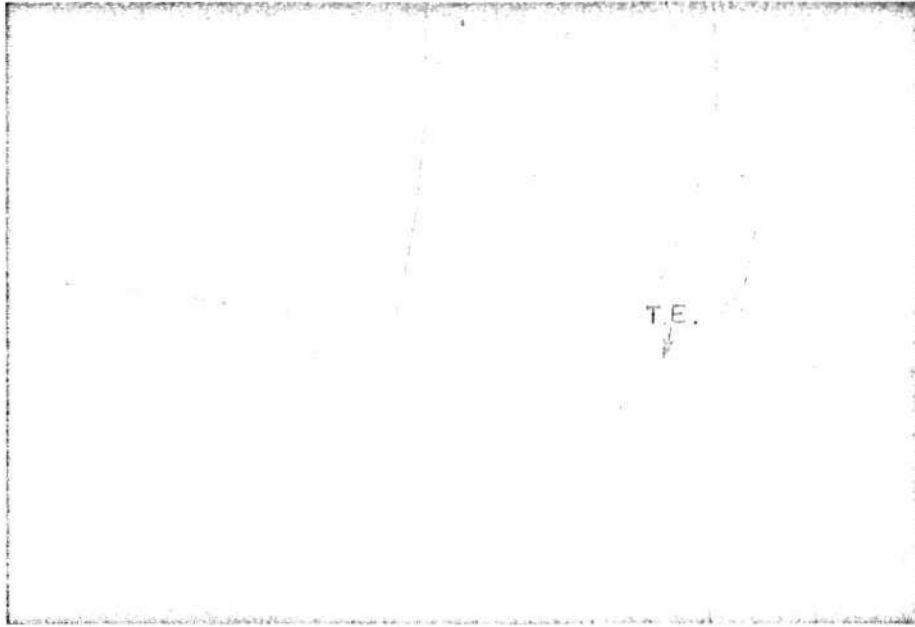


(a) LOCAL INCIDENCE INCREASING WITH DISTANCE FROM APEX



(b) LOCAL INCIDENCE DECREASING WITH DISTANCE FROM APEX

Fig. 32 Vortices for Cambered Delta Plate, $\Lambda = 80$ Deg; Water Tunnel
 $U = 2$ in./sec (Ref. 58)

(a) $M = 0.90$ (b) $M = 0.95$

Reproduced from
best available copy.

Fig. 33 Interaction of Shock Wave With Leading-Edge Vortices; Schlieren Observation, Sharp-Edged Plate Delata; $\Lambda = 50$ Deg, $\alpha = 10$ Deg (Ref. 58)

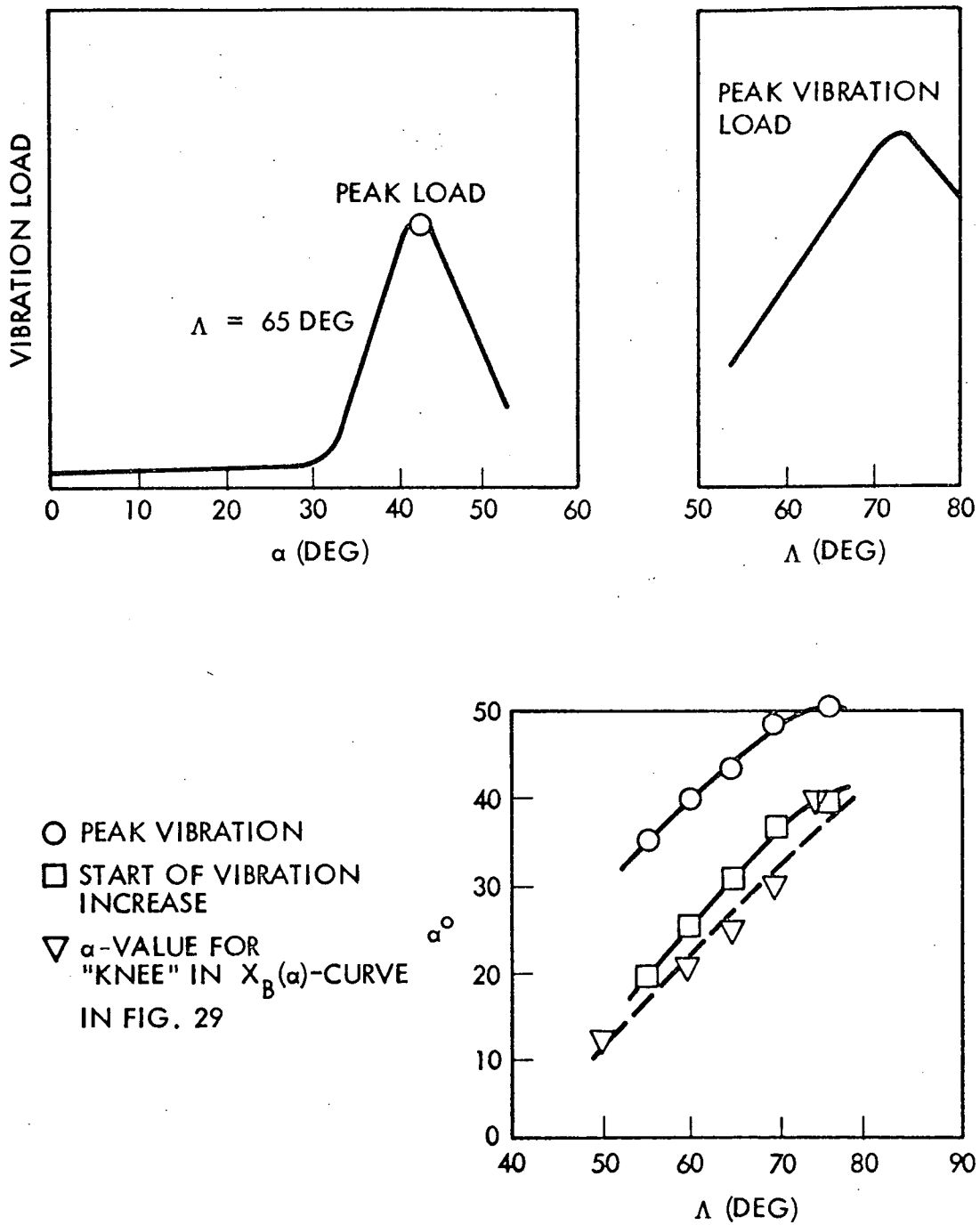


Fig. 34 Low-Frequency ($f\bar{c}/U = 0.05$) Vibration Load on Delta Wings Due to Vortex Burst (Ref. 63)

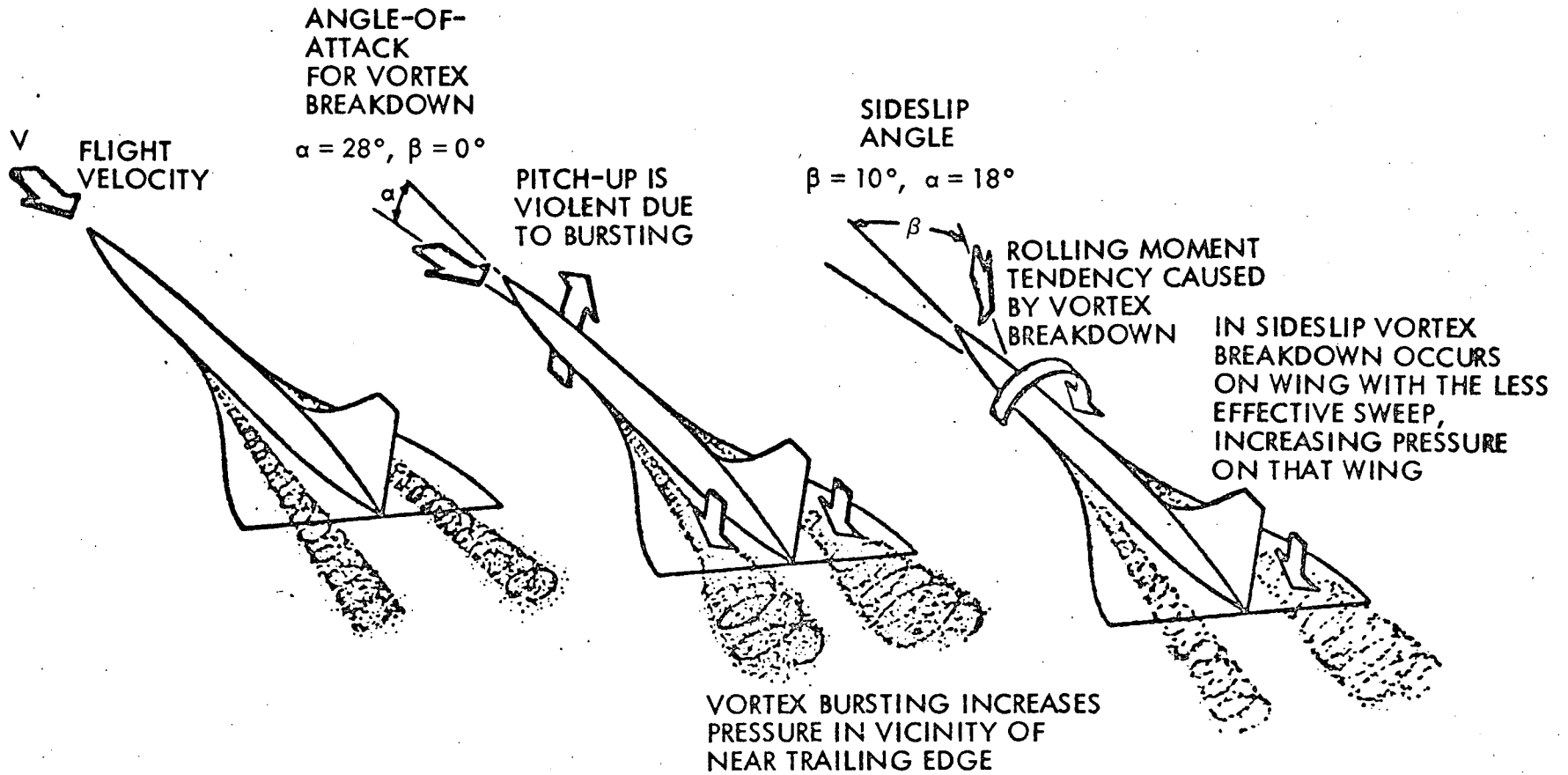


Fig. 35 Vortex Burst Effects on the Concorde Aircraft (Ref. 64)

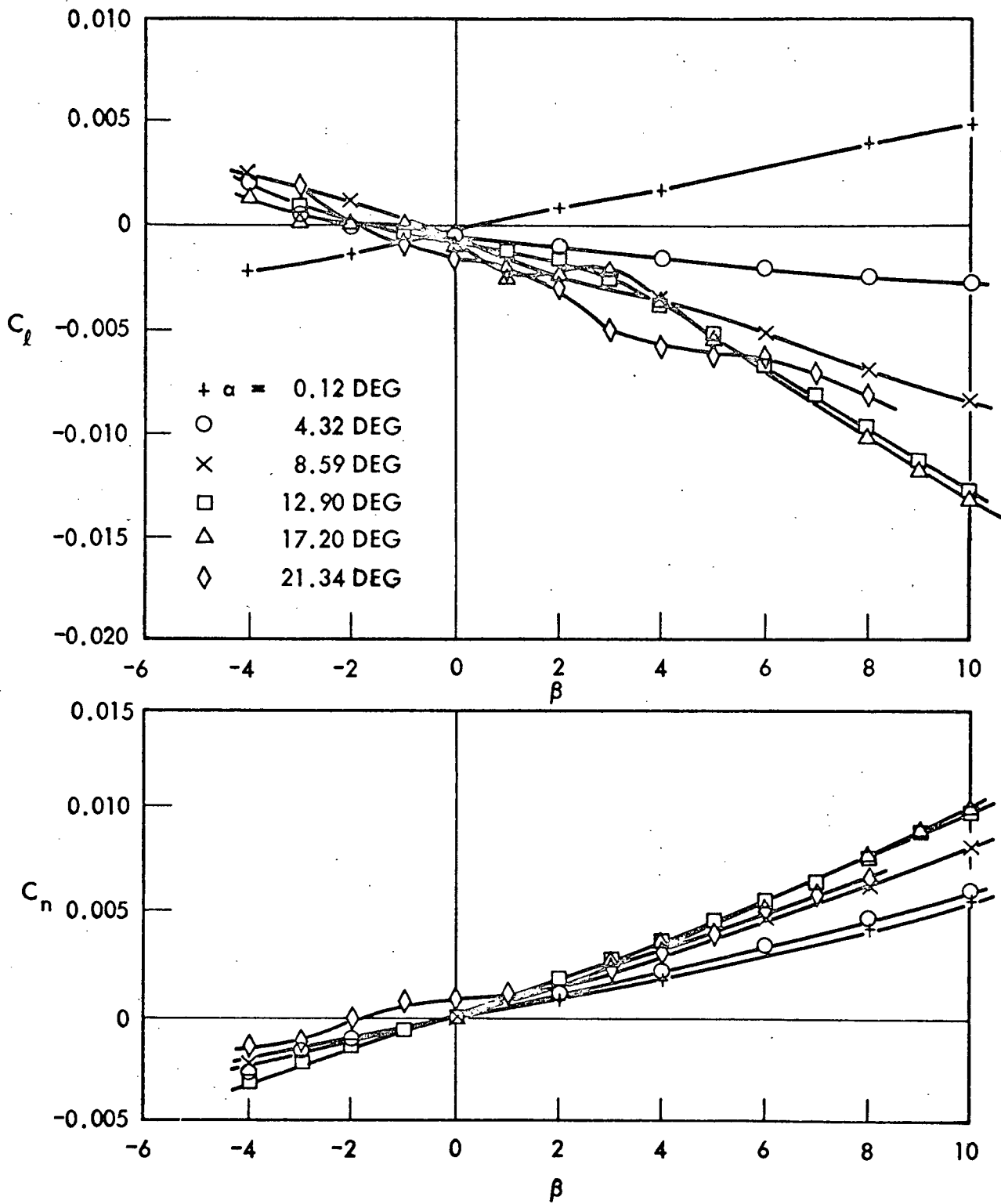
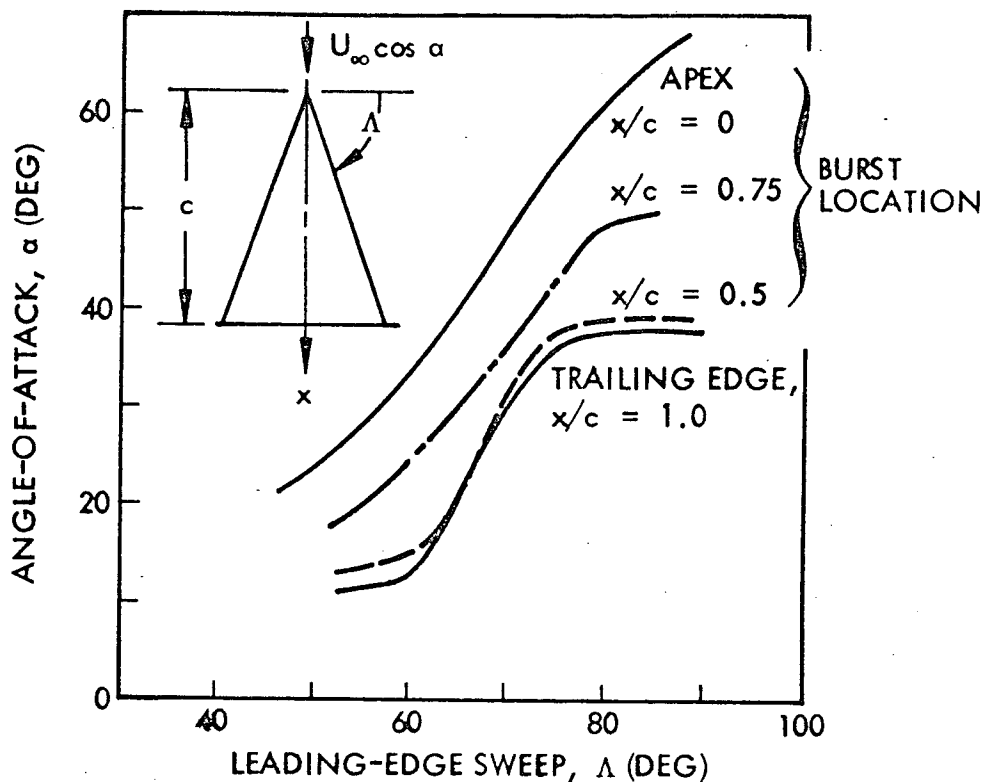
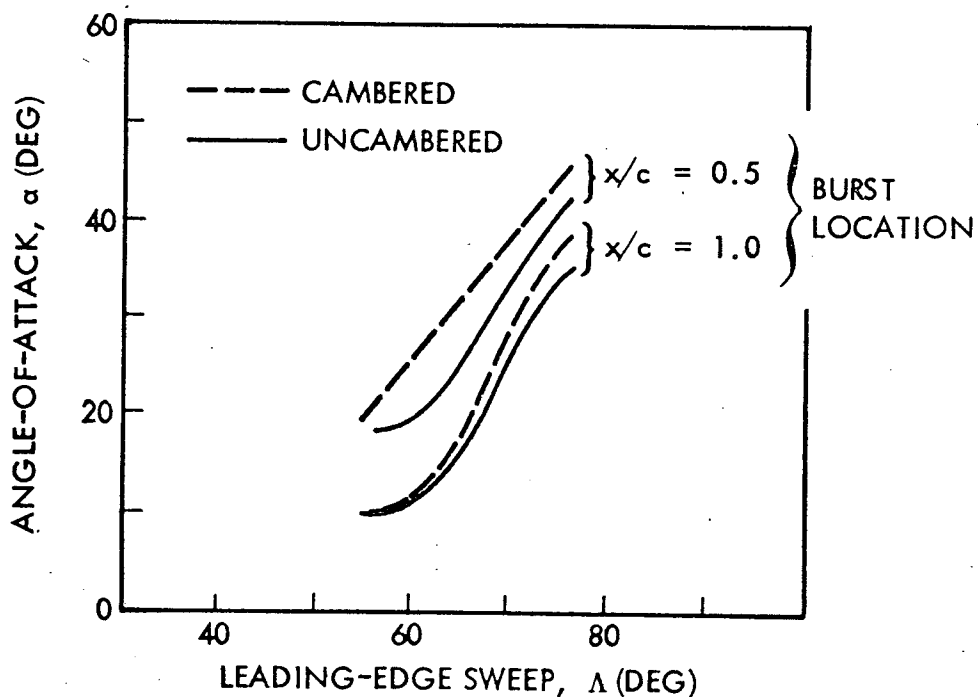


Fig. 36 Lateral Characteristics of Cone-Flow Wave Rider (Ref. 65)



(a) EFFECT OF SWEEP (REF. 60)



(b) EFFECT OF CAMBER (REF. 63)

Fig. 37 Sensitivity of Vortex Burst to Planform and Section Geometry

sweep is the dominant planform effect (Fig. 38). Thus, yaw, which effectively changes windward and leeward side sweep, is a degree of freedom that will have a great impact on the vehicle dynamics. This is especially true when there are tail surfaces and a fuselage with which the vortices can interact as in the case of the space shuttle vehicle. Some early lateral-directional stability results on the NAR orbiter (Ref. 66) show nonlinear roll, yaw, and side force coefficients with possible hysteresis loops for the wing-body combination (Fig. 39a). Likewise, the incremental effect of adding rolled out tip fins is nonlinear with possible hysteresis loops (Fig. 39b), and the pitch plane characteristics show the typical nonlinearities resulting from vortex burst (Fig. 39c). Yaw locks burst near the apex of the windward wing and causes it to move aft on the leeward wing (Refs. 48 and 59). The result is a reduced lift on the windward wing and an increase on the leeward wing (Fig. 40a). Likewise, the fuselage interaction results in a loss of windward and an increase of leeward suction. This explains the large positive $C_{l\beta}$ near $\beta = 0$ (and the correspondingly less negative $C_{n\beta}$ and more negative $C_{y\beta}$) (Fig. 39a). The addition of the tip fins not only gives additional surfaces for the vortex burst phenomenon to work on, but they also affect burst location. Thus, vortex burst is fixed at the leeward fin-wing juncture causing a negative incremental wing loading which dominates $\Delta C_{l\beta}$ making it negative (Figs. 39b and 40b). The windward fin loads are larger than those on the leeward fin due to the more extensive windward side vortex burst, thus causing a positive $\Delta C_{y\beta}$ and a negative $\Delta C_{n\beta}$. As β is increased further the burst induced load variation becomes negligible and the attached flow fin effects become dominant (e. g., $-\Delta C_l$, $+\Delta C_n$, $-\Delta C_y$, Fig. 39b).

The nonlinear interference effects of vortex burst are reminiscent of the nonlinear interference loads caused by the attachment of the vortices emanating from the wing fuselage juncture of the straight wing orbiter (Fig. 41 and Ref. 67). The result was stable nonzero yaw trim at $M = 0.6$ and bang-bang yaw characteristics at $M = 0.25$ and 1.5 with β -hysteresis near $\beta = 0$ and an unstable yaw trim for $\beta = 4$ deg at $M = 0.25$ (Fig. 42). This undoubtedly contributed to the disastrous results experienced in the subscale, free flight tests of the pitchover maneuver (Ref. 68).

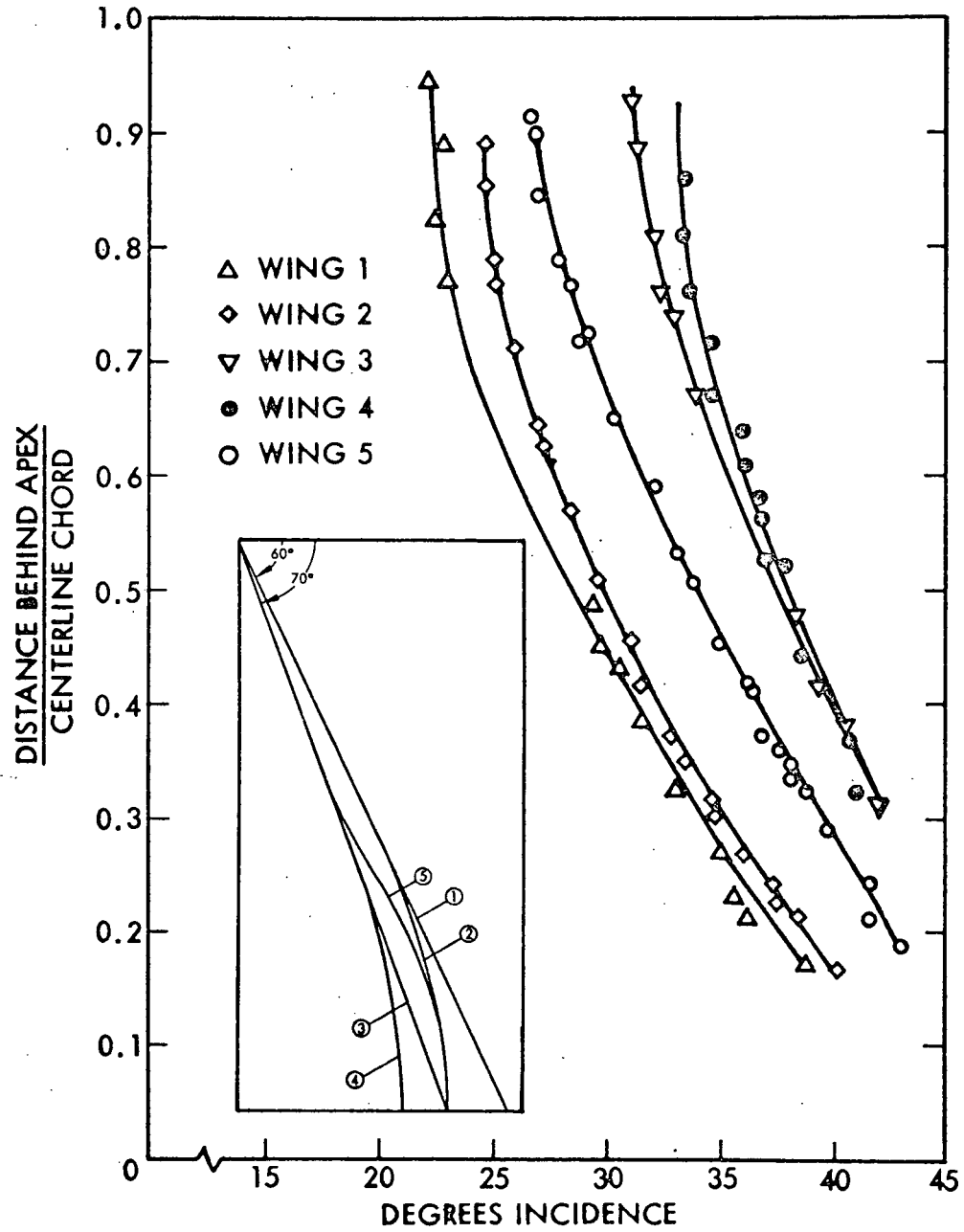


Fig. 38 Variation of Breakdown Position With Incidence (Ref. 62)

20

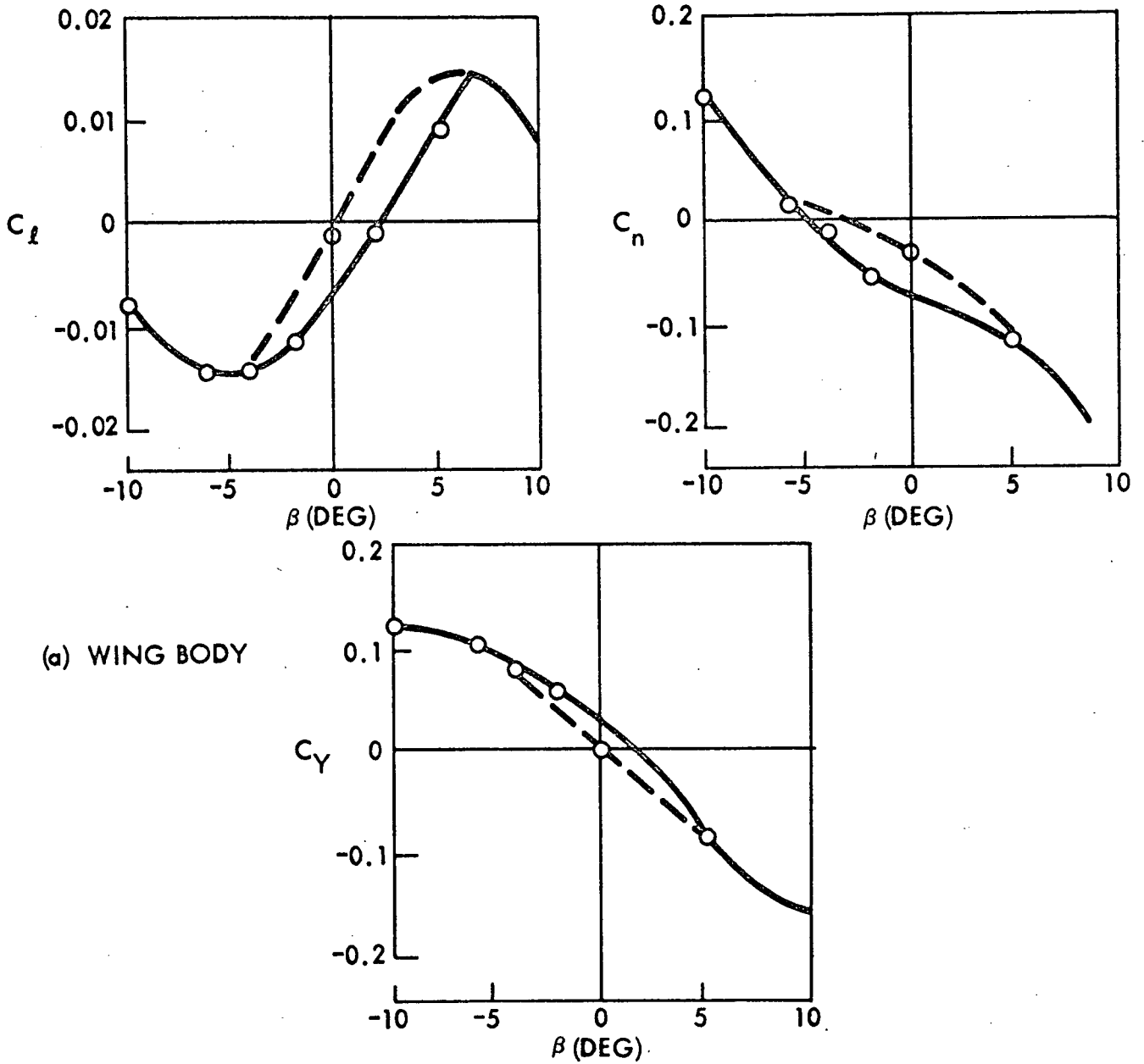


Fig. 39a Effect of Vortex Burst on the Aerodynamic Characteristics of the NAR Orbiter, $M = 0.6$ (Ref. 66)

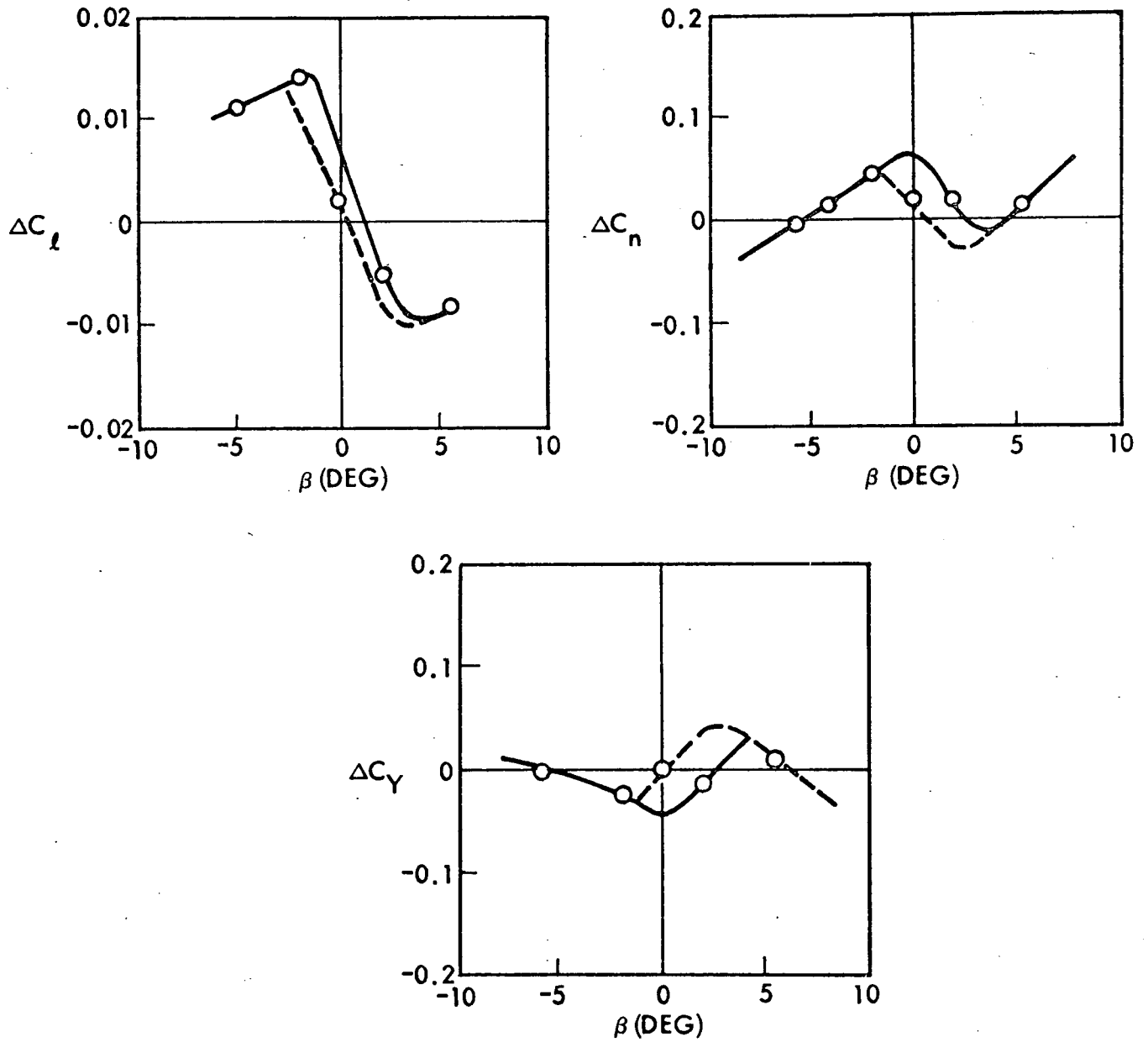


Fig. 39b Effect of Vortex Burst on the Aerodynamic Characteristics of the NAR Orbiter, $M = 0.6$ (Ref. 66)

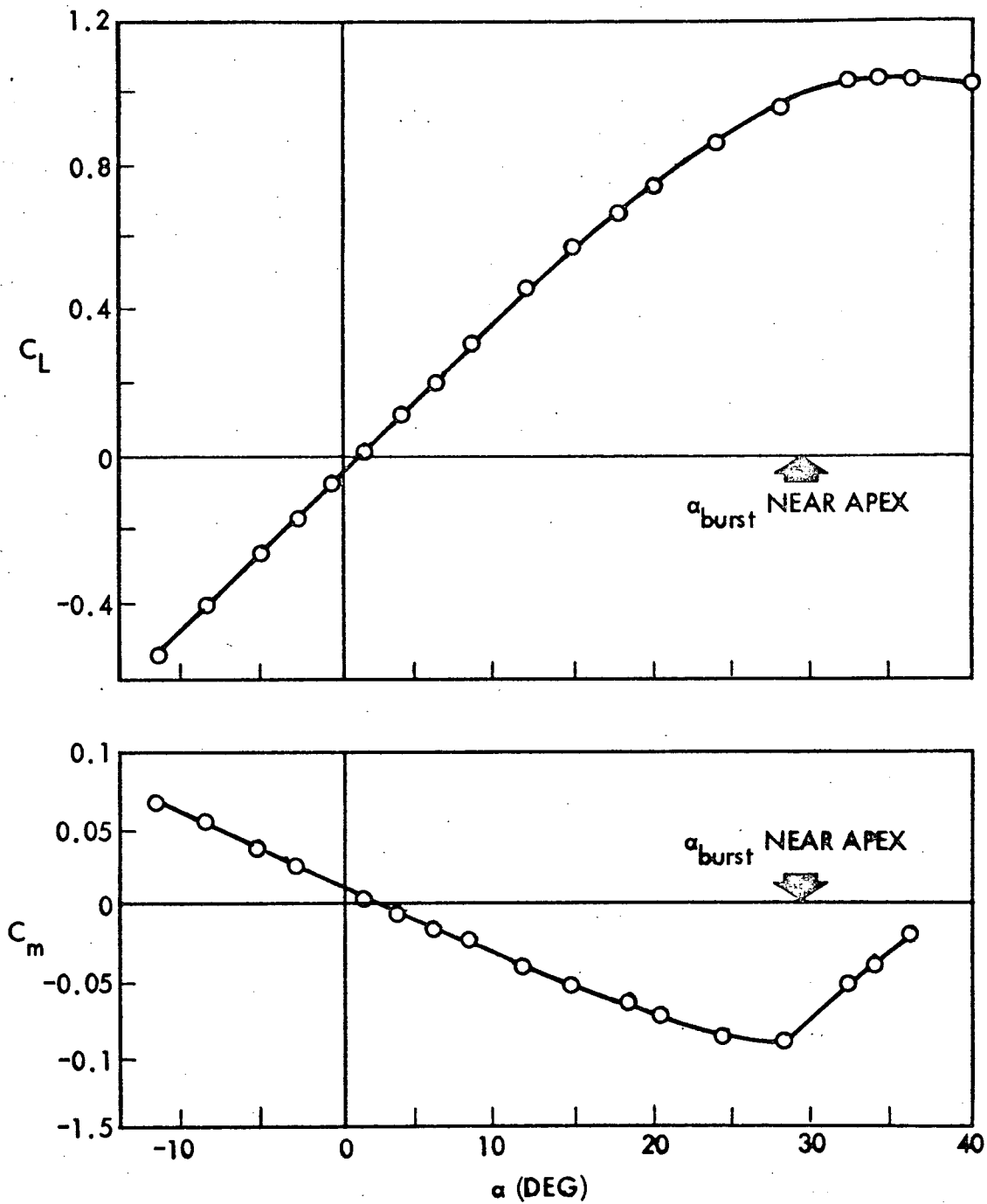
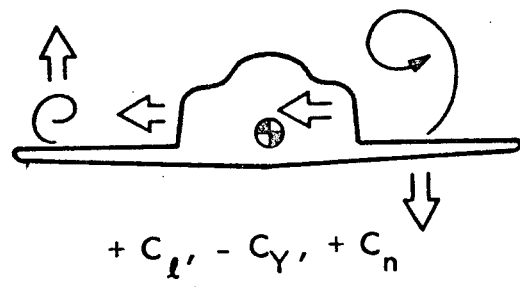
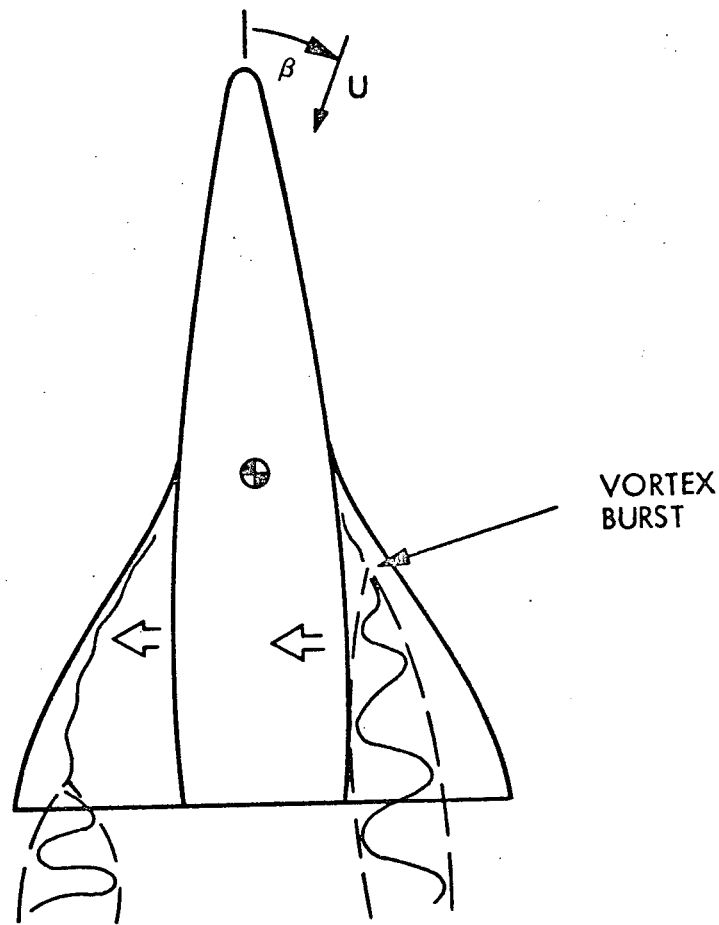


Fig. 39c Effect of Vortex Burst on the Aerodynamic Characteristics of the NAR Orbiter, $M = 0.6$ (Ref. 66)



(a) WING-BODY

Fig. 40a Vortex Burst Interference Effects

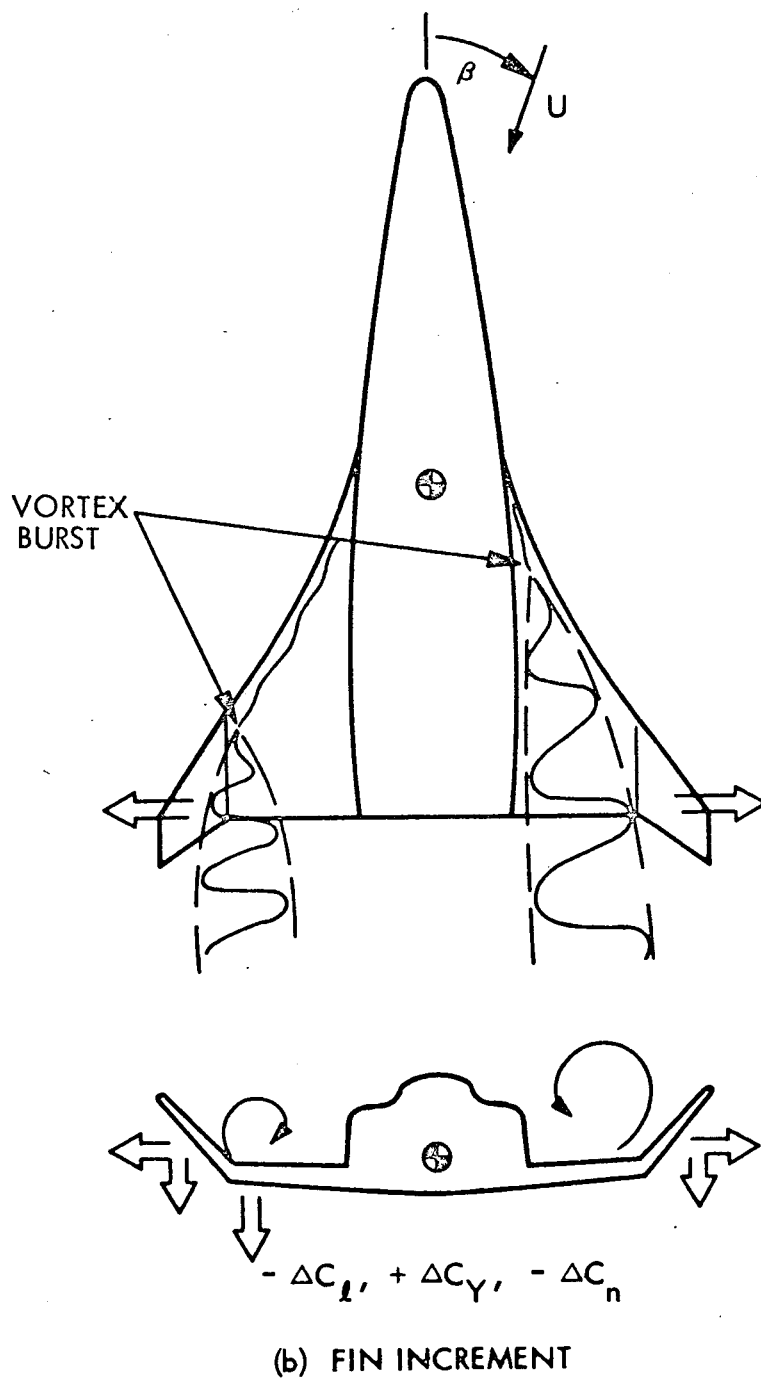


Fig. 40b Vortex Burst Interference Effects

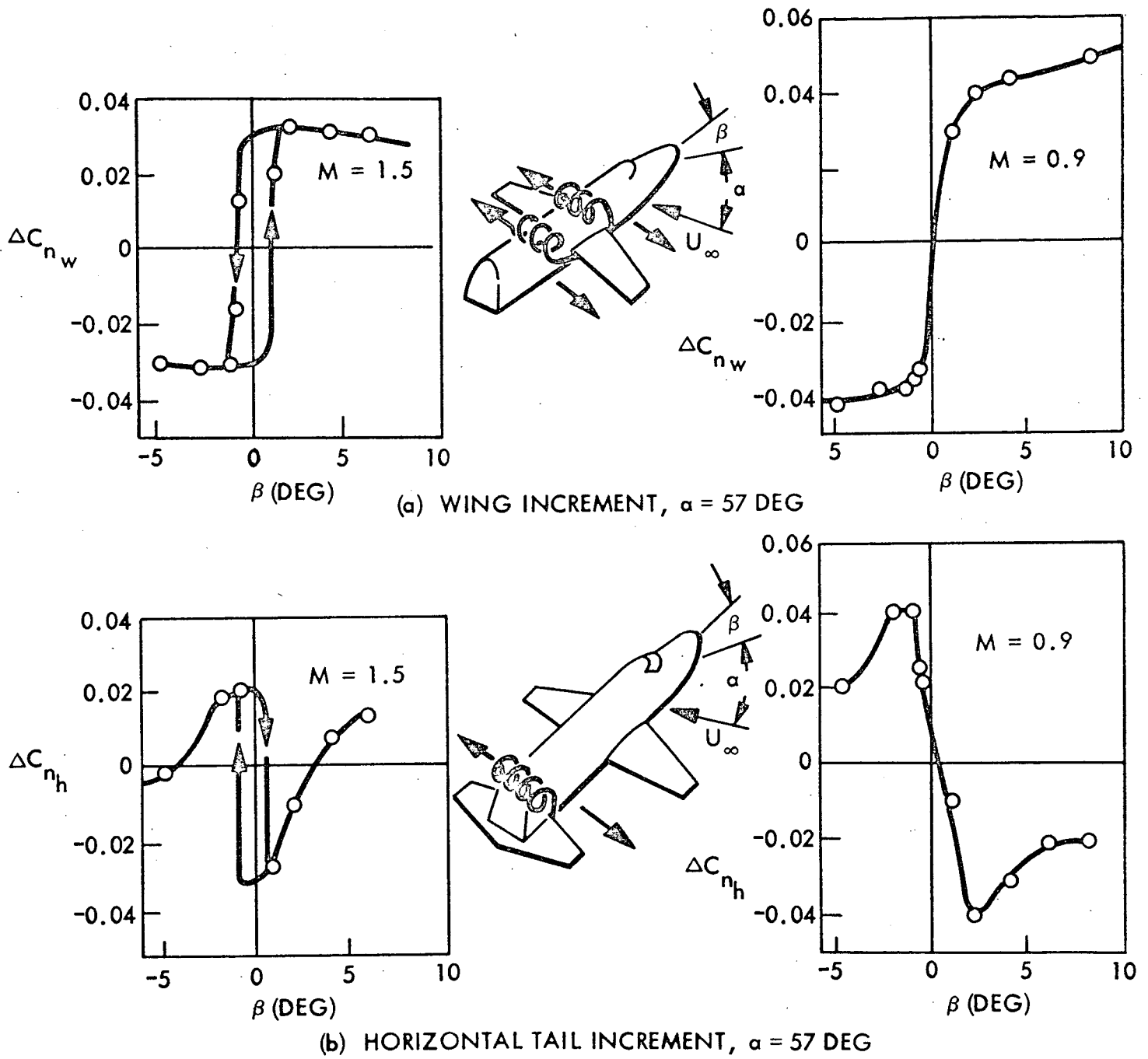


Fig. 41 Yaw Interference Loads on Straight Wing Orbiter, $\alpha = 57$ deg (Ref. 67)

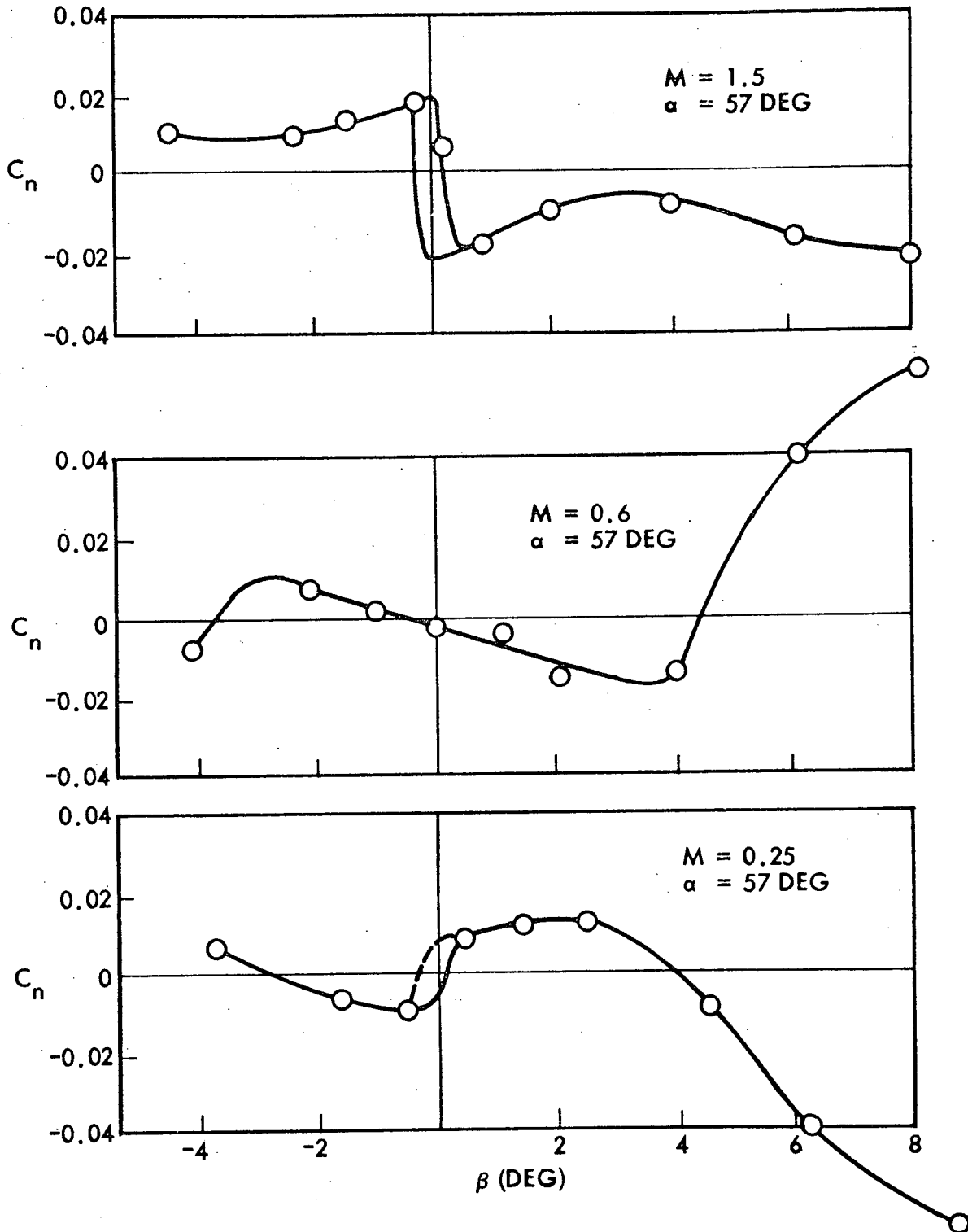


Fig. 42 Yaw Stability on Straight Wing Orbiter, $\alpha = 57$ deg (Ref. 67)

Vortex effects are not restricted to delta wing vehicles. The Lockheed delta body configuration (the only proposed lifting body orbiter) shows the typical nonlinear pitch and yaw moment characteristics of vortex lift (Ref. 69 and Fig. 43). The oil flow photograph in Fig. 44a shows the beginning of leading edge vortex formation over the rolled out tip fin emanating at the fin-body juncture. At $\alpha = 25$ deg (Fig. 44b) the vortex has burst and the scrubbing patterns from the large unstable vortices are evident.

Vortex burst is a phenomenon common to all the delta orbiter configurations. It is certainly to be avoided considering the associated nonlinear characteristics and adverse dynamic effects. Fortunately, all the proposed shuttle vehicles fly at angles of attack well below those for severe vortex burst effects. Furthermore, the slightly ogee planform of the shuttle delta wings tends to delay the occurrence of burst and also makes the burst process less violent, i. e., less prone to cause large discontinuous changes of the aerodynamic characteristics. On the other hand, vortex burst is sensitive to back pressure, such as would be produced by the deflection of a trailing edge control surface, and a careful analysis of the problem is needed. This will be discussed in detail in the next section along with other control interference effects.

2.4 CONTROL INTERFERENCE

Up until now the effect of back pressure on the leeward flow field of the delta wing has not been considered. It is well known that the extent of shock induced separation is sensitive to back pressure (Ref. 70). Flap controls will often cause boundary layer separation, especially in hypersonic low density flow, where less than 10 deg flap deflection often will cause boundary layer separation (Refs. 70 to 73 and Fig. 45). Thus, the deflection of a trailing edge control surface will affect the extent of shock induced separation. Such back pressure effects are of practical concern since it is desirable to control the shuttle with leeward control deflections, wherever possible, in order to minimize control surface heating. Data obtained on the NAR orbiter (Refs. 24 and 74) show an elevon effectiveness greater than Newtonian for small deflections ($\delta = -10$ deg) at low angles of attack (Fig. 46). This is the likely result of

2-58

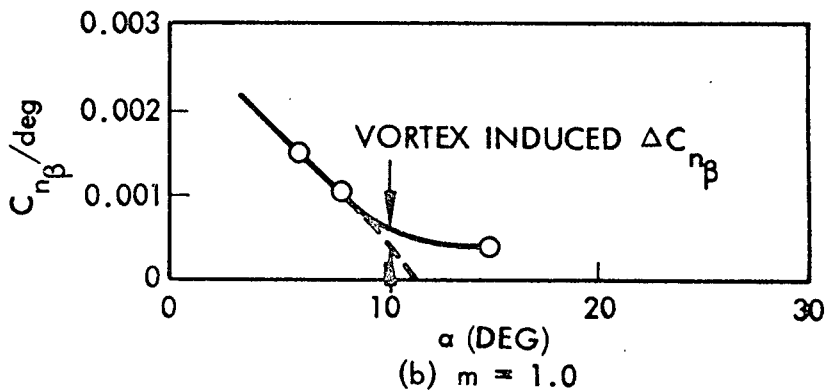
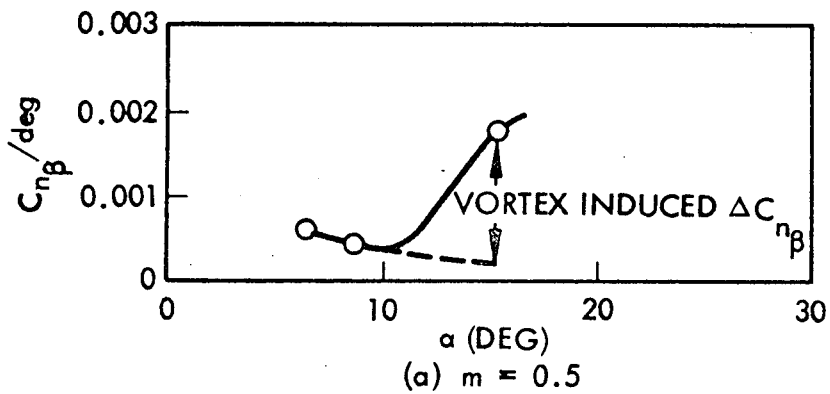
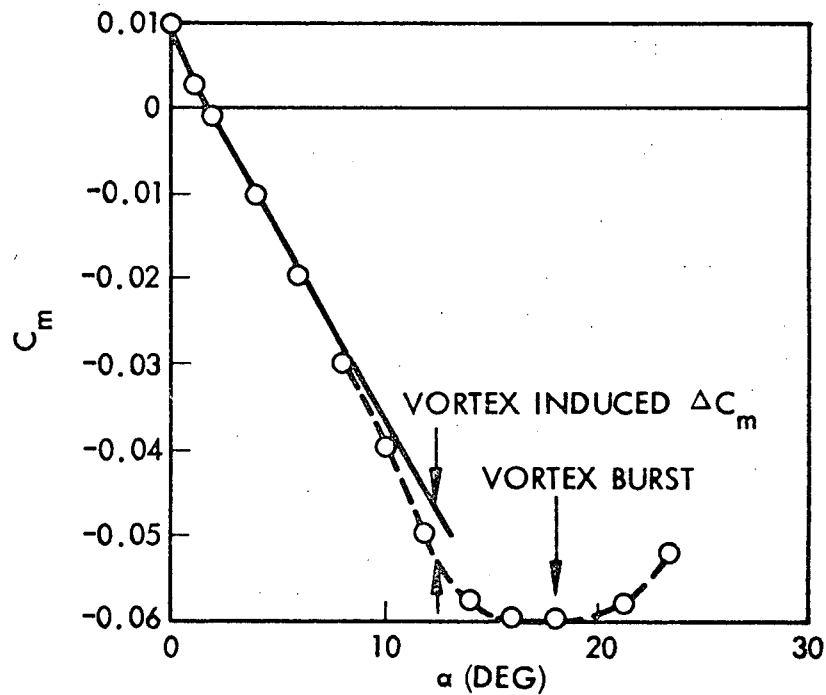
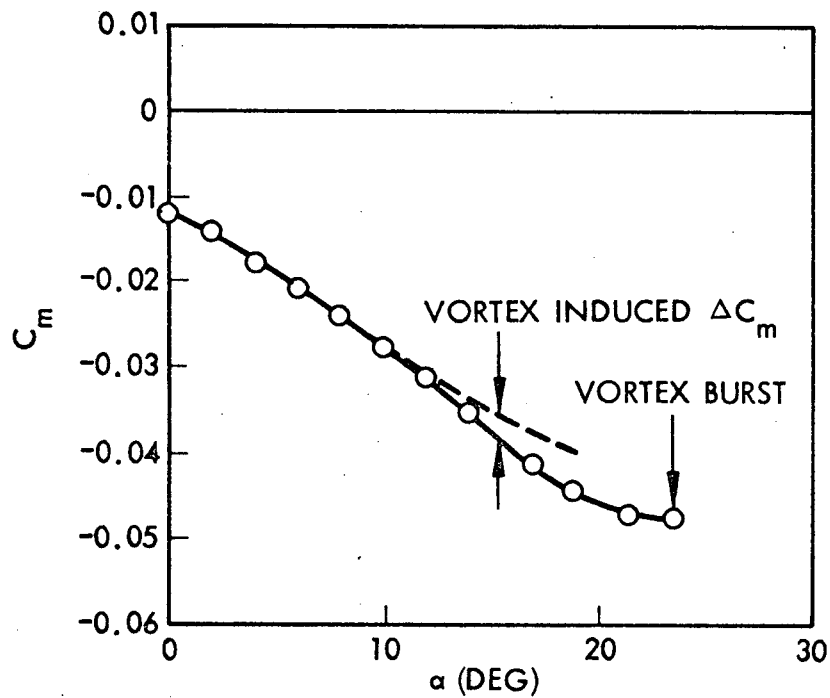


Fig. 43 Correlation of Delta Body Pitch and Yaw Characteristics (Ref. 69)



(a) ATTACHED FLOW
 $\alpha = 10 \text{ DEG}$



(b) VORTEX BURST
 $\alpha = 20 \text{ DEG}$

Fig. 44 Delta Body Leaside Flow Patterns, $M = 1.0$ (Ref. 69)

2-60

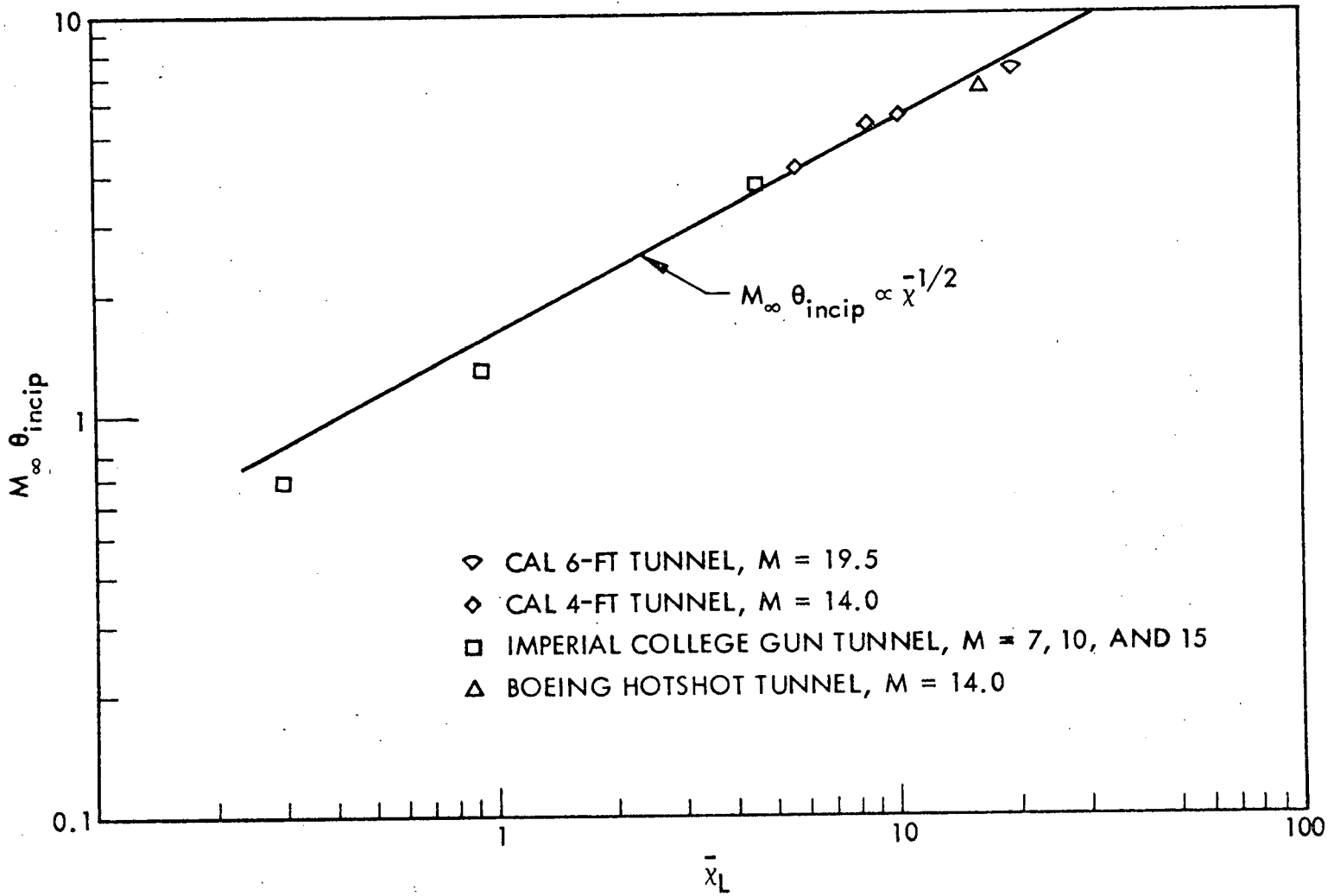


Fig. 45 $M_\infty \theta_{incip}$ Versus \bar{x}_L for Incipient Separation Condition (Ref. 71)

2-61

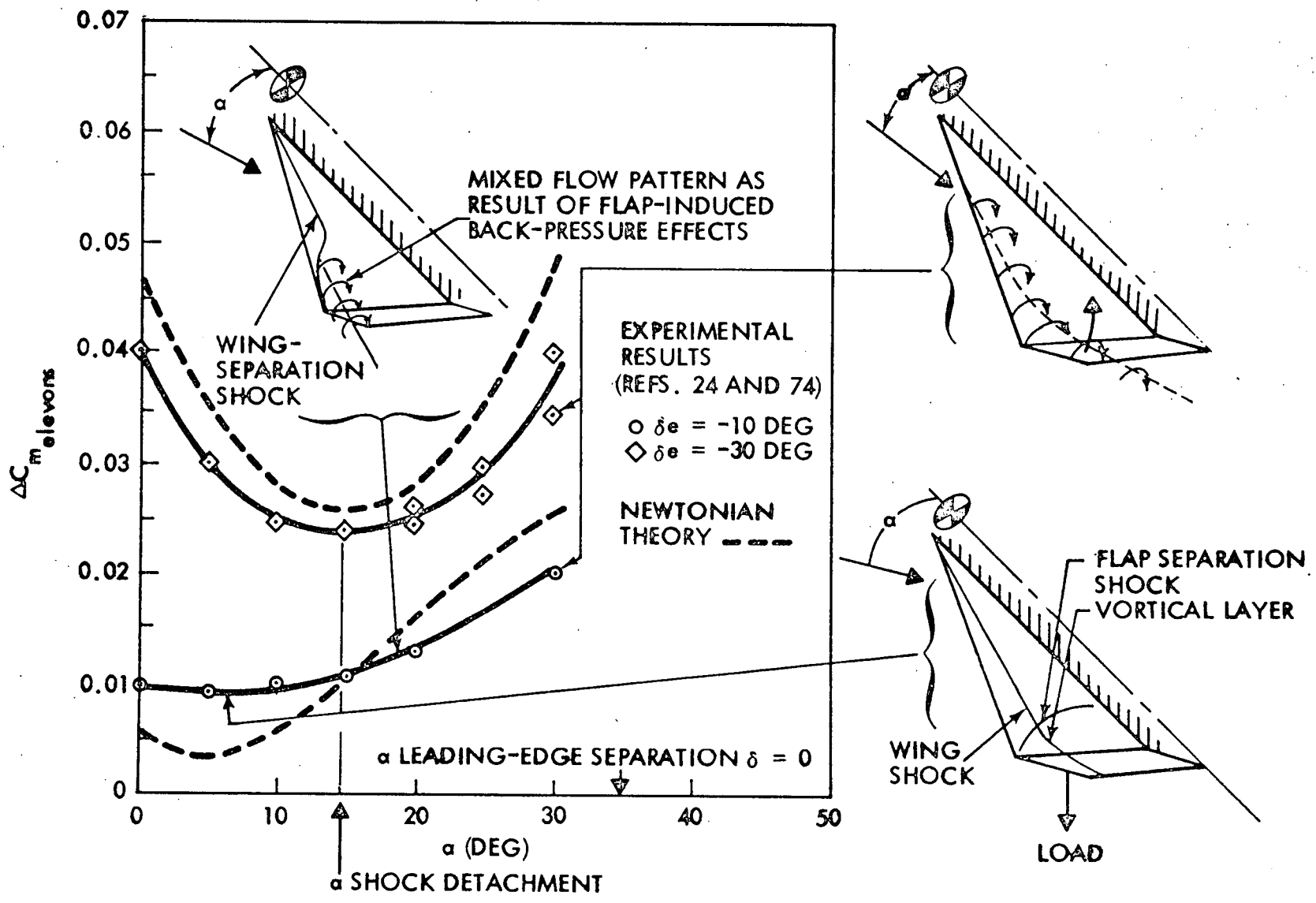


Fig. 46 Supersonic Control Interference for NAR Orbiter, M = 5

shock induced separation of the leeside flow. The separation extent (for fixed flap deflection $\delta = -10$ deg) increases initially with angle of attack. However, the back pressure effect from the flap causes the transition between shock induced separation and leading edge stall to start near the flap and progress forward with increasing angle of attack (see inset sketch in Fig. 46); at high angle of attack the positive lift produced by the vortices outweighs the negative lift generated by the flap induced flow separation over the inner wing surface. The result is a loss of flap effectiveness below the Newtonian windward side value (i. e., a more stable ΔC_m than predicted by Newtonian theory for $\delta = -10$ deg). At the high deflection $\delta = 30$ deg the mixed flow field may still occur and the overall force data are not sensitive enough to detect it. Generally, the leeside effects seem to vary less drastically and Newtonian theory seems to predict the trends rather well.

Experimental results also indicate that roll reversal occurs as a result of the back-pressure-induced change in flow field (Ref. 25 and Fig. 47). If hysteresis does occur when switching between the various separated flow types (as indicated in Fig. 6), then a residual control force will remain after the control deflection is removed. The control force is made up of two components: the force on the control surface itself and the induced load on the wing (due to a control induced change in the flow field (separation type) on the wing. The former will go away when the control deflection is removed. The latter will persist (if flow field hysteresis is present) until the angle of attack is reduced sufficiently to get out of the hysteresis region (Fig. 48).

As one would expect, vortex burst is also sensitive to back pressure. In agreement with Ludwig's theory, Hummel finds that supplying an adverse pressure gradient by using an obstacle one chord length downstream of the trailing edge on the right half span causes vortex breakdown (Fig. 49 and Ref. 48). An upward flap deflection, e. g., for a roll maneuver, will of course have a similar effect, thus causing a "super response" to a roll command. Thus, control deflection will induce burst where ordinarily it would not occur. Furthermore, vortex burst is definitely associated with hysteresis (Fig. 30), and subsonic control-induced burst is a problem of serious concern. There is experimental evidence of control-induced burst on a proposed shuttle configuration

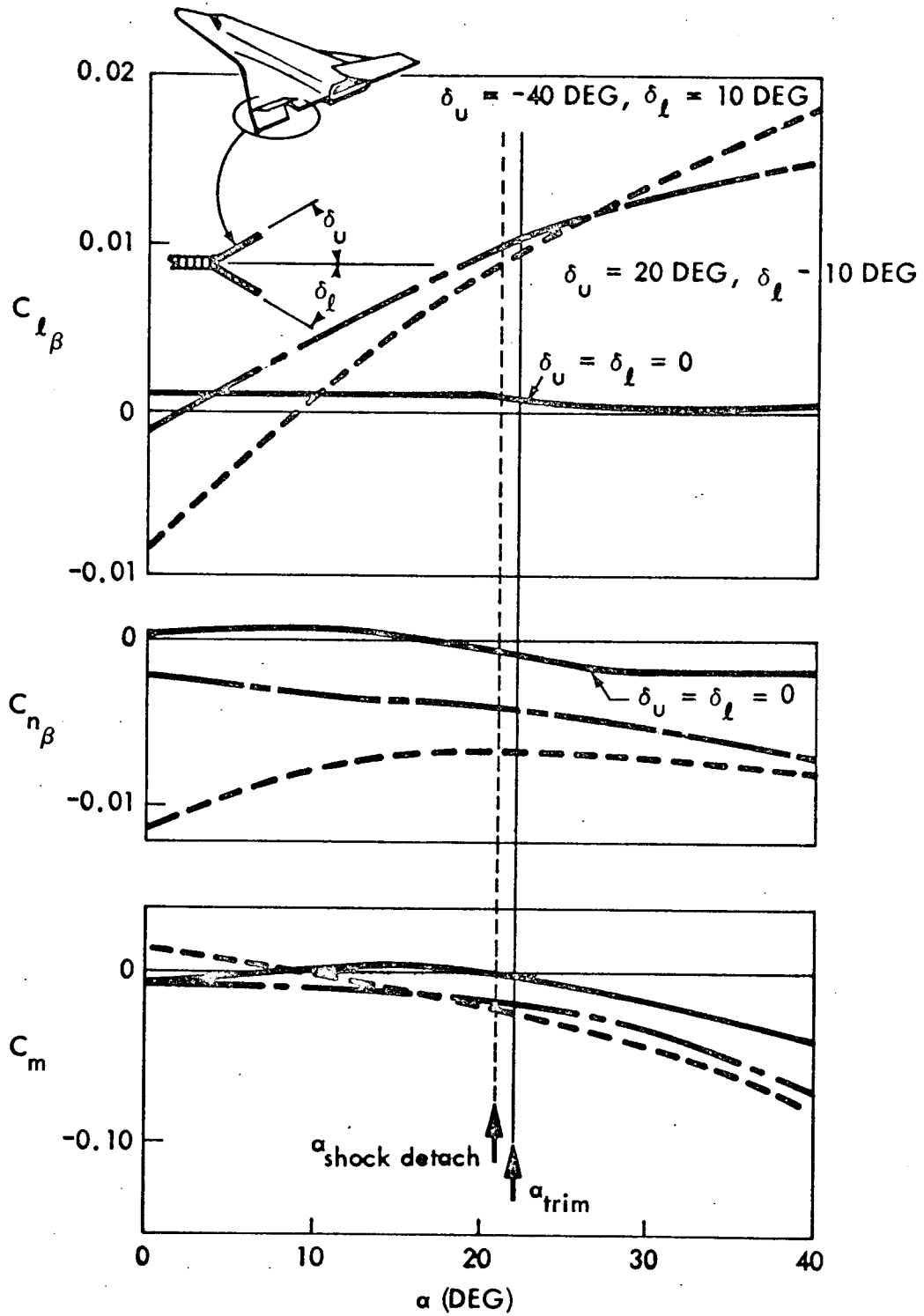


Fig. 47 Effect of Combined Elevator - Aileron Deflection on Aerodynamic Characteristics, NAR Orbiter With Split Elevon, $M = 60$ (Ref. 24)

2-64

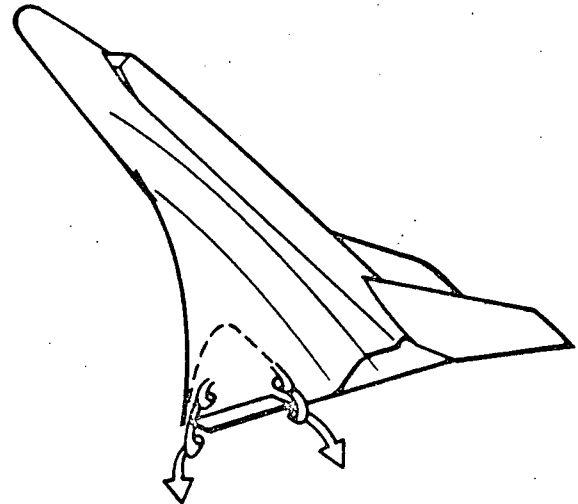
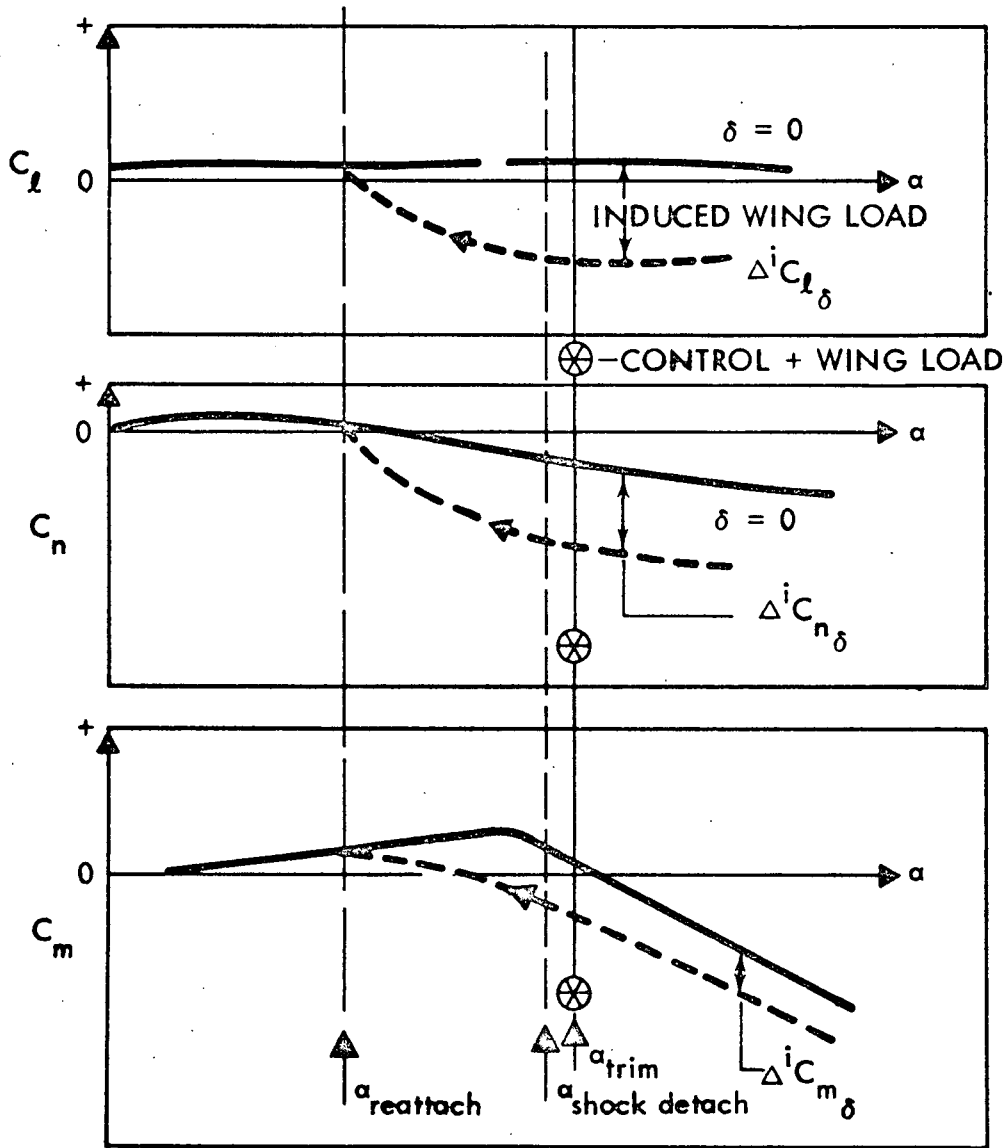


Fig. 48 Possible Control Induced Hysteresis

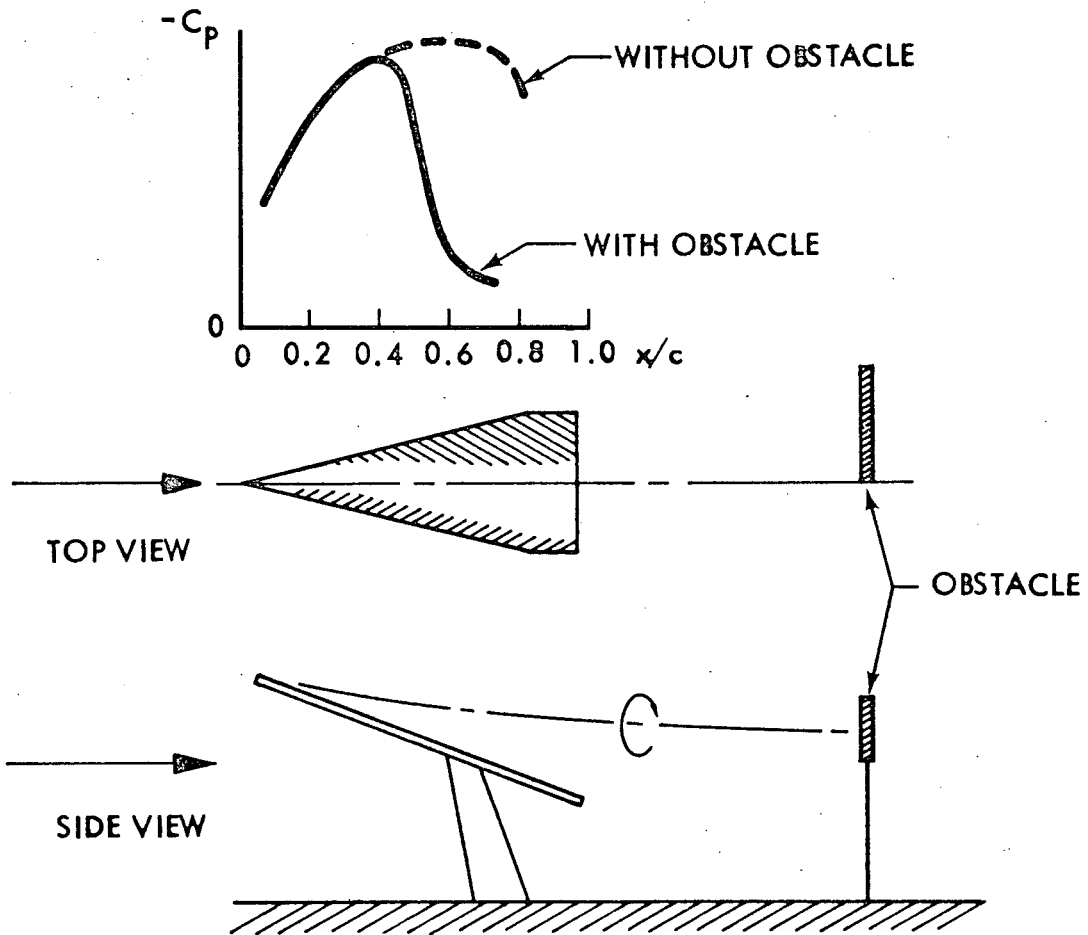


Fig. 49 Vortex Burst Caused by Downstream Obstacle on 76-deg Delta Wing at $\alpha = 20$ deg (Ref. 48)

(Fig. 50 and Ref. 24). At $M = 0.6$ vortex burst is caused by the left elevon at $\alpha = 12$ deg for a combined pitch-roll command which results in $\delta_L = -45$ deg. After burst, there is a reduction in control effectiveness until burst is caused also by the right elevon. Nearly all control force is lost when burst occurs near the wing apex. At $M = 1.5$ the characteristics are similar but less drastic. At $M = 2.0$ the typical shock induced leeside separation characteristics are evident (compare Fig. 48 with Fig. 46).

This loss of control effectiveness during vortex burst has been observed in flight (Fig. 51 and Ref. 75). Vortex burst was observed to occur over the outboard wing between $\alpha = 15$ deg and $\alpha = 18$ deg. At this time increased pitch control activity was necessary (Fig. 51b). Likewise, increased yaw and roll deflections were necessary (Fig. 51c) to maintain control.

Even though the shuttle vehicle may largely avoid the vortex burst and shock induced separation, control deflection will cause the realization of both, with the attendant undesirable dynamic effects. The NAR orbiter will certainly experience shock induced separation as the result of control deflection, as it flies just below the lower bound of the shock induced separated flow region (Fig. 52).

Incidentally, there is one other control interference effect worth mentioning, and that is bow shock-flap shock interaction (Refs. 11 and 75 to 77). Leeward control deflections do not cause bow shock-flap shock interactions, but if the vehicle is trimmed near zero elevator deflection, as indicated from the test data of Ref. 25 (Fig. 53a), and a sufficiently large aileron deflection is required, it could happen (Fig. 53b). This can result in aerodynamic undamping in pitch (Fig. 53c) which is coupled aerodynamically with the two other angular degrees of freedom. Of course, one can through diligent design assure that large aileron deflections are not necessary (in this case $\delta \leq 15$ deg is acceptable). But one must recognize the problem in order to be sure to avoid it. Even for smaller flap deflections than those causing the drastic flap shock-bow shock interaction, the curved bow shock can through the generated inviscid shear flow, the "entropy wake," generate loads on aft body and flap (Ref. 78). "Entropy

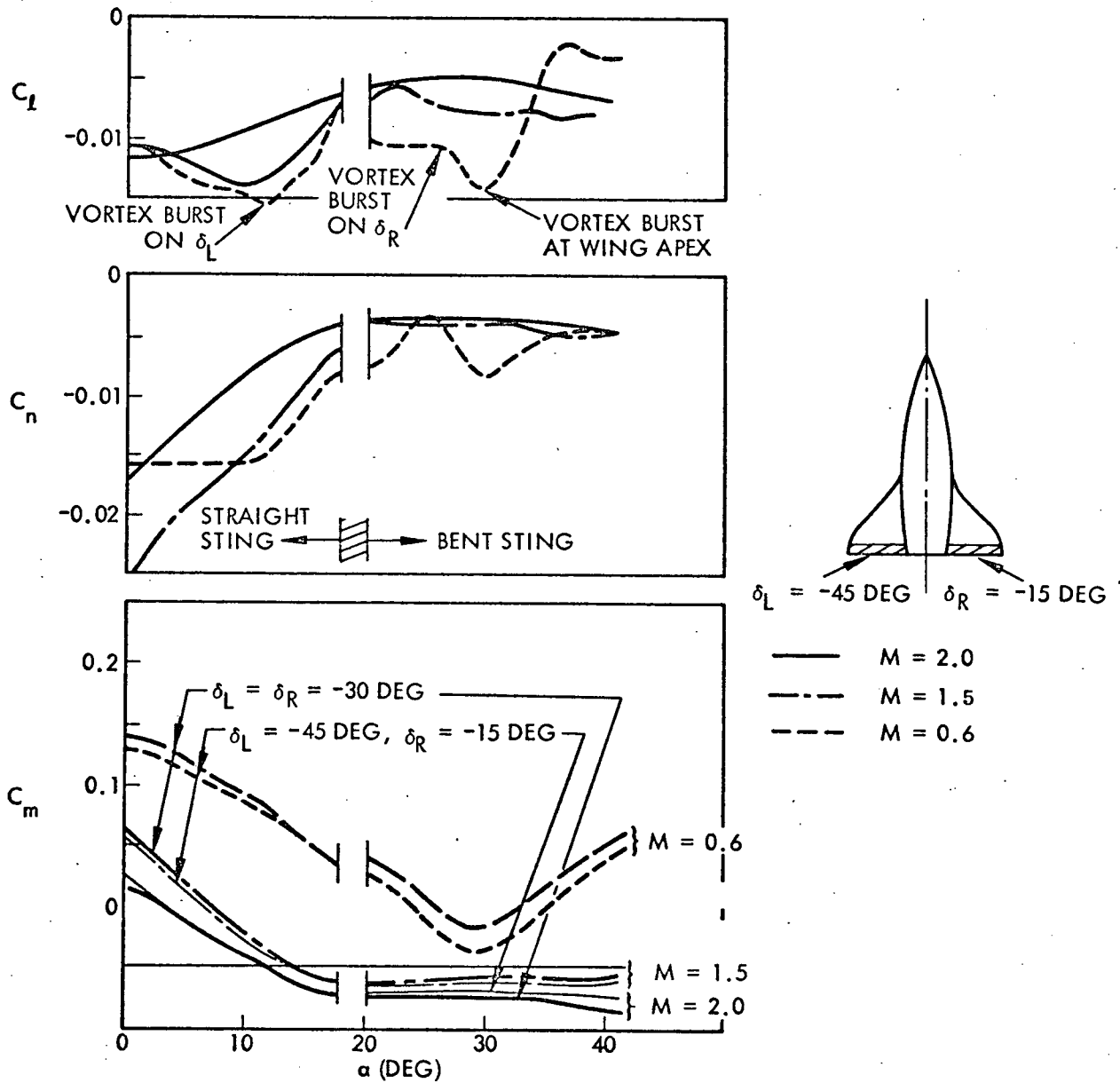
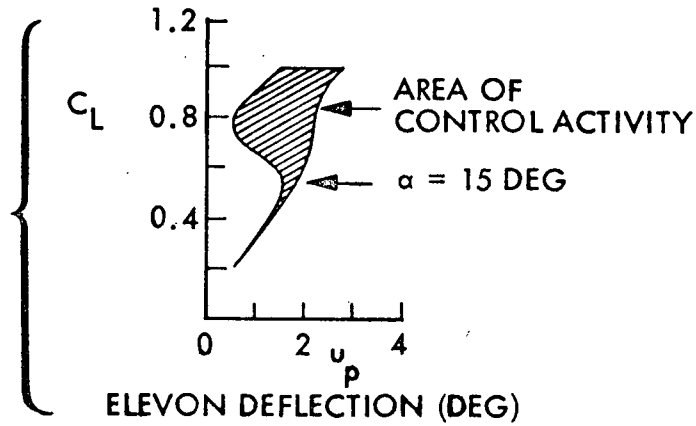
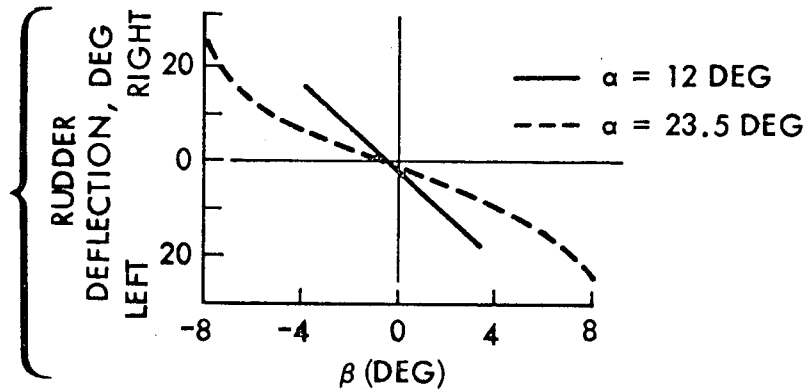


Fig. 50 Control-Reduced Vortex Burst (Ref. 24)

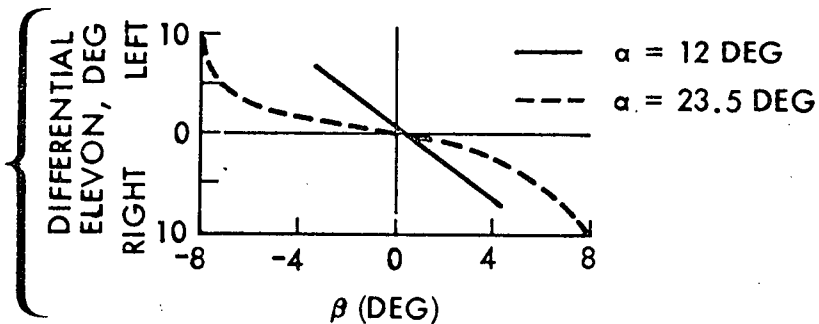
(a) PITCH CONTROL



(b) YAW CONTROL



(c) ROLL CONTROL



UNSTEADY FLOW

$\alpha = 15 \text{ DEG}$ INCIPIENT VORTEX BURST

$\alpha = 18 \text{ DEG}$ VORTEX BURST

Fig. 51 Effect of Vortex Burst on Control Demand, Flight Results on Modified F5D Aircraft (Ref. 75)

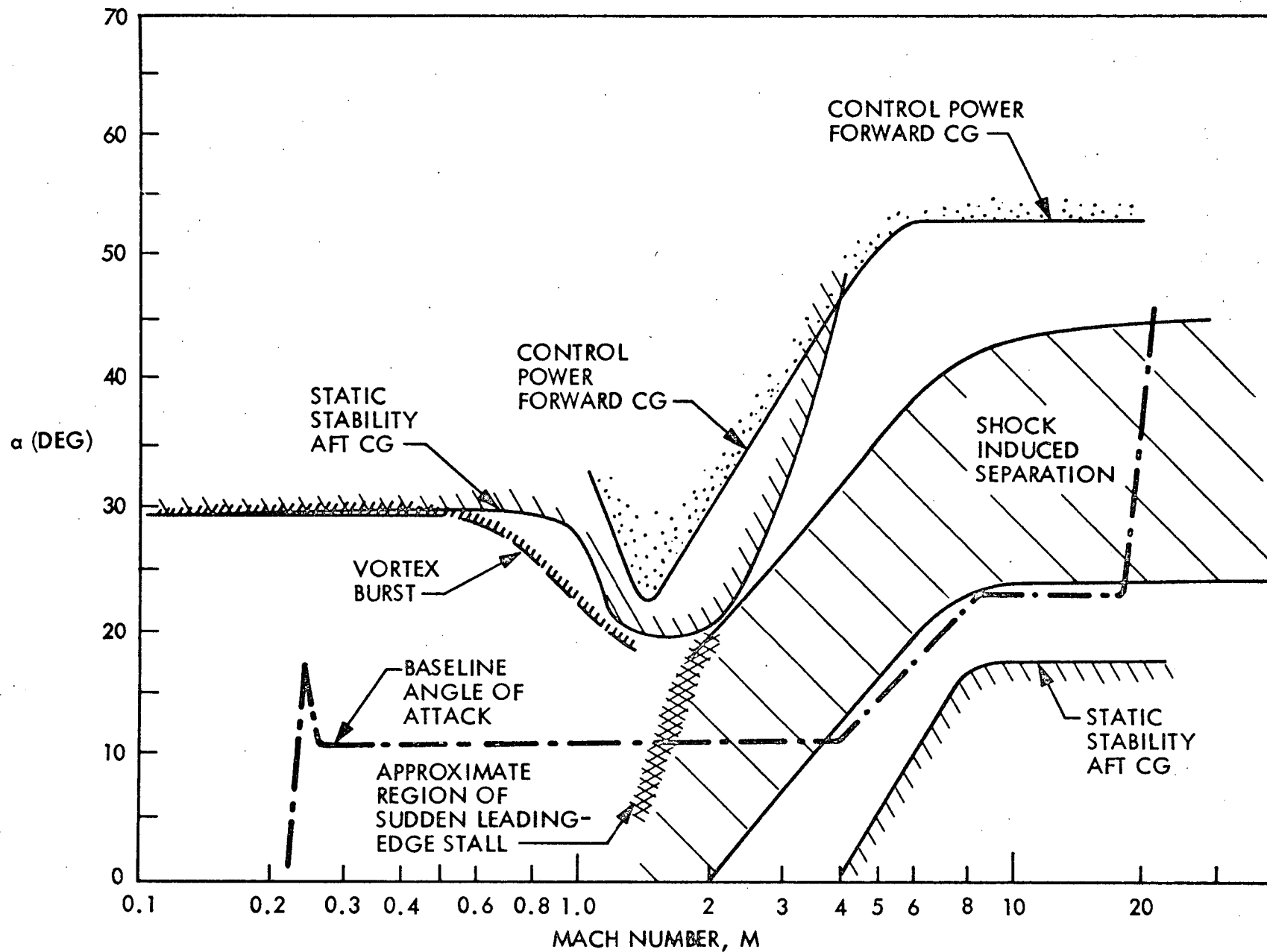
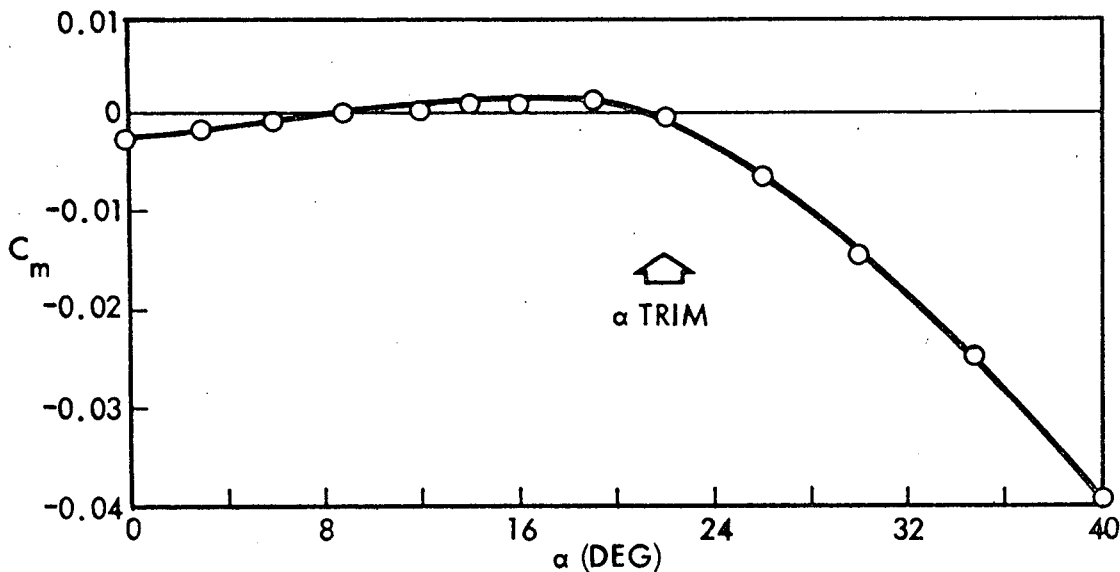
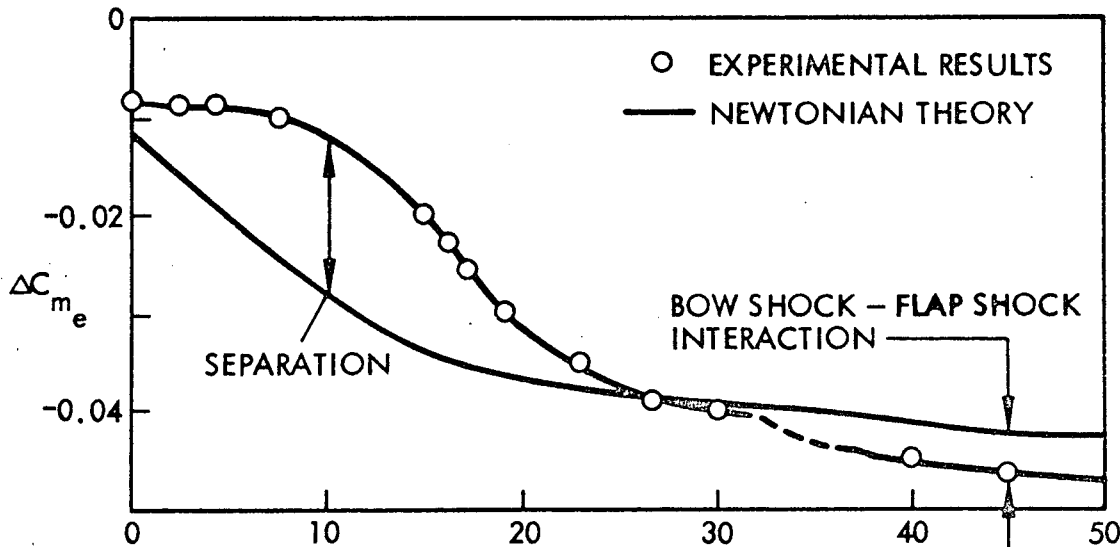
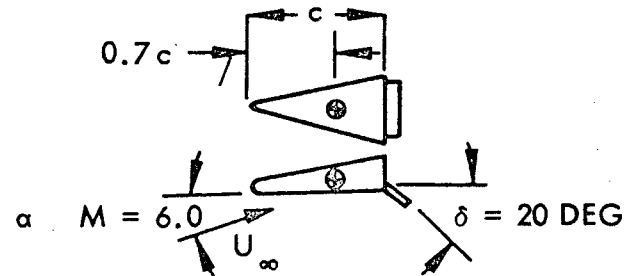


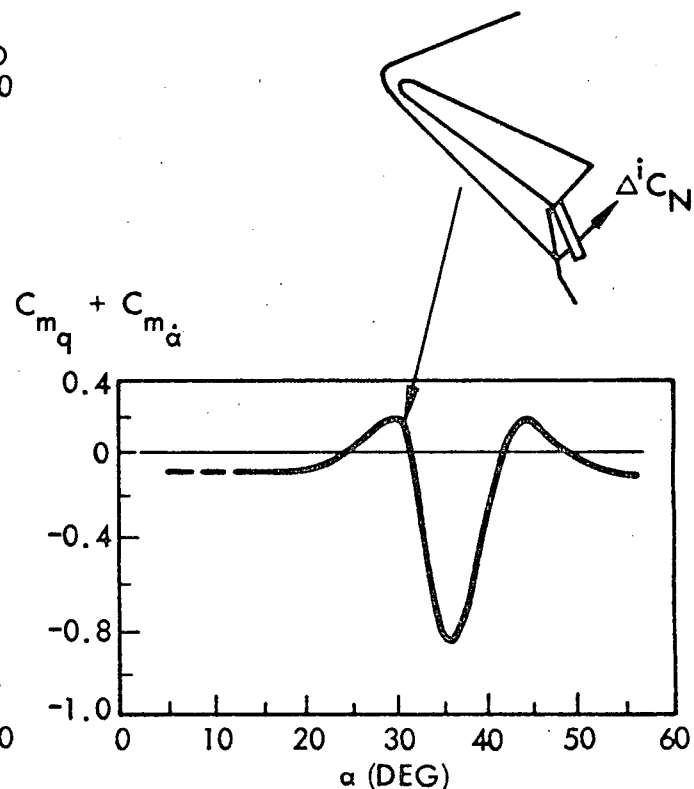
Fig. 52 Unsteady Aerodynamic Flow Boundaries Superimposed on NAR Orbiter Entry Corridor (Ref. 21)



(a) $M = 6.0$ PITCHING MOMENT



(b) ELEVON INDUCED MOMENT
WINDWARD DEFLECTION, $\delta_e = 15$ DEG, (REF. 25)



(c) PITCH DAMPING RESULTS
(REF. 11)

Fig. 53 Probable Occurrence and Possible Results of Bow Showk-Flap Shock Interference

vortices" generated by discontinuities in the shock envelope are another means of generating loads on the aft body, as Maikapar has shown for a half-cone lifting entry geometry (Ref. 79).

Pitch-roll coupling through bow shock induced crossflow, in addition to the dynamic pressure deficit, could be another entropy wake effect, according to Hart's findings (Ref. 80). The Edney-effect, i. e., bow shock-wing shock interaction, is another interference effect that can cause problems (Ref. 81). However, the problem is mainly one of increased heating and is not causing any substantial vehicle dynamics problem. In addition, it is not likely to occur as readily for the delta winged vehicles as for the straight winged ones, where it is unavoidable unless the angle of attack is very, very large (Refs. 82 and 83).

2.5 FOREBODY VORTICES

It is now well documented that long slender bodies start to develop free vortices at moderate angles of attack, and that the vortex shedding becomes asymmetric at some high angle of attack (Refs. 84 to 86) with the result that large side forces and yawing moments are generated at zero sideslip (Refs. 87 to 90 and Fig. 54). The phenomenon shows α -hysteresis (Fig. 55 and Ref. 88). The direction of the side force and moment is determined by minute model asymmetries as it seems to be body-fixed (Fig. 56 and Ref. 89). The magnitude is determined by the nose geometry, a slender nose giving larger magnitudes than a more blunt nose, and by the nose boundary layer, mainly because of the decreased wake width (Ref. 89). As the angle of attack is increased more vortices are shed, the axial separation distance being that fixing a separation in time in the cross flow plane determined by von Karman's theory. At some angle of attack below $\alpha = 90$ deg this space-time equivalence breaks down and von Karman type vortex shedding starts (Refs. 86 and 89). As a result of this, the direction of the side moment can change sign several times for a long body as vortices are added with increased α (Fig. 57 and Refs. 85 and 87). An asymmetric roughness strip on the nose fixes the asymmetry and can cause greatly increased side forces (and moments) (Fig. 58 and Ref. 88). Even the unintentional body asymmetry completely dominates over roll

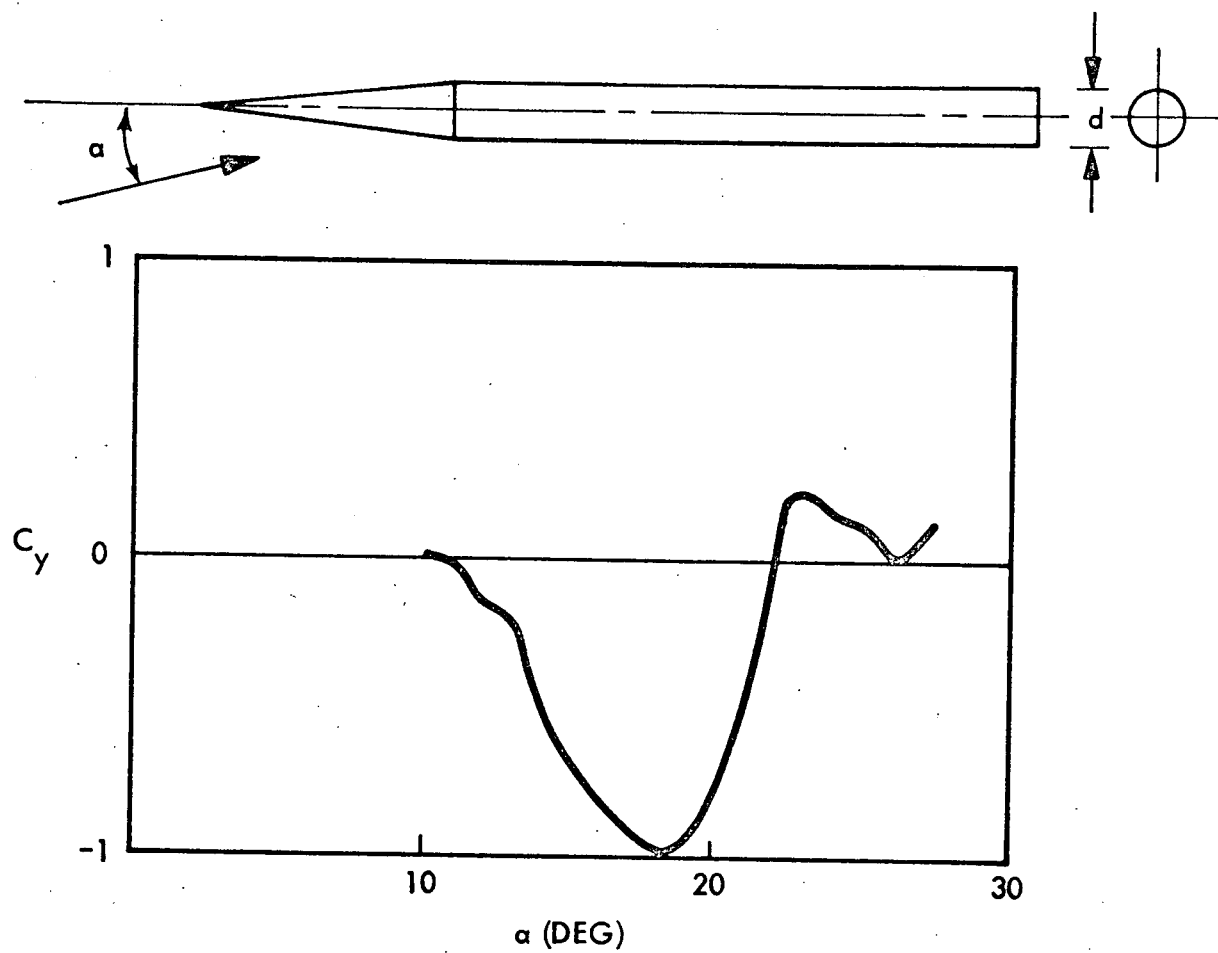


Fig. 54 Side Force at Zero Yaw as Function of Angle-of-Attack for Cone-Cylinder Body at $M = 2$ and $R_d = 2.6 \times 10^6$ (Ref. 87)

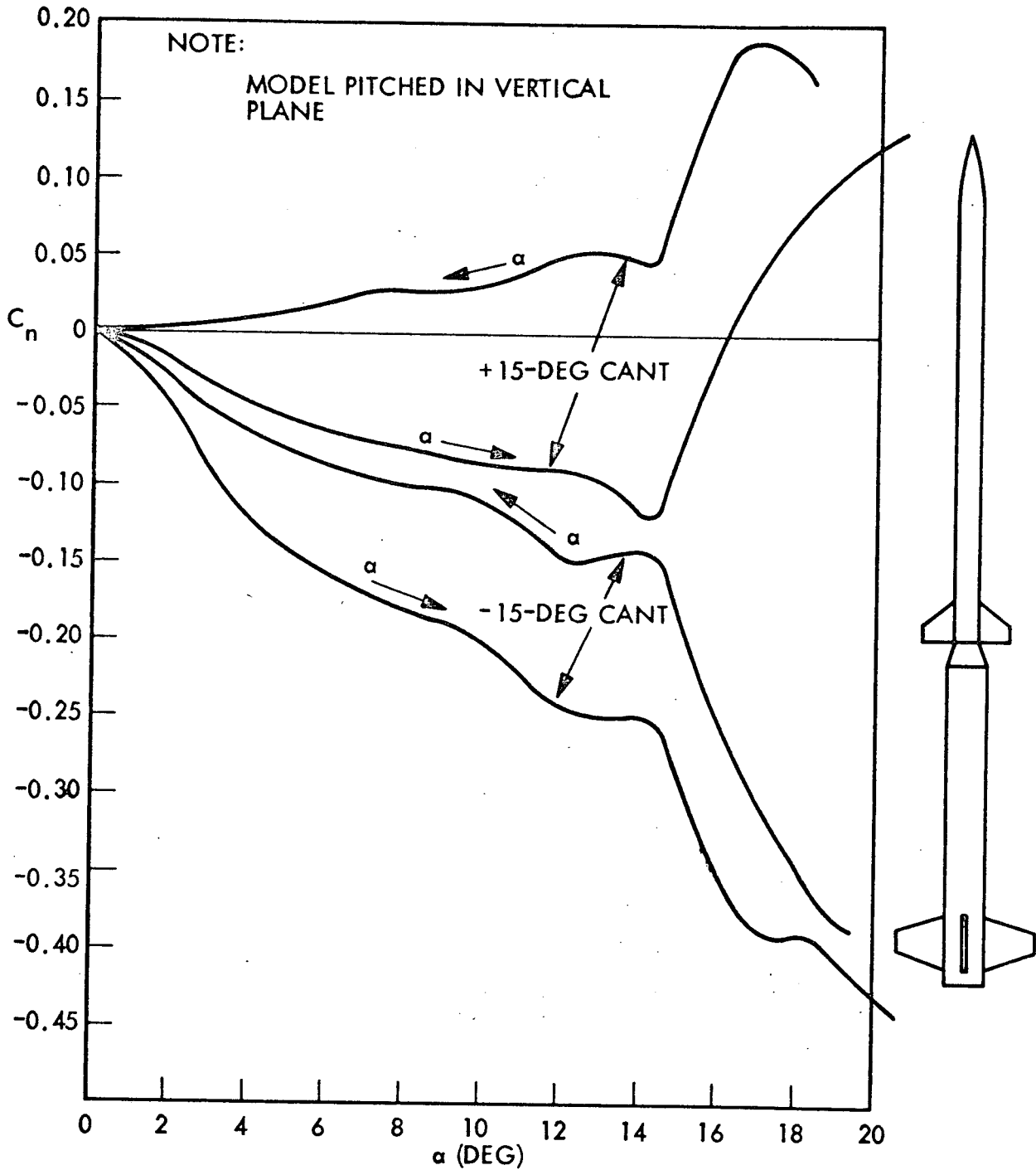


Fig. 55 Side Moment Coefficients Measured on Tomahawk With ± 15 -deg Fin Cant (Ref. 88)

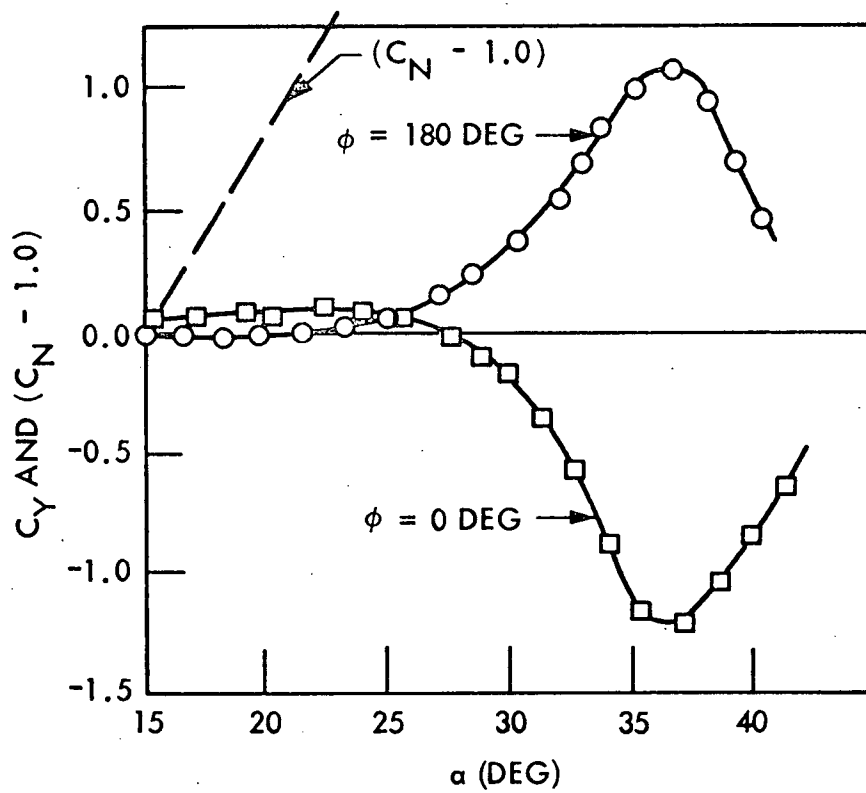
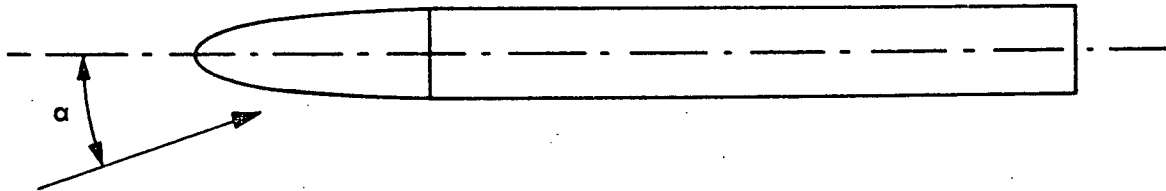


Fig. 56 Side Force at Zero Yaw and Various Roll Angles For an Ogive-Cylinder at $M = 0.7$ (Ref. 89)

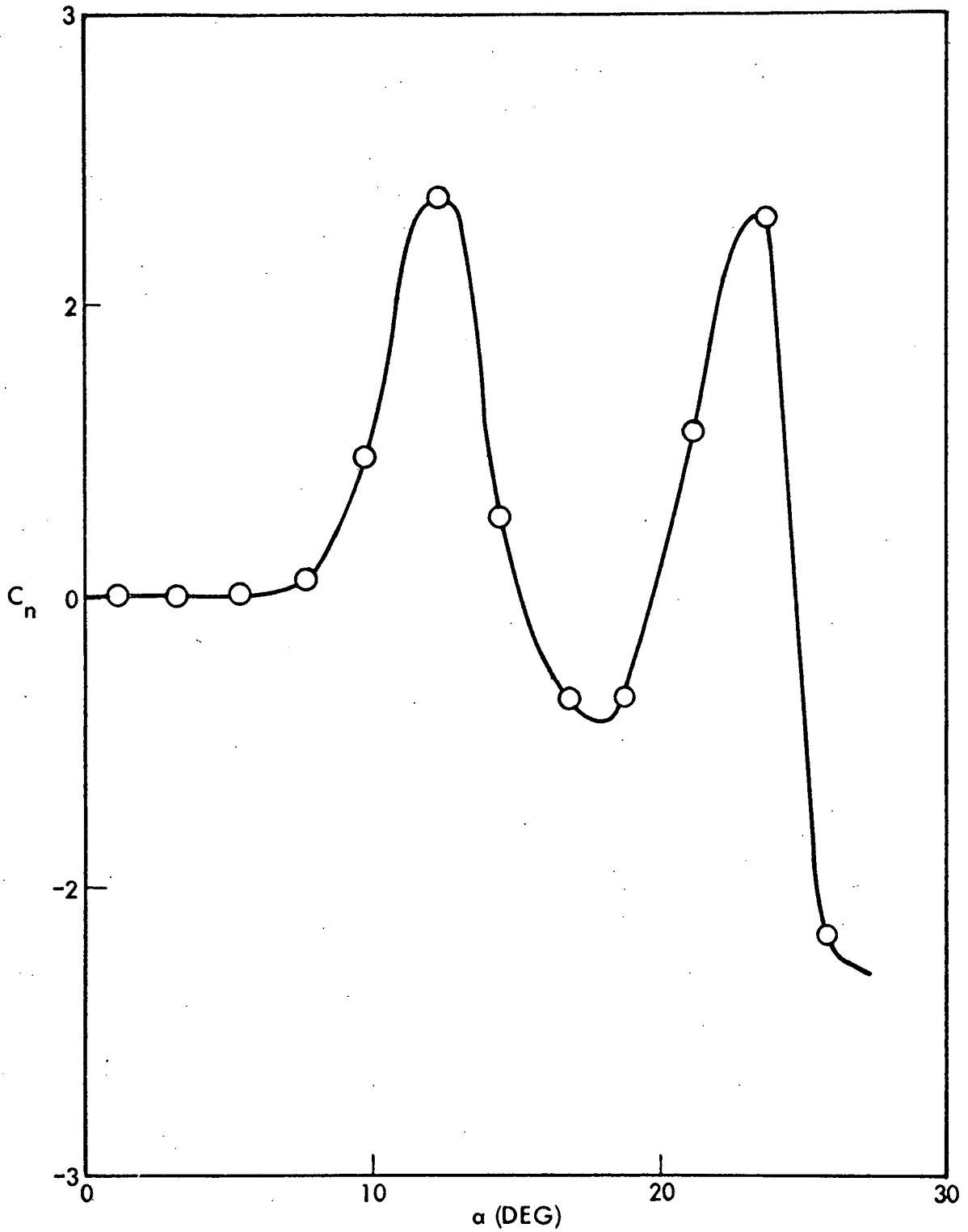


Fig. 57 Side Moment at Zero Yaw for Cone-Cylinder at $M = 0.5$ (Ref. 87)

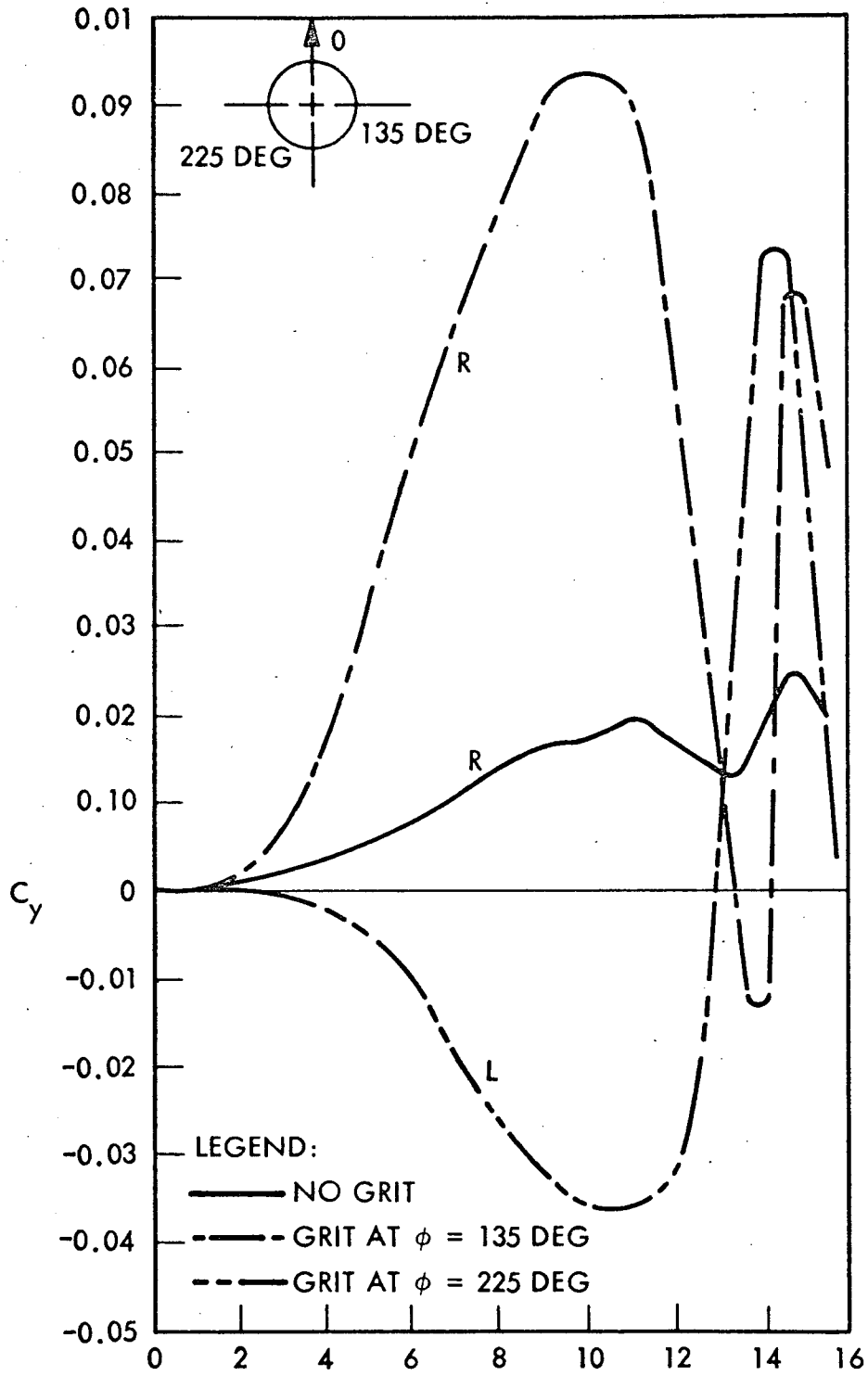


Fig. 58 Side Force Coefficients on Tomahawk at Zero Spin With and Without 1/4-in.-Wide Longitudinal Strips of No. 40 Grit (Ref. 88)

rate effects (Fig. 59 and Ref. 87). For a blunt nose the steady asymmetric vortex geometry is more difficult to establish, i. e., the vortices usually show some degree of unsteadiness (Ref. 90). Pick shows how the vortex induced asymmetric aerodynamic characteristics can be determined through simple analytic expressions (Ref. 89).

It has been recognized for some time now that free vortices from the slender forebody of modern fighters can cause adverse lateral characteristics strong enough to make the flat spin modes unrecoverable (Fig. 60 and Refs. 91 to 93). In one investigation the adverse yawing moment characteristics were very repeatable (Fig. 61 and Ref. 92), whereas in other experimental investigations large differences between repeat runs have been found (Fig. 62 and Refs. 93, 94). Even if the cross section is noncircular, rounded corners usually lead to problems with large jumpwise changes in aerodynamic characteristics when the crossflow changes from subcritical to supercritical (Ref. 95).

In aeroballistics and reentry body industry the effects of asymmetry have long been recognized (Refs. 96 to 99), resulting in roll-lock in and coning motions which are the low angle of attack equivalent to the aircraft spins (Refs. 91 to 93). The asymmetry can in this case be a combination of mass and geometric asymmetries (Refs. 98 and 100). At slightly higher angles of attack the tilting of the symmetric vortex pair shed from a slender forebody can provide the driving force. It has been shown that the induced crossflow at the nose sets the vortex asymmetry, thus accounting for the major portion of the induced side moment (Fig. 63, Refs. 101 and 102). The remainder of the side load is probably the result of unequal vortex strength.

In addition to the local effect at the nose, the forebody vortices can affect the vertical tail loads.* The oilflow photograph in Fig. 2a shows stagnation region on the leeward fuselage which is the result of the flow entrained by the forebody vortices stagnating on the upper surface (Fig. 3). Incidentally, the photograph also shows a constant azimuth for the stagnation region, i. e., the "tilting" of the forebody vortices is set at the nose. The entrained flow constitutes a region of excess velocity (Fig. 64). Thus,

*Such forebody vortices have been found to cause roll lock-in due to interaction with folded out fins on a square bomb (Ref. 103) and have also been observed to interact with flap induced flow separation regions (Ref. 104).

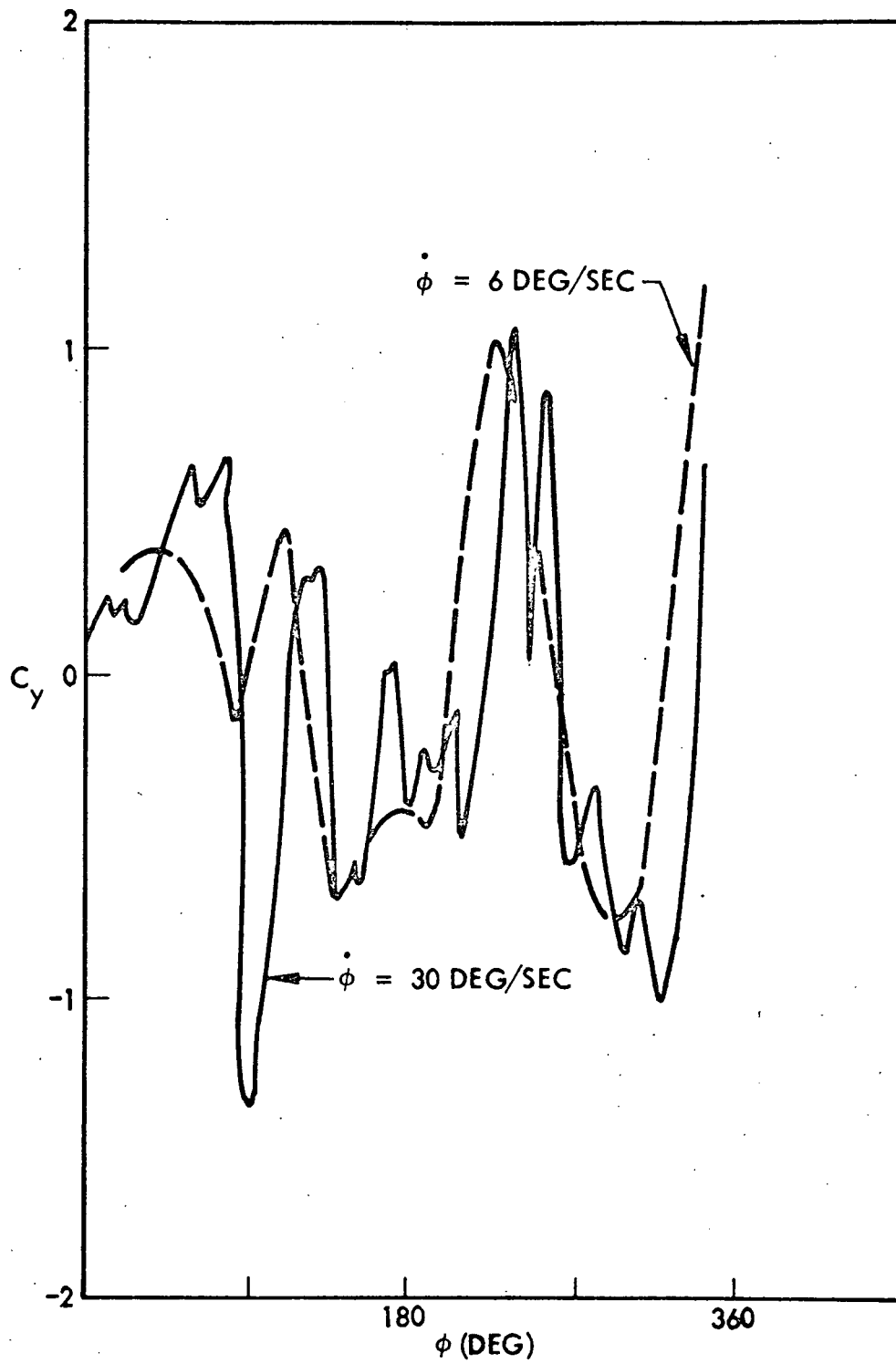


Fig. 59 Effect of Roll Orientation and Roll Rate on Side Force at $\alpha = 18$ deg and $\beta = 0$ for Cone-Cylinder at $M = 0.5$ (Ref. 87)

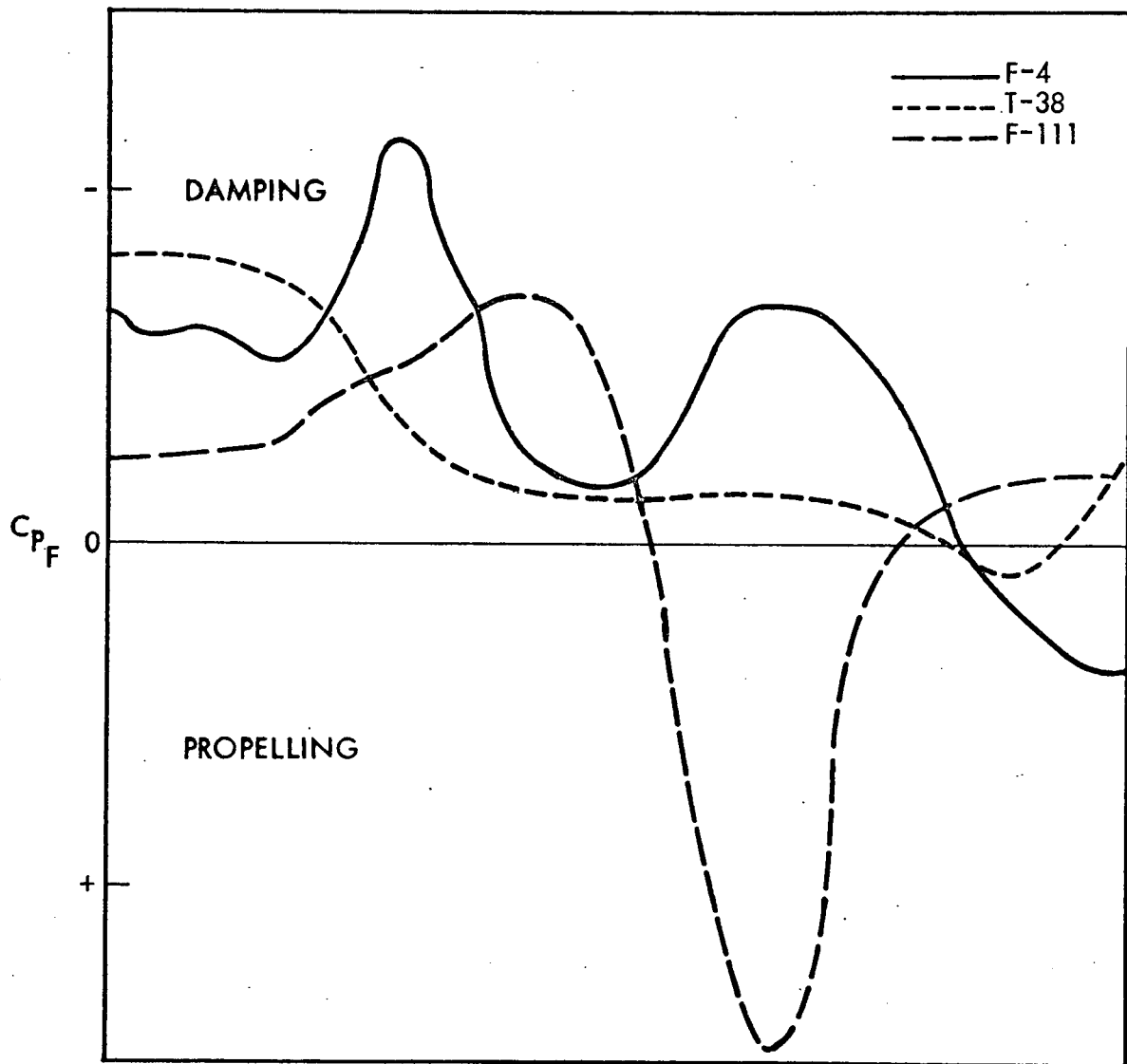


Fig. 60 Yaw Rate Damping Characteristics as Function of Angle of Attack for Several High Performance Fighter Aircraft (Ref. 91)

2-80

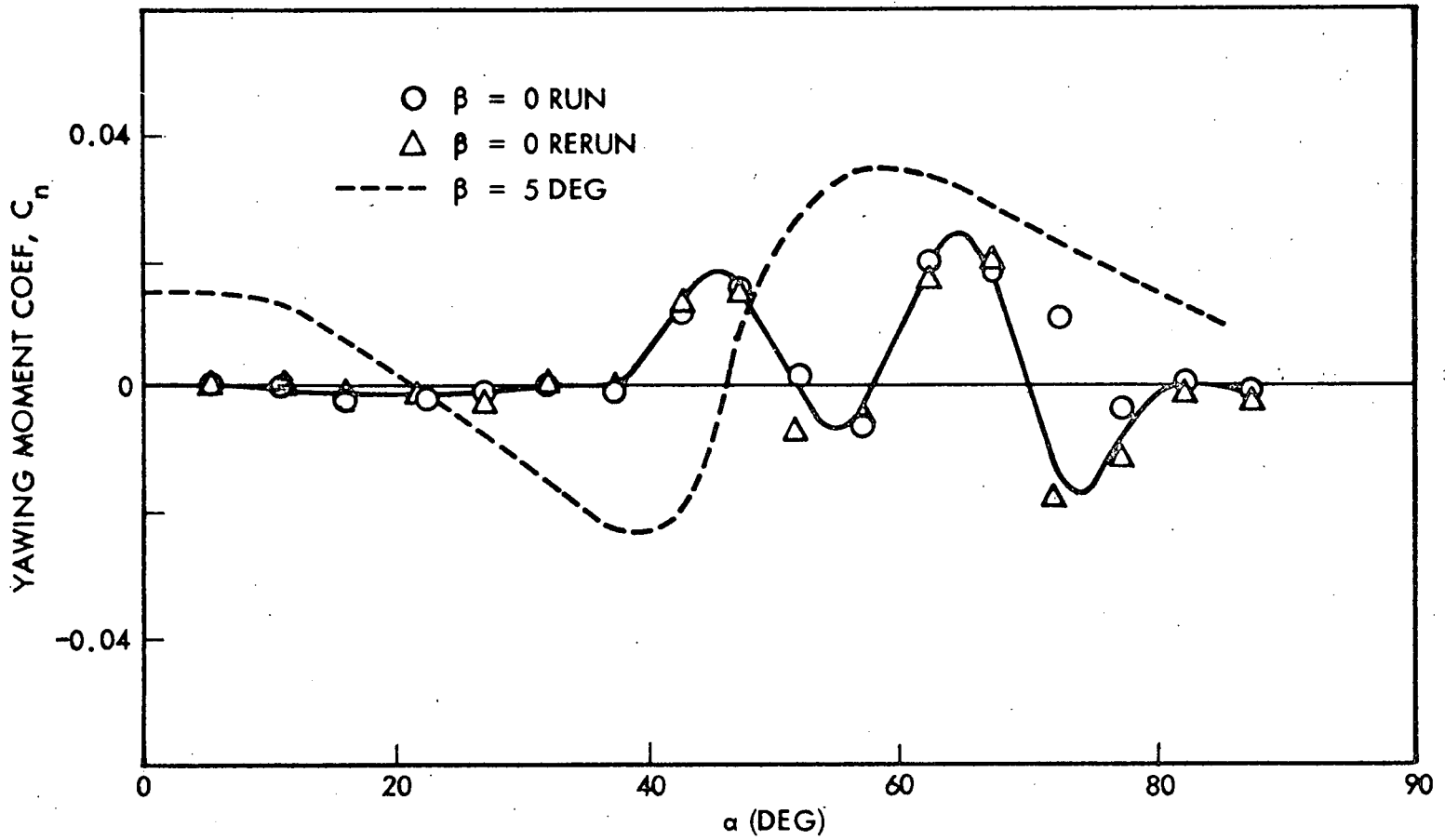
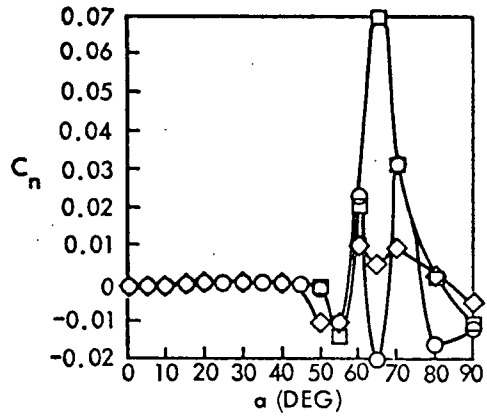
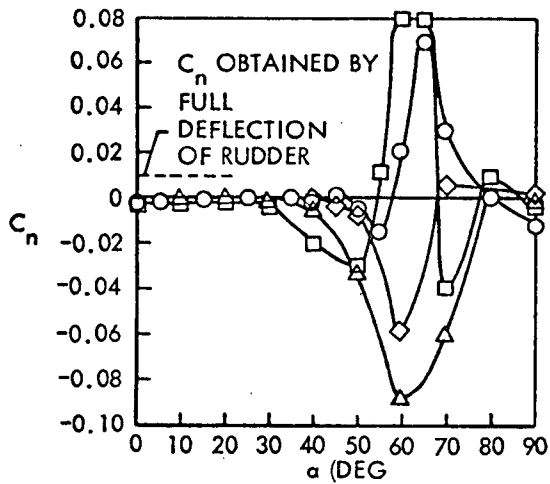
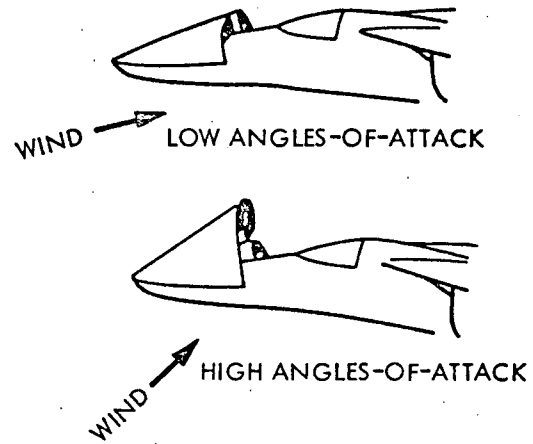


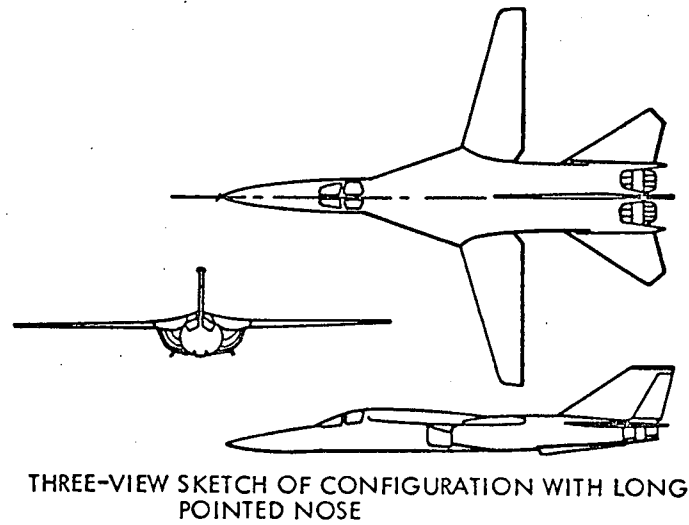
Fig. 61 Example of Yawing Moments at $\beta = 0$ (Ref. 92)



(a) VARIATION OF YAWING-MOMENT COEFFICIENT WITH ANGLE-OF-ATTACK; SYMBOLS INDICATE VALUES OBTAINED IN SEVERAL REPEAT TESTS



(b) VARIATION OF STATIC YAWING-MOMENT COEFFICIENT WITH ANGLE-OF-ATTACK FOR SEVERAL MODELS OF THE CONFIGURATION; $\beta = 0$ DEG



THREE-VIEW SKETCH OF CONFIGURATION WITH LONG POINTED NOSE

Fig. 62 Lack of Repeatability of Side Moments Induced by Free Forebody Vortices at Zero Yaw (Ref. 93)

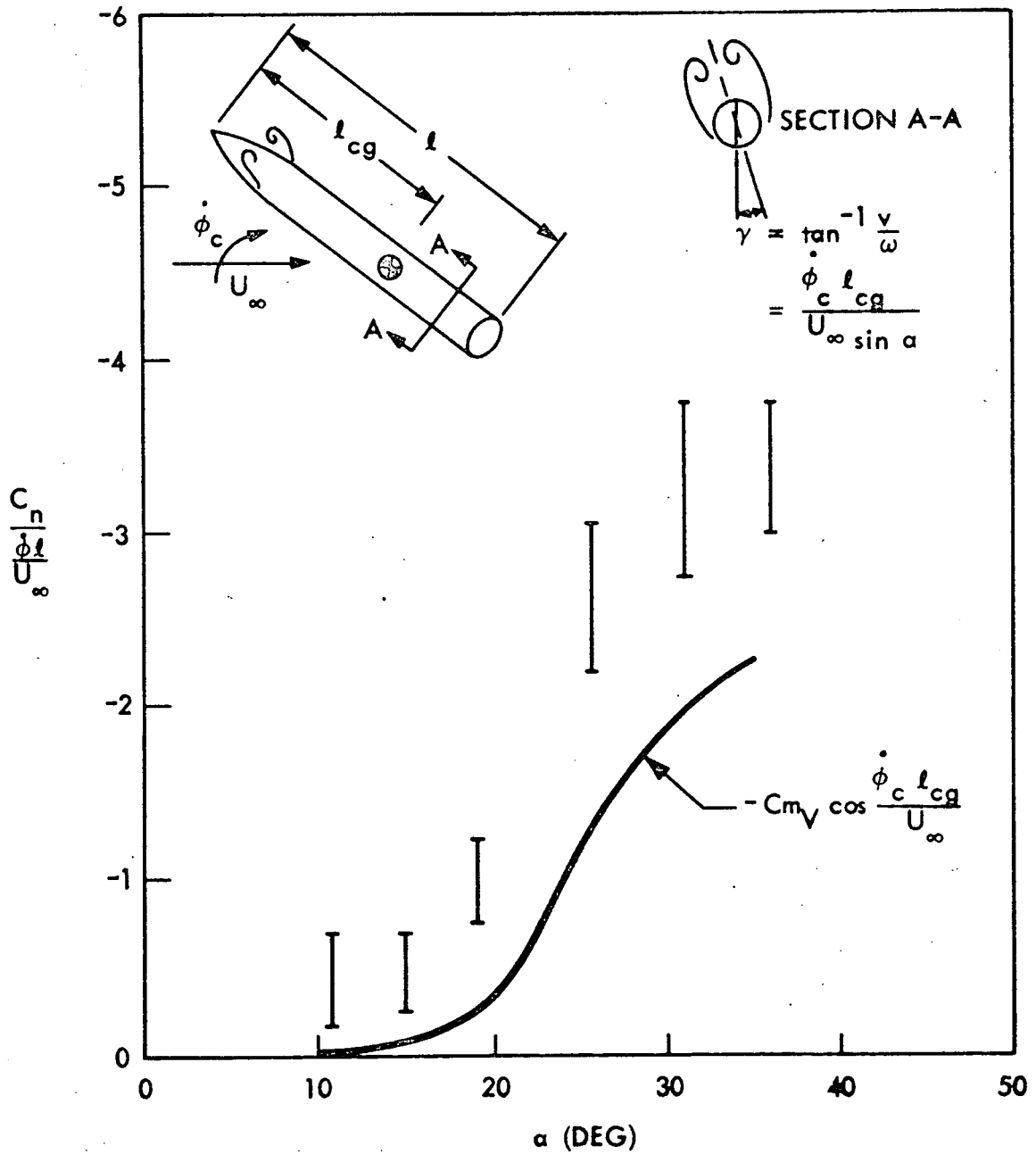


Fig. 63 Correlation of Dynamic Vortex Induced Yaw Moment (Ref. 101)

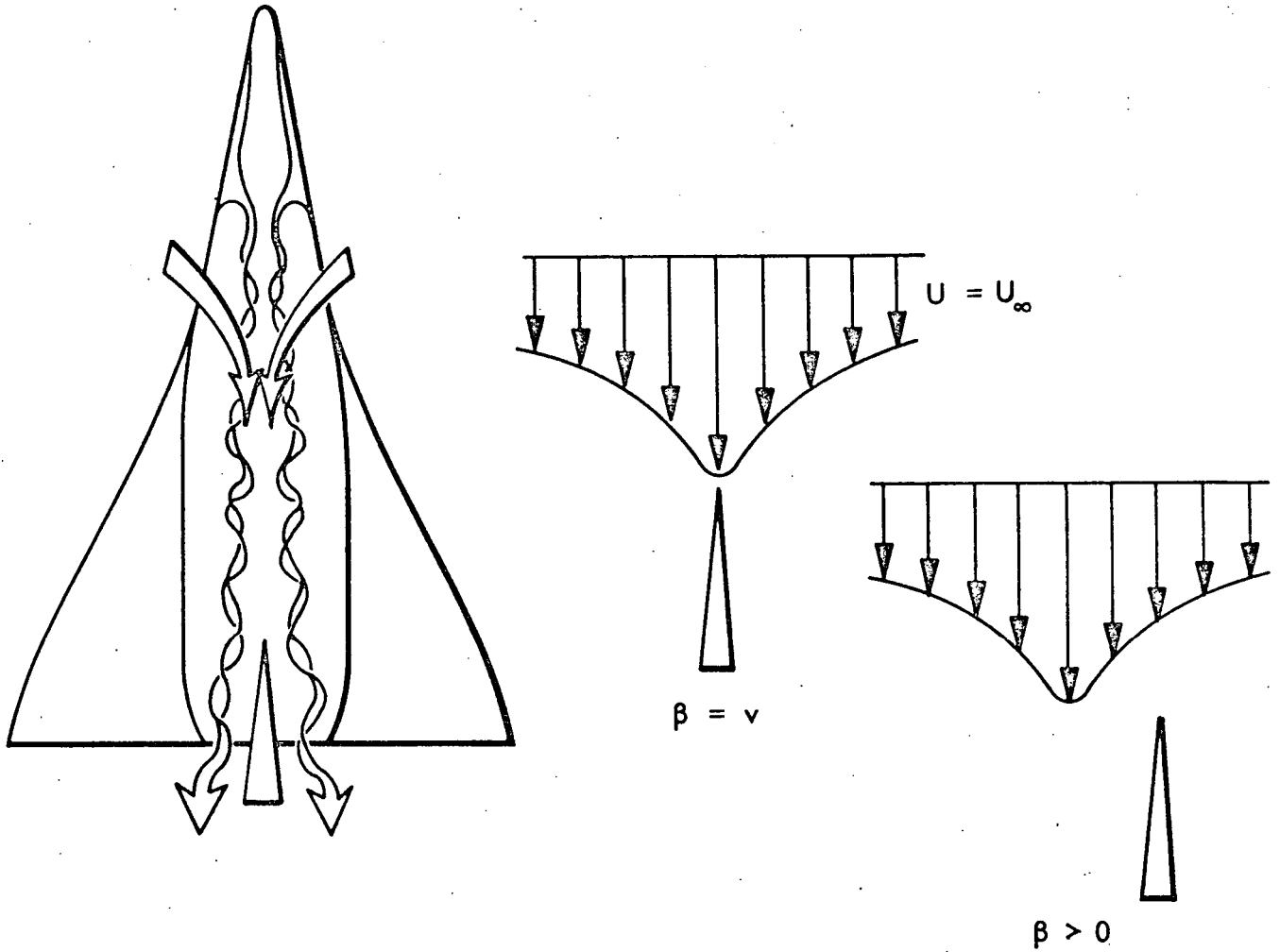


Fig. 64 Effect of Forebody Vorticity on Velocity Profile at Tail

when the vehicle yaws the vertical tail is subjected to decreasing velocities (i. e., decreasing dynamic pressures). The velocity gradient, however, subjects one side of the wedge tail to higher dynamic pressures than the other. This is similar to the wedge fin submerged in the shear flow generated by nose induced separation (Fig. 65 and Ref. 105); a load is induced in the direction of decreasing velocity. Likewise, for positive β a positive induced side force will result. Increasing the wedge angle effectively increases the average differential dynamic pressure, which increases the induced load (Fig. 66 and Ref. 24). The induced load may or may not be larger than the load component due to the local flow angle. In the case of the tail with drag brake the induced load is large enough to cause a reversal in the incremental drag brake load at $M = 2.5$ and to nearly eliminate it at $M = 4.6$. This is not the result of an ordinary loss of tail effectiveness at high angle of attack due to body shielding. One would expect the shielding effect to be the same for both the pure 10 deg wedge tail and the tail with the simulated 70 deg drag brake. Certainly shielding effects would not cause a reversal in the sign of the drag brake load. What is more likely is that the local load vanishes or nearly vanishes due to shielding, allowing the vortex induced load to dominate. The effect of forebody vortices, both the local effect at the nose and the induced effect at the tail, are statically destabilizing in yaw (Fig. 67 and Ref. 25). Thus, the induced tail load will add dynamic stability due to the finite time lag required to convect the vortices from the nose to tail. However, static instability is in itself a serious problem that can result in a sustained spin (Ref. 27). Furthermore, in the case of the shuttle it would require large amounts of reaction control propellant to maintain stability (Refs. 106 and 107). Thus, it appears highly desirable to eliminate or minimize these effects, if at all possible.

2.6 AVOIDING THE PROBLEMS

Perhaps the best way to eliminate these stability problems is to traverse the regions of instability quickly, and to avoid flying close to an unstable flow boundary (see Fig. 52); thus avoiding involuntary realization of adverse unsteady flow effects due to control deflection, gust, etc. From the preceding discussions the flow phenomena to avoid are:

1. High speed shock induced separation
2. Sudden leading edge stall

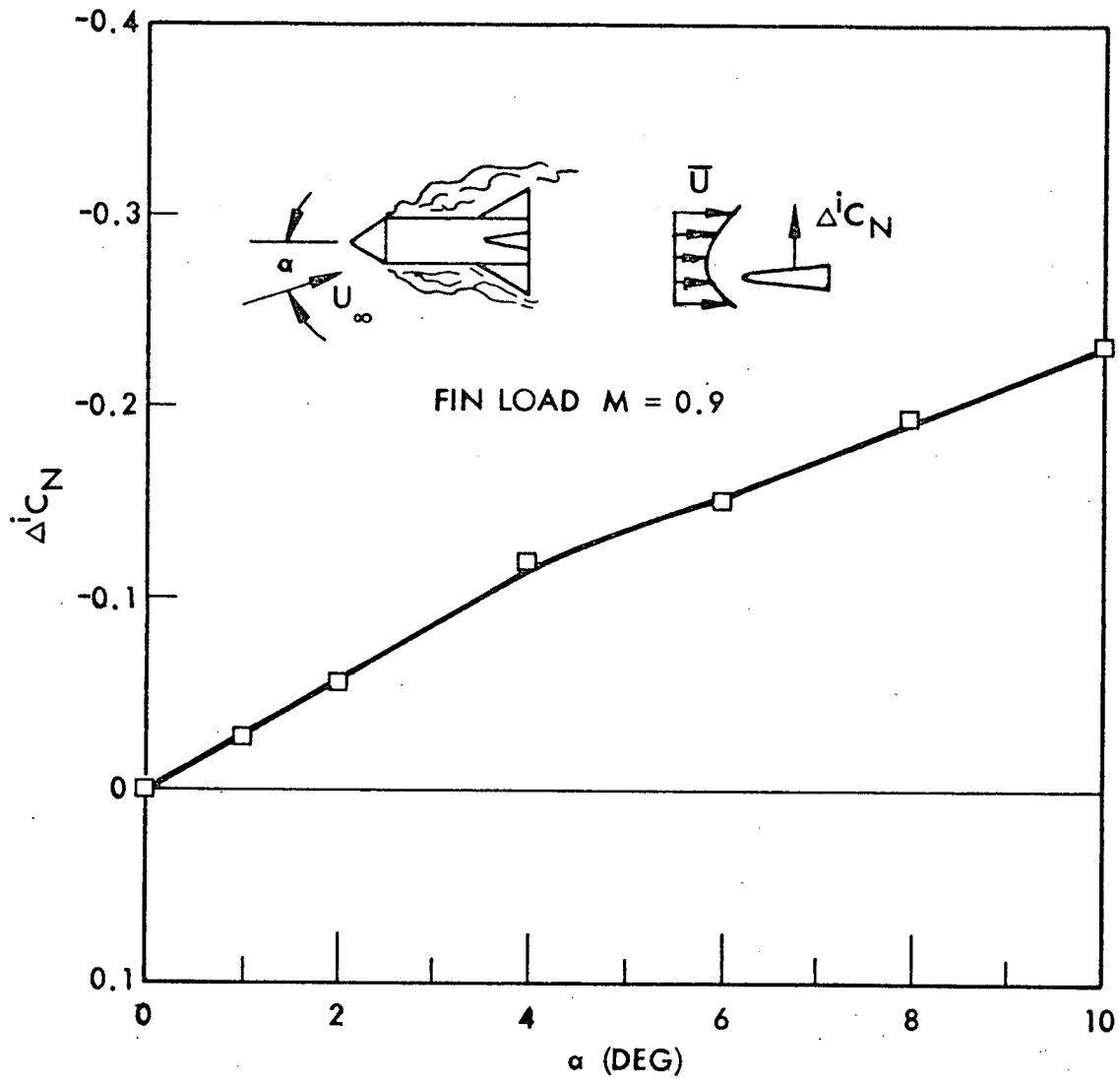


Fig. 65 Effect of Shear Flow on Fin-Induced Pitching Moment (Ref. 105)

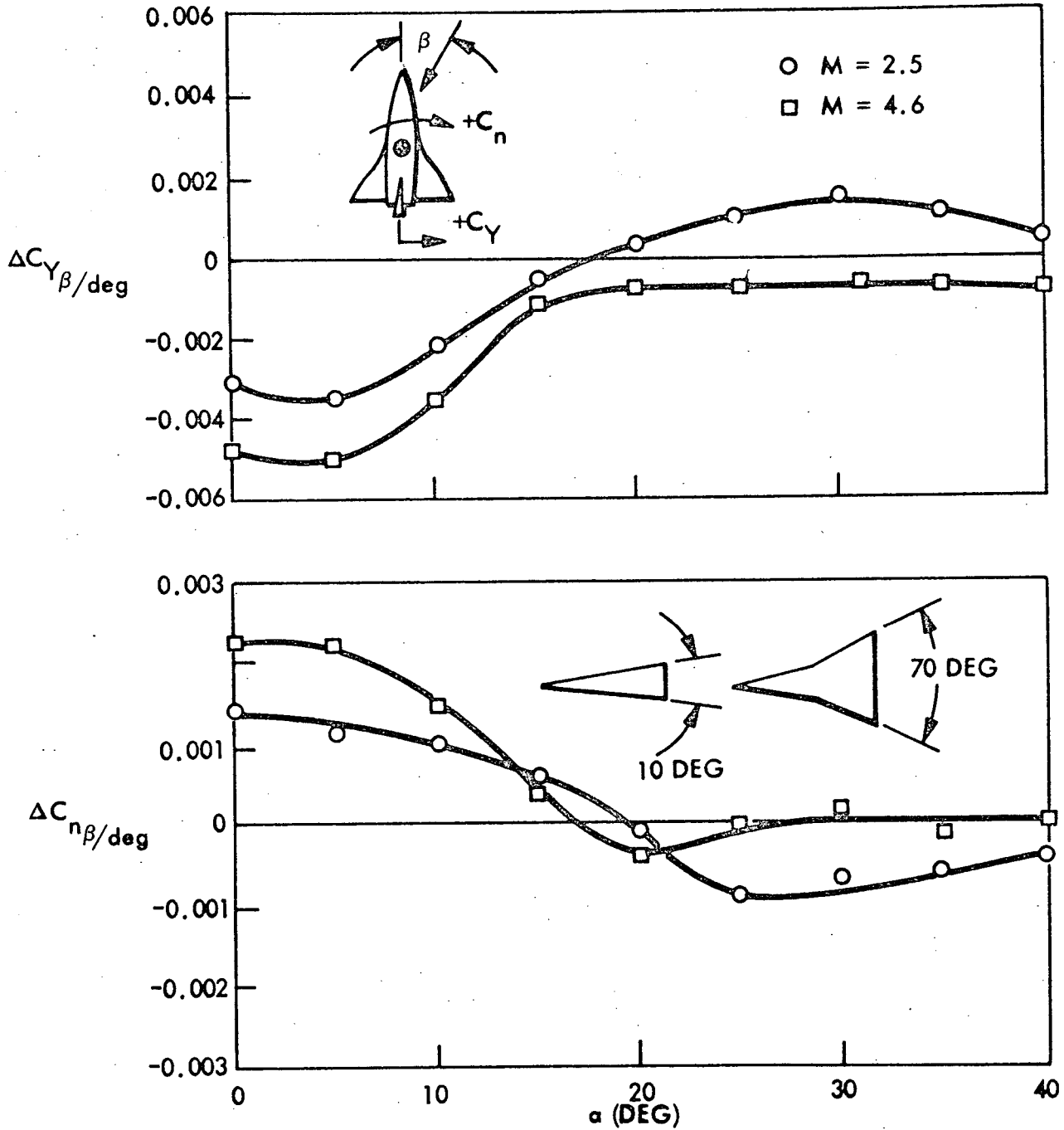


Fig. 66 Effect of Drag Brake on Directional Stability, NAR Orbiter (Ref. 24)

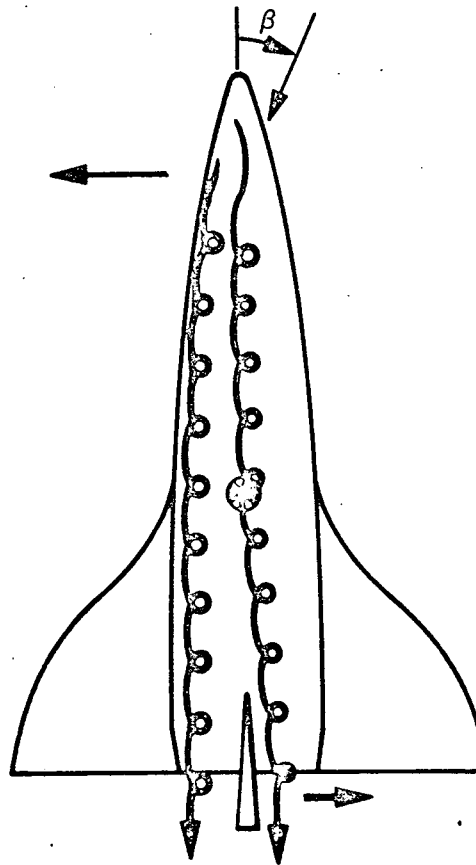
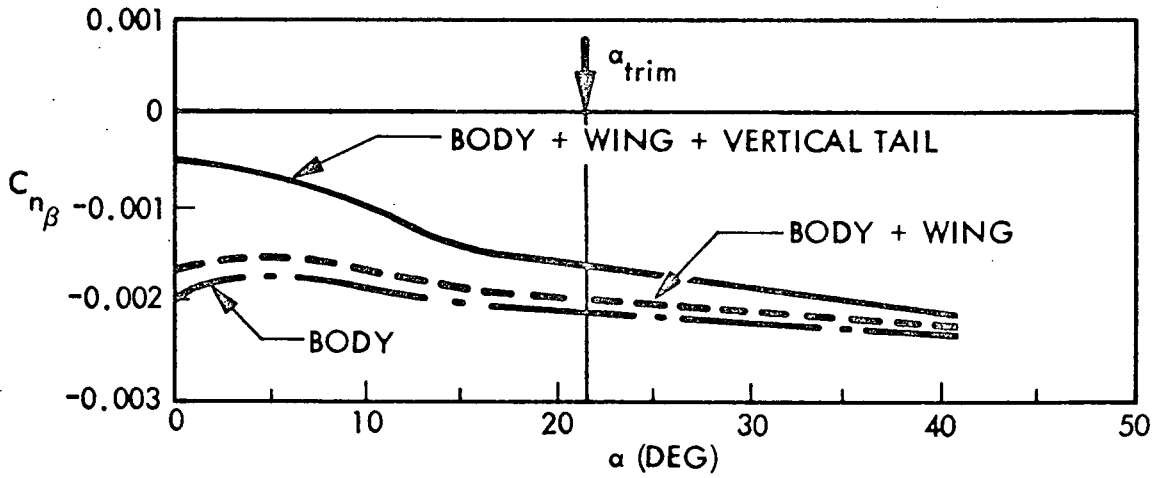


Fig. 67 Component Buildup Yaw Characteristics, NAR Orbiter, $M = 6.0$ (Ref. 25)

3. Vortex burst
4. Bow shock-flap shock interaction
5. Forebody vortices

The last item, the effect of forebody vortices, cannot be avoided by trajectory shaping alone, since the shuttle must fly at high angles of attack because of aerodynamic heating considerations.

A fictitious entry trajectory is superimposed on the boundaries of the NAR entry corridor as an illustration of one way of minimizing the deleterious effects of unsteady flow phenomena (Fig. 68). The trajectory is fictitious in the sense that it was constructed without regard to meeting cross range and aerodynamic heating requirements.* It is only an illustration of the philosophy of avoiding unfavorable flow regions. At any rate, the philosophy is to stay above the region of shock induced separation as long as possible; then to traverse it quickly and remain well below the lower bound to avoid control induced separation. In addition, it may be necessary to limit control deflection. Thus, the trajectory resembles the ones in Fig. 52 except for staying farther away from the lower bound of the shock induced separation region. The second passage through the shock induced separation region should be made at low angle of attack. It appears that by so doing it may be possible to avoid the region of sudden L. E. stall (Figs. 18 and 19, Ref. 39). At lower Mach number a return to the baseline trajectory seems permissible; however, it may be necessary to limit control deflection to avoid control induced vortex burst.

An alternate scheme that might be applied to a reduced cross range trajectory (Ref. 108) could be to stay above the shock induced separation region and below the control power limit, thus reaching the subsonic cruise attitude at about $M = 1.2$ (alternate trajectory of Fig. 68). This, of course, supposes that a means can be found for moving the aft center of gravity stability boundary upward. Both the stability boundary and the control limit seem to be associated with vortex burst; either subsonic burst, or breakdown of the diffuse hypersonic L.E. vortex. As the location of

*If cross range requirements were relaxed it would certainly simplify the flight dynamics problem.

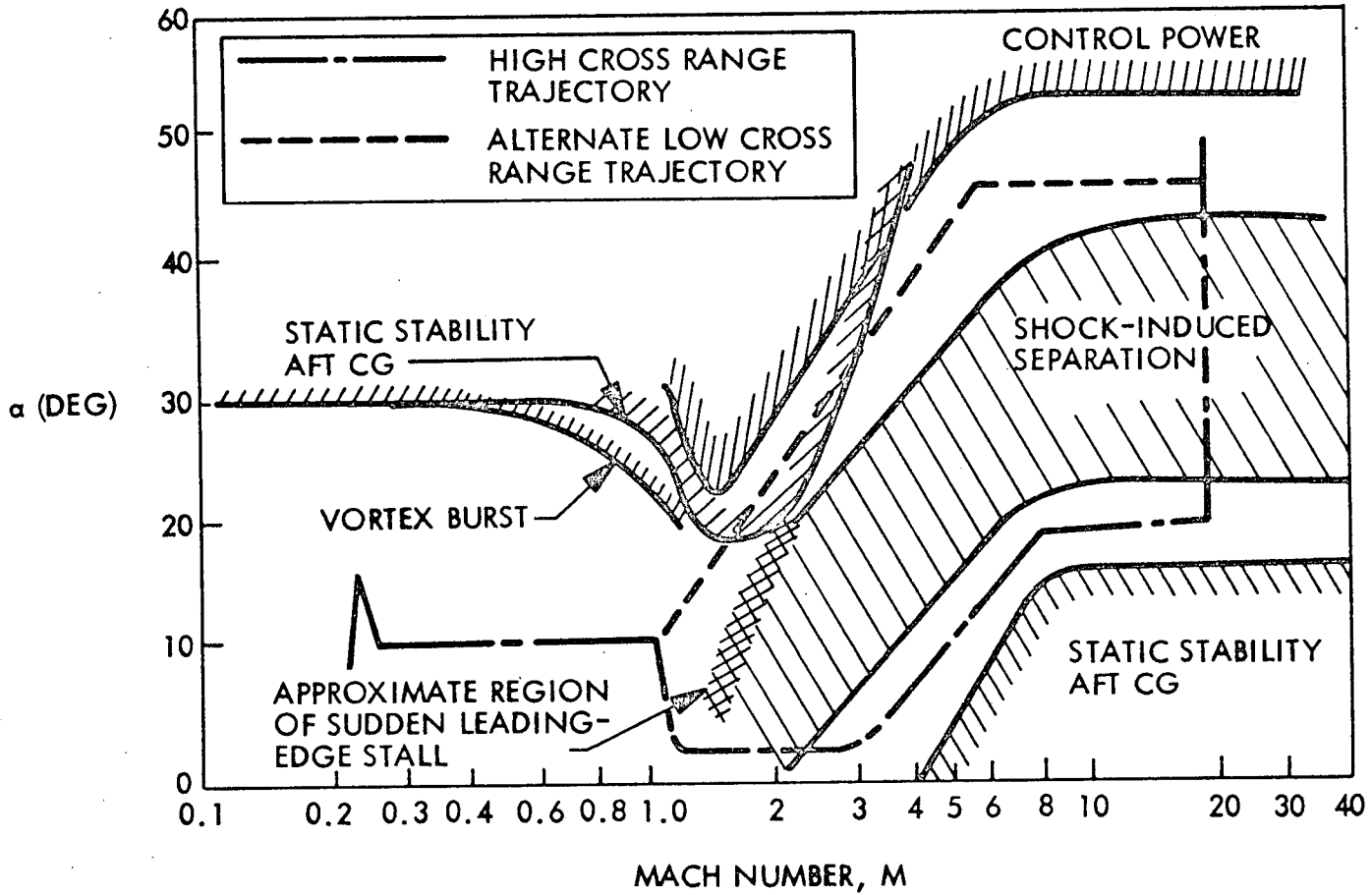


Fig. 68 Sample Trajectories to Minimize Unsteady Aerodynamic Effects

the vortex burst boundary between $M = 1.2$ and 2.0 is unknown, the alternate trajectory could still traverse the region of vortex burst.

It might be possible to gain leeway for a trajectory like this by increasing the leading edge sweep, thereby lowering the upper angle of attack boundary for shock-induced separation (see Figs. 5, 6, and 68). This would also delay vortex burst, thereby widening the space shuttle reentry corridor by raising the stability and control boundaries to higher angles of attack since increasing sweep angle delays subsonic vortex burst (Fig. 27 and Ref. 58). There is no reason to believe it would do otherwise at higher speeds. When L. E. stall occurs the leading edge flow is subsonic, and increased sweep will energize the vortex core flow to delay burst just as in the low speed case. Increasing sweep also eliminates the dangerous mixed leading edge flow condition shown earlier in Fig. 22 (Ref. 109 and Fig. 69).

As the vortex breakdown moves aft with increasing sweep, it should be possible to find a double-delta planform that does not get vortex burst forward of the trailing edge for the operational α - β -range of the space shuttle vehicle. That is, the inner wing is given high enough sweep and the less swept outer wing is made short enough to keep vortex breakdowns off the wing area. McMahan and Kohlman (Refs. 60, 110, and 111) have tested double delta planforms and find that the vortex burst is delayed. Their inner wing is very short - they correctly name it a strake - and the outer wing vortex is by far the stronger vortex, wrapping the strake vortex around itself starting already at $\alpha = 7$ deg (Fig. 70a). This results in smooth C_L - and C_m -characteristics up until vortex burst for the combined ogee-type leading edge vortex. It is interesting to note that the added forebody strake or inner delta wing induces substantial lift on the aft (main delta) wing surface, balancing the forebody strake lift (Fig. 70b). Sachs et al. investigate a similar double-delta planform (Ref. 112), although the difference in sweep angles between inner and outer wings is larger, resulting in larger reshaping of the combined vortex (Fig. 70c). When the inner wing is large, i. e., not a strake, the inner vortex is dominant and will wrap the outer vortex around itself at some angle of attack considerably below that for inner vortex breakdown. This lift-off of the outer vortex

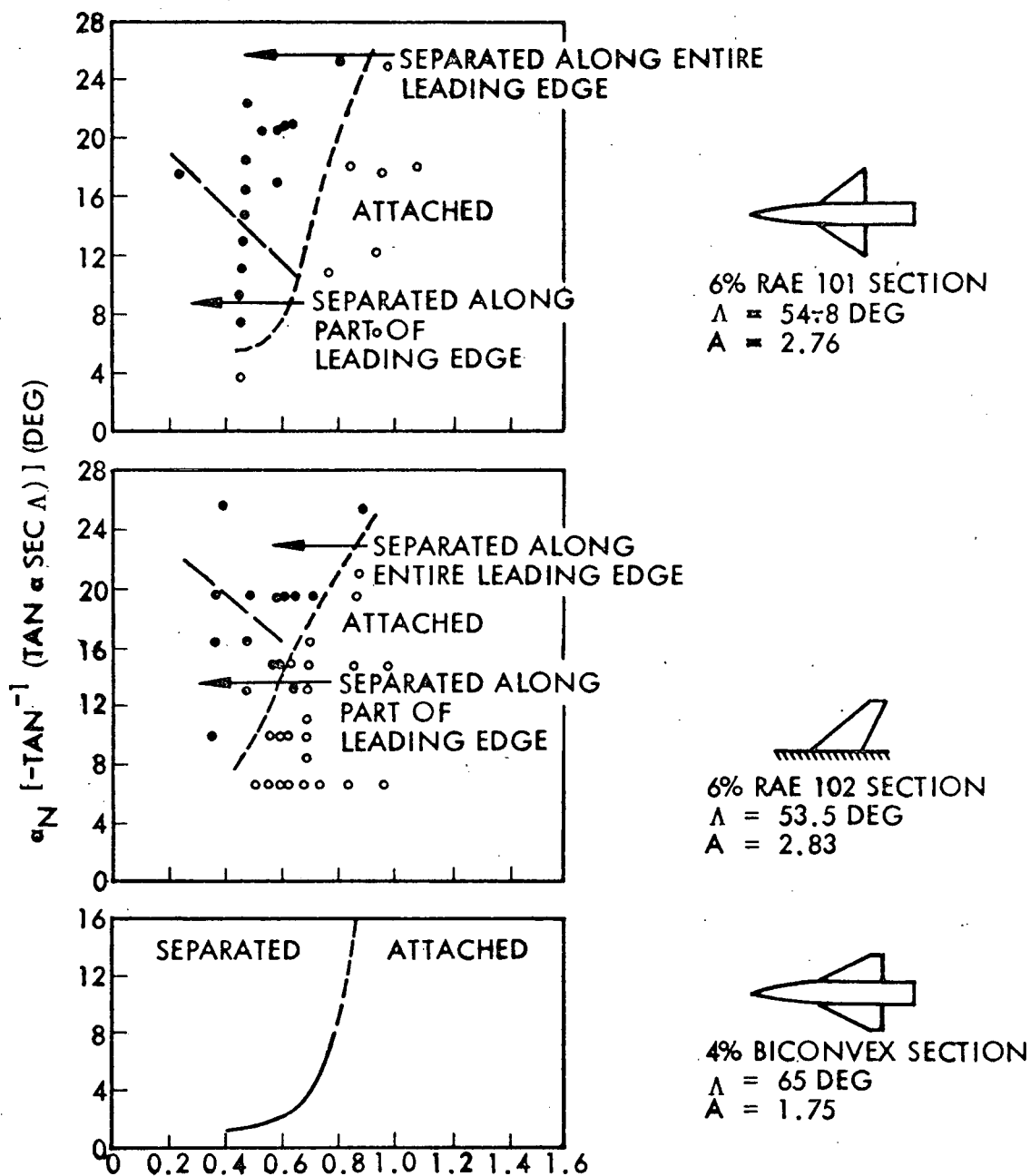
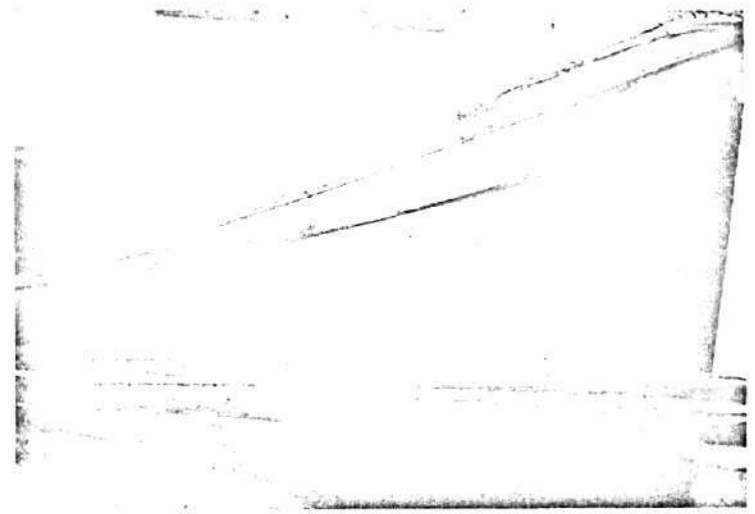


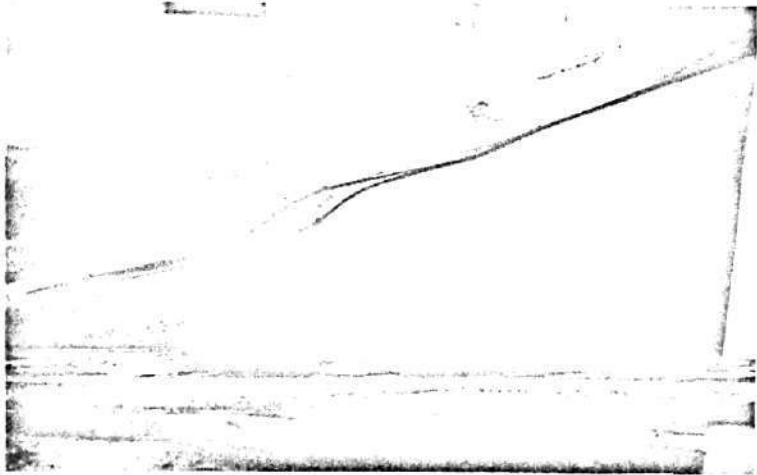
Fig. 69 Effect of Leading Edge Sweep on Mixed Leading Edge Flow Conditions



$\alpha = 5 \text{ DEG}$



$\alpha = 7 \text{ DEG}$



$\alpha = 10 \text{ DEG}$



$\alpha = 15 \text{ DEG}$

Fig. 70a Leading Edge Vortex Flow Characteristics of Double-Delta Wings

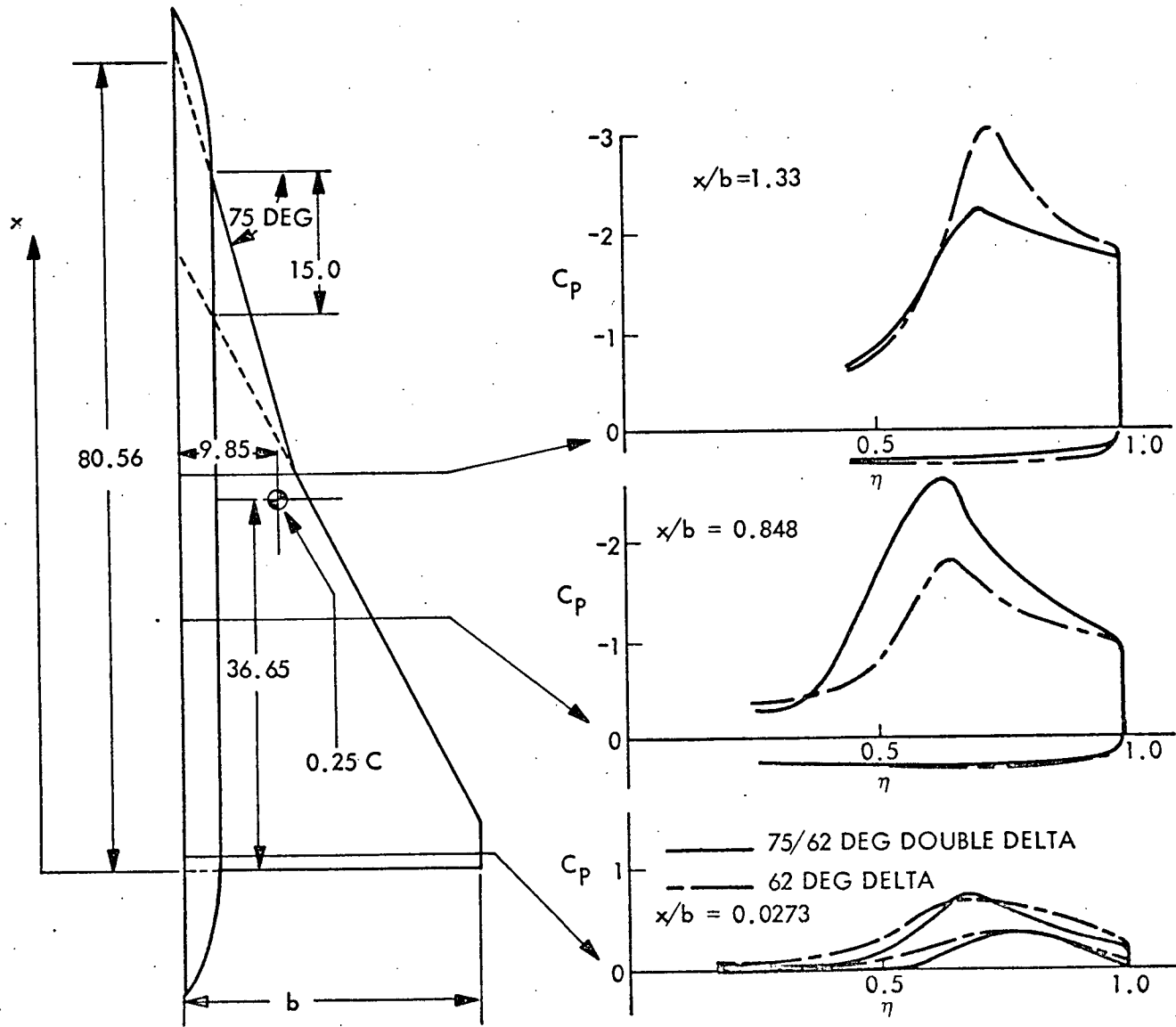
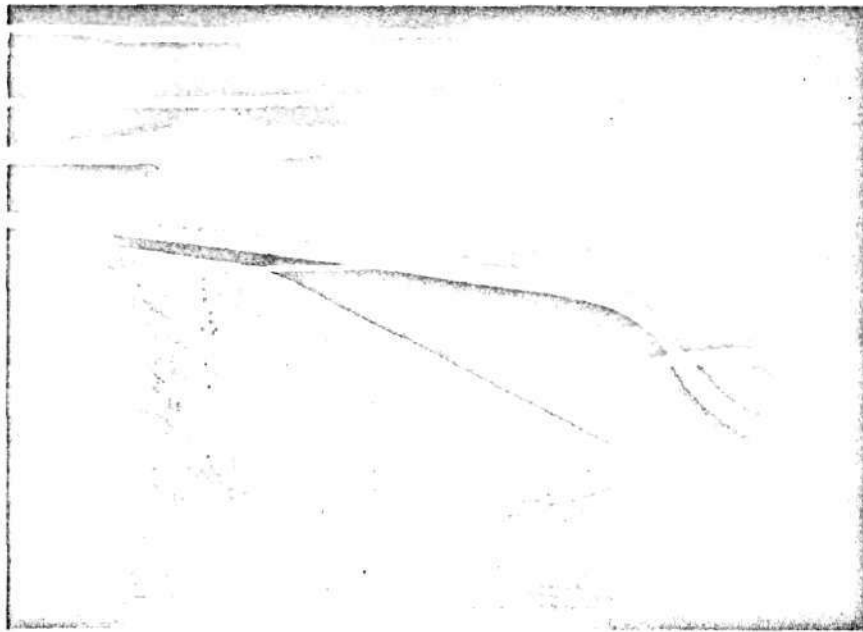
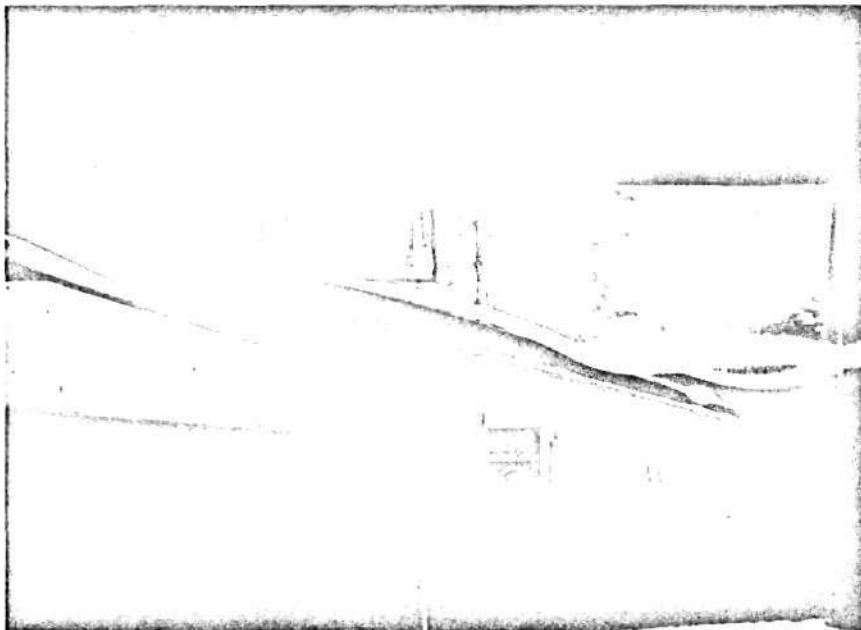
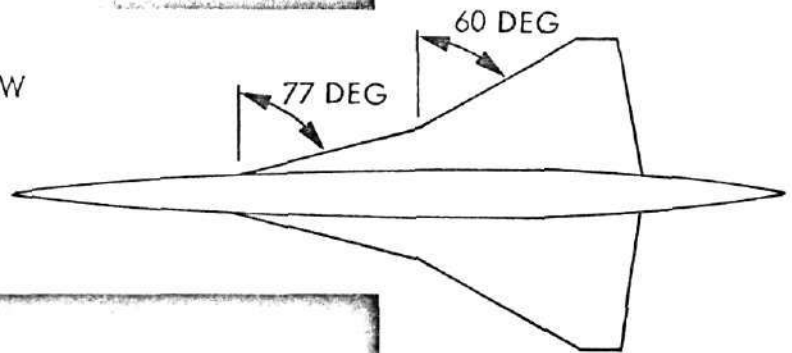


Fig. 70b Leading Edge Vortex Flow Characteristics of Double-Delta Wings



PLAN VIEW



SIDE VIEW

Reproduced from
best available copy.

Fig. 70c Leading Edge Vortex Flow Characteristics of Double-Delta Wings

deloads the outer wing and is as disastrous as vortex burst in regard to vehicle dynamics. This phenomenon was investigated extensively on the Swedish double-delta fighter "Draken" (Fig. 71) by one of the authors. The angle of attack for this interaction could be delayed by separating inner and outer vortices more in the spanwise direction, or by decreasing the strength of the inner wing vortex, e. g., by shortening the chord or by using nose droop or camber. Even if outer wing vortex lift-off occurs, flap controls on the inner wing would still remain effective, contrary to what is the case for delta wing vortex burst. It seems likely that some planform between that of the Swedish "Draken" (Fig. 71) and those tried by Wendtz and others (Refs. 68 to 70) should provide the needed solution for the space shuttle vehicle. It would also solve the alternating separated-attached leading edge problem discussed earlier (provided the inner wing is not just a strake) by fixing the demarcation line between attached and separated leading edge flow.

As vortex breakdown is caused by or associated with a stagnation of the core flow, and increasing sweep energizes the core flow, one would assume that a planform in which the sweep is increasing towards the trailing edge would delay vortex burst, and it does (Fig. 37 and Ref. 62). However, the effect is small compared to the beneficial effect of a double delta or ogee planform (compare wings 2 and 5 in Fig. 37) in which case better static stability characteristics is an additional bonus. Strategically placed tangential blowing slots could delay the vortex breakdown further (Refs. 114 and 115). This delay of vortex burst to a higher angle of attack means also a gain in lift. This is not always true if the delay is accomplished by delaying the initial vortex formation, e. g., by leading edge droop or apex drooping (Refs. 116 and 117). It appears, however, that a combination of curving the leading edge planform and convexing the upper surface could lead to some optimum design (Refs. 62, 65, 118).

The bow shock-flap shock interaction is avoided if windward side elevon deflections are limited such that they will not intercept the bow shock even under combined elevator-aileron deflections.

2-96

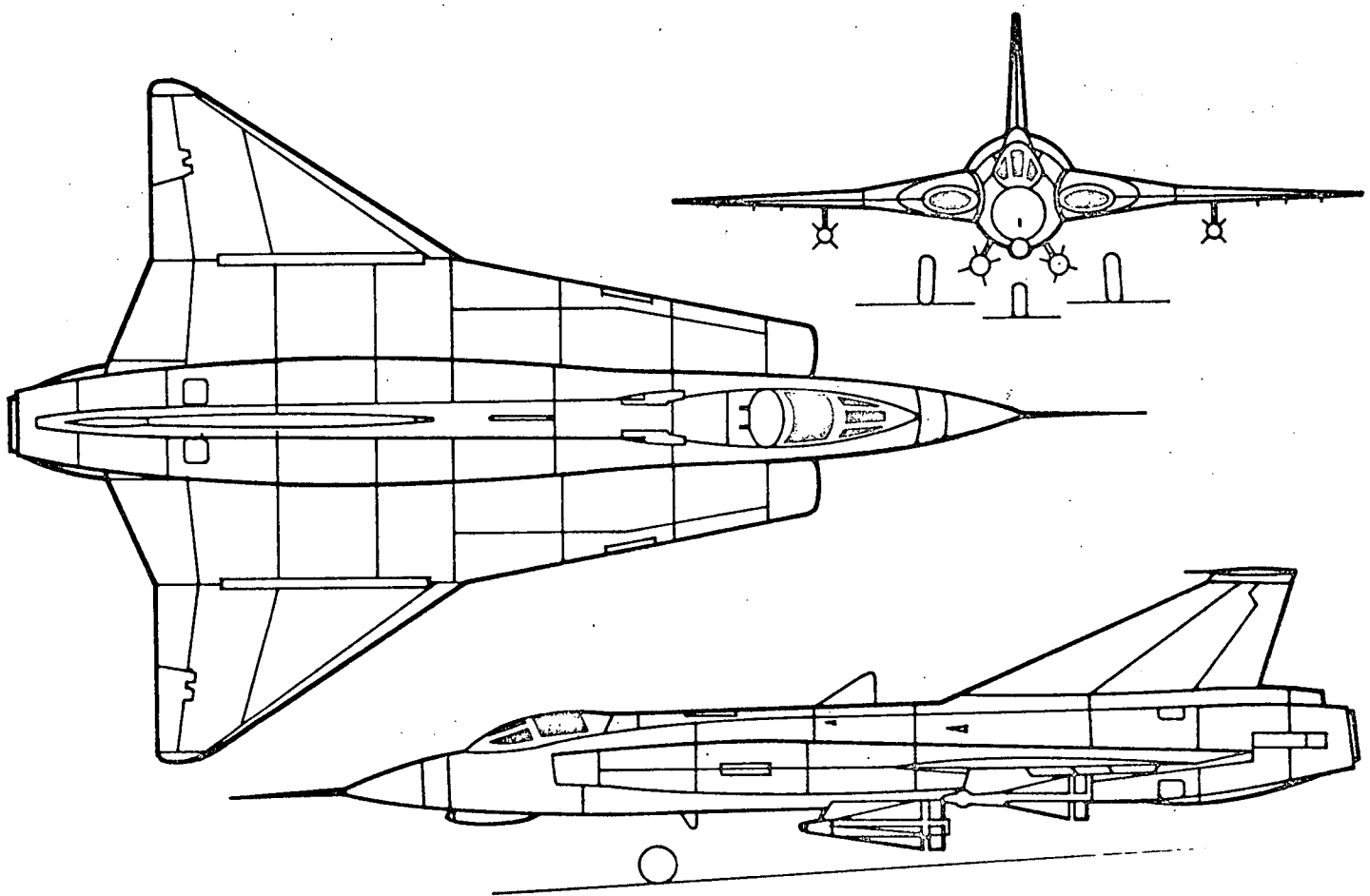


Fig. 71 Swedish Fighter Aircraft Draken

The effect of forebody vortices is not easy to avoid completely as was discussed earlier. However, it is quite possible to fix the vortex separation point, thus eliminating the asymmetric vortex shedding and thereby the major portion of the destabilizing load. This may be accomplished by fuselage shaping (Ref. 119), strakes (Ref. 106 and Fig. 72), or a combination of both. The strakes can be integrated into the design of an efficient double delta configuration. This has the added advantage of delaying vortex burst and maintaining good control effectiveness to high angles of attack, as discussed previously. Strakes will only extend the range for symmetric vortex shedding to higher angles of attack. Even a low aspect ratio delta wing starts shedding asymmetric vortices at high α (Ref. 120) as does also a rectangular wing (Ref. 84). Maltby et al. (Ref. 84) have shown that a flat top cross-section with sloping bottom sides, e.g., triangular and semi-circular sections, works the same way as the flat plate, i.e., have the same α -range for symmetric vortex shedding. However, it takes only a small disturbance in the top centerline, such as that caused by a spline (Fig. 73), to force early asymmetric vortex shedding. A detail in cockpit design could cause such an effect, as all that is needed is a short flow fence. The flow cannot find a stable stagnation condition on top of the centerline spline (Fig. 73a). As a result, the stagnation point moves to one side of the centerline spline forcing an asymmetry into the vortex geometry (Fig. 73b). This disturbance causes the vortex pair to deform into the more stable space-time equivalence to the von Karman vortex shedding (Fig. 73c). There is, of course, a critical spline height associated with this phenomenon. For larger heights than the critical the spline starts acting as a splitter plate, stabilizing the occurrence of two symmetric vortices. It is quite possible that minute differences in cockpit design rather than in wing and aft body design caused the different characteristics shown in Fig. 74 for three high performance aircraft geometries (Ref. 94).

Not only are surface details on the top side of the forebody important, also the nose-tip geometry is critical. Noretip bluntness has been shown to have large influence on the asymmetric vortex shedding off ogive-cylinder bodies (Fig. 75 and Ref. 89). The same effect has been observed for a high performance aircraft (Fig. 76 and Ref. 94). If the noretip is given a small asymmetric flat spot the direction of the asymmetric

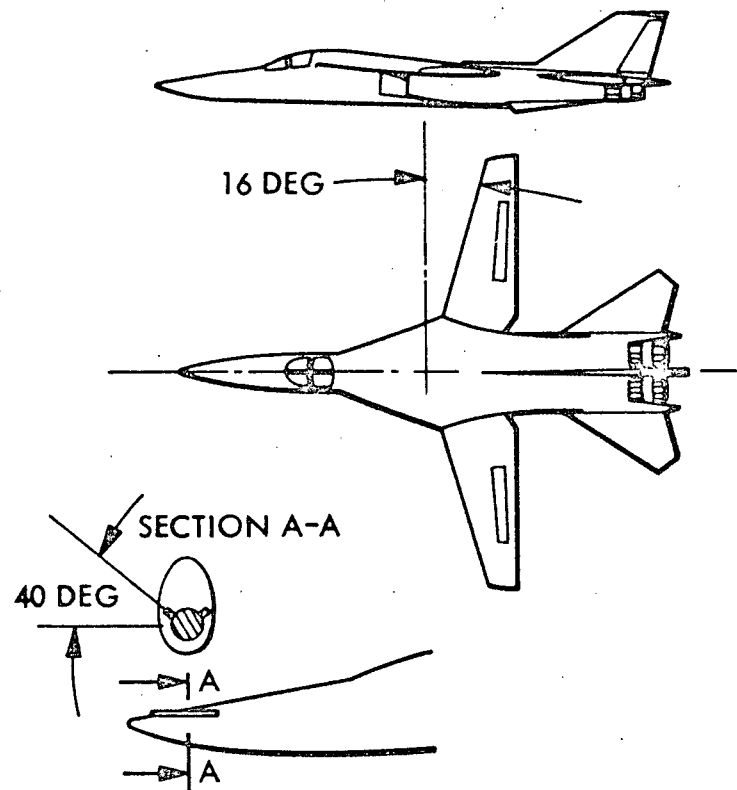
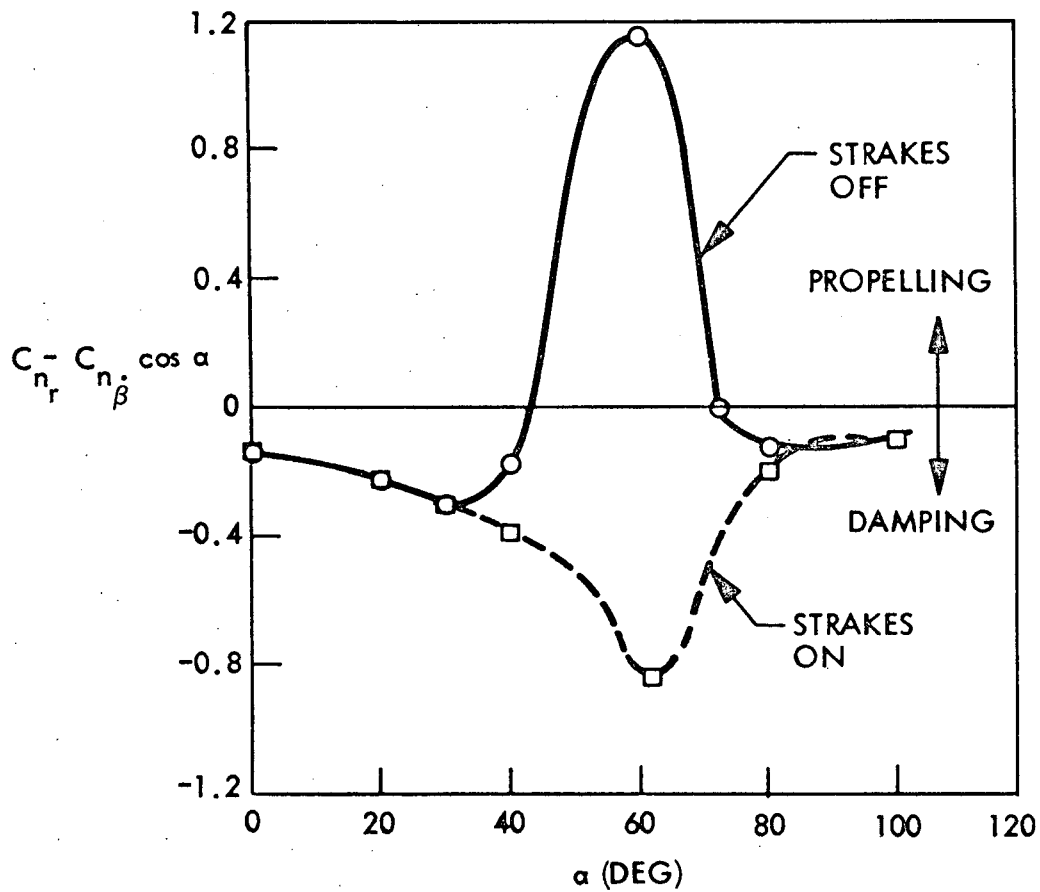
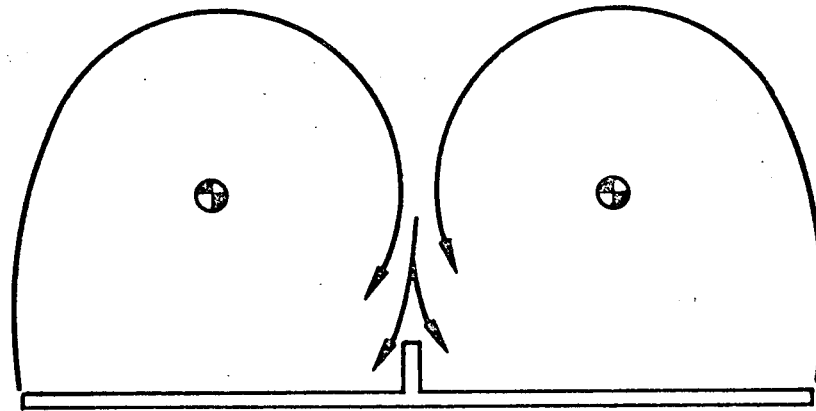
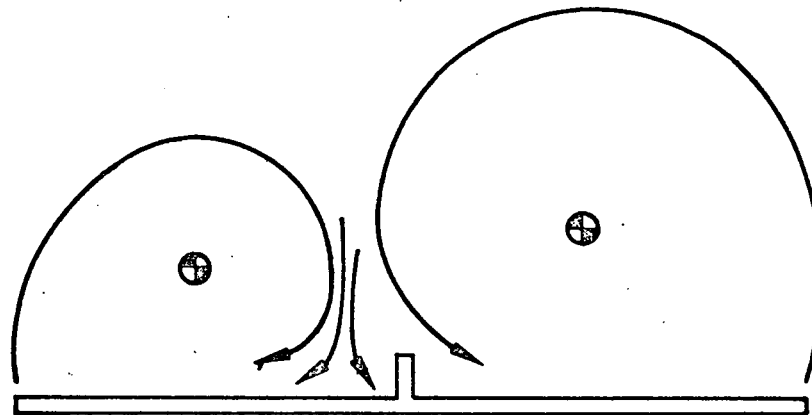


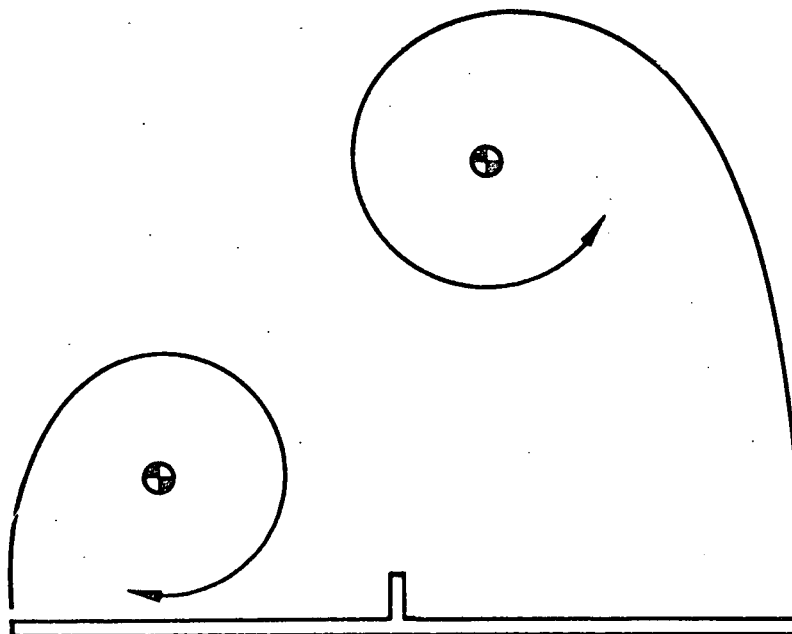
Fig. 72 Effect of Double-Strake Configuration on Aerodynamic Damping in Yaw With Angle-of-Attack For a High Performance Aircraft Configuration (Ref. 84)



(a) UNSTABLE STAGNATION POINT FOR SYMMETRIC VORTEX PAIR



(b) UNSTABLE ASYMMETRIC VORTEX PAIR



(c) STABLE ASYMMETRIC VORTEX PAIR

Fig. 73 Mischievous Centerline Spline Effects on Vortex Shedding

2-100

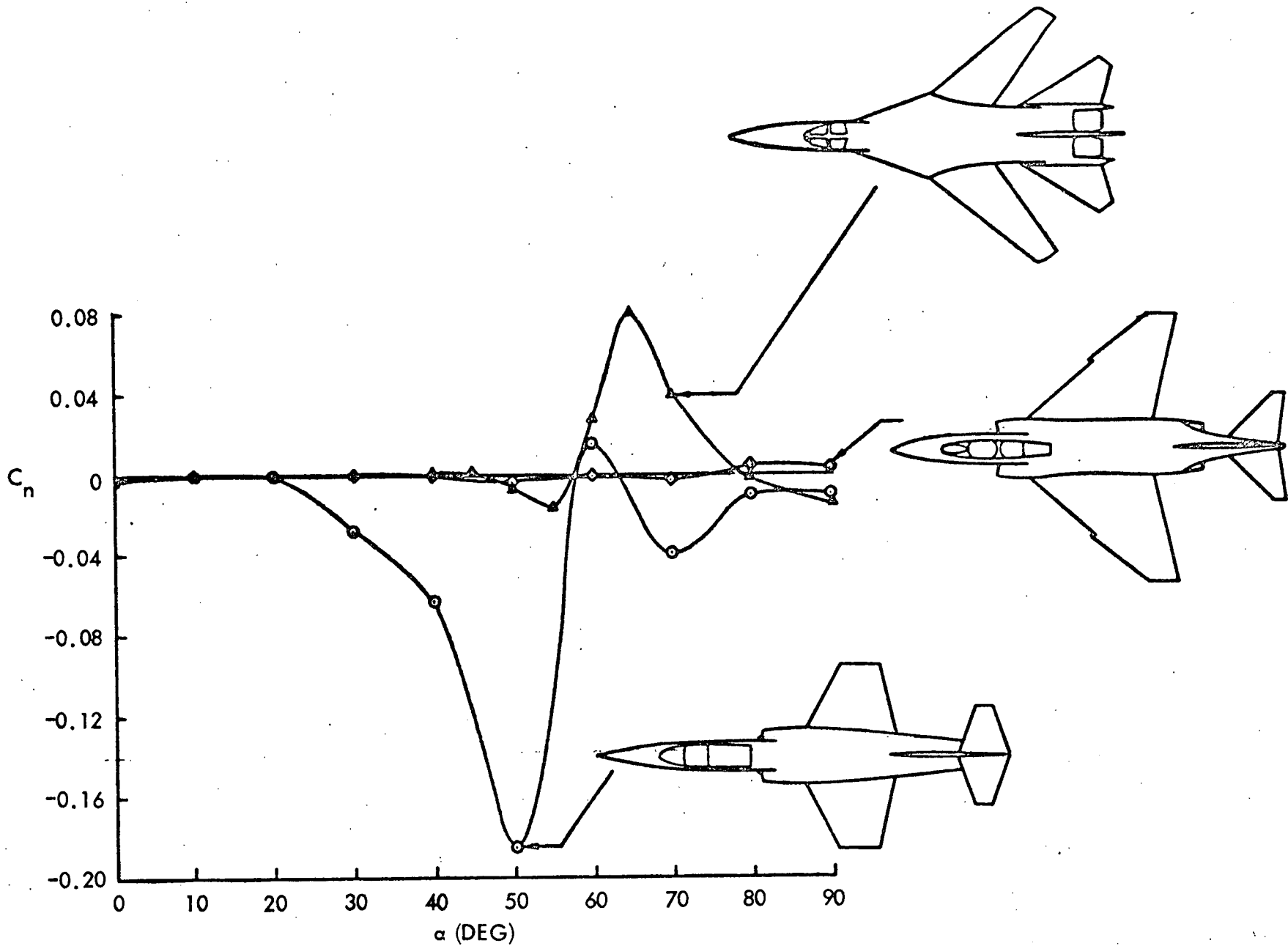


Fig. 74 Variation of Yawing-Moment Coefficient With Angle-of-Attack for Several Aircraft Configurations at $\beta = 0$ deg, $R = 0.3 \times 10^6$ (Ref. 94)

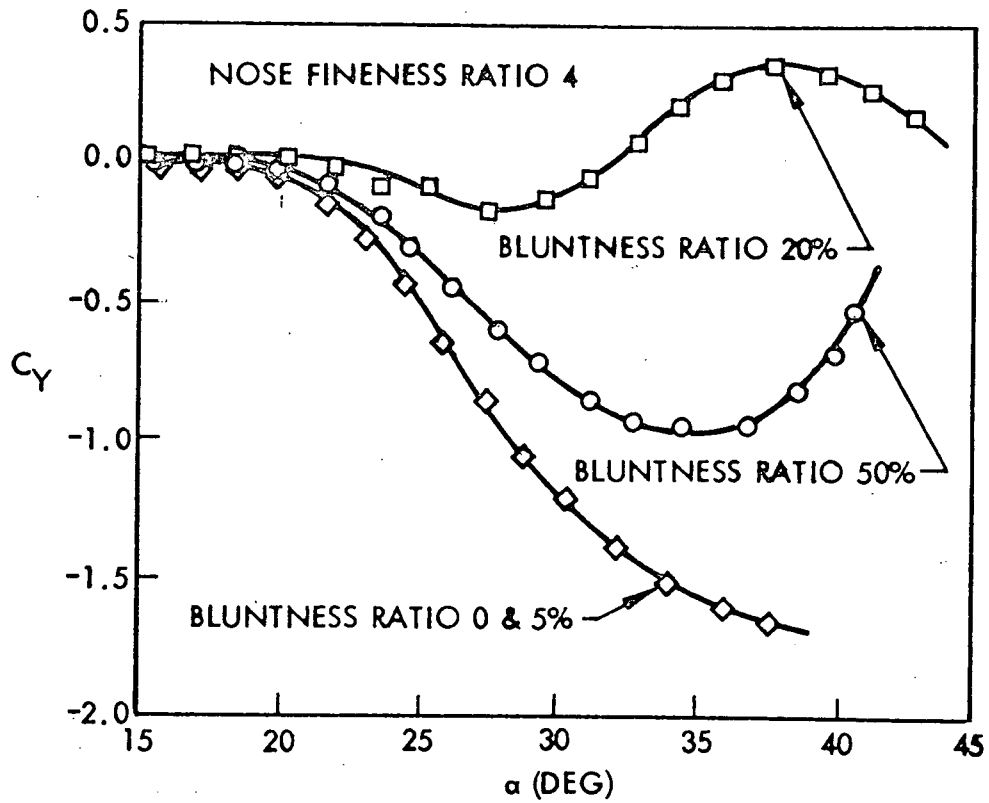
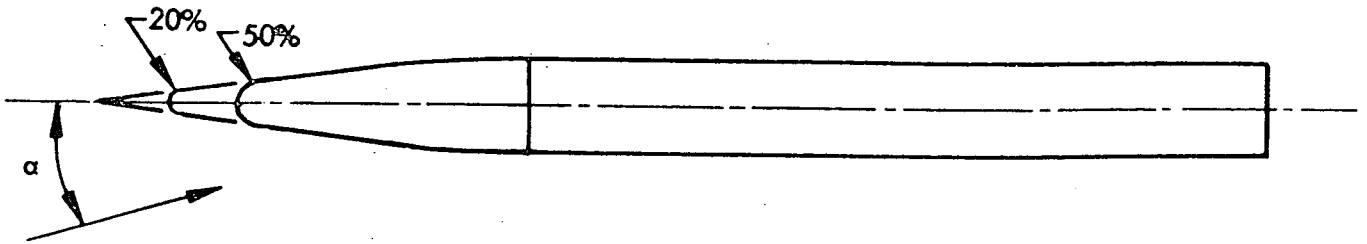


Fig. 75 Side Force Coefficient at Zero Yaw for an Ogive-Cylinder With Various Nose Tip Bluntness Ratios, $M = 0.6$ (Ref. 89)

DIMENSIONS IN: INCHES (CENTIMETERS)

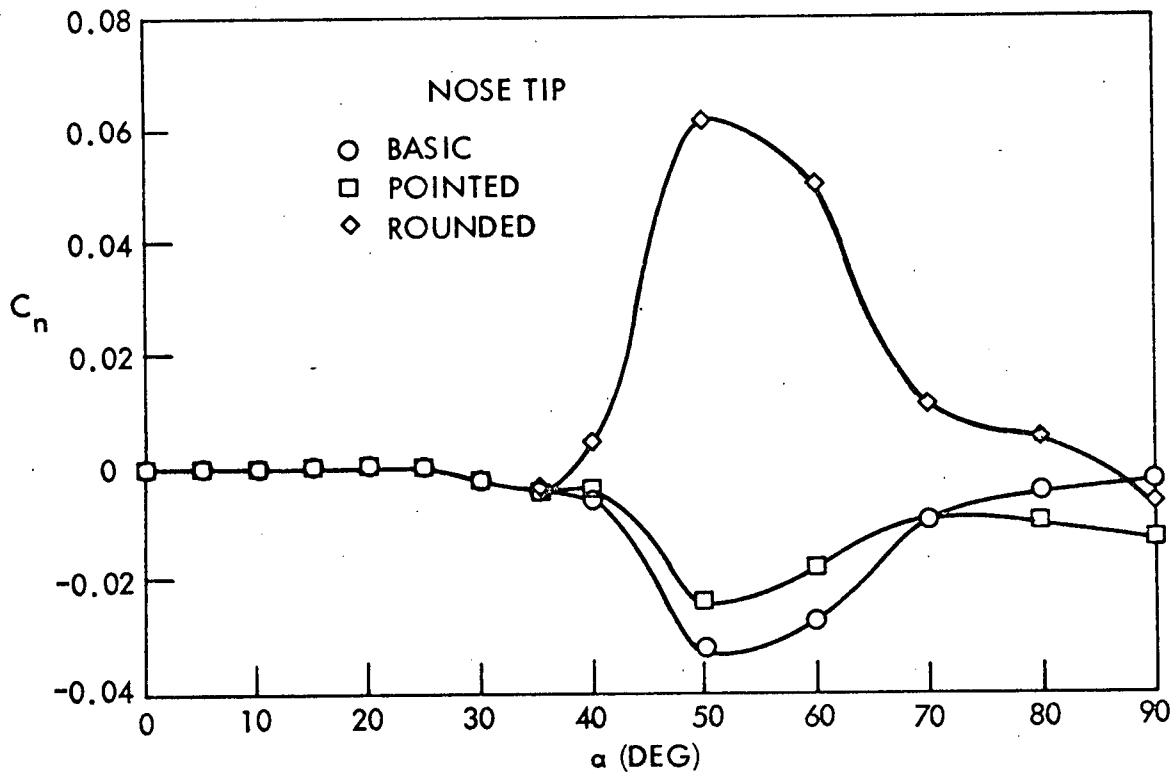
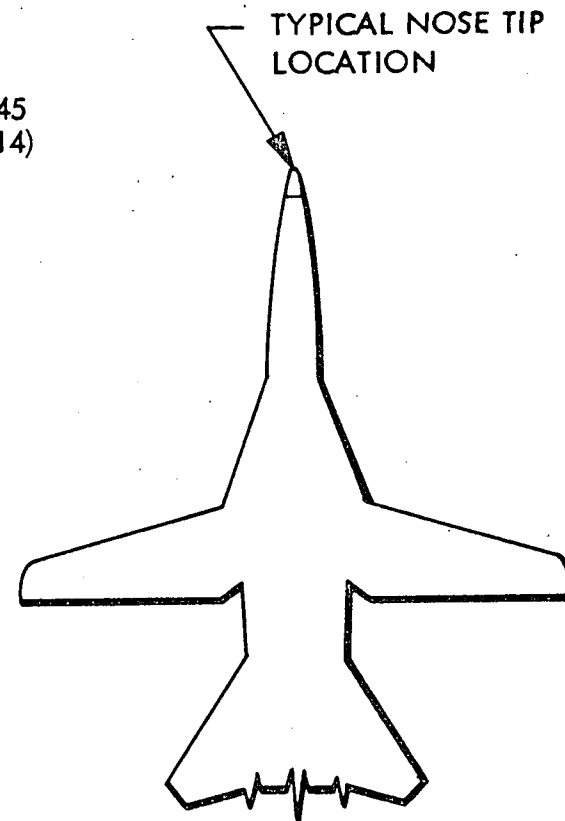
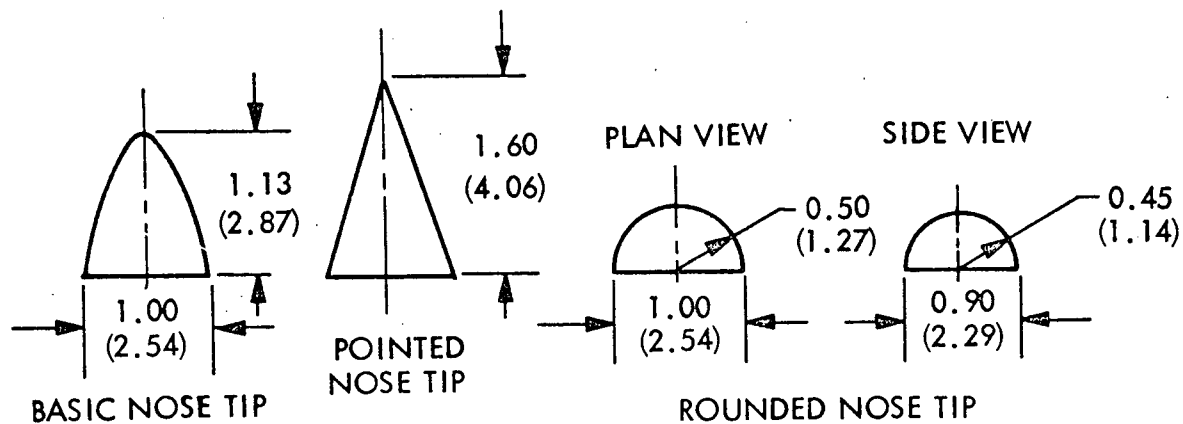


Fig. 76 Effect of Nose-Tip Shape on Side Moment of a High Performance Aircraft at Zero Yaw (Ref. 94)

vortex shedding effect can be controlled as effectively as where an asymmetric strake is used (Fig. 77). How sensitive the vortex shedding is to minute differences is demonstrated by the side moment characteristics in Fig. 78 for several models with supposedly identical nose design.* The variation between the side moment generated by asymmetric vortex shedding for the models used is an order of magnitude larger than the maximum capability of the rudder! In contrast, changing the wing plan form geometry greatly has a negligible effect.

Also ground wind loads on launch vehicles have shown this tremendous sensitivity to nosetip geometry (Ref. 121). The similarity is not accidental, but rather supports the space-time equivalence between steady asymmetric vortex shedding at high angles of attack and the periodic von Karman vortex shedding at near 90 deg flow incidence. It is the minute surface and geometry details that determine the birth process of the vortex (Ref. 122), and thereby the future downstream development of the vortex with associated induced aerodynamic loads. The process is irreversible, i. e., it is very difficult to change the course of the vortex development after its "birth." These profound effects of small changes in nose geometry are particularly disconcerting for ablative noses.

Forebody strakes may not completely eliminate the directional instability, as one shuttle contractor has shown (Fig. 80 and Ref. 106). The hard chine results represent the effect of fixing vortex shedding locations. However, the symmetric vortex shedding from the forebody can also induce significant adverse effects, especially when the vortices can interact with a vertical tail. Only after the addition of a ventral fin was a stable $C_{n\beta}$ measured. Using a twin fin arrangement could possibly have eliminated the symmetric vortex interference effect (illustrated in Fig. 64).

During the transition maneuver it will be necessary to fix the flow conditions over the wing to avoid the possibility of experiencing snap roll. That is, when traversing the flow boundaries it is likely that one wing will reestablish attached leading edge flow before the other. The result may be an unprogrammed snap roll similar to that

*The small variation in Reynolds number has a negligible effect. Compare 1/10- and 1/15-scale models for which the Reynolds number is the same.

2-104

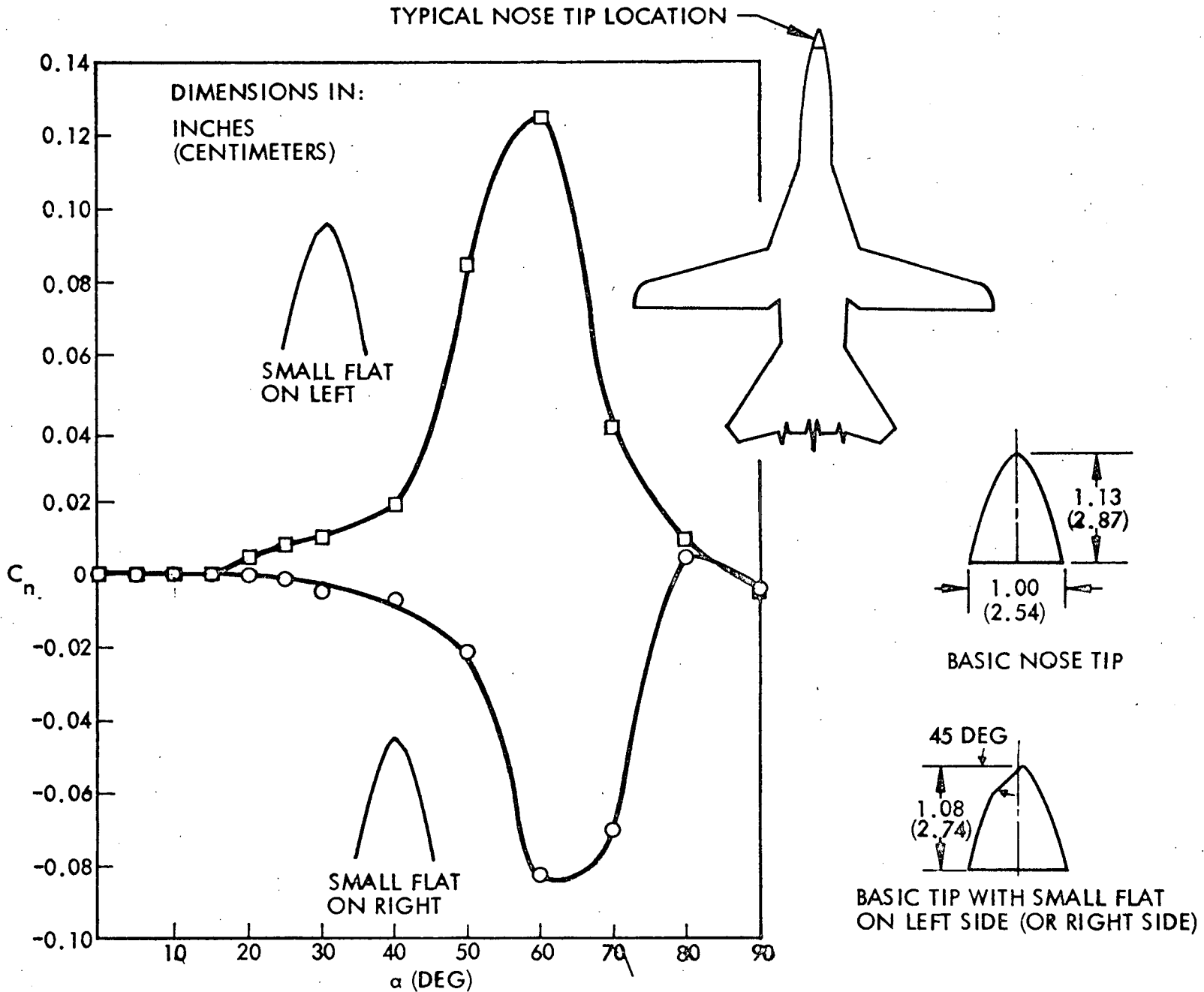


Fig. 77 Effect of Asymmetric Nose-Tip on Side Moment of a High Performance Aircraft at Zero Yaw (Ref. 94)

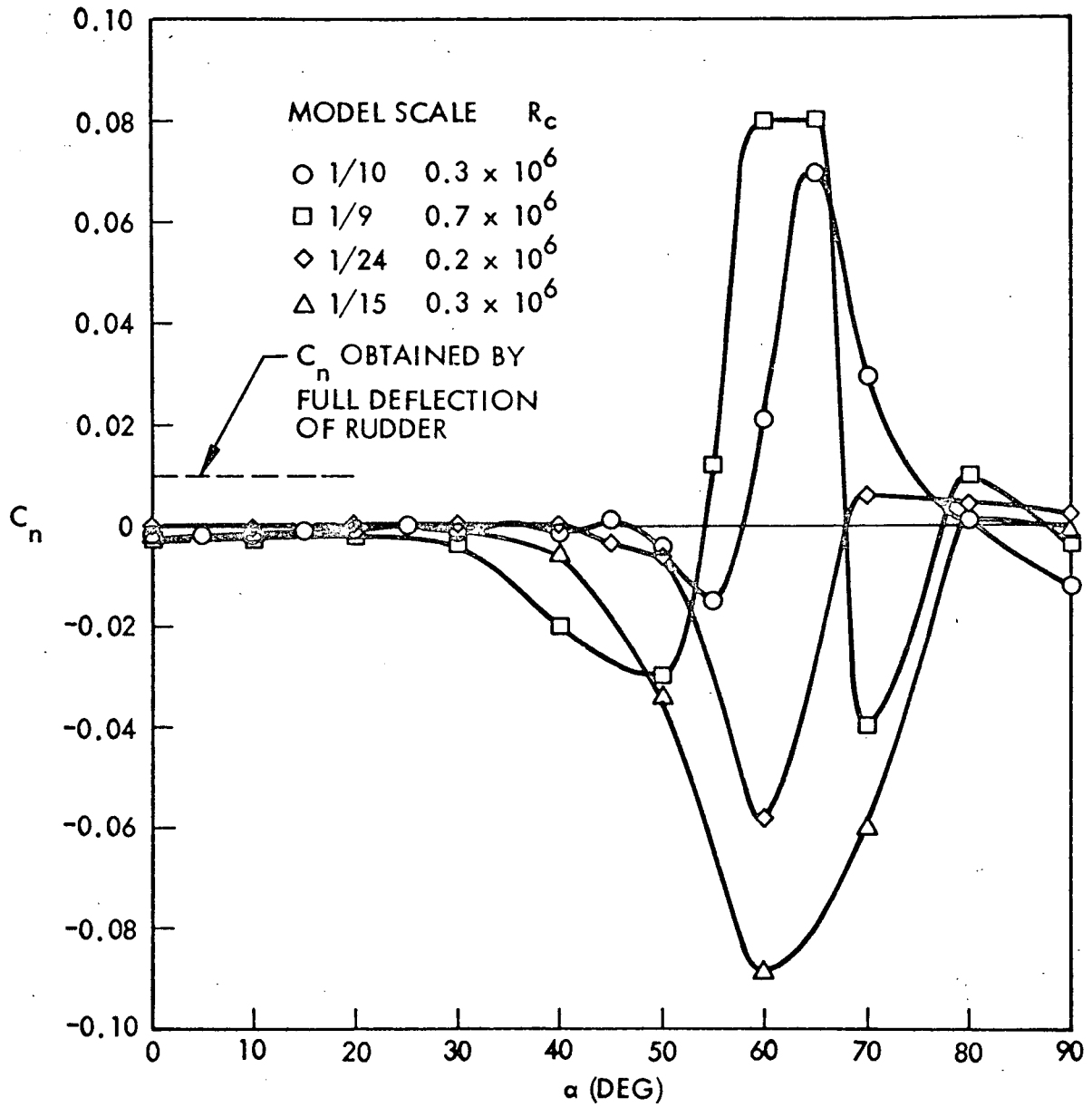


Fig. 78 Variation of Side Moment at Zero Yaw Between "Identical" Models (Ref. 94)

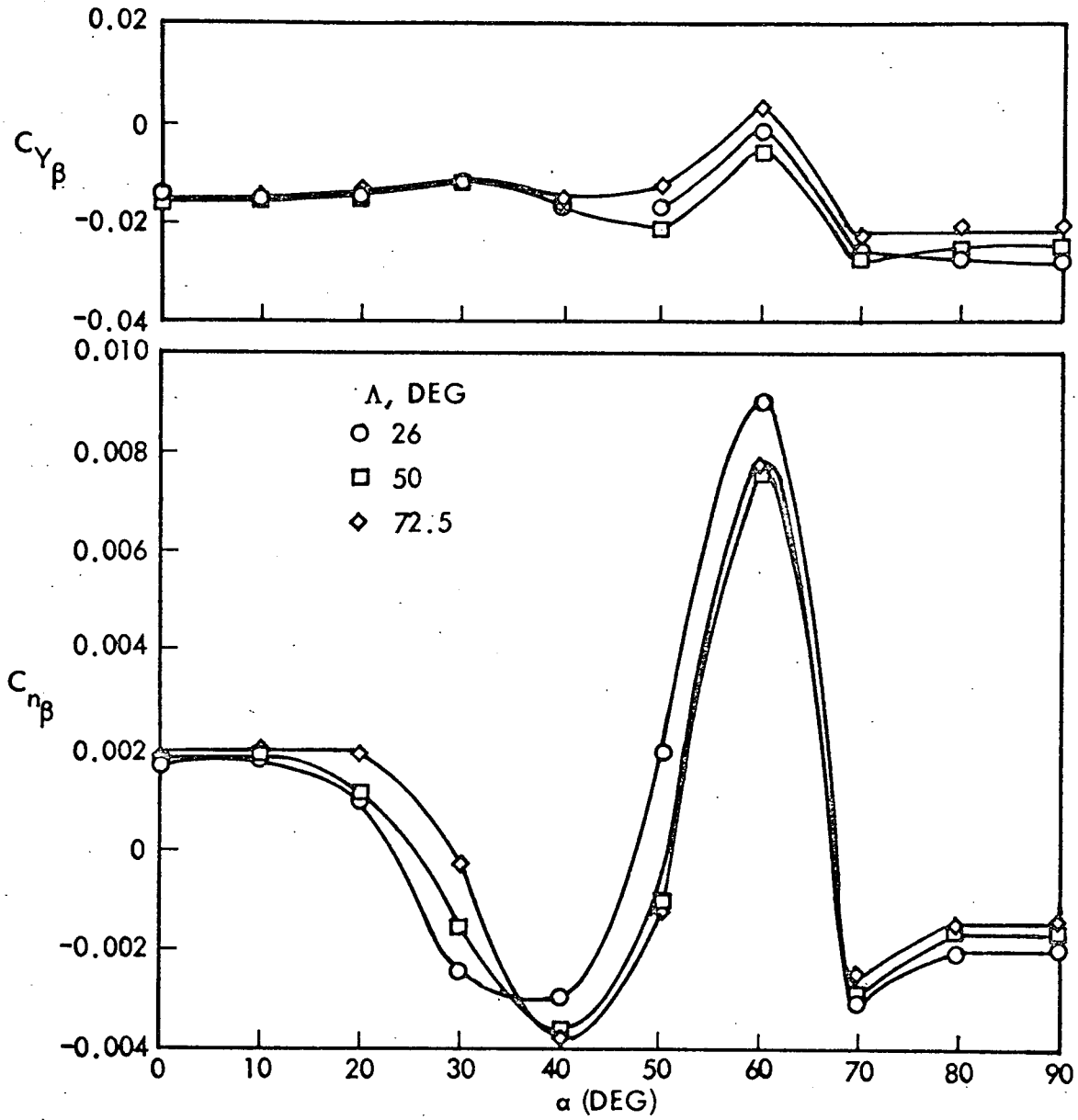


Fig. 79 Effect of Wing Sweep Angle on $C_{Y\beta}$ and $C_{n\beta}$ of a High Performance Aircraft at Zero Yaw

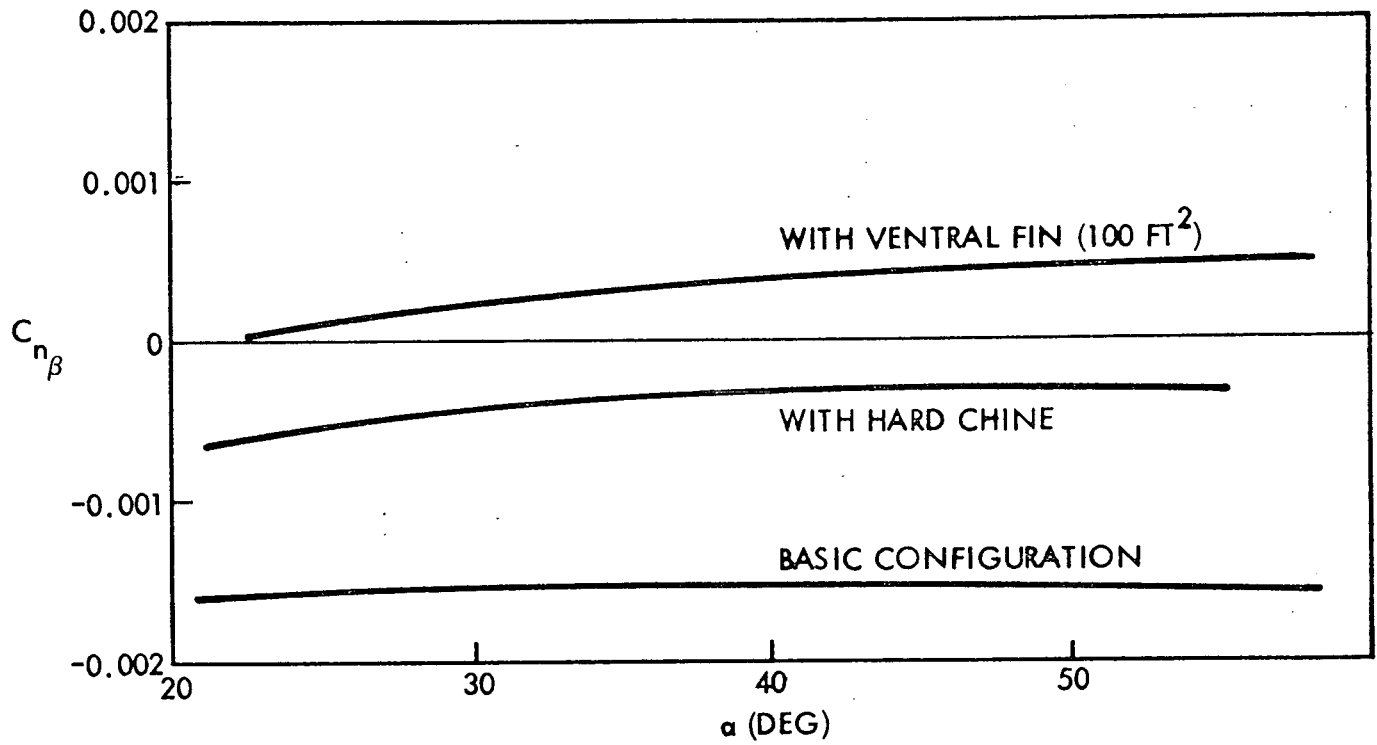


Fig. 80 Effect of Configuration Modifications on Directional Stability of Grumman Orbiter (Ref. 106)

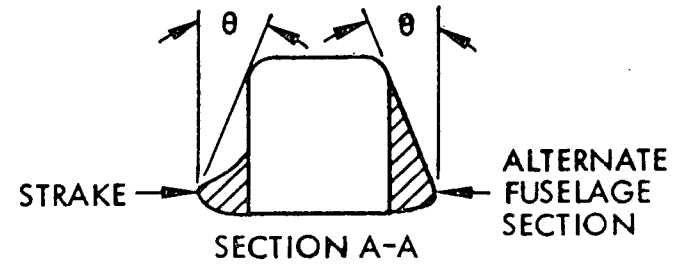
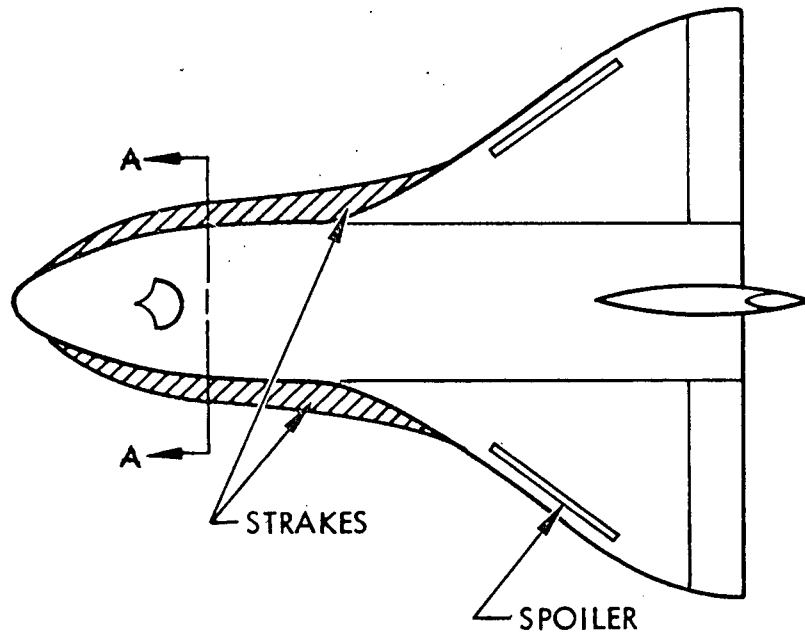
experienced with the straight winged shuttle orbiter during the drop tests (Ref. 68). Spoilers probably provide the simplest means of fixing separation. When the transition maneuver has been completed down to subcritical angles of attack, the spoilers would be retracted, causing instantaneous flow reattachment on both wings simultaneously.

The configuration modifications just discussed are summarized in Fig. 81. Like the trajectory modifications, these are fictitious and are meant to illustrate philosophy only. No evaluation of their effects on longitudinal stability, drag, center of gravity location, etc., has been made. Strakes, spoilers, and ventral fins constitute the preferred modifications. The ventral fin (or fins) would have to be folding or jettisonable for landing. If the ventral fin (or fins) prove undesirable from aerodynamic heating considerations or negative dihedral effects (Ref. 123), it may be possible to achieve directional stability with two vertical tails. If the cross range requirements could be relaxed it might be possible to fly the vehicle at very high angles of attack ($\alpha \approx 45$ deg) over most of the trajectory and delay pitch-over to lower speeds as in the sample low cross range trajectory (Fig. 68). This relaxes the lateral stability requirements somewhat (Ref. 107) allowing a negative $C_{n\beta}$ at high Mach numbers.

2.7 EXPERIMENTAL PROGRAM

In order to implement the suggested configuration modifications, it will be necessary to resort to wind tunnel tests. There is no other reliable means of determining the effectiveness of the various fixes and the necessary gradients for design optimization. There are no theoretical techniques that will predict the boundaries of the various pertinent flow conditions, although a great deal can be done with existing experimental results.

The tests would consist of the usual configuration buildup with six component force and moment data. The force data should be obtained for both increasing and decreasing angles of attack when traversing a flow boundary to define hysteresis if it is present. Six component data are essential because the cross coefficients give valuable insight into the phenomenon. For instance, the occurrence of asymmetric forebody vortex



NOTE: θ MUST BE LARGE ENOUGH TO AVOID HYPERSONIC REATTACHMENT

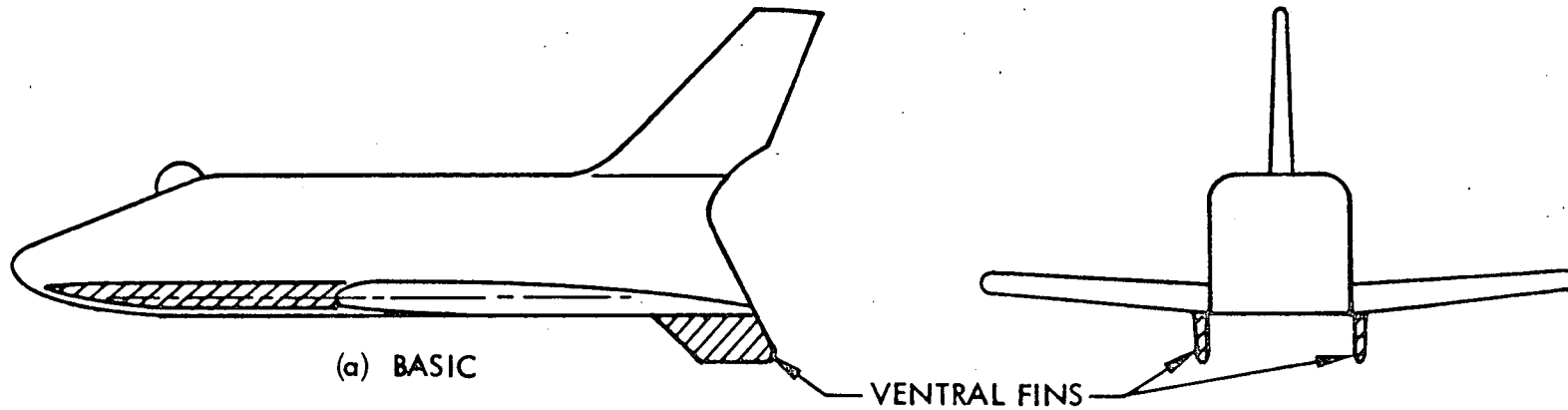
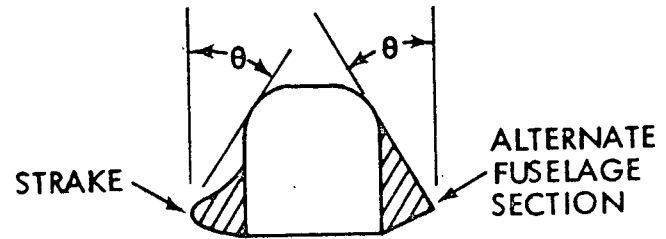
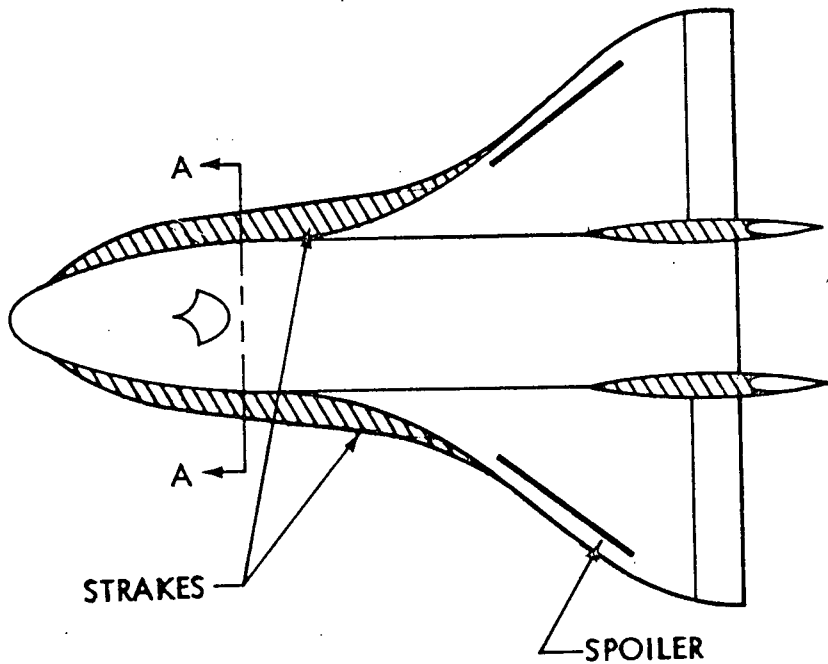
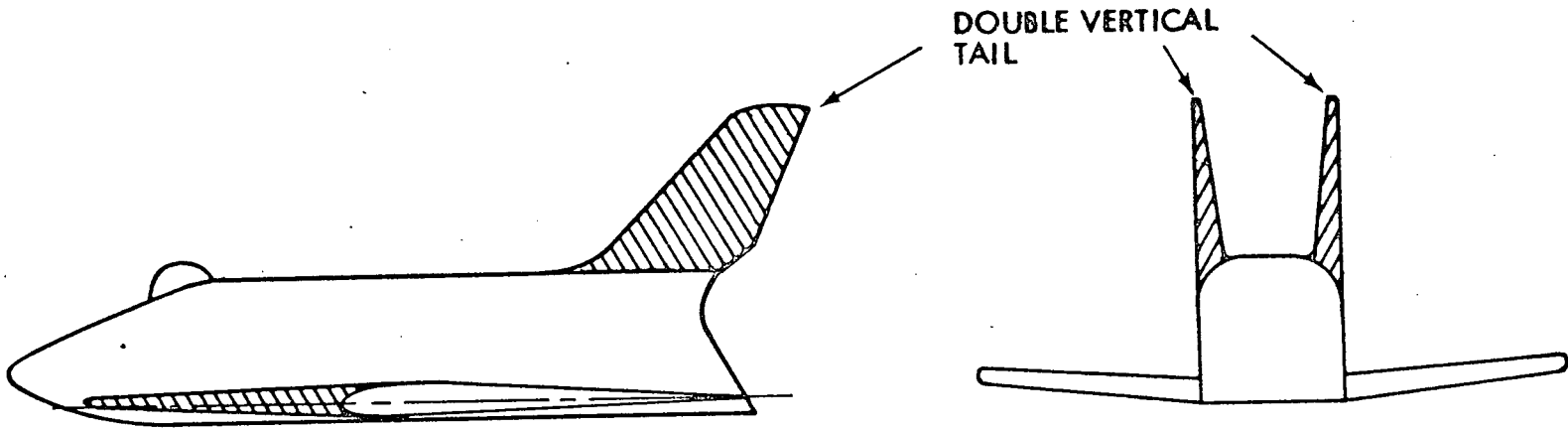


Fig. 81 Suggested Orbiter Modifications



SECTION A-A

NOTE: θ MUST BE LARGE ENOUGH TO AVOID HYPERSONIC REATTACHMENT



(b) ALTERNATE

Fig. 81 (Cont.)

shedding is accompanied by large side forces as the body is pitched, even at zero yaw. Furthermore, it is essential that complete flow visualization results are obtained, both shadowgraph coverage and surface flow visualization such as oil flow. Surface flow visualization is a fast and reliable means of determining the boundaries between the various flow types.

The most drastic variation of the various flow boundaries occurs between $M = 0.5$ and $M = 6.0$. Thus, it is suggested that a so-called trisonic tunnel be used, at least for the first preliminary investigations. Eventually the entire flight regime must be well documented to assure that the vehicle will not inadvertently experience any of the five undesirable flow conditions. Particular attention would have to be paid to obtain widest possible Reynolds number coverage to provide much needed information about the very difficult scaling problem.

In order to apply the test data to the transient flight conditions existing during the pitch-over maneuver, it will probably be necessary to run some specialized static tests with deformed models to supply needed input for a quasi-steady analysis of the vehicle dynamics.

Section 3 CONCLUSIONS

This study of the unsteady aerodynamics of the high cross range, delta planform, shuttle orbiter indicates that the shuttle vehicle will be subject to five unsteady flow phenomena which can have deleterious effects on the flight dynamics.

1. Leaside shock induced separation
2. Sudden leading edge stall
3. Vortex burst
4. Bow shock-flap shock interaction
5. Free forebody vortices

Furthermore, many of these undesirable flow conditions may be induced by control deflection.

Because the shuttle enters at a high angle of attack ($\alpha \geq 30$ deg) and eventually must pitch over to a low cruise angle of attack ($\alpha \leq 10$ deg), it will necessarily traverse at least one of the three stall regions (Items 1 through 3). This should be accomplished as quickly as possible. It is essential that stall be controlled (e.g., via spoilers) such that simultaneous reattachment can be accomplished on both wings after traversing stall. This prevents the disastrous snap roll which can result when the flow attaches on one wing while remaining stalled on the other. If necessary, the separation boundaries may be altered by wing planform or section modifications.

The unsteady flow regimes must be well mapped to insure that control deflection will not cause stall. Combined elevator and aileron deflections are particularly dangerous since they may induce stall on only one wing, again subjecting the vehicle to all the dangers of asymmetric stall effects. Bow shock-flap shock interaction may also be avoided by carefully programming control deflection.

Much of the undesirable effects of forebody vortices can be eliminated by fixing vortex locations. This is a relatively simple matter of shaping the body cross section or adding strakes.

A careful review of the unsteady flow problems of the delta wing shuttle orbiters indicates that there is every reason to believe that the problems can be dealt with successfully.

It appears that the boost configurations, both parallel and series stage configurations, will experience unsteady aerodynamic effects that could cause undamping of one or more of the lower elastic modes.

Section 4

RECOMMENDATIONS FOR FUTURE STUDY

The present study has documented several flow mechanisms with potentially disastrous influence on the space shuttle vehicle dynamics. Various fixes have been outlined that could minimize or possibly eliminate these detrimental effects. It remains to conduct the experiments and further analysis needed to determine the effectiveness of suggested fixes, and to determine the sensitivity of the effectiveness to various configuration variables, thus generating the inputs for configuration optimization. It is obvious that some of the suggested fixes will conflict with basic stability and trim requirements, and that the best possible compromise would have to be sought.

The suggested trajectory shaping reduces the time the space shuttle vehicle spends at critical flight conditions. However, the transient conditions now become important. Essentially, the delta wing vehicle will perform a transition maneuver similar to that of the straight winged space shuttle vehicle. Vortex burst and reattachment of leading edge flow play the same role for the delta wing as airfoil stall did for the straight wing. Available experimental and theoretical results indicate that reestablishing attached leading edge flow or steady leading edge vortex flow will be associated with the same problems as the reestablishment of attached airfoil flow. The phenomena are associated with α -hysteresis and basic tendencies towards asymmetry with snap roll as likely results during the transition maneuver.

For both vehicles, the delta winged as well as the straight winged space shuttle vehicle, the obvious solution is to try to delay reestablishment of regular vortex flow and attached flow, respectively, until the transition maneuver has been completed. This can be done by use of spoilers and other flow separation devices which are popped up before the transition maneuver is started and retracted when the cruising attitude has been reached.

On the surface, the program sketched above is rather straightforward. However, some further scrutinizing reveals that such a well recognized problem as that of scaling wind tunnel test data to full scale flight conditions can present formidable difficulties. Already the scaling of steady separated flow is difficult, as is the scaling of attached unsteady flow. In the present case we are faced with the problem of scaling unsteady separated flow. Already in the case of two-dimensional flow, e. g., unsteady airfoil stall, this can be quite difficult (Ref. 124). As the delta orbiter transition maneuver takes place at high speeds, flight tests are more difficult, both technically and economically, than for the subsonic transition maneuver of the straight winged space shuttle (Ref. 68). Consequently, it becomes very important to devise a combined theoretical-analytical approach to solve the scaling problem.

All the stability and control boundaries will be affected by rate effects. Also the design optimization will be affected. For example, suppose the wing planform is altered to avoid unsteady mixed flow, e. g., leading edge separation inboard and retarded separation outboard. When the vehicle rolls, the roll rate induced decelerating wall effect (the mechanism responsible for stall overshoot, Refs. 14 to 16) will be the greatest near the tip since the leading edge velocity is highest there (Ref. 15). This will result in a longer delay of stall at the tip than at the root for the upward moving wing, and the converse for the downward moving wing. Thus, the mixed flow pattern could reappear dynamically. The induced force is upward at the tip of the ascending wing and downward on the descending wing, thus driving the motion (i. e., it is undamping).

Perhaps the most fundamental problem associated with the unsteady aerodynamics of delta wings is that of scaling of separated flow effects. The shock induced separation is difficult to scale already for stationary flow on airfoils and straight wings (Refs. 125 to 127 and Fig. 82). It is only recently that a criterion for simulation of terminal shock boundary layer interaction in two-dimensional subsonic-transonic flow was established (Ref. 128). Whitehead has shown that transition has a drastic effect on control induced separation on delta wings (Ref. 77). Because the boundary layer approach length varies along the span the leeside separating patterns will exhibit a spanwise variation. Transition also has a significant effect on leading edge vortex formation (Ref. 59 and Fig. 83). Thus, a wind tunnel test must simulate both the spanwise and

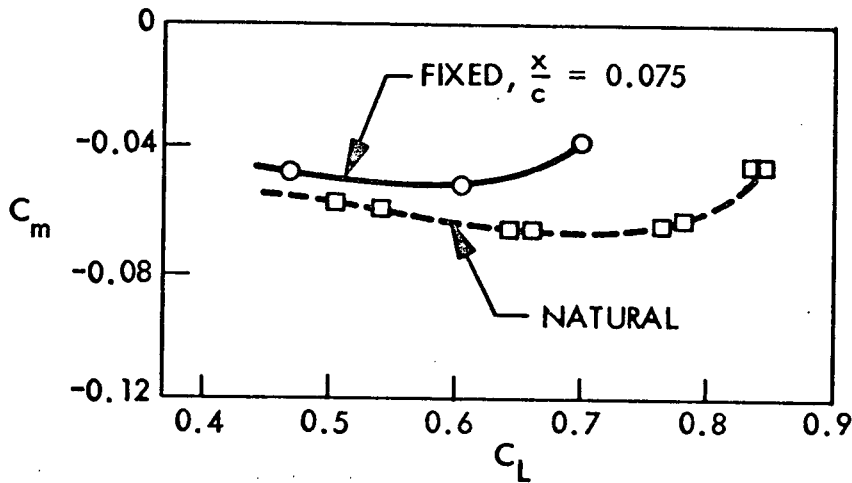
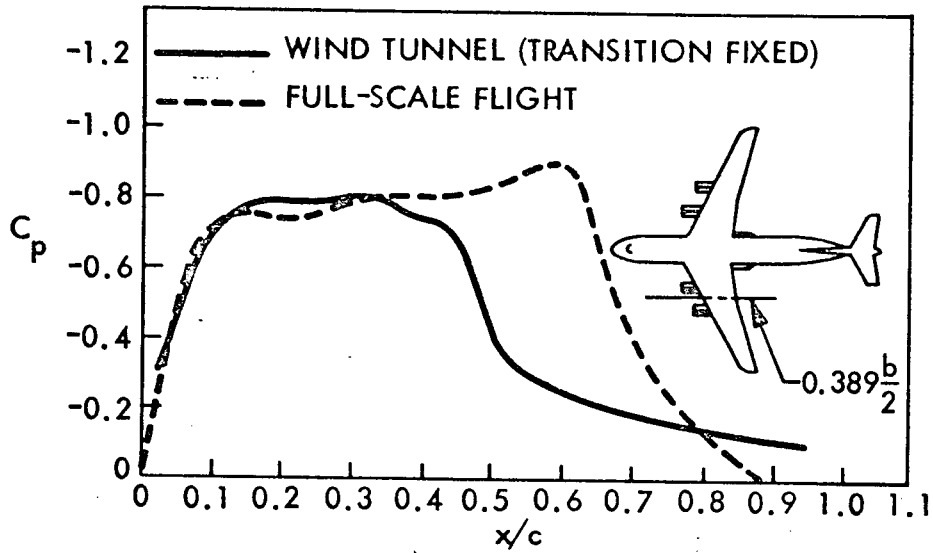
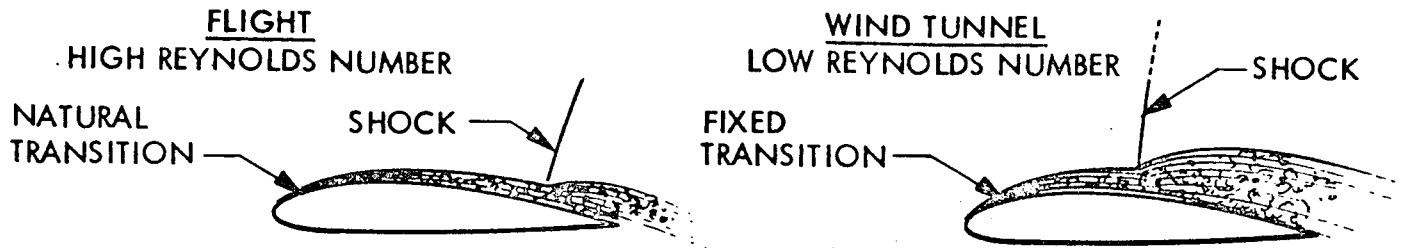


Fig. 82 Shock Induced Separation, Comparison Between Wind Tunnel and Flight-Test Results (Ref. 127)

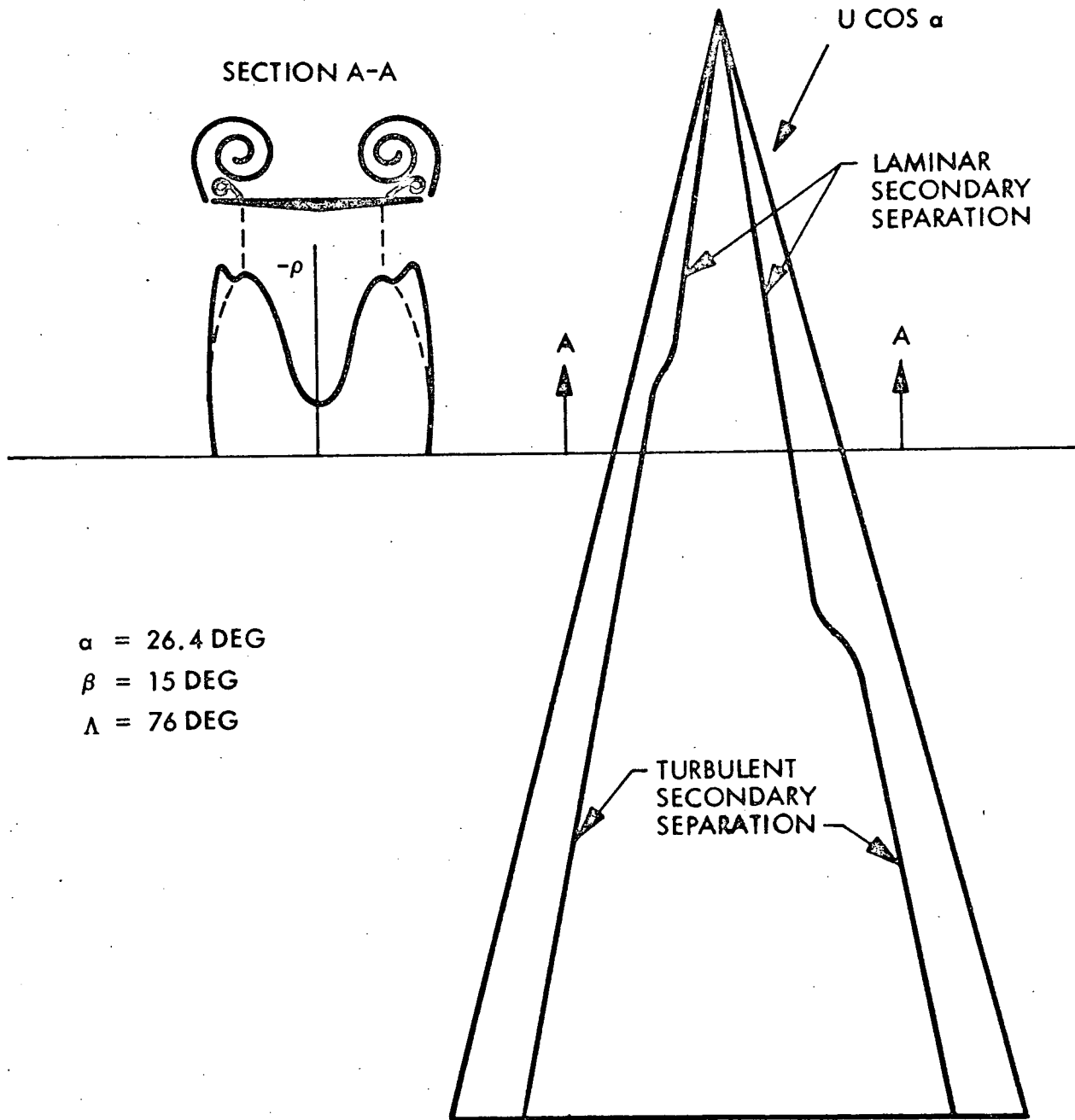


Fig. 83 Effect of Boundary Layer Transition on Leading Edge Vortex Formation (Ref. 59)

chordwise position of transition, and at hypersonic down to subsonic speeds in the case of the space shuttle vehicle.

The vortex shedding from slender forebodies is also sensitive to boundary layer conditions, supercritical flow conditions, i. e., turbulent boundary layers, giving significantly smaller induced side moments (Refs. 89 and 94, Fig. 84).

As boundary layer transition is very sensitive to accelerated flow effects, it is very much affected by the vehicle motion (Refs. 129 and 130).

In the case of spoiler design great care has to be exercised that it will not revert to a preseparation device (Refs. 5, 131, and 132). This presents a real problem when covering the α - β -M-range for the space shuttle vehicle, including the transient effects during the transition maneuver. A "spoiler design" utilizing a flap located at quarter- or midchord is probably the best way of avoiding these dangerous preseparation effects.

In summary, three major problems must be solved to assure a safe transition from orbit to cruise conditions for the shuttle vehicle. They are, in order of increasing difficulty, as follows:

1. Documentation of stability and control boundaries for both static and dynamic flight conditions.
2. A complete analysis of the unsteady aerodynamics of the shuttle vehicle including effects of "fixes".
3. Development of means for scaling of both static and unsteady aerodynamic characteristics.

The first item may be accomplished simply by performing the wind tunnel tests described earlier in the main report.

The second item, however, requires some analysis. Quasi-steady techniques developed at LMSC have successfully predicted dynamic stall loops resulting from pitch

4-6

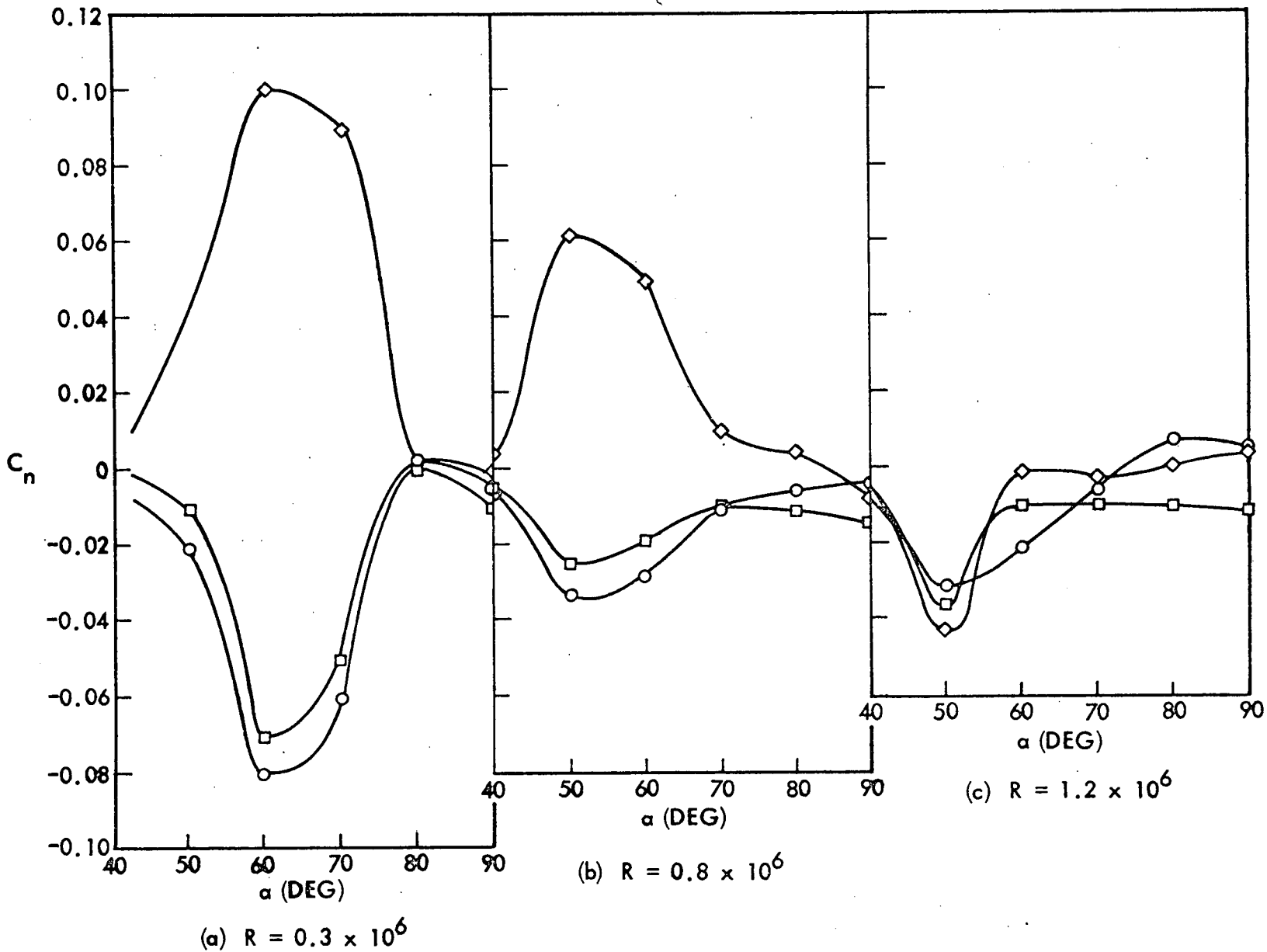


Fig. 84 Effect of Reynolds Number on Forebody Asymmetric Vortex Shedding at Zero Yaw (Ref. 94)

rate induced stall overshoot (Refs. 14 to 16). These methods can be extended to the delta wing, thus allowing computation of the rate induced delay of the various unsteady stall boundaries, mixed flow conditions, etc. In addition, the rate induced effects on the forebody vortices and their interaction with the tail must be described. This is effectively an extension of earlier work on bodies of revolution (Refs. 1 to 5).

The third item, finally, requires a considerable amount of analysis and perhaps some specialized testing. It seems prudent to first assess the impact of spanwise variation in transition location on vehicle dynamics. This then provides the means for determination of the error band for the predicted full scale vehicle dynamics.

In summary, one needs to perform a study similar to the one just completed and reported herein, with the emphasis shifted from a broad-brush look at the overall problems of the delta wing orbiter to a more quantitative analysis of the specific problems associated with various modes of transition from orbit to atmospheric cruise conditions.

Section 5
REFERENCES

1. Woods, P. and Ericsson, L. E., "Aeroelastic Considerations in a Slender Blunt-Nose, Multistage Rocket," Aerospace Engineering, Vol. 21, No. 5, May 1962, pp. 42-51.
2. Ericsson, L. E. and Reding, J. P., "Analysis of Flow Separation Effects on the Dynamics of a Large Space Booster," J. Spacecraft and Rockets, Vol. 2, No. 4, July-August 1965, pp. 481-490.
3. Ericsson, L. E. and Reding, J. P., "Dynamics of Separated Flow Over Blunt Bodies," Lockheed Missiles & Space Company, Report 2-80-65-1, NASA Contract NAS 8-5338, December 1965.
4. Ericsson, L. E., French, N. J., and Guenther, R. A., "The Aeroelastic Characteristics of the Saturn 1B Launch Vehicle With Biconic Payload Shroud," Lockheed Missiles & Space Company, Report M-37-67-1, NASA Contract NAS 8-11238, July 1967.
5. Ericsson, L. E., "Aeroelastic Instability Caused by Slender Payloads," J. Spacecraft and Rockets, Vol. 4, No. 1, January 1967, pp. 65-73.
6. Ericsson, L. E., and Reding, J. P., "Ablation Effects on Vehicle Dynamics," J. Spacecraft and Rockets, Vol. 3, No. 10, October 1966, pp. 1476-1483.
7. Reding, J. P., and Ericsson, L. E., "Loads on Bodies in Wakes," J. Spacecraft and Rockets, Vol. 4, No. 4, April 1967, pp. 511-518.
8. Ericsson, L. E. and Reding, J. P., "Aerodynamic Effects of Bulbous Bases," NASA CR-1339, August 1969.
9. Ericsson, L. E. and Reding, J. P., "Re-entry Capsule Dynamics," J. of Spacecraft and Rockets, Vol. 8, No. 6, June 1971, pp. 575-586.

10. Jecmen, D. M., Reding, J. P., and Ericsson, L. E., "An Application of Automatic Carpet Plotting to Wind Tunnel Data Reduction," *J. Spacecraft and Rockets*, Vol. 4, No. 3, March 1967, pp. 408-410.
11. Ericsson, L. E. and Reding, J. P., "Dynamic Stability Problems Associated With Flare Stabilizers and Flap Controls," *J. Spacecraft and Rockets*, Vol. 7, No. 2, February 1970, pp. 132-137.
12. Ericsson, L. E., "Universal Scaling Laws for Hypersonic Nose Bluntness Effects," *AIAA Journal*, Vol. 7, No. 12, December 1969, pp. 2222-2227.
13. Ericsson, L. E., " α -Effects are Negligible at Hypersonic Speeds - Fact or Fiction?," Vol. 3, *Proceeding of the 19th Congress of the International Astronautical Federation*, New York, 13-19 October 1968, pp. 547-561.
14. Ericsson, L. E. and Reding, J. P., "Unsteady Airfoil Stall," NASA CR 66787, July 1969.
15. Ericsson, L. E. and Reding, J. P., "Unsteady Airfoil Stall and Stall Flutter," NASA CR-111906, June 1971.
16. Ericsson, L. E. and Reding, J. P., "Unsteady Airfoil Stall, Review and Extension," *Journal of Aircraft*, Vol. 8, No. 8, August 1971, pp. 609-616.
17. Reding, J. P. and Ericsson, L. E., "Unsteady Aerodynamics of Manned Space Vehicles; Past, Present, and Future," *Proceedings First Western Space Congress*, Santa Maria, California, October 27-29, 1970, pp. 882-893.
18. Hanson, P. W. and Dogget, R. V., Jr., "Wind-Tunnel Measurements of Aerodynamic Damping Derivatives of a Launch Vehicles Vibrating in Free-Free Bending Modes at Mach Numbers from 0.7 to 2.87 and Comparisons With Theory," NASA TND-1391 (1962).
19. Rainey, A. G., "Progress on the Launch Vehicle Buffeting Problem," *J. Spacecraft and Rocket*, Vol. 2, No. 3, May-June 1965, pp. 289-299.
20. Ericsson, L. E. and Reding, J. P., "Technical Summary Report, Aeroelastic Characteristics of Saturn 1B and Saturn V Launch Vehicles," Lockheed Missiles and Space Company, Report M-37-67-5, Contract NAS 8-11238, December 1967.

21. Young, J. C., "Aerodynamic Comparisons of the Space Shuttle Phase B Two Stage Fully Reusable Vehicles," Aero-Configuration Working Group Meeting, MSFC, Houston, Texas, 16 September 1971.
22. Seegmiller, H. L., "Surface Flow Visualization Investigation of a High Cross Range Shuttle Configuration at a Mach Number of 7.4 and Several Reynolds Numbers," NASA SSPD-8, June 2, 1970.
23. Cross, E. J., "Analytical Investigation of the Expansion Flow Field over a Delta Wing at Hypersonic Speeds," ARL 68-0027, February 1968.
24. Foster, G., Graves, E., Mennell, R., Olsen, D. C. and Comeron, B., "Supersonic Stability and Control Characteristics of NR Delta Wing Orbiter," -134D/161B, NASA SADSAC DMS-DR-1096, May 1971.
25. Goldberg, G., Emery, C., Olsen, R., and Munnell, R., "Hypersonic Stability and Control Investigation and Evaluation of Split Elevon Concept for Yaw Control for the 0.00763 Scale NR Delta Wing Orbiter, NCR 134D/161B," NASA SADSAC DMS-DR-1095, May 1971.
26. Cleary, J. W., "Hypersonic Stability and Control Characteristics of a High-Cross Range Orbital Vehicle," NASA SSPD-7, May 22, 1970.
27. Weaver, J., Allen, E. C., and Glynn, J., "Static Stability and Control Investigation of NR Delta Wing (134D) and Straight Wing (130G) Space Shuttle Orbiters," NASA SADSAC DMS-DR-1076, March 1971.
28. Space Shuttle Aerodynamics Group, "North American Rockwell Space Shuttle Program Aerodynamic Design Data Book, Volume II - Delta Wing Orbiter, DB 2.1.5 - 13000-10," Space Division, North American Rockwell Corporation, May 1971.
29. Lamborne, H. C., "Some Current and Proposed Investigations into the Flow for Slender Delta and Other Wings in Unsteady Motion," ARC 21844, April
30. Lamborne, N. C., Bryer, D. W., and Mayberg, J. F. M., "A Preliminary Note on the Behavior of the Leading-Edge Vortices of a Delta Wing Following a Sudden Change of Incidence," NPL AERO Note 1006, March 13, 1962.

31. Jones, W. P., "Research on Unsteady Flow," the Sixth Minta Martin Lecture, *Journal of Aerospace Sciences*, Vol. 29, No. 3, March 1962, pp. 249-263.
32. Hayes, W. D. and Probstein, R. F., "Hypersonic Flow Theory," Vol. 1, *Inviscid Flows*, Academic Press, 1966, pp. 50-51.
33. Randall, R. E., Bell, D. R., and Burk, J. L., "Pressure Distribution Tests on Several Sharp Leading Edge Wings, Bodies, and Body-wing Combinations at Mach 5 and 8," AEDC TN-60-173, September 1960.
34. Rainbird, W. J., Crabbe, R. S., Peake, D. J., and Meyer, R. F., "Some Examples of Separation in Three-dimensional Flows," *Canadian Aeronautics and Space Journal*, Vol. 12, No. 10, December 1966, pp. 409-423.
35. Charwat, A. F., and Redekopp, L. G., "Supersonic Interference Flow Along the Corner of Intersecting Wedges," *AIAA Journal*, Vol. 5, No. 3, March 1967, pp. 480-488.
36. Watson, R. D. and Weinstein, L. M., "A Study of Hypersonic Corner Flow Intersections," AIAA 70-227 (1970).
37. Kaufman, L. G., Meckler, L., and Hartofilis, S. A., "An Investigation of Flow Separation and Aerodynamic Controls at Hypersonic Speeds," *J. Aircraft*, Vol. 3, No. 6, Nov.-Dec. 1966, pp. 555-561.
38. Korkegi, R. H., "Viscous Interactions and Flight at High Mach Number," AIAA 70-781 (1970).
39. Lindsey, W. F., and Landrum, E. J., "Compilation of Information on the Transonic Attachment of Flows at the Leading Edges of Airfoils," NACA TN 4204, February 1958.
40. Chevalier, H. L., and Robertson, J. E., "Pressure Fluctuations Resulting From Alternating Flow Separation and Attachment at Transonic Speeds," AEDC TDR 63-204 (November 1963).
41. Ericsson, L. E. and Reding, J. P., "Dynamic Stall of Helicopter Blades," Preprint No. 422, 26th Annual Forum of the American Helicopter Society, Washington, D.C., June 16-18, 1970.

42. Hanson, P. W. and Dogget, R. V., Jr., "Aerodynamic Damping and Buffet Response of an Aeroelastic Model of the Saturn I Block II Launch Vehicle," NASA TND-2713, March 1965.
43. Rogers, E. W. E., Berry, C. J., and Townsend, J. E. C., "A Study of the Effect of Leading Edge Modifications on the Flow Over a 50-Deg Sweptback Wing at Transonic Speeds," Great Brit. R&M No. 3270 (1962).
44. Goetz, R. C., "Exploratory Study of Buffet and Stall Flutter of Space Shuttle Vehicle Wing Concepts," NASA LWP-872, May 22, 1970.
45. Erickson, L. L., Gambucci, B. J., and Wilcox, P. R., "Initial Transition Flutter Results for a Straight Wing Version of the Space Shuttle Vehicle," NASA SSPD-17, December 15, 1970.
46. Polhamus, E. C., "A Concept of the Vortex Lift of Sharp-Edge Wings Based on a Leading Edge Suction Analogy," NASA TND-3767, December 1966.
47. Polhamus, E. C., "Application of the Leading-Edge-Suction Analogy of Vortex Lift to the Drag Due to Lift of Sharp-Edge Delta Wings," NASA TND-4739.
48. Hummel, D., "Untersuchungen über das Aufplatzen der Wirbel an schlanken Deltaflügeln," Z. Flugwiss 13 (1965), pp. 158-168.
49. Ludwig, H., "Zur Erklärung der Instabilität der über angestellten Deltaflügeln auftretenden freien Wirbelkerne," Zeitschrift für Flugwissenschaften, Vol. 10, 1962, pp. 242-249.
50. Benjamin, T. B., "Theory of the Vortex Breakdown Phenomenon," J. Fluid Mech., Vol. 14, 1962, pp. 593-629.
51. Harvey, J. K., "Some Observations of the Vortex Breakdown Phenomenon," J. Fluid Mech., Vol. 14, 1962, pp. 585-592.
52. Sarpkaya, T., "Vortex Breakdown in Swirling Conical Flows," AIAA 71-52, January 1971.
53. Peterschn, E., "The Stability Criterion for Vortices by Ludwig and Its Application to Some Experimental Results," FFA Report 119, The Aeronautical Research Institute of Sweden, 1970.

54. Hall, M. G., "The Structure of Concentrated Vortex Cores," Progress in Aeronautical Sciences, Pergamon Press, London, Vol. 7, 1966, pp. 53-110.
55. Elle, B. J., "On the Breakdown at High Incidence of the Leading Edge Vortices on Delta Wings," J. Royal Aeronautical Society, Vol. 94, August 1960, pp. 491-493.
56. Bossel, H. H., "Stagnation Criteria for Vortex Flows," AIAA J., Vol. 6, No. 6, June 1968, pp. 1192, 1193.
57. Crow, S. C., "Stability Theory for a Pair of Trailing Vortices," AIAA 70-53, January 1970.
58. Lambourne, N. C. and Bryer, D. W., "The Bursting of Leading-Edge Vortices - Some Observations and Discussion of the Phenomenon," Great Brit. R&M No. 3282 (1962).
59. Hummel, D., "Experimentelle Untersuchung der Strömung auf der Saugseite eines Schlanken Deltaflügels," Zeitschrift für Flugwissenschaften, Vol. 13, No. 7, July 1965, pp. 247-252.
60. Wendtz, W. H., and Kohleman, D. L., "Vortex Breakdown on Slender Sharp-Edged Wings," AIAA 69-778, July 1969.
61. Lawson, M. V., "Some Experiments With Vortex Breakdown," J. Royal Aeronautical Society, Vol. 68, May 1964, pp. 343-346.
62. Earnshaw, P. B., "Measurements of Vortex-Breakdown Position at Low Speed on a Series of Sharp-Edged Symmetrical Models," Great Brit. ARC CP No. 828 (1965).
63. Earnshaw, P. B., and Lawford, J. A., "Low-Speed Wind Tunnel Experiments on a Series of Sharp-Edged Delta Wings," Great Brit. RAE Tech. Note Aero 2780, August 1961.
64. Sforza, P. M., "Aircraft Vortices, Benign on Baleful?", Space-Aeronautics, April 1970, pp. 42-48.
65. Keating, R. F. A. and Mayne, B. L., "Low-Speed Characteristics of Wave-rider Wings," Great Brit. RAE Tech. Rpt. 69051.

66. Malcolm, G. N., "Aerodynamic Characteristics of the North American Rockwell Delta Wing Orbiter at Mach Numbers From .25 to 2.0," NASA SADSAC DMS-DR-1078, November-December 1970.
67. Brownson, J. C. "Static Stability Characteristics of MSC Orbiter Preliminary Tests at Mach No. 0.25-2.0," NASA SSPD-1, December 22, 1969.
68. Hamilton, E. J. and Ryals, W. G., "Review of 1/10 Scale Space Shuttle Air Drop Test Results," NASA MSC Internal Document 5-2950-1-NOV-126, June 24, 1970.
69. Donselman, R. W., "Data for the SS-9 Force Test of LMSC Orbiter Spacecraft Configuration in the NASA MSFC 14 x 14-inch Wind Tunnel," LMSC Report to be published.
70. Needham, D. A., and Stollery, J. L., "Boundary Layer Separation in Hypersonic Flow," AIAA 66-455, June 1966.
71. Holden, M. S., "Theoretical and Experimental Studies of Separated Flow Induced by Shock-Wave Boundary Layer Interaction," AGARD Specialist Conference on Separated Flows, Rhode-Saint-Genese Belgium, 10-13 May 1966, Conference Proceedings No. 4, pp. 153-180.
72. Marvin, J. G., Seegmiller, H. L., Lockman, W. K., Mateer, G. G., Pappas, C. C., and DeRose, C. E., "Surface Flow Patterns and Aerodynamic Heating on Space Shuttle Vehicles," Paper 71-594, AIAA 4th Fluid and Plasma Dynamics Conference, Palo Alto, California, June 21-23, 1971.
73. Maltby, R. L. et al., "Low Speed Flow Studies of the Vortex Patterns Above Inclined Slender Bodies Using a New Smoke Technique, Great Brit. RAE-TN-Aero-2482, November 1957.
74. Freeman, D. C., "Supersonic Aerodynamic Stability, Control, and Performance of a Modified NR-134D Orbiter Configuration," NASA SADSAC DMS-DR-1101, June 1971.
75. Rolls, L. S., Koenig, D. G., and Drinkwater, F. J., III, "Flight Investigation of the Aerodynamic Properties of an Ogee Wing," NASA TND-3071, December 1965.

76. Morkovin, M. V., Donahue, J. C., and Larson, H. K., "Exploratory Investigation of the Effects of Gas Injection Through a Porous Model on Separation, Transition, Static Stability, and Control Effectiveness of a Blunt Entry Body at Mach Number 7.3," AIAA 68-27, January 1968, and Report ER 14598, Contract NAS 2-3873, July 1967, Martin Marietta Corp.
77. Whitehead, A. H., Jr. and Keyes, J. W., "Flow Phenomenon and Separation Over Delta Wings With Trailing-Edge Flaps at Mach 6," AIAA Journal, Vol. 6, No. 12, December 1968, pp. 2380-2387.
78. Ericsson, L. E., "Unsteady Aerodynamics of an Ablating Flared Body of Revolution Including Effects of Entropy Gradient," AIAA Journal, Vol. 6, No. 12, December 1968, pp. 2395-2401.
79. Maikapar, G. E., "Aerodynamic Heating of Lifting Bodies," Paper Re-126, 19th Congress of the International Astronautical Federation, New York, 13-19 October 1968.
80. Hart, H., "Wing/Tail Interference in Hypersonic Missile Configurations," 8th Navy Symposium on Aeroballistics, Naval Weapons Center, Corona, Calif., May 6-8, 1969.
81. Edney, B. E., "Effects of Shock Impingement on the Heat Transfer Around Blunt Bodies," AIAA Journal, Vol. 6, No. 1, January 1968, pp. 15-21.
82. Katzen, E. D., Marvin, H. L., Seegmiller, H. L., Axelson, J. A., Brownson, J. J., Cleary, J. W., Kickman, W. K., and Kaattari, G. E., "Static Aerodynamics, Flow Fields, and Aerodynamic Heating of Space Shuttle Orbiters," Space Transportation System Technology Symposium, Vol. I, NASA TM X-52576, July 15-17, 1970.
83. Edney, B. E., "Shock Interference Heating and the Space Shuttle," Space Transportation System Technology Symposium, Vol. I, NASA TM X-52876, July 15-17, 1970.
84. Maltby, R. L., et al., "Low Speed Flow Studies of the Vortex Patterns Above Inclined Slender Bodies Using a New Smoke Technique," RAE-TN-AERO-2482, November 1957.

85. Gapcynski, J. P., "An Experimental Investigation of the Flow Phenomena Over Bodies at High Angles of Attack at a Mach Number of 2.01," NACA RML 55H29, October 1955.
86. Fiechter, M., "Über Wirbelsysteme an schlanken Rotationskörpern und ihren Einfluss auf die aerodynamischen Beiwerte," Deutsch-Französisches Forschungsinstitut Saint-Louis, Bericht 10/66, December 1966.
87. Astraghji, E. G., "The Influence of Mach Number, Reynolds Number, Semi-Nose Angle and Roll Rate on the Development of the Forces and Moments Over a Series of Long Slender Bodies of Revolution at Incidence," NAE Data Report 54510020, Ottawa, 1967.
88. Curry, W. H. and Reed, J. F., "Measurement of Magnus Effects on a Sounding Rocket Model in a Supersonic Wind Tunnel," AIAA 66-754, September 1966.
89. Pick, G. S., "Investigation of Side Forces on Ogive-Cylinder Bodies at High Angles of Attack in the M 0.5 to 1.1 Range," AIAA 71-570, June 1971.
90. Hall, I. M., Roger, E. W. E., and Davis, B. M., "Experiments With Inclined Blunt-Nosed Bodies at $M=2.45$," Great Brit. R&M No. 3218.
91. McElroy, G. E. and Sharp, P. S., "An Approach to Stall/Spin Development and Test," AIAA 71-772, July 1971.
92. Casteel, G. R. and Weyl, C. J., "A Design Approach to Provide Satisfactory Spin Characteristics for a Modern Fighter Aircraft," AIAA 70-928, July 1970.
93. Chambers, J. R. and Bowman, J. S., Jr., "Recent Experience With Techniques for Prediction of Spin Characteristics of Fighter Aircraft," Journal of Aircraft, Vol. 8, No. 7, July 1971, pp. 548-553.
94. Chambers, J. R., Anglin, E. L., and Bowman, J. B., Jr., "Effects of Pointed Nose on Spin Characteristics of a Fighter Airplane Model Including Correlation With Theoretical Calculations," NASA TN-D5921, September 1970.
95. Polhamus, E. C., "Effect of Flow Incidence and Reynolds Number on Low-Speed Aerodynamic Characteristics of Several Non-circular Cylinders With Applications to Directional Stability and Spinning," NASA TR R-29 (1959).

96. Nelson, R. L., "The Motions of Rolling Symmetrical Vehicles Referred to a Body-Axis System," NACA TN 3737 (1956).
97. Pettus, J. J., "Persistent Re-entry Vehicle Roll Resonance," AIAA 67-49, New York, 1966.
98. Price, D. A., Jr., "Sources, Mechanisms, and Control of Roll Resonance Phenomena for Sounding Rockets," Journal of Spacecraft and Rockets, Vol. 4, No. 11, November 1967, pp. 1516-1525.
99. Kanno, J. S., "Spin Induced Forced Resonant Behavior of a Ballistic Body Reentering the Atmosphere," Lockheed Missiles & Space Division, Report LMSD 288139, Vol. 3, January 1960.
100. Price, D. A., Jr. and Ericsson, L. E., "A New Treatment of Roll Pitch Coupling for Ballistic Re-entry Vehicles," AIAA Journal, Vol. 8, No. 9, September 1970, pp. 1608-1615.
101. Schiff, L. B., and Tobak, M., "Results from a New Wind-Tunnel Apparatus for Studying Coning and Spinning Motions of Bodies of Revolution," AIAA Journal, Vol. 8, No. 11, November 1970, pp. 1953-1957.
102. Kuhn, G. D., Spangler, S. B., and Nielsen, J. N., "Theoretical Analysis of Vortex Shedding from Bodies of Revolution in Coning Motion," AIAA 70-52, January 1970 (Also NASA CR 1440).
103. Lucero, E. F., "Pitch Control Effectiveness of Flap Controls Mounted on a Body of Revolution," 8th Navy Symposium on Aeroballistics, Naval Weapons Center, Corona, California, 6-8 May 1969.
104. Hobbs, J., "A Study to Eliminate Flight Instabilities on a High-Drag Air-Delivered Mine," 8th Navy Symposium on Aeroballistics, Naval Weapons Center, Corona, California, 6-8 May 1969.
105. Treon, S. L., "Effects of Nose-Cone Angle on the Transonic Aerodynamic Characteristics of a Blunt Cone-Cylinder Body Having a Cylindrical Flared, or Blunt-Finned Afterbody," NASA TMX-582, October 1961.

106. Raymes, F., "Alternate Space Shuttle Concepts Study, Part II Tech. Summary, Vol. I Orbiter Definitions," Contract NAS 9-11160, Grumman Report DRL M-010-Line Item 11, B 3543RD-12, July 6, 1971.
107. Wawrzyniak, M. E., "To What Extent Should Space Shuttle Stability and Control be Provided Through Stability Augmentation?", Space Transportation Systems Technology Symposium, Volume I, NASA TMX-52876, July 15-17, 1970.
108. Stengel, R. F., "Strategies for Control of the Space Shuttle Transition," AIAA Paper 71-923, August 1971.
109. Stanbrook, A. and Squire, L. C., "Possible Types of Flow at Swept Leading Edges," The Aer. Quarterly, February 1964, pp. 72-82.
110. Wendtz, W. H., Jr. and McMahan, M. C., "An Experimental Investigation of the Flow Fields About Delta and Double-Delta Wings at Low Speeds," NASA CR-521, August 1966.
111. Wendtz, W. H., Jr. and McMahan, M. C., "Further Experimental Investigations of Delta and Double-Delta Wing Flow Fields at Low Speeds," NASA CR-714, February 1967.
112. Sacks, A. H., Lundberg, R. E., and Hanson, C. W., "A Theoretical Investigation of the Aerodynamics of Slender Wing-Body Combinations Exhibiting Leading-Edge Separation," NASA CR-719.
113. Jane's All The World's Aircraft, 1971, p. 191.
114. Cornish III, J. J., "High Lift Application of Spanwise Blowing," ICAS 7th Congress, Roma, Italy, September 14-18, 1970, Paper 70-09.
115. Dixon, C. J., "Lift Augmentation by Lateral Blowing Over a Lifting Surface," AIAA 69-193, 1969.
116. Squire, L. C., Jones, J. C., and Stanbrook, A., "An Experimental Investigation of the Characteristics of Some Plane and Cambered 65° Delta Wings at Mach Numbers From 0.7 to 2.0," Great Brit. R&M No. 3305 (1963).

117. Rao, D. M., "Hypersonic Lee-Surface Heating Alleviation on Delta Wing by Apex-Drooping," AIAA Journal, Vol. 9, No. 9, September 1971, pp. 1875-1876.
118. Whitehead, A. H., Jr., and Bertram, M. H., "Alleviation of Vortex-Induced Heating to the Lee Side of Slender Wings in Hypersonic Flow," AIAA Journal, Vol. 9, No. 9, September 1971, pp. 1870-1872.
119. Kirkpatrick, D. L. I. and Field, J. D., "Experimental Investigation of the Positions of the Leading Edge Vortices Above Slender Delta Wings With Various Rhombic Cross-Sections in Subsonic Conical Flow," Great Brit. RAE Tech. Report No. 66068 (1966).
120. Bird, J., "Tuft-Grid Surveys at Low Speeds for Delta Wings," NASA TND-5045, February 1969.
121. Buell, D. A., "Some Sources of Ground-Wind Loads in Launch Vehicles," Proceedings of AIAA Fifth Annual Structures and Materials Conference, Palm Springs, California, 1-3 April 1964, pp. 178-183, (see also NASA TND-1893, 1963).
122. Morkovin, M. V., Prepared Comment to the Above Paper by Buell, AIAA Fifth Annual Structures and Materials Conference, Palm Springs, California, 1-3 April 1964.
123. Moul, M. J. and Paulson, J. W., "Dynamic Lateral Behavior of High Performance Aircraft," NACA RML 58E16, August 1958.
124. Ericsson, L. E. and Reding, J. P., "Dynamic Stall Simulation Problems," Journal of Aircraft, Vol. 8, No. 7, July 1971, pp. 579-583.
125. Stanewsky, E. and Hicks, G., "Scaling Effects on Shock-Boundary Layer Interaction in Transonic Flow," AFFDL-TR-68-11, March 1968.
126. Zonars, D., Lowndes, H. B., and Kolb, A. W., "Ground Testing," AIAA 68-1084, October 1968.
127. Loving, D. L., "Wind-Tunnel-Flight Correlation of Shock-Induced Separation Flow," NASA TN D-3580, 1966.

128. Blackwell, J. A., Jr., "Preliminary Study of Effects of Reynolds Number and Boundary-Layer Transition Location on Shock-Induced Separation," NASA TN D-5003, January 1969.
129. Ericsson, L. E., "Effect of Boundary Layer Transition on Vehicle Dynamics," J. Spacecraft and Rockets, Vol. 6, No. 12, December 1969, pp. 1404-1409.
130. Obremski, H. J. and Morkovin, M. V., "Application of a Quasi-Steady Stability Model to Periodic Boundary Layers," AIAA Journal, Vol. 7, No. 7, July 1969, pp. 1298-1301.
131. Ericsson, L. E., "Loads Induced by Terminal-Shock Boundary-Layer Interaction on Cone-Cylinder Bodies," J. Spacecraft and Rockets, Vol. 7, No. 9, September 1970, pp. 1106-1112.
132. Ericsson, L. E., "Unsteady Aerodynamics of Separating and Reattaching Flow on Bodies of Revolution," IUTAM Symposium on Unsteady Boundary Layers, Laval University, Quebec, 24-28 May 1971.
133. Ericsson, L. E., Reding, J. P., and Guenther, R. A., "Gust Penetration Loads and Elastic Vehicle Response for Saturn V Launch Vehicles," Lockheed Missiles & Space Company, Report M-3C-70-2, July 1970.
134. Reding, J. P., "Partial Simulation of Elastic-Body Dynamics for the Upper-Stage Apollo-Saturn Launch Vehicle," Lockheed Missiles & Space Company Report M-37-67-4, December 1967.
135. Reding, J. P., "Forces Induced on Bodies in Free Wakes and Three-Dimensional Cavities," Lockheed Missiles & Space Company, Report LMSC/6E7990, December 1968.
136. Coats, J. P., "Static and Dynamic Testing of Conical Trailing Decelerators for the Pershing Re-Entry Vehicle," Arnold Engineering Development Center, TN-60-188, October 1960.
137. Brownson, J. J. and Whitnah, A. M., "Determination of Drag, Stability, and Control Characteristics for the MSC Launch Configuration (Straight Wings)," NASA SADSAC DMS-DR-1063, (SSPD-31), March 1971.

138. Muhlstein, L., Jr., "Buffet Response of Space Shuttle Launch Configurations as Determined by Tests of an Aeroelastic Model," NASA Space Shuttle Technology Conference, Vol. II, NASA TM-X-2274, March 2-4, 1971.
139. Coe, C. F., Dods, J. B., Robinson, R. C., and Mayes, W. H., "Preliminary Measurements and Flow Visualization Studies of Pressure Fluctuations on Space Shuttle Configurations," NASA Space Shuttle Technology Conference, Vol. II, NASA TM X-2274, March 2-4, 1971.
140. Watts, L., "Study to Develop a Solution for Configuration Instability for the 0.003366 Scale S-IC/NR NCR Orbiter," NASA SADSAC DMS-DR-1091, May 1971.
141. Glauz, W. D. and Blackburn, R. R., "Study of Indicial Aerodynamic Forces on Multistage Space Vehicle Systems, Vol. I Application of Theory to Basic Geometries and to the Saturn V," Midwest Research Institute Final Report 28 June 1962-September 1968.

Appendix A
NOMENCLATURE

A	axial force, kg: coefficient $C_A = A/(\rho_\infty U_\infty^2/2)S$
a	speed of sound, m/sec
AR	aspect ratio, $AR = b^2/S$
b	wing span, m
c and \bar{c}	reference length, m, c = delta wing root chord
d	reference length, m (maximum diameter for body of revolution)
D_ν	equivalent elastic body damping derivative
f	frequency, cycles per second
L	lift, kg: coefficient $C_L = L/(\rho_\infty U_\infty^2/2)S$
ℓ	rolling moment kg-m: coefficient $C_\ell = \ell/(\rho_\infty U_\infty^2/2)Sc$ length, m
M	Mach number, $M = a/U$
M_p	pitching moment, kg-m: coefficient $C_m = M_p/(\rho_\infty U_\infty^2/2)Sc$
N	normal force, kg: coefficient $C_N = N/(\rho_\infty U_\infty^2/2)S$
n	yawing moment, kg-m: coefficient $n/(\rho_\infty U_\infty^2/2)Sc$
p	pressure, kg/m^2 : coefficient $C_p = (p - p_\infty)/(\rho_\infty U_\infty^2/2)$ roll rate, rad/sec
q	pitch rate rad/sec
R and R_c	Reynolds number based on c
S	reference area, m^2
t	time, sec
U and U_∞	free stream velocity, m/sec
\bar{U}	convection velocity, m/sec

x	horizontal coordinate, m
Y	side force, kg: coefficient $C_Y = Y/(\rho_\infty U_\infty^2/2)S$
y	lateral coordinate, m
z	vertical coordinate, m
α	angle of attack, radian or deg
β	sideslip angle, radian or deg
γ	rotation of plane of symmetry of forebody vorticies, radian or deg (Fig. 63)
Δ	increment
η	nondimensional span, y/c
δ	control deflection, radian or deg
δ_1	modal deflection at first antinode, m
δ_{\max}	maximum modal deflection, m
δ_{TE}	trailing edge modal deflection
ζ	damping, fraction of critical
Λ	sweep angle of leading edge, radian or deg
θ	flow reattachment angle, radian or deg (Fig. 81)
$\Delta\theta$	angle of attack perturbation, radian or deg
ρ	air density, $\text{kg}\cdot\text{sec}^2/\text{m}^4$
φ	roll angle, radian or deg
φ_c	coning angle, radian or deg
ψ	yaw angle, radian or deg
ω	oscillation frequency, radians/sec: $\omega = 2\pi f$

Subscripts

AC	aerodynamic center
b	base

CG	center of gravity
det	detached shock wave
L	left
l	lower
incip	incipient
p	$\partial/\partial p$
q	$\partial/\partial q$
R	right
r	rudder
s	separated flow or stall
TE	trailing edge
u	upper
V	vortex induced
∞	free stream conditions
α	$\partial/\partial\alpha$
β	$\partial/\partial\beta$
δ	$\partial/\partial\delta$

Superscripts

i induced, e. g. $\Delta^i C_L \equiv$ separation induced lift coefficient

Differential

$\dot{\alpha}$ $\partial\alpha/\partial t$
 $\dot{\beta}$ $\partial\beta/\partial t$

Appendix B*

LAUNCH CONFIGURATION AEROELASTIC STABILITY

In addition to the study of the unsteady aerodynamics of the delta orbiter a small companion study was made of the unsteady aerodynamics of the boost configuration. The objective was to determine if there were unsteady aerodynamic effects at work which might degrade the aeroelastic stability of the boost configurations.

As mentioned in the introduction it is this application of the quasi-steady technique to the aeroelastic stability of launch vehicles dominated by separated flow that is its most notable success. In order to establish the veracity of the technique the results of its application to the Saturn boosters will be reviewed.

That the Apollo-Saturn V booster is dominated by separated flow is evident in the shadowgraph in Figure B-1. The various regions of separated flow drastically affect the aerodynamic loads over the command module and the various interstage frustums (Figure B-2). The wake of Apollo escape rocket is the most striking separated flow feature in the flow photograph of Figure B-1. Measurements of the time history of the time history of the escape rocket load indicate that the load lags the motion of the escape rocket. This lag is well predicted from the attached to separated flow axial force ratio (Figure B-3 and Ref. 134). That is $(C_{A\infty}/C_{AS})^{1/2} = (q_{\infty}/q_S)^{1/2} = U_{\infty}/U_S$. This, of course, tacitly assumes incompressible flow which should not be too bad an assumption for the induced wake flow. The axial force ratio is also used to extract the load induced by the escape rocket from force distribution measurements (Ref. 2). Using this quasi-steady technique, the aerodynamic damping of the escape rocket - command module combination was predicted. The results are in good agreement with experiment (Figure B-4 and Ref. 135). The most notable feature of this comparison is that the aerodynamic undamping of the disk on configuration is well predicted.

*The authors gratefully acknowledge the contributions made by Lt. H. G. Chalkley, U. S. N. to this launch vehicle analysis during his Education-With-Industry tour at LMSC, July 6 - August 13, 1971.

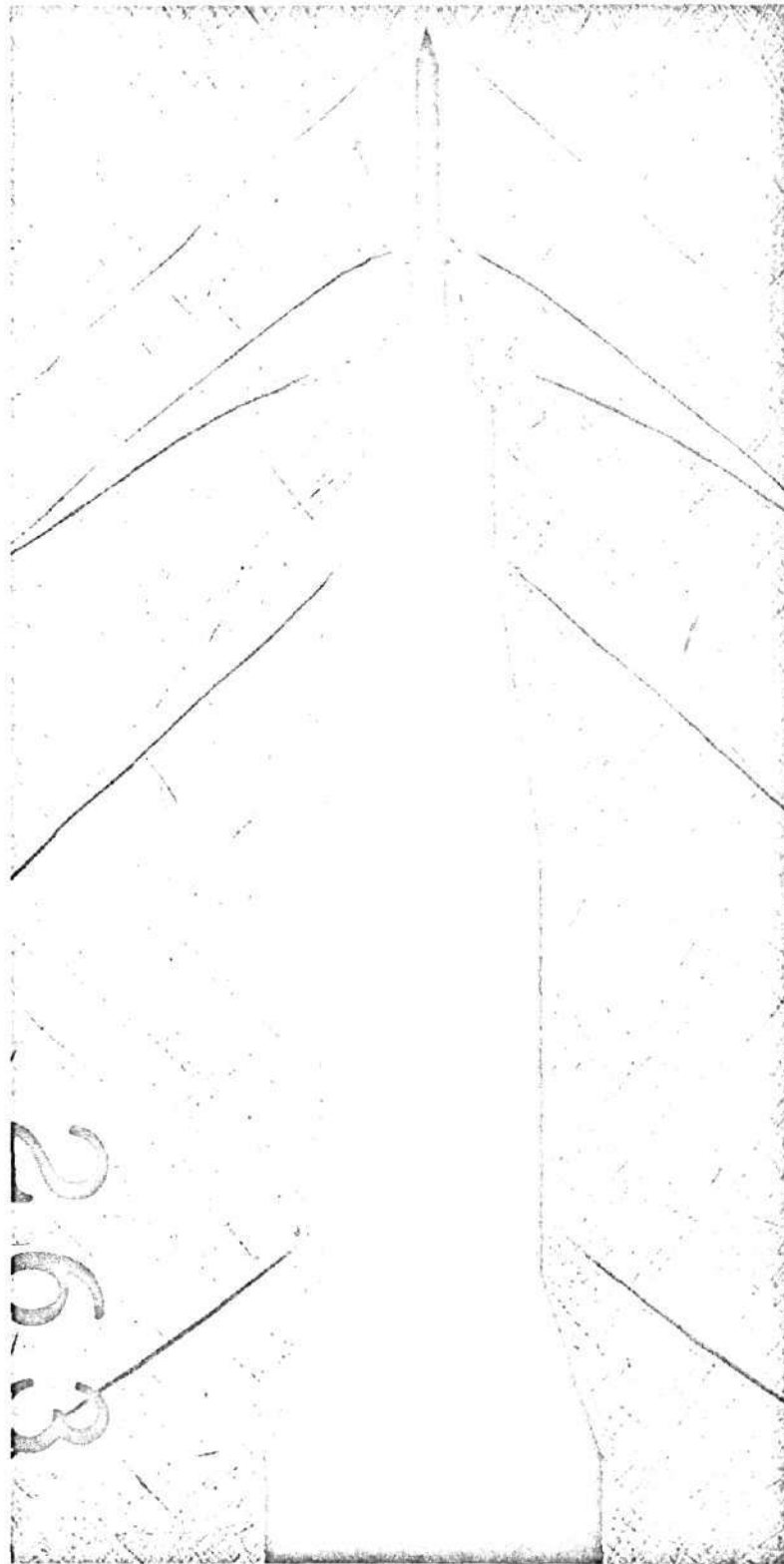


Fig. B-1 Shadowgraph of Flow Over Saturn-V Launch Vehicle at $M = 1.46$

B-2

Reproduced from
best available copy.

B-3

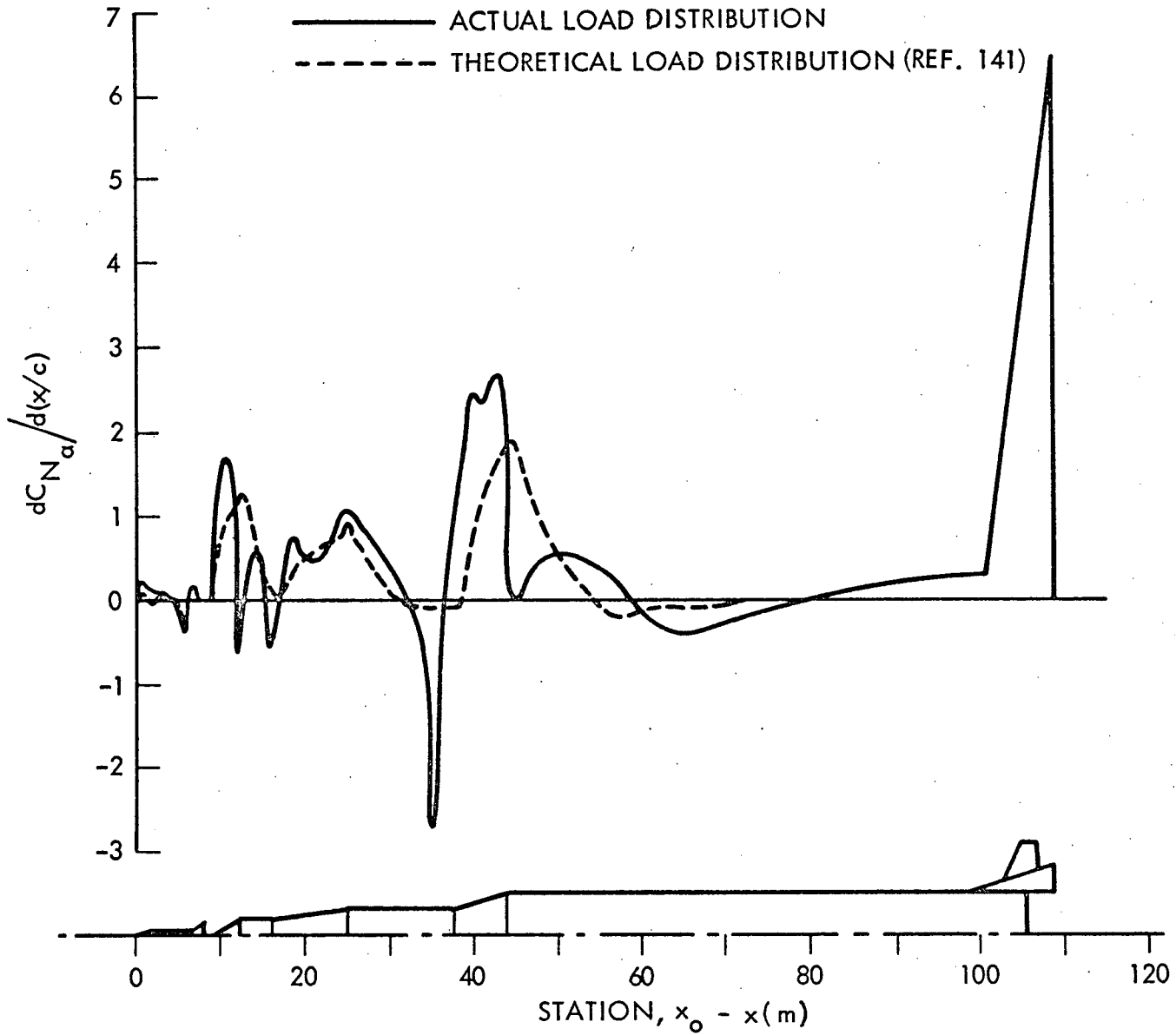


Fig. B-2 Static Load Distribution on the Saturn-V Launch Vehicle at $M = 1.3$ (Ref. 133)

ω_{cps}	$\Delta \theta \approx 1^\circ$	$\approx 1.5^\circ$	$\approx 2^\circ$	$\Delta \theta \approx 0.5^\circ$	$\approx 1^\circ$	$\approx 2^\circ$
100	○	○	♂	●	♂	♂
50	□	□	♂	■	♂	♂

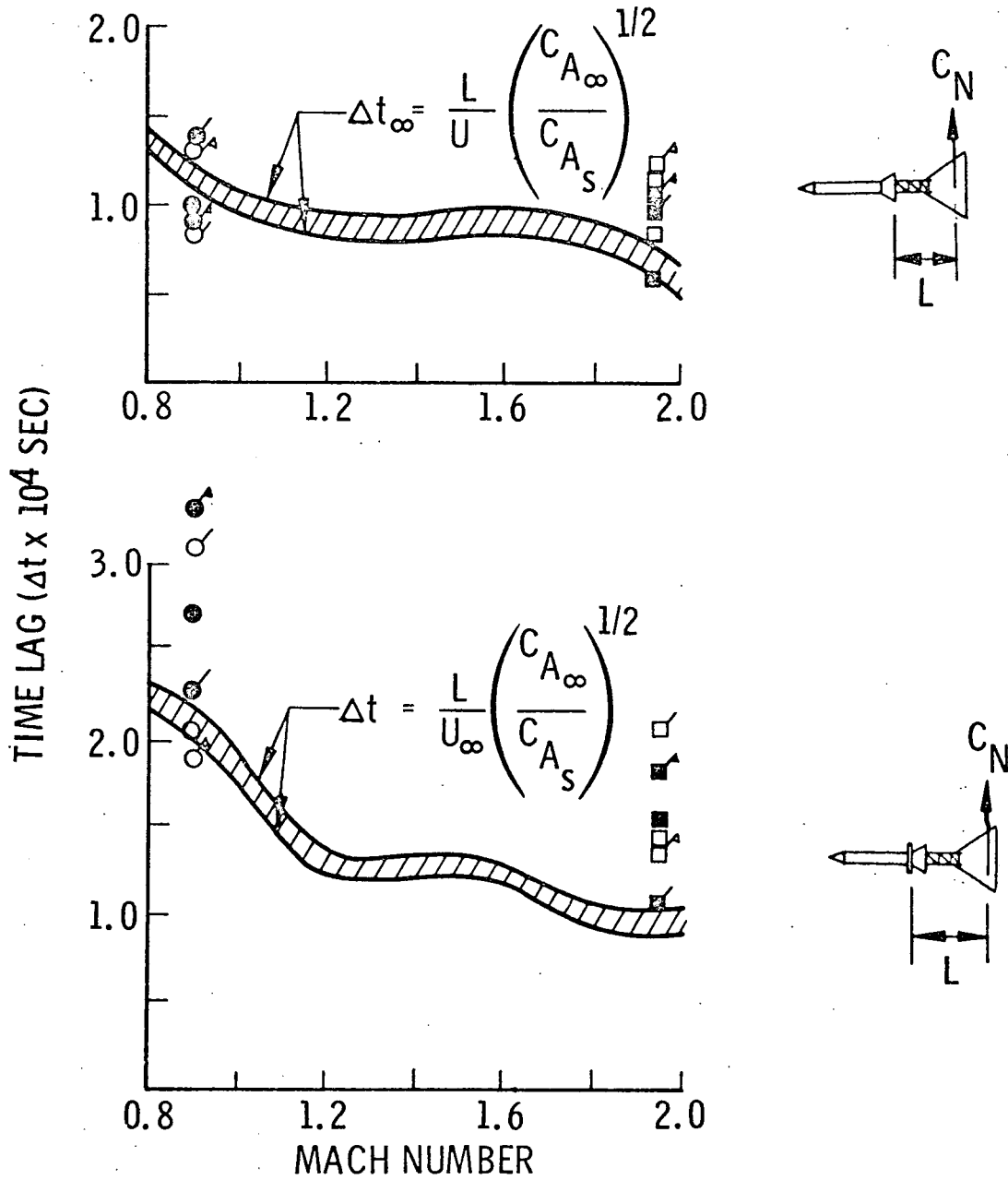


Fig. B-3 Comparison Between Computed and Measured Time Lags in Escape-System Wake (Ref. 134)

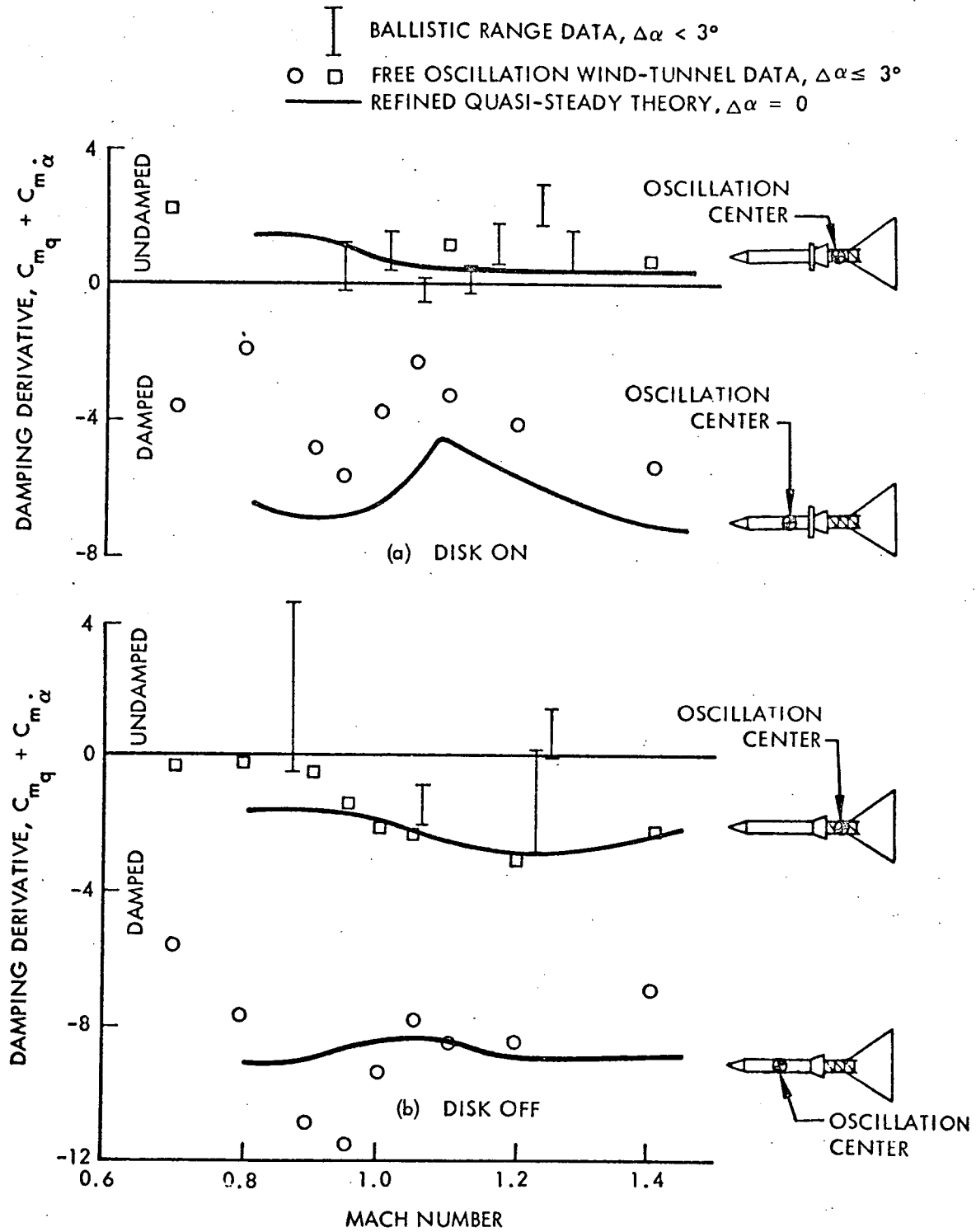


Fig. B-4 Comparison Between Quasi-Steady Predictions and Rigid-Body Experimental Results (Ref. 135)

Likewise, the technique successfully predicted the aerodynamic damping of a fully elastic model (Ref. 18) of the Saturn I booster (Figure B-5 and Ref. 2).

There was some good fortune involved in the Apollo-Saturn results. Later measurements of the loads on bodies in wakes (Ref. 135) indicate the existence of so-called "upstream communication" effects (Figure B-6). That is, when the submerged body penetrates the wake neck the cross flow developed on the submerged body at angle of attack causes an upwash in the recirculation region that induces a further wake asymmetry and greater submerged body load. This is opposed by a tendency of the windward wake boundary to be pushed outward due to back pressure effects. It so happened that the Apollo escape tower was a critical length such that these two effects just cancelled, Fig. B-6. This is very fortunate as the Apollo-Saturn dynamics would otherwise have been a whole lot more complicated as indicated by the dynamics of trailing decelerators. This "upstream communication" effect has been shown to be the cause of one type of decelerator instability (Figure B-7 and Ref. 7).

There is evidence that upstream effects can occur on the parallel stage shuttle boost configuration (Figure B-8 and Ref. 137). The booster tail evidently affects the orbiter loads through the wake recirculation region.

These upstream loads are neglected in the presented estimate of the yaw damping of a parallel stage, straight wing, ascent configuration. The elastic modes were taken from Ref. 138 (Fig. B-9). It is assumed that the orbiter wake affected only the booster tail load for yaw oscillations, which is a reasonable first order approximation. However, it is unknown how much of the total tail load (from Ref. 137) is the result of the orbiter wake. Thus, Figure B-10 presents the aerodynamic damping of the first two yaw modes assuming the tail load varies all the way from being completely the result of the orbiter wake ($\Delta^i C_{Y_{tail}}/C_{Y_{tail}} = 1.0$) to being completely insensitive to the orbiter ($\Delta^i C_{Y_{tail}}/C_{Y_{tail}} = 0$). The first mode shows very little likelihood of aerodynamic undamping while the second mode shows a considerable likelihood of aerodynamic undamping. The likelihood of aerodynamic undamping seems considerable when one considers that the Apollo escape rocket wake accounted for as much as 80 percent of the command module load. It would seem that the thin booster tail will be equally as dominated by the orbiter wake flow.

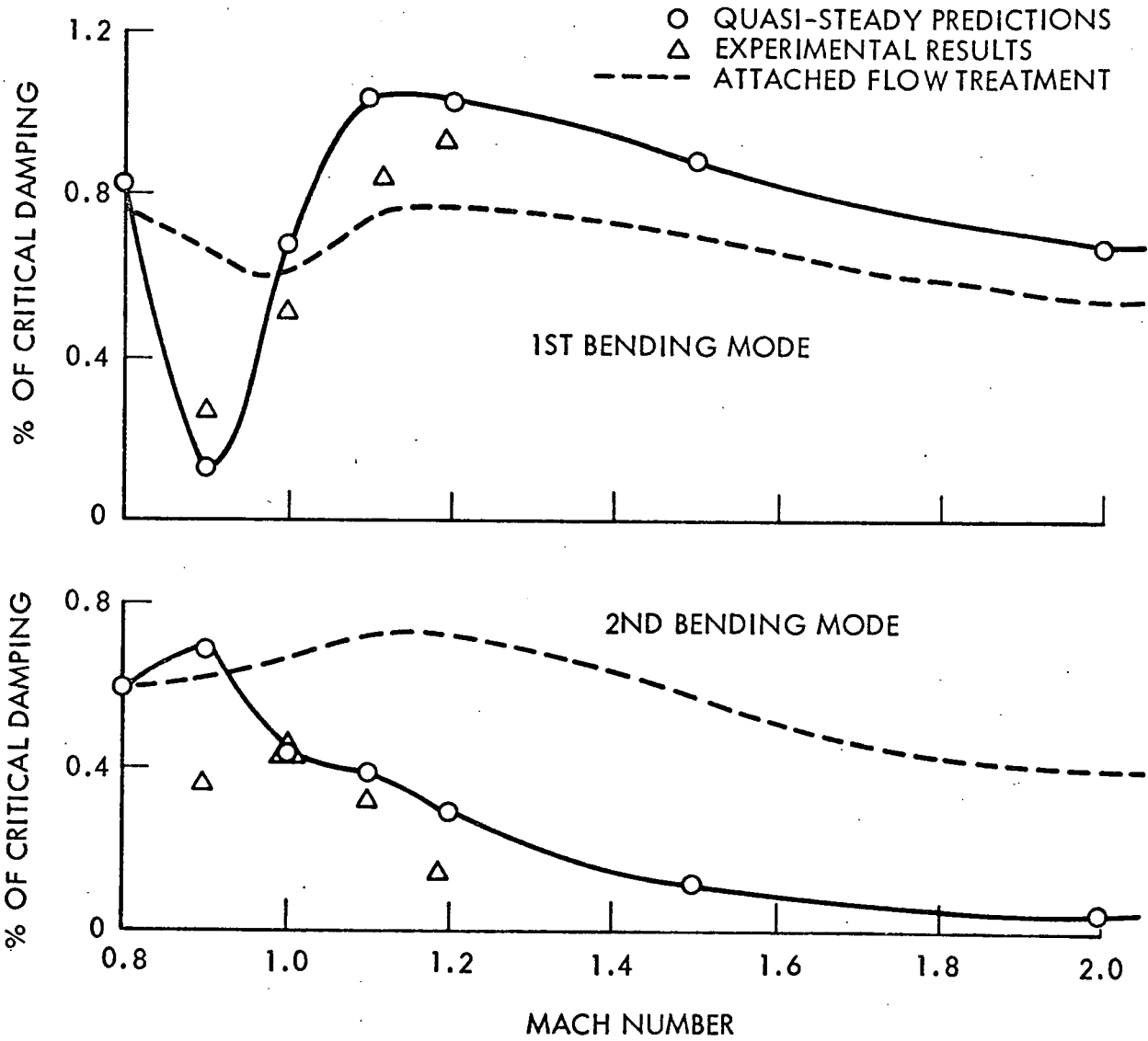


Fig. B-5 Aerodynamic Damping at $\alpha = 0$ of Apollo-Saturn I Launch Vehicle with Disk-On Escape Rocket (Ref. 3)

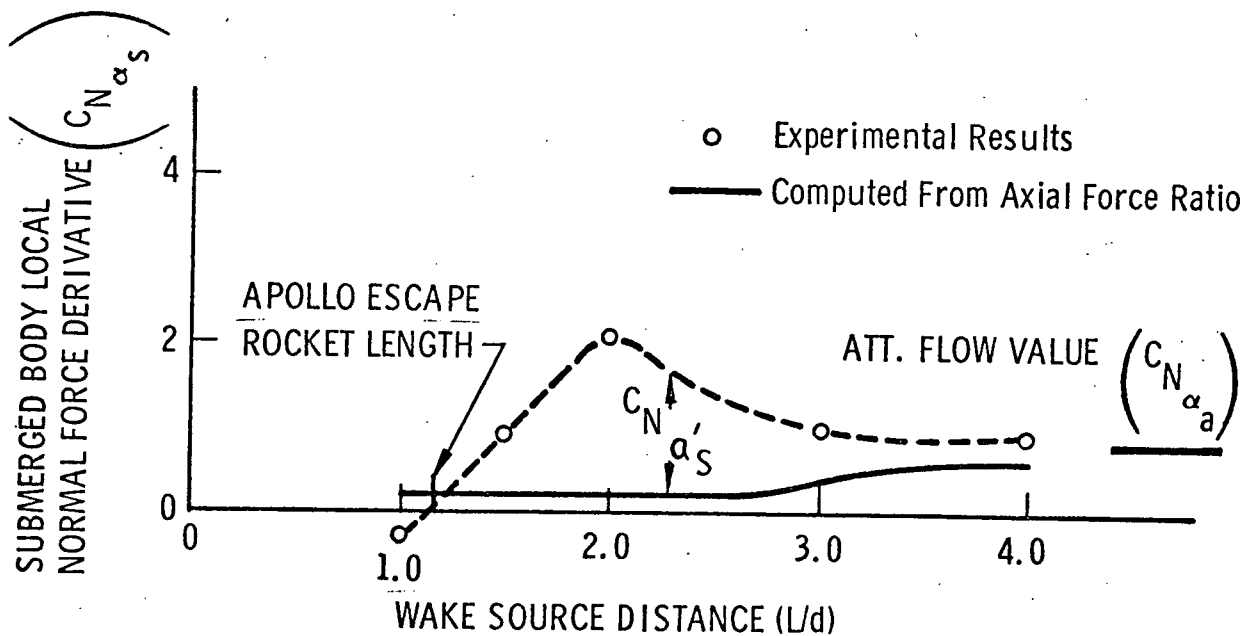
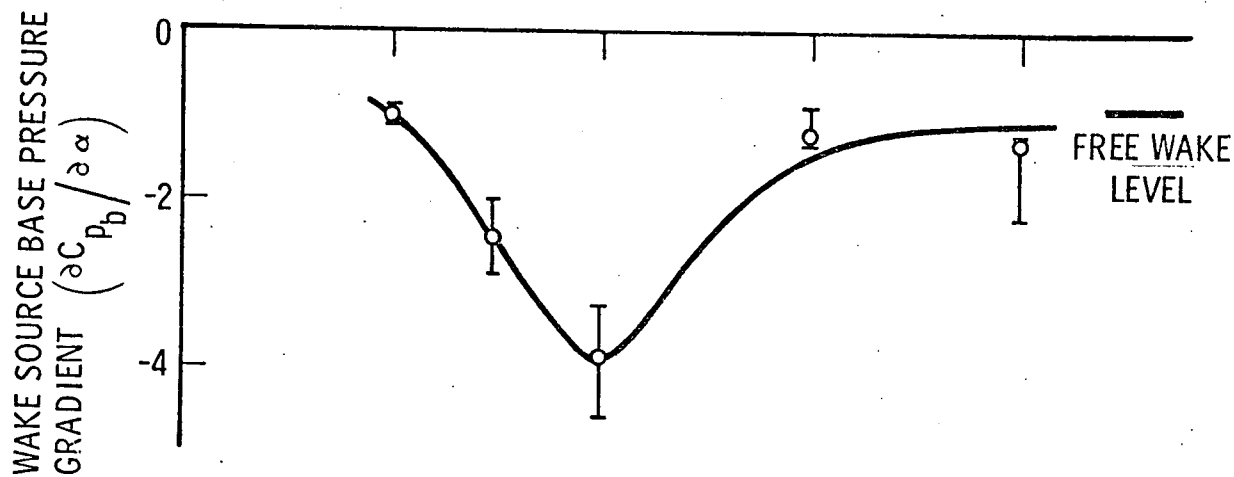
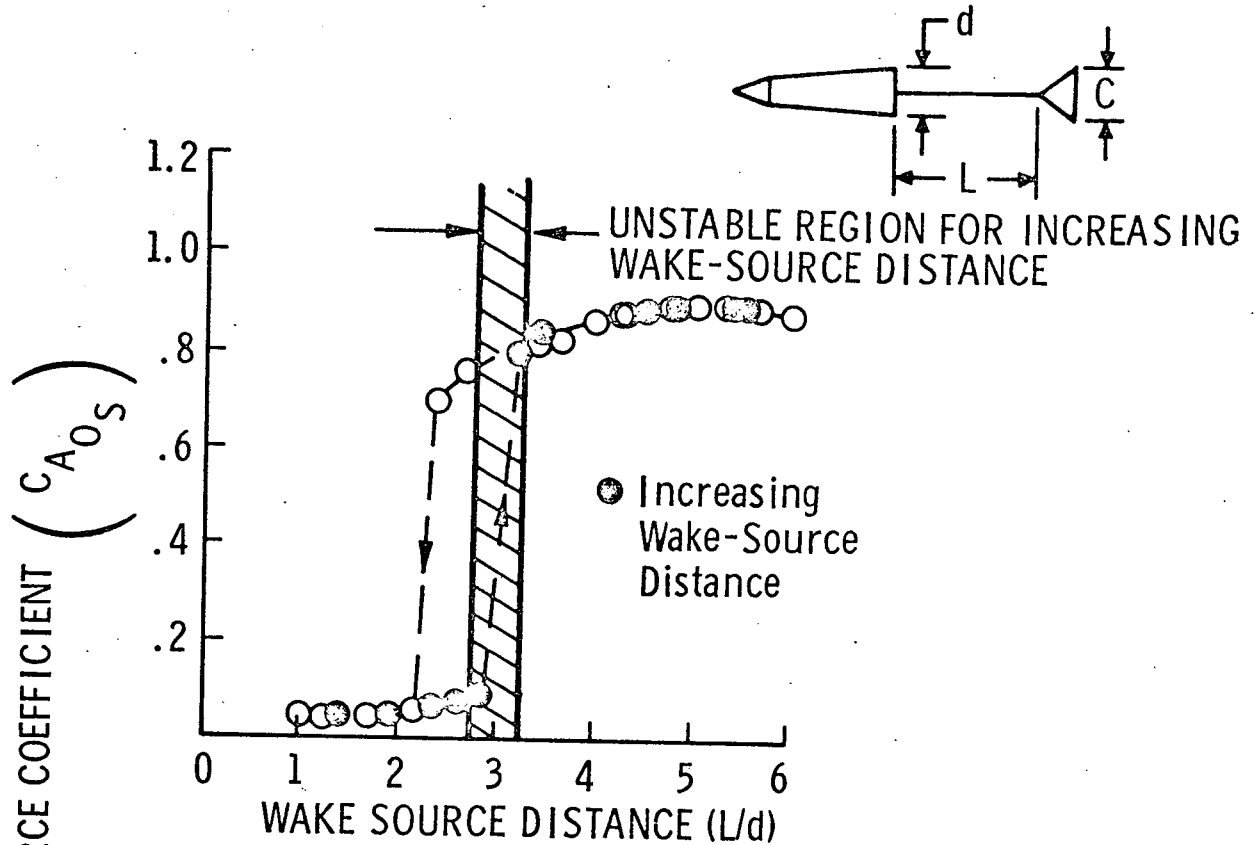
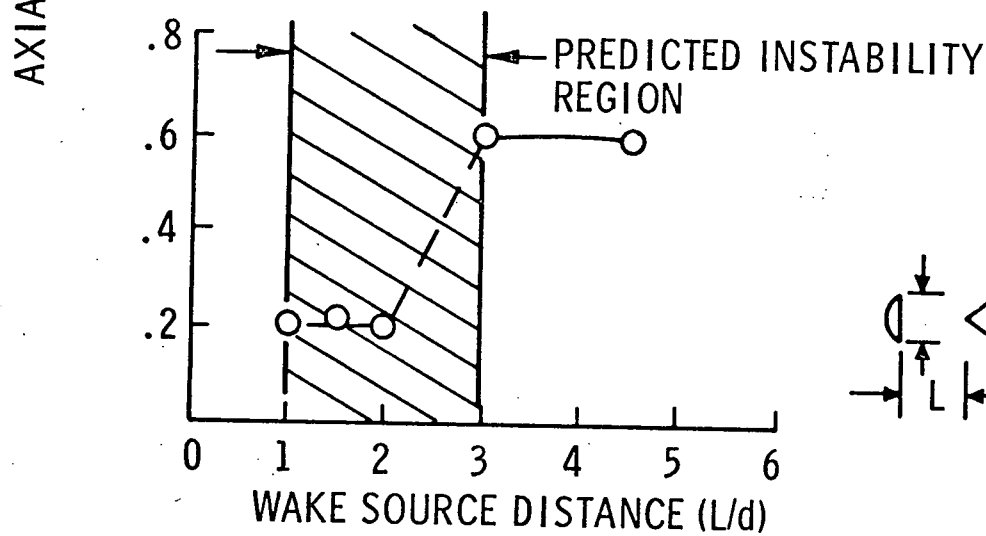


Fig. B-6 Correlation of Wake Source Base Pressure Sensitivity With Submerged Conic Forebody Local Loads (Ref. 135)



a) 45° Decelerator ($M = 6.0$)



b) 30° Decelerator ($M = 1.96$)

Fig. B-7 Correlation of Instability Region With Wake Neck Induced Drag Rise

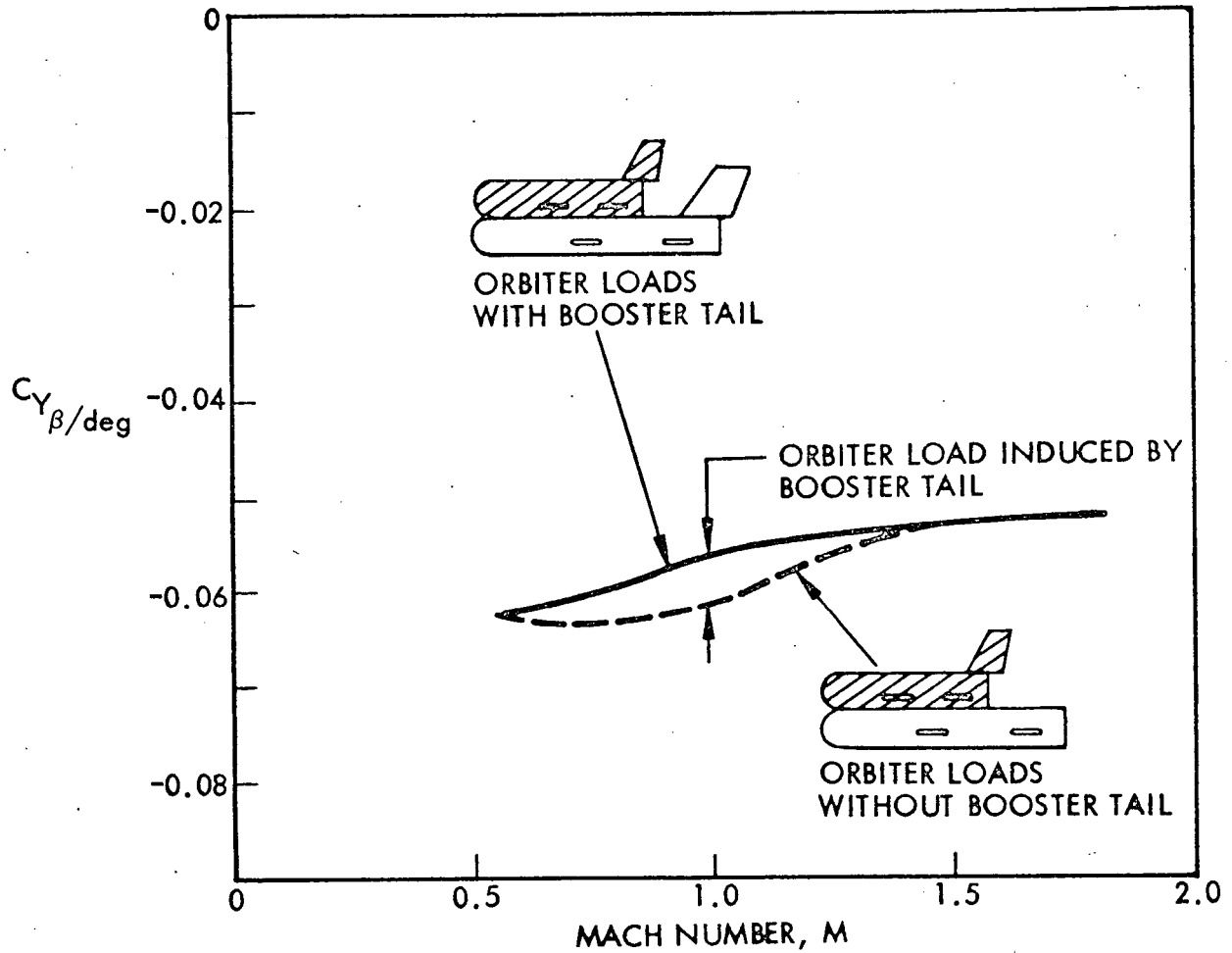


Fig. B-8 Launch Configuration, Upstream Communication Load (Ref. 137)

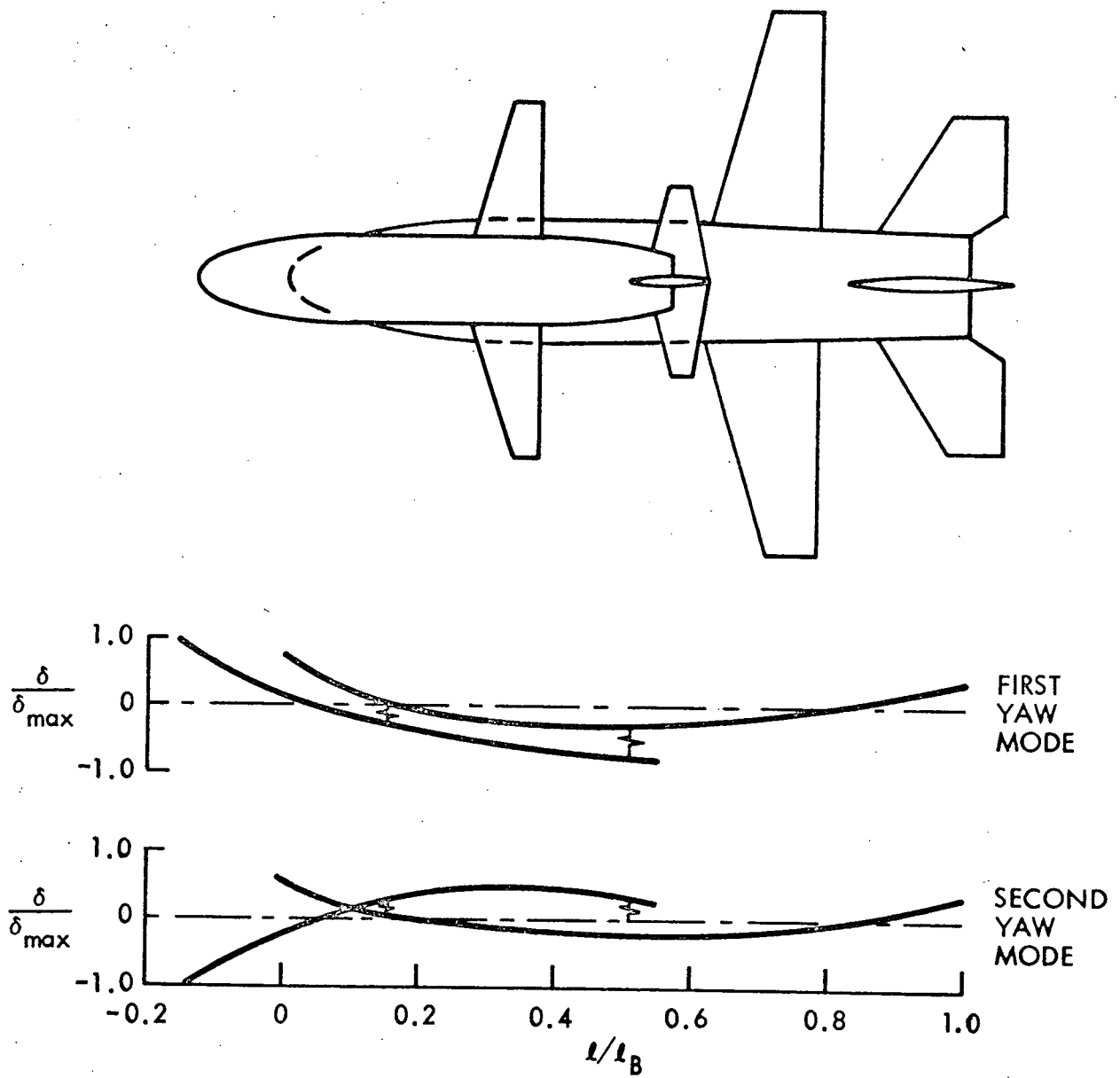
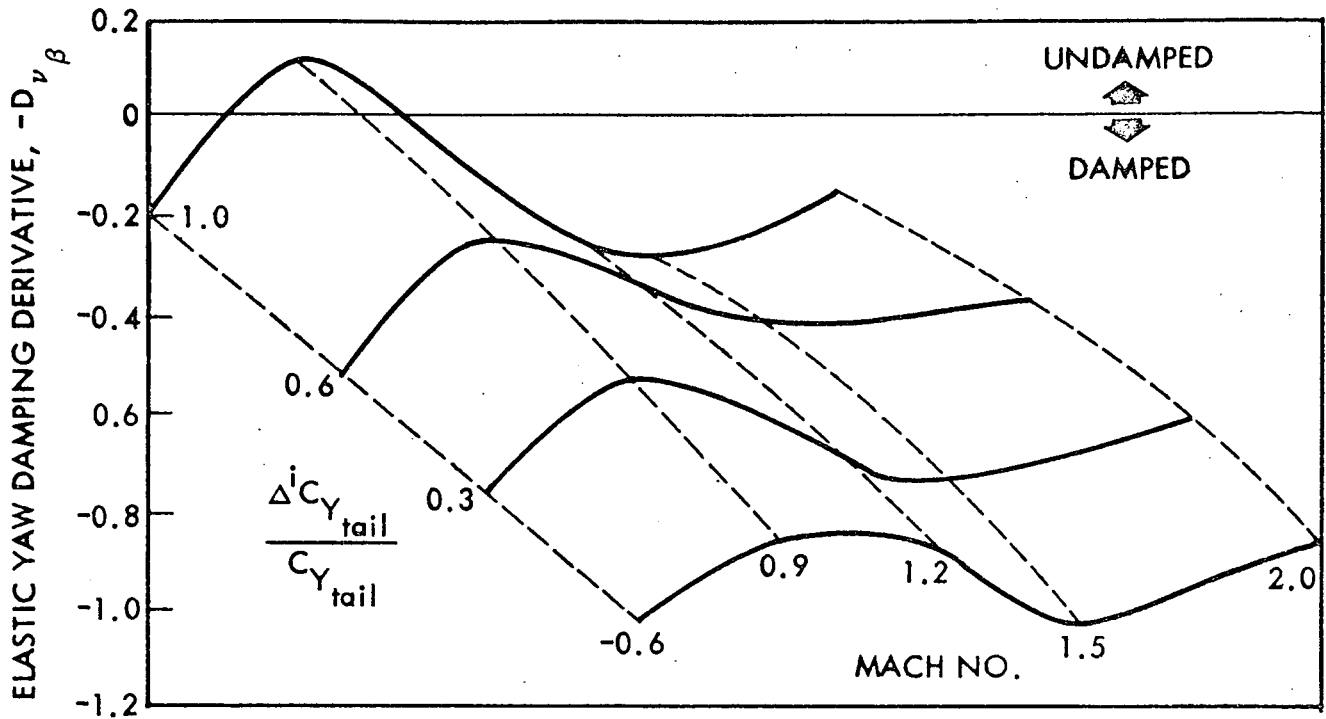
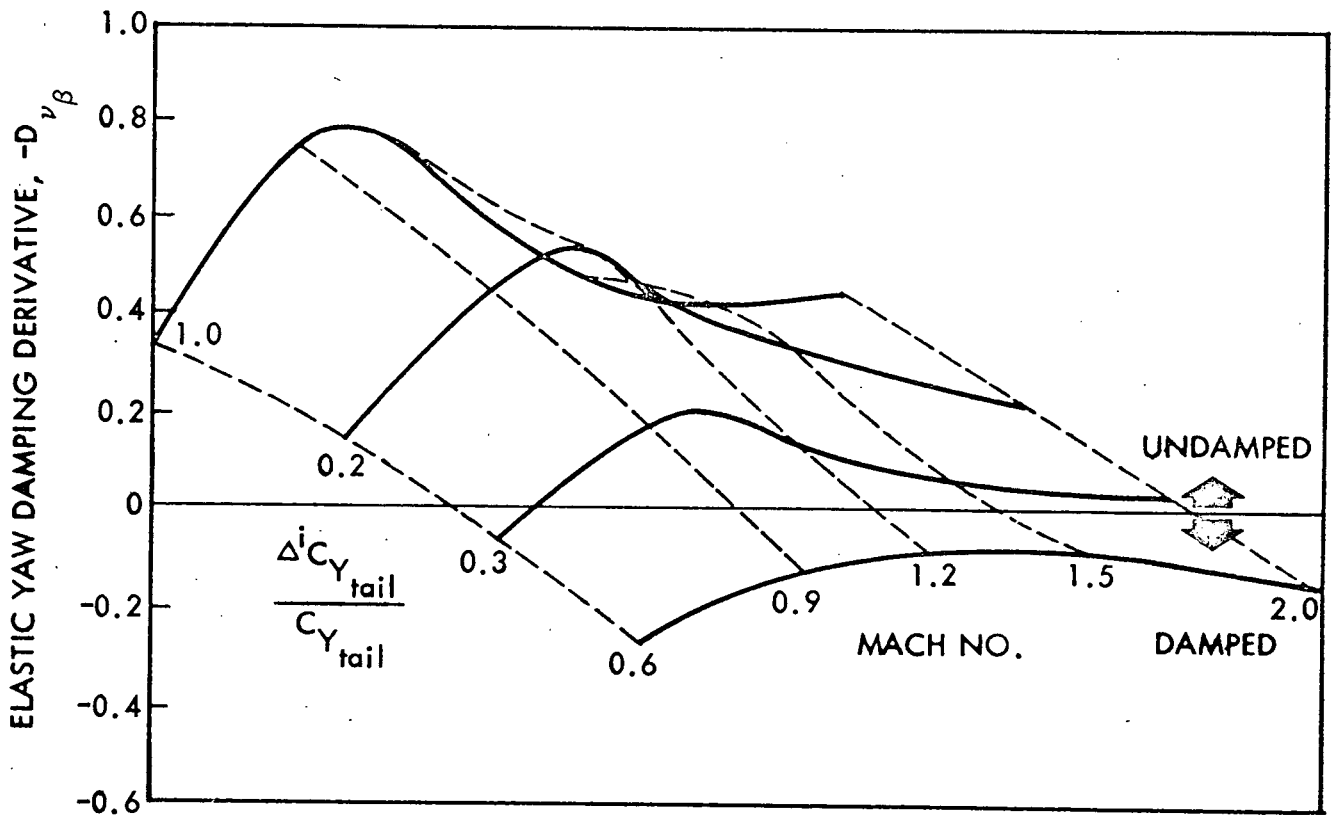


Fig. B-9 Yaw Plane Bending Modes (Ref. 138)



(a) FIRST YAW MODE



(b) SECOND YAW MODE

Fig. B-10 Effect of Relative Magnitude of Induced Booster Tail Load on Yaw Damping

Calculations of the aerodynamic damping of the first two pitch modes (Figure B-11) were also accomplished (mode shapes again from Ref. 138). The booster wing and horizontal tail surfaces are affected by booster interference as indicated by static experimental results (Ref. 137). These data allowed extraction of the interference loads. Coe's flow visualization results (Ref. 139) indicate that the downwash from the orbiter wing is the primary source of interference on the booster wing while the downwash from the orbiter horizontal tail dominates the booster horizontal tail loads. The resulting estimates of the damping derivatives show that the first pitch mode will be aerodynamically damped while the second mode is undamped (Figure B-12).

Similar computations were carried out on a series stage configuration. The configuration was a NAR delta orbiter atop a S-1C stage. The S-1C stage had large tail fins for static stability during boost (e.g. sketch in Figure B-15). There were sufficient wind tunnel results (Ref. 140) to deduce the magnitude of the orbiter wing-booster tail interference load. This interference effect was assumed to be the result of the downwash induced by the orbiter wing which in turn is the result of wing lift, thus, of wing angle of attack. No mode shape estimates were available so it was assumed that the mode shape was similar to that of the Saturn 203 vehicle which was essentially two stiff stages with a weak interstage (the interstage is an antinode of the first three bending modes). Thus, the first three modes were approximated by straight line segments and the critical interstage to tail deflection ratio was computed.* Only the second mode indicated undamping. The second mode stability boundaries for $M = 0.9$ and 1.2 are presented in Figure B-13. That the mode shapes defined by the stability boundary are realistic is indicated by the comparison with an actual Saturn 203 mode shape, Figure B-14.

In conclusion, rough order of magnitude estimates of the aerodynamic damping of parallel and series stage shuttle launch configurations indicate that aerodynamic undamping of the at least one of the lower elastic modes is likely. The likelihood is considered great enough to warrant more detailed analysis.

*By using straight line segments the interstage deflection is related to the slope of the delta wing which in turn determines downwash. Thus, the interstage deflection (δ_1) and the tail or fin deflection ($\delta_{T, E.}$) are indicative of the relative magnitude of local and induced loads.

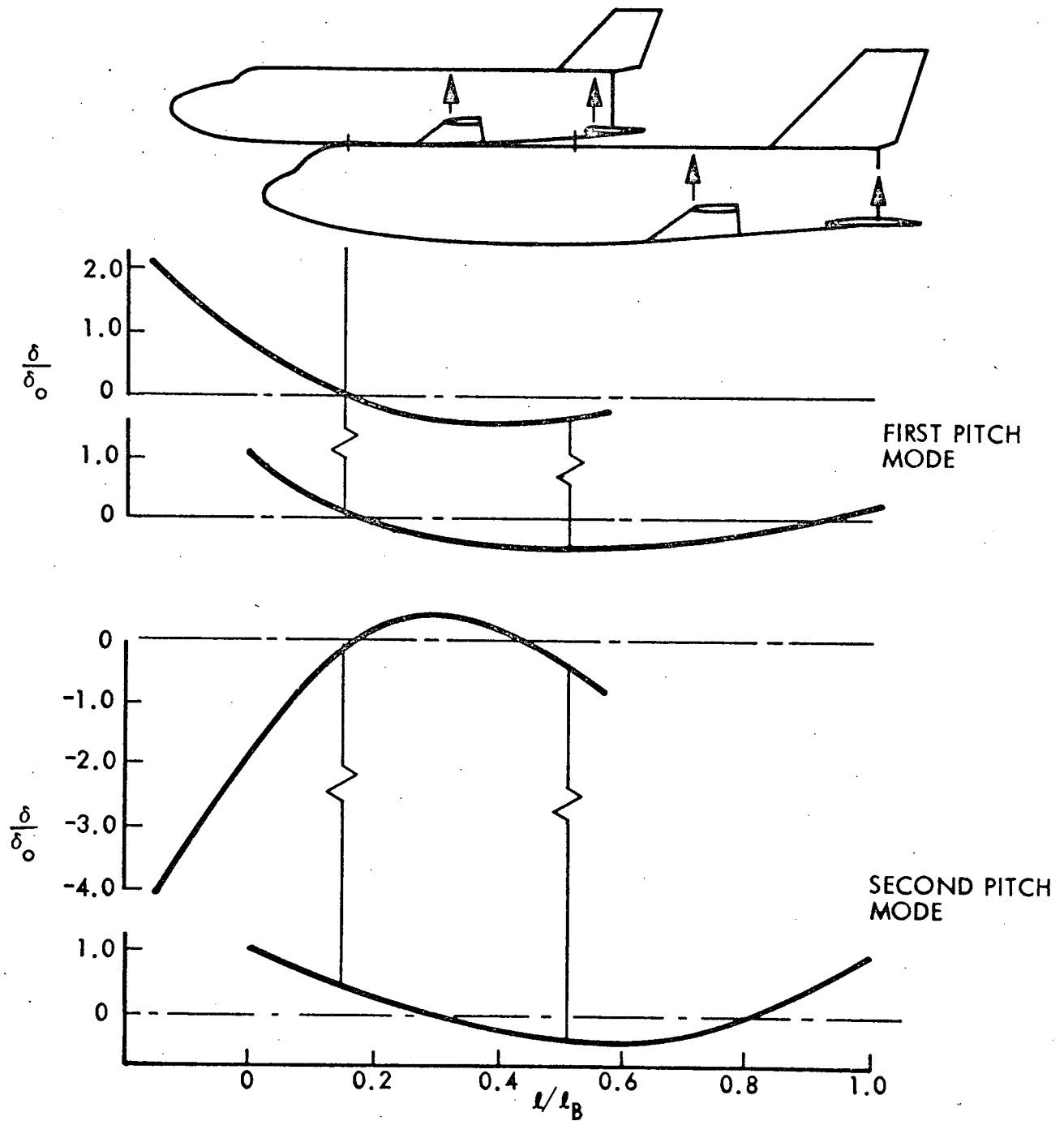


Fig. B-11 Pitch Plane Mode Shapes (Ref. 138)

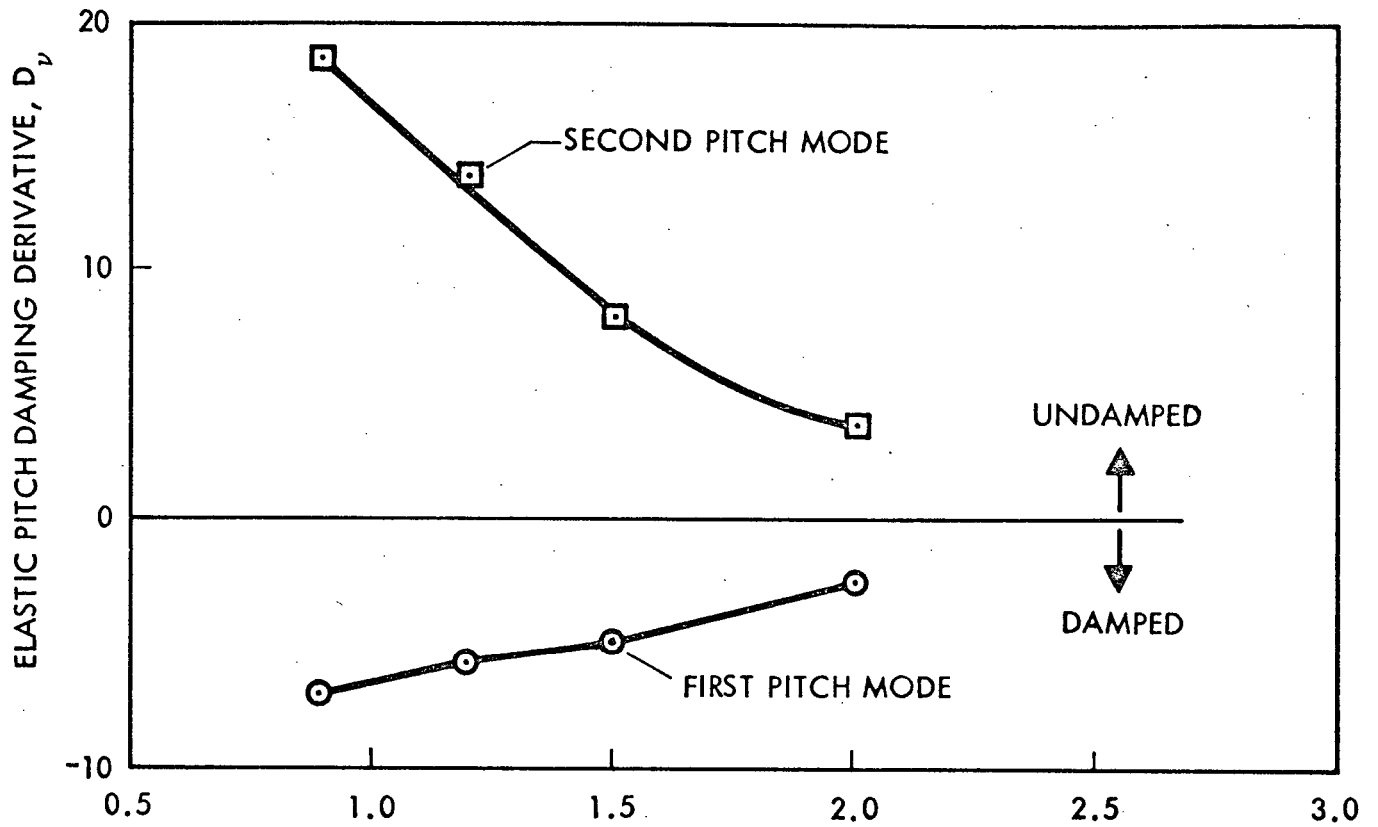


Fig. B-12 Straight Wing Boost Configuration Free-Free Mode Aerodynamic Damping

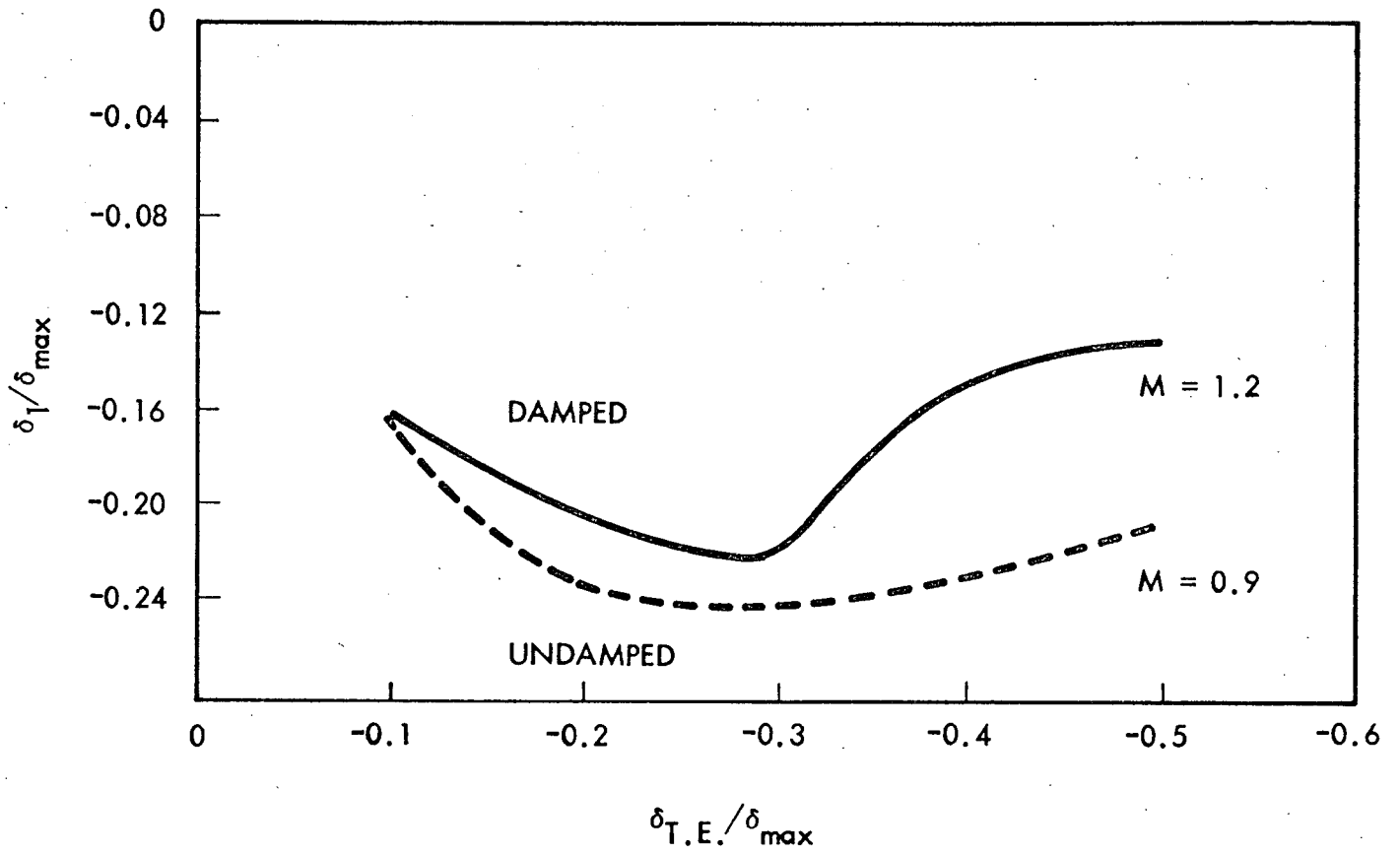


Fig. B-13 Second Mode Aerodynamic Damping Bounds for S-1C NAR Orbiter Launch Configuration

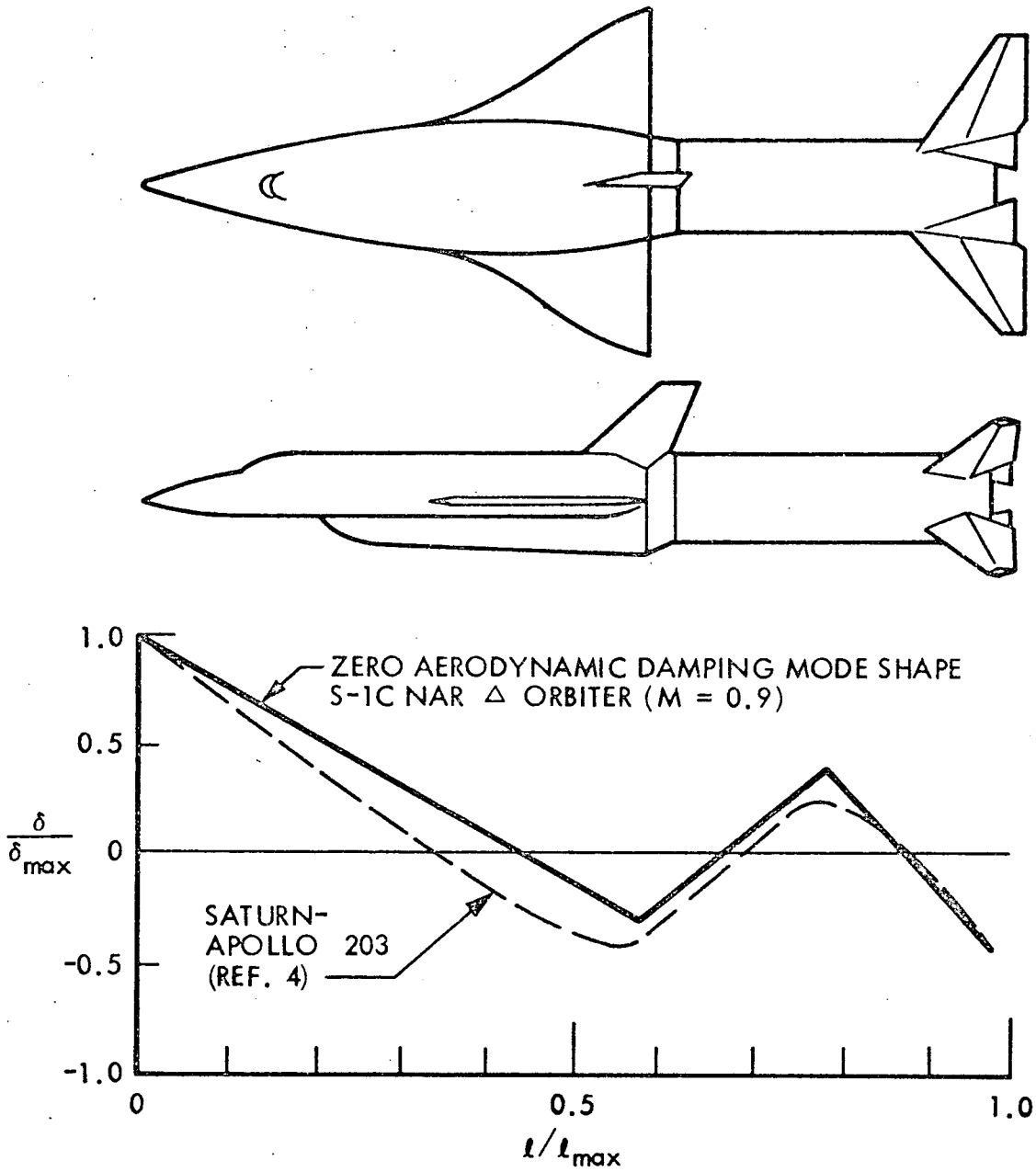


Fig. B-14 Mode Shape Comparison for S-1C-NAR Orbiter Launch Configuration and the Saturn 203 Launch Vehicle

A Reproduced Copy
OF

Reproduced for NASA
by the
NASA Scientific and Technical Information Facility